BEILSTEIN JOURNAL OF ORGANIC CHEMISTRY

Novel macrocycles: from synthesis to supramolecular function

Edited by Pablo Ballester, Konrad Tiefenbacher,Carmine Gaeta, Carmen Talotta,Margherita De Rosa and Paolo Della Sala

Imprint

Beilstein Journal of Organic Chemistry
www.bjoc.org
ISSN 1860-5397
Email: journals-support@beilstein-institut.de

The *Beilstein Journal of Organic Chemistry* is published by the Beilstein-Institut zur Förderung der Chemischen Wissenschaften.

Beilstein-Institut zur Förderung der Chemischen Wissenschaften
Trakehner Straße 7–9
60487 Frankfurt am Main
Germany
www.beilstein-institut.de

BEILSTEIN JOURNAL OF ORGANIC CHEMISTRY

Acyclic cucurbit[*n*]uril bearing alkyl sulfate ionic groups

Christian Akakpo, Peter Y. Zavalij and Lyle Isaacs*

Full Research Paper

Open Access

Address:
Department of Chemistry and Biochemistry, University of Maryland, College Park, Maryland 20742, United States

Email:
Lyle Isaacs* - LIsaacs@umd.edu

* Corresponding author

Keywords:
cucurbituril; host–guest chemistry; isothermal titration calorimetry; molecular container; X-ray crystallography

Beilstein J. Org. Chem. **2025,** *21,* 717–726.
https://doi.org/10.3762/bjoc.21.55

Received: 09 January 2025
Accepted: 28 March 2025
Published: 03 April 2025

This article is part of the thematic issue "Novel macrocycles: from synthesis to supramolecular function".

Guest Editor: C. Gaeta

Abstract

We report the synthesis and characterization of a new acyclic cucurbit[*n*]uril (CB[*n*]) host **C1** that features four alkyl sulfate ionic groups. The X-ray crystal structure of the **C1·Me$_6$CHDA** complex is reported. Host **C1** is significantly less soluble in water (4 mM) compared to the analogous acyclic CB[*n*] host **M1** which features sulfonate ionic groups (346 mM). Host **C1** does not undergo significant self-association according to the results of ^{1}H NMR dilution experiments. The molecular recognition behavior of the hosts **C1** and **M1** toward a panel of seven ammonium ions was explored by ^{1}H NMR spectroscopy and isothermal titration calorimetry (ITC). We find that **C1** generally binds slightly more tightly than **M1** toward a specific guest. **C1** binds more tightly to quaternary ammonium guests compared to the corresponding primary ammonium ions.

Introduction

Molecular recognition interactions are key elements of life processes including self- versus non-self-recognition, biosynthesis, molecular and ion transport, and replication. Beginning with the pioneering works of Pedersen, Lehn, and Cram, supramolecular chemists have studied the fundamental aspects of non-covalent interactions in organic solvents and water [1-4]. Building on this fundamental knowledge, supramolecular chemists created a variety of functional systems including supramolecular polymers, sensing ensembles, molecular machines, supramolecular separation phases, and drug delivery systems [5-9]. A primary subfield of supramolecular chemistry involves the synthesis of macrocyclic hosts and studies of their molecular recognition properties. The most widely studied macrocyclic host systems include those created entirely by covalent bonds (crown ethers, cyclodextrins, calixarenes, cyclophanes, pillararenes, cucurbit[*n*]urils (CB[*n*])), and those prepared by metal ligands and H-bonding self-assembly processes [1,2,10-20]. Macrocycles have played key roles in important real-world products including the household deodorizer Febreeze^{TM}, glucose monitors, and as solubilizing excipients [21-26]. Within these families of macrocyclic hosts, CB[*n*] molecular containers have proven particularly versatile because they form high affinity

CB[*n*]–guest complexes in aqueous solution that are responsive to various stimuli (e.g., photochemical, electrochemical, chemical) [27-30]. For this reason, macrocyclic CB[*n*] have been used as key elements of separations processes [31,32], sensing systems [33,34], in pharmaceutical applications [35-38], in bioimaging systems [39,40], and even in household deodorizing products [41].

An important subclass of CB[*n*] hosts are acyclic CB[*n*]-type receptors which have been extensively studied by our lab and others over the past decade [42-52]. Figure 1 shows the chemical structure of the prototypical acyclic CB[*n*]-type known as **M1** [53,54]. **M1** features a central glycoluril tetramer, two aromatic *o*-xylylene walls, and four sulfonates as solubilizing ionic groups. In accord with these structural features, **M1** binds a variety of hydrophobic and cationic guest molecules by the hydrophobic effect, π–π interactions, and electrostatic (ion–dipole and ion–ion) interactions. Although acyclic CB[*n*] are not macrocycles, they are preorganized into a C-shaped geometry by virtue of their polycyclic chemical structure and display binding affinities approaching those of macrocyclic CB[*n*]. **M1** and analogues display outstanding biocompatibility and have been used for a number of in vivo biomedical applications including as a solubilizing excipient for anticancer agents and as an in vivo sequestrant to reverse the biological activity of neuromuscular blocking agents, anesthetics, and drugs of abuse (e.g., methamphetamine and fentanyl) [54-60].

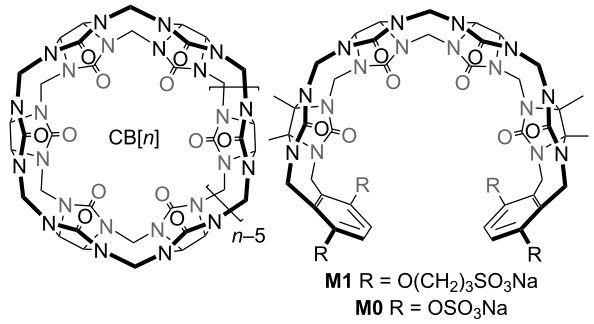

Figure 1: Chemical structures of CB[n] and selected acyclic CB[*n*]-type molecular containers **M1** and **M0**.

As a result of their modular synthesis, acyclic CB[*n*] can be easily modified synthetically [42-47,61]. Acyclic CB[*n*]-type receptors featuring different length glycoluril oligomers (monomer–pentamer) and different aromatic walls (e.g., naphthalene, anthracene, triptycene) have been studied [42,62-67]. Previously, we have studied the influence of the length of the $O(CH_2)_nSO_3Na$ sidearm (n = 0, 2, 3, 4) and found that the **M0** host – where the hydrophobic linker $(CH_2)_n$ was completely removed – displayed higher binding affinity than **M1** which we attributed to the location of the ionic group closer to the ureidyl C=O portals [68,69]. However, a close examination of the structures of **M0** and **M1** show that the ionic group for **M1** is a sulfonate and for **M0** is a sulfate. Accordingly, **M1** and **M0** differ in two ways: a) different $(CH_2)_n$ linker length and b) different ionic group (sulfonate versus sulfate). In this paper, we present the synthesis and molecular recognition properties of a new acyclic CB[*n*]-type receptor **C1** which allows us to disentangle these two effects.

Results and Discussion

This results and discussion section is organized as follows: First, we present the design, synthesis, and spectroscopic characterization of **C1** along with determination of its inherent aqueous solubility and self-association properties. Next, we present the X-ray crystal structure of **C1** as its **C1**·**Me$_6$CHDA** complex. Subsequently, we describe a qualitative investigation of **C1**·guest and **M1**·guest complexation by ^{1}H NMR spectroscopy and quantitative investigation by isothermal titration calorimetry (ITC). Finally, we discuss the trends in binding affinity observed for **C1**·guest and **M1**·guest complexation.

Design, synthesis and characterization of **C1**

In order to disentangle the effects of the ionic group (sulfonate versus sulfate) while maintaining the distance of the ionic group from the ureidyl C=O portal we designed acyclic CB[*n*]-type receptor **C1** (Scheme 1). The only structural difference between **M1** and **C1** is the swapping of one CH_2 group for one O atom in each alkyl chain which effectively changes the sulfonate group to a sulfate group. The synthetic route to **C1** starts with the double electrophilic aromatic substitution reaction of methylene-bridged glycoluril tetramer (**TetBCE**) with **W1** in TFA/Ac_2O 1:1 which adds the sidewalls and transforms the OH groups into OAc groups to give **TetW1$_{OAc}$** in 71% yield as described previously [70]. Saponification of **TetW1$_{OAc}$** with LiOH at 50 °C followed by acidification with 0.1 M HCl gives **TetW1** in 69% yield [70]. Finally, the sulfation of **TetW1** occurs upon treatment with py·SO_3 (20 equiv) in dry pyridine to yield **C1** as a white solid in 68% yield. In accord with the depicted C_{2v}-symmetric geometry (Scheme 1), the ^{1}H NMR spectrum of **C1** displays one aromatic resonance (H_a), two methyl resonances $(CH_3)_j$ and $(CH_3)_k$, two equatorial methine doublets (H_l and H_m), along with three doublets for the diastereotopic methylene bridges around 5.5 ppm (H_d, H_f, H_h) in the expected 2:2:1 ratio (Figure 2a). The 4.0–4.5 ppm region is crowded which precludes precise assignments of the expected resonances for H_e, H_g, H_i, H_b, and H_c. Similarly, the ^{13}C NMR spectrum recorded for **C1** (Figure 2b) shows 15 of the 16 resonances expected based on time averaged C_{2v}-symmetry in solution. For example, we observe two resonances for the C=O groups, three resonances for the aromatic C-atoms, two methyl

resonances, three resonances for the bridging CH_2 groups, and five of the six resonances for the sidearm (b and c) and equatorial glycoluril C-atoms. The negative-ion electrospray ionization mass spectrum shows an ion at m/z = 751.13 which corresponds to $[\mathbf{C1} - 2Na]^{2-}$.

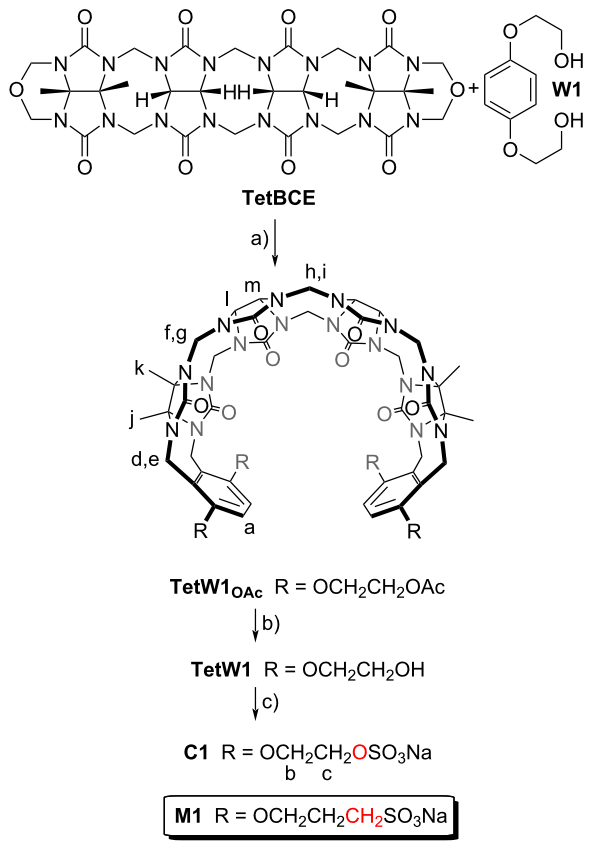

Scheme 1: Synthesis of **C1**. Conditions: a) TFA/Ac_2O, 70 °C, 3.5 h, 71%; b) LiOH, 50 °C, 69%; c) dry pyridine, pyridine sulfur trioxide complex (20 equiv), 90 °C, 18 h, 68%.

Inherent aqueous solubility of C1

After having firmly established the structure of **C1** we decided to determine its inherent aqueous solubility. For this purpose, we added an excess of solid **C1** to D_2O and stirred the solution at room temperature overnight. Afterwards, the mixture was centrifuged (4400 rpm, 10 min) to pellet excess insoluble **C1**. An aliquot of the supernatant and a solution of dimethyl malonic acid as a non-binding internal standard of known concentration were transferred to an NMR tube followed by collection of a ^{1}H NMR spectrum using a delay time between pulses of 20 seconds to ensure accurate integration. The inherent aqueous solubility of **C1** was determined to be 3.97 mM by comparison of the integrals for H_a of **C1** with that of the CH_3-resonance for dimethyl malonic acid (Figure S5 in Supporting Information File 1).

Qualitative study of C1·guest recognition properties by ^{1}H NMR spectroscopy

Next, we decided to perform a qualitative investigation of the host–guest properties of **C1** by ^{1}H NMR spectroscopy. Figure 3 shows the chemical structures of a panel of guests that were studied and the complexation-induced changes in chemical shift (Δδ) for **C1**·guest. As the central hydrophobic binding domain of the guests we selected alkylene, *p*-xylylene, cyclohexane, and adamantane moieties that are known to bind well to (acyclic) CB[*n*] receptors [71-73]. The cross-sectional area of this hydrophobic moiety increases as follows: **PDA** ≈ **HDA** < **PXDA** < **CHDA** < **AdA**. Given that (acyclic) CB[*n*] often bind to ammonium ion guests (e.g., NH_3^+ form) weaker than they do to the corresponding methonium ion guests (e.g., NMe_3^+ form) we elected to study both forms to elucidate related preferences for the sulfated **C1** host relative to the sulfonated **M1** host [69,71,74]. Figure 4 shows a ^{1}H NMR stack plot created for uncomplexed **C1** (Figure 4d), uncomplexed **Me_6PXDA** (Figure 4d), and 1:1 and 1:2 mixtures of **C1** and **Me_6PXDA**. Several spectroscopic features are noteworthy. First, the Ar–H

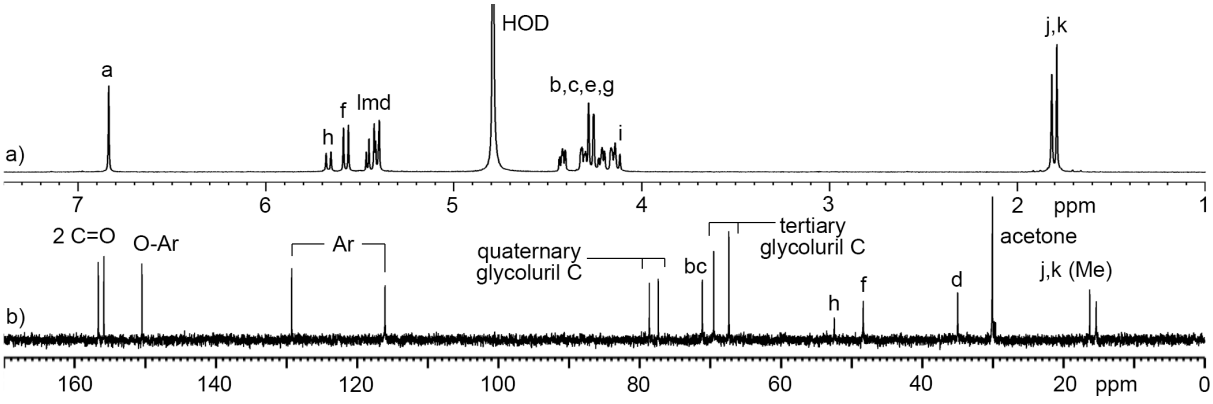

Figure 2: a) ^{1}H NMR spectrum (600, D_2O, rt) and b) ^{13}C NMR spectrum recorded (150 MHz, D_2O, rt) for **C1**.

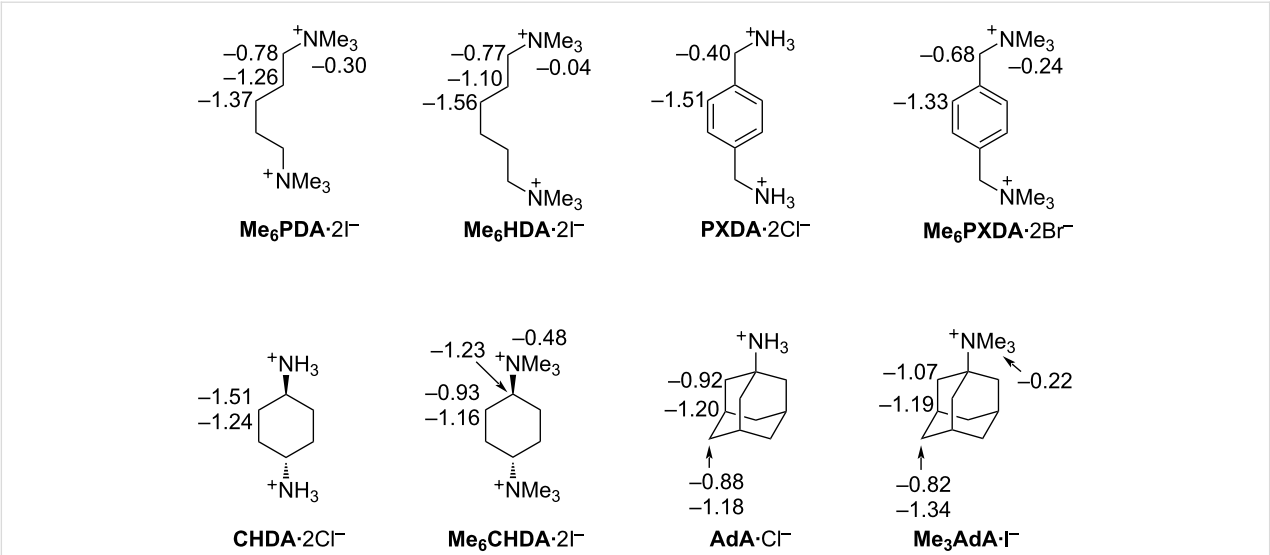

Figure 3: Chemical structures of guests used in this study along with the complexation induced changes in chemical shift (Δδ) upon formation of the **C1**·guest complexes. Negative Δδ values represent upfield shifts upon complexation.

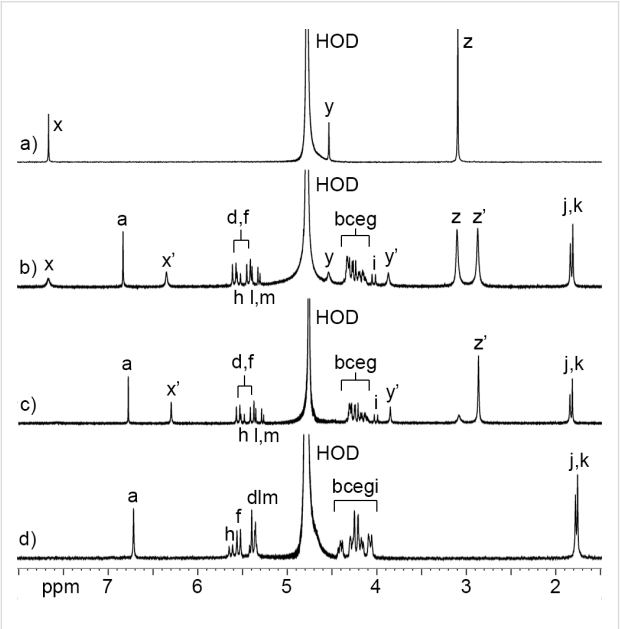

Figure 4: ^{1}H NMR spectra recorded (400 MHz, D_2O, rt) for: a) **Me$_6$PXDA** (0.5 mM), b) a mixture of **C1** (0.5 mM) and **Me$_6$PXDA** (1.0 mM), c) a mixture of **C1** (0.5 mM) and **Me$_6$PXDA** (0.5 mM), and d) **C1** (0.5 mM).

resonance for **Me$_6$PXDA** undergoes a large upfield shift (Δδ = −1.33) upon formation of **C1**·**Me$_6$PXDA** (Figure 4c) whereas the CH_2 (Δδ = −0.68) and NMe_3 (Δδ = −0.24) groups undergo smaller upfield shifts. This observation strongly suggests that the Ar–H protons are located nearer the center of the magnetically shielding cavity of **C1** which is defined by the aromatic sidewalls and the ureidyl π-systems. The small changes in chemical shift for the methonium group suggests it is located near the ureidyl C=O portals and not inside the magnetically shielding cavity. Related complexation-induced changes in chemical shift are observed for the other **C1**·guest complexes (Figure 3 and Supporting Information File 1) which confirms that the hydrophobic central region of the guest binds inside the hydrophobic cavity of **C1** whereas the hydrophilic ammonium and methonium groups reside at the electrostatically negative ureidyl C=O portals. Second, at a 1:2 **C1**/**Me$_6$PXDA** ratio (Figure 4b), we observe separate resonances for free **Me$_6$PXDA** and complexed **C1**·**Me$_6$PXDA** which means that the rate of guest exchange is slow on the chemical shift timescale. Slow kinetics of guest exchange is commonly observed for tight host·guest complexes. In contrast, the kinetics of guest exchange are in the intermediate exchange regime on the chemical shift timescale for the complexes of **C1** with **CHDA**, **Me$_6$CHDA**, **AdA**, **Me$_3$AdA** (Supporting Information File 1, Figures S10–S13) which is typical of weaker complexes. Third, we observe changes in the chemical shift for the H_a resonance of **C1** upon formation of the **C1**·guest complexes. In uncomplexed **C1** the tips of the aromatic rings are pointing toward each other which places H_a in the magnetically shielding region of the opposing sidewall. Upon formation of the **C1**·guest complexes, the tips of the aromatic sidewall change their orientation to accommodate the hydrophobic region of the guest which changes the orientation of H_a with respect to the magnetically shielding region [54,63,64].

X-ray crystal structure of **C1**

We were fortunate to obtain single crystals of the **C1**·**Me$_6$CHDA** complex and solved the crystal structure by X-ray diffraction (CCDC 2411723). Figure 5 shows a cross-

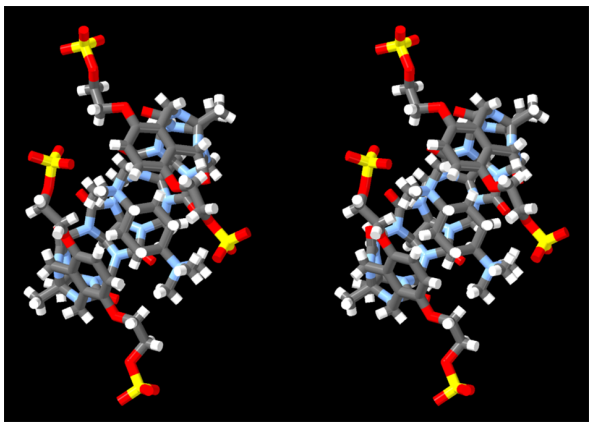

Figure 5: Cross-eyed stereoview of the **C1·Me$_6$CHDA** complex in the crystal. Color code: C, gray; H, white; N, blue; O, red; S, yellow.

eyed stereoview of one **C1·Me$_6$CHDA** complex in the crystal. Several features of this structure are noteworthy. First, the crystal structure confirms the molecular structure of **C1** and its overall C-shaped geometry. Second, within the **C1·Me$_6$CHDA** complex, the aromatic sidewalls are splayed away from the equator of **C1** resulting in a helical geometry [63,65]. Both senses of helical chirality are present in the crystal; values in parenthesis given below refer to the complex with opposite helical chirality. The guest **Me$_6$CHDA** possesses a mirror plane and is therefore achiral. In solution, host **C1** is flexible and the two senses of helicity – and other conformations – undergo rapid equilibrium rendering the **C1** and the **C1·Me$_6$CHDA** complex achiral. The centroids of the aromatic sidewall are 0.9698 Å (1.1193 Å) above and 1.3090 Å (1.4832 Å) below the mean plane of the glycoluril methine and glycoluril quaternary C-atoms. Third, the **Me$_6$CHDA** guest is not symmetrically oriented with respect to the ureidyl carbonyl portals of **C1**. Specifically, one of the methonium N-atoms is located inside the cavity of **C1** at 1.4476 Å (0.6162 Å) below the mean plane of the ureidyl carbonyl O-atoms whereas the other methonium N-atom is located 1.7980 Å (0.9686 Å) outside the cavity.

Figure 6 shows the packing of four molecules of the **C1·Me$_6$CHDA** complex in a single unit cell along with four molecules of **Me$_6$CHDA** located outside the cavity of **C1** to ensure overall charge neutrality. It is well known that CB[*n*]·guest complexation is driven by ion–dipole interactions at the ureidyl C=O portals [75]. Previously, we found that the $Me_3N^+\cdots O{=}C$ distances in the ultratight CB[7]·diamantane$(NMe_3)_2$ complex averaged 4.38(7) Å [74]. For comparison, a histogram of $Me_3N^+\cdots O{=}C$ distances drawn from 89 CCDC structures that contain an acetylcholine-type unit ($Me_3NCH_2CH_2O(C{=}O)R$) range from 3.5 Å to 5 Å with a maximum probability of 4.4 Å [74]. Figure 6 shows $Me_3N^+\cdots O{=}C$ contacts that are less than 4.40 Å. The large number of contacts that are significantly shorter than 4.40 Å establishes that $Me_3N^+\cdots O{=}C$ cation–dipole interactions play an important role driving the inclusion of **Me$_6$CHDA** inside of **C1** to form the **C1·Me$_6$CHDA** complex. Of course, the inclusion of the hydrophobic cyclohexyl moiety inside the cavity of **C1** provides a hydrophobic driving force for complexation in water. Given that **C1** is a tetraanion and that **Me$_6$CHDA** is a dication, an additional molecule of **Me$_6$CHDA** is present per molecule of **C1** to ensure overall charge neutrality in the crystal. Among the four molecules of **Me$_6$CHDA** outside the cavity of **C1** in the molecular cell (Figure 6, only two external **Me$_6$CHDA** are shown for clarity), only one $Me_3N^+\cdots O{=}C$ contact (4.548 Å) with a distance < 5.5 Å is observed. Given the anionic nature of

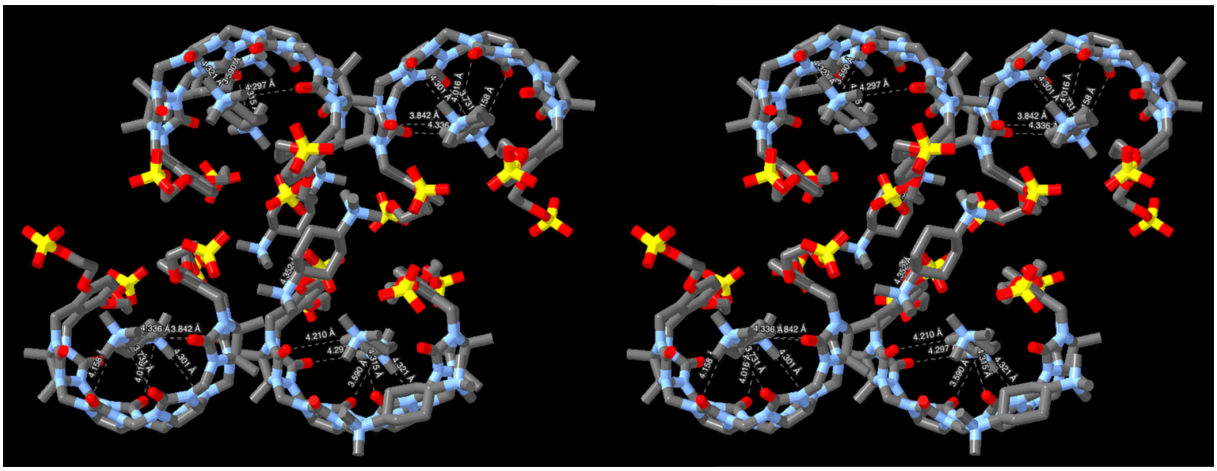

Figure 6: Cross-eyed stereoview of the crystal packing observed in the molecular cell of **C1·Me$_6$CHDA**. H-atoms are omitted for clarity. N···O distances less than 4.40 Å are indicated with dashed lines. Color code: C, gray; N, blue; O, red; S, yellow.

the sulfate substituents, one might expect to observe $Me_3N^+\cdots{}^-O_3SO$ interactions in the crystal. Somewhat surprisingly, only a single short $Me_3N^+\cdots{}^-O_3SO$ contact (4.352 Å) is observed with distance < 4.4 Å. There are, however, numerous longer $Me_3N^+\cdots{}^-O_3SO$ contacts with distances in the 4.4–5.4 Å range which suggests they play a supporting role during crystallization.

Measurement of the self-association of **C1**

Before proceeding to investigate the molecular recognition properties of **C1** by ITC, we wanted to determine whether **C1** undergoes self-association in phosphate-buffered saline (PBS) which might impinge on guest binding and complicate the determination of **C1**·guest binding constants. For this purpose, we performed dilution experiments monitored by ^{1}H NMR spectroscopy. We prepared a series of NMR samples of **C1** in D_2O (from 4 mM to 125 μM) and monitored the chemical shift of H_a (Supporting Information File 1, Figure S14). Over this dilution range, the resonance for H_a remains a sharp singlet at 6.94 ppm. Accordingly, we conclude that **C1** remains monomeric at the low concentration (100 μM) typically employed for isothermal titration calorimetry measurements.

Use of isothermal titration calorimetry to measure the thermodynamic parameters of complexation

Acyclic CB[*n*]-type receptors are known to bind tightly ($K_a > 10^6$ M^{-1}) to hydrophobic diammonium ions [42,65,71]. Accordingly, we elected to use isothermal titration calorimetry (ITC) to measure the binding between **C1** or **M1** with the panel of guests. A single ITC run is capable of delivering both the binding constant (K_a, M^{-1}) and the enthalpy of complexation (ΔH, kcal mol^{-1}). Direct ITC titrations are most appropriate for host·guest complexes with $K_a \leq 10^7$ M^{-1} where Wiseman c-values from 5–500 can be achieved by changing the concentration of host in the ITC cell [76-78]. Figure 7a presents the thermogram recorded when a solution of **C1** (100 μM) in phosphate-buffered saline (PBS) in the ITC cell was titrated with a solution of **CHDA** (1 mM) from the ITC injection syringe. The DP versus time data in Figure 6a was integrated and then plotted as ΔH versus molar ratio in Figure 7b. The ΔH versus molar ratio data was then fitted to the single-set-of-sites binding model in the PEAQ ITC data analysis software which delivered $K_a = (6.49 \pm 0.10) \times 10^5$ M^{-1} and $\Delta H = -7.82 \pm 0.02$ kcal mol^{-1} for the **C1**·**CHDA** complex (Table 1). All ITC experiments were performed in triplicate and the reported values represent the mean ± standard deviation. For stronger complexes, where the Wiseman c-value cannot be adjusted into the ideal range by reducing the host concentration in the ITC cell due to the insufficient heat evolved, competitive ITC titrations must be used. In competitive ITC titrations a solution of the host and an excess of a weak binding competitive guest in the ITC cell is titrated with a solution of the tighter binding guest from the ITC injection syringe [78]. The analysis of competitive titrations requires that the K_a and ΔH values for the host·competitor complexes have been previously determined and used as known inputs to the competitive binding model in the PEAQ data analysis software. To maximize the

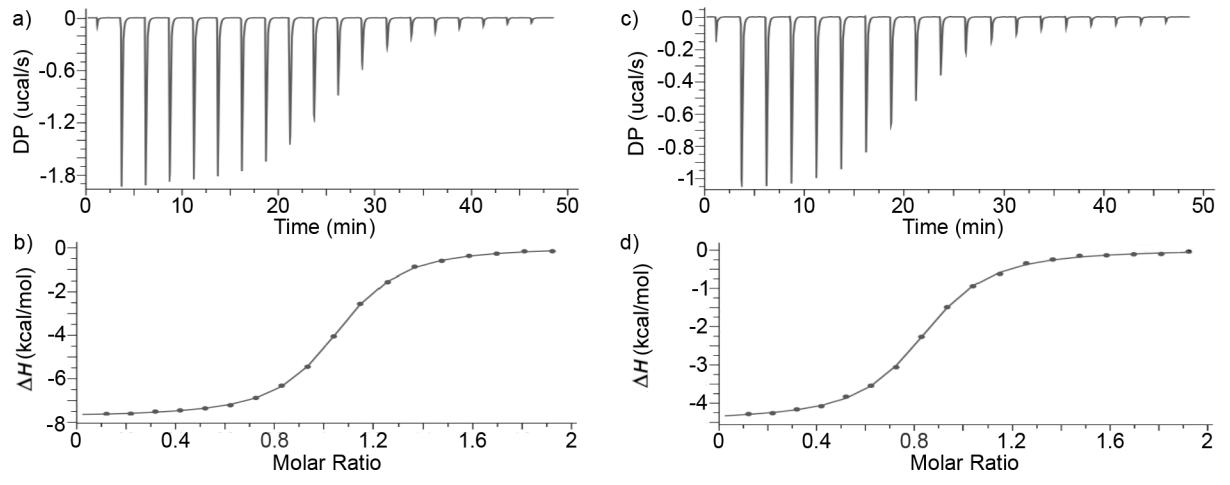

Figure 7: a) Representative plot of DP (μcal s^{-1}) versus time from the titration of **C1** (0.1 mM) in the ITC cell with a solution of **CHDA** (1.0 mM) from the ITC syringe. b) Plot of ΔH versus the **C1**:**CHDA** molar ratio. The solid line represents the best fit of the data to the single-set-of-sites binding model implemented in the PEAQ ITC data analysis software. The measurements were performed in triplicate and yielded $K_a = (6.49 \pm 0.10) \times 10^5$ M^{-1} and $\Delta H = -7.82 \pm 0.02$ kcal mol^{-1}. c) Representative plot of DP versus time from the competitive titration of **C1** (0.1 mM) and **CHDA** (0.8 mM) in the cell with a solution of **Me$_6$PXDA** (1.0 mM) from the syringe. d) Plot of ΔH versus the **C1**:**Me$_6$PXDA** molar ratio. The solid line represents the best fit of the data to the competitive binding model implemented in the PEAQ ITC data analysis software. The measurements were performed in triplicate and yielded $K_a = (2.47 \pm 0.06) \times 10^8$ M^{-1} and $\Delta H = -12.43 \pm 0.02$ kcal mol^{-1}.

Table 1: Thermodynamic parameters (K_a (M^{-1}), $\Delta H°$ (kcal/mol) determined for the **C1**·guest, **M1**·guest and **M0**·guest complexes by ITC. Conditions: 298.0 K, phosphate-buffered saline, pH 7.4.

Guest	**C1**		**M1**	
	K_a	$\Delta H°$	K_a (M^{-1})	$\Delta H°$
Me_6PDA	(3.40 ± 0.09) × 10^{7d}	−13.47 ± 0.03	(1.31 ± 0.05) × 10^{6a}	−5.98 ± 0.03
Me_6HDA	(6.54 ± 0.59) × 10^{7b}	−10.13 ± 0.02	(2.95 ± 0.12) × 10^{6a}	−5.27 ± 0.02
PXDA	(1.44 ± 0.03) × 10^{8c}	−10.07 ± 0.01	(3.42 ± 0.05) × 10^{7c}	−5.67 ± 0.01
Me_6PXDA	(2.47 ± 0.06) × 10^{8b}	−12.43 ± 0.02	(7.52 ± 0.18) × 10^{7b}	−8.64 ± 0.02
CHDA	(6.49 ± 0.10) × 10^{5a}	−7.82 ± 0.02	(2.79 ± 0.07) × 10^{5a}	−4.38 ± 0.02
Me_6CHDA	(1.75 ± 0.06) × 10^{6a}	−7.83 ± 0.03	(1.20 ± 0.04) × 10^{6a}	−7.44 ± 0.03
AdA	(2.41 ± 0.04) × 10^{6a}	−7.54 ± 0.03	(1.99 ± 0.06) × 10^{6a}	−4.11 ± 0.03
Me_3AdA	(2.31 ± 0.07) × 10^{6a}	−11.00 ± 0.04	(2.09 ± 0.07) × 10^{6a}	−7.42 ± 0.02

[a]Measured by direct ITC titration of host (100 μM) in the cell with guest (1 mM) in the syringe. [b]Measured by ITC competition assay using **CHDA** (0.8 mM) as competitor included in the cell. [c]Measured by ITC competition assay using **CHDA** (0.5 mM) as competitor included in the cell. [d]Measured by ITC competition assay using **CHDA** (0.1 mM) as competitor included in the cell.

heat evolved in the competitive ITC titrations, the host·competitor and host·tight guest complexes should have very different ΔH values. Figure 7c shows the competitive ITC titration of a mixture of **C1** (0.1 mM) and **CHDA** (0.8 mM) in the ITC cell with a solution of **Me_6PXDA** (1.0 mM) from the syringe. The DP versus time plot was integrated and a plot of ΔH versus molar ratio was created (Figure 7d) and fitted to the competitive binding model in the PEAQ ITC data analysis software to determine K_a = (2.47 ± 0.06) × 10^8 M^{-1} and ΔH = −12.43 ± 0.02 kcal mol^{-1} for the **C1**·**Me_6PXDA** complex. The K_a and ΔH values for the remaining **C1**·guest and **M1**·guest complexes were determined by analogous direct or competitive ITC titrations (Table 1 and Supporting Information File 1).

Comparison of the thermodynamic parameters for **C1**·guest and **M1**·guest complexation

Overall, **C1** is the more potent host with K_a values ranging from 2.41 × 10^5 (**AdA**) to 2.49 × 10^8 M^{-1} (**Me_6PXDA**) relative to **M1** whose K_a values range from 1.99 × 10^5 (**AdA**) to 7.52 × 10^7 M^{-1} (**Me_6PXDA**). Similarly, the enthalpic contributions to binding are more favorable for **C1** with ΔH values ranging from −7.54 (**AdA**) to −13.47 kcal mol^{-1} (**Me_6PDA**) than for **M1** with ΔH values ranging from −4.11 (**AdA**) to −8.64 kcal mol^{-1} (**Me_6PXDA**). The more favorable enthalpic contributions to binding is likely due to stronger electrostatic interactions between the guest and the sulfate ionic groups. For both **C1** and **M1**, the **Me_6HDA** and **Me_6PXDA** are the strongest binding guests whereas the cyclohexane and adamantane-based guests with a larger cross-sectional area bind 10–100-fold more weakly. The ratio of the binding constants of a common guest to **C1** versus **M1** is as follows: **Me_6PDA** (26.0), **Me_6HDA** (22.2), **PXDA** (4.2), **Me_6PXDA** (3.3), **CHDA** (2.3), **Me_6CHDA** (1.3), **AdA** (1.2), **Me_3AdA** (1.1). The **C1** host is both a tighter and more selective host for the narrower guests than **M1**. We can also tease out the effect of chain length by a comparison of **Me_6PDA** with **Me_6HDA**. We find that the longer and more hydrophobic **Me_6HDA** guest binds 1.92-fold stronger to **C1**; similarly, **Me_6HDA** binds 2.25-fold stronger to **M1**. These differences are likely due to the increased hydrophobicity of the additional CH_2 group. Finally, we can compare the binding of the primary ammonium versus the corresponding quaternary ammonium ion guest toward **C1** and separately **M1**. We find that **C1** binds the quaternary ammoniums somewhat stronger: **Me_6PXDA** vs **PXDA** (1.72-fold), **Me_6CHDA** vs **CHDA** (2.42-fold), **Me_3AdA** vs **AdA** (4.59-fold). A similar trend holds for **M1**: **Me_6PXDA** vs **PXDA** (2.20-fold), **Me_6CHDA** vs **CHDA** (4.30-fold), **Me_3AdA** vs **AdA** (10.50-fold).

Conclusion

In summary, we have designed, synthesized, and characterized a new acyclic CB[*n*]-type receptor **C1** that bears sulfate ionic groups and compared its properties with **M1** which features sulfonate ionic groups. We find that **C1** is much less soluble (4 mM) than **M1** (346 mM) in water. Host **C1** does not undergo self-association in PBS buffer according to ^{1}H NMR dilution experiments. Analysis of complexation-induced changes in chemical shifts establish that the hydrophobic regions of the guests bind within the anisotropic shielding cavity of **C1** whereas the ionic groups reside closer to the ureidyl carbonyl portals of **C1**. Direct and competitive ITC titrations were used to measure the thermodynamic parameters of binding for **C1**·guest and **M1**·guest complexes in PBS solution. Overall, we find that **C1** – with its sulfate ionic groups – binds tighter than **M1** toward each member of the guest panel with largest differences observed for the narrowest **Me_6PDA** (26-fold) and **Me_6HDA** (22.2-fold) guests. Similarly, we find that **C1** binds the quater-

nary ammonium stronger than the corresponding primary ammonium ion guest by 1.72 to 9.59-fold. In conclusion, we find that **C1** displays somewhat enhanced molecular recognition properties than **M1** but possesses less desirable aqueous solubility properties.

Experimental

General experimental details

All chemicals were purchased from commercial suppliers and were used without further purification. Guest molecules were available from previous studies [65,71]. Compounds **TetW1$_{OAc}$** and **TetW1** were prepared according to the literature procedures with slight modifications [70]. NMR spectra were recorded using commercial spectrometers operating at 600 or 400 MHz for ^{1}H and 150 or 100 MHz for ^{13}C. Melting points were measured on a Meltemp apparatus in open capillary tubes and are uncorrected. IR spectra were measured on a Thermo Nicolet NEXUS 670 FT/IR spectrometer by attenuated total reflectance (ATR) and are reported in cm^{-1}. Mass spectrometry was performed using a JEOL AccuTOF electrospray instrument. ITC data was collected on a Malvern Microcal PEAQ-ITC instrument with a cell volume of 200 µL and an injection syringe with a capacity of 40 µL. For ITC experiments, the host and guest solutions were prepared in a 20 mM phosphate-buffered water (pH 7.4). The sample cell was filled (200 µL) with the host solution and the guest solution was titrated (first injection = 0.4 µL, subsequent 18 injections = 2 µL) into the cell. All ITC experiments were analyzed using the MicroCal PEAQ-ITC data analysis software.

Compound **C1**

A mixture of **TetW1** (0.430 g, 0.376 mmol) and pyridine sulfur trioxide (1.1838 g, 7.437 mmol) was dissolved in dry pyridine (57 mL). The resulting mixture was heated at 90 °C under N_2 for 18 h and then cooled to rt. The precipitate was collected by first decanting some of the solvent and then the remaining mixture was transferred to a 50 mL centrifuge tube and centrifuged (7200 rpm, 5 min). The supernatant was carefully poured off. Next, the crude solid was dissolved in 1 M NaOH (25 mL) which results in a yellow and then red solution. Afterwards, EtOH (144 mL) was added which gave a white precipitate that was collected by centrifugation (7200 rpm, 10 min). The crude solid was analyzed by ^{1}H NMR which showed residual pyridine. The crude solid was subsequently dissolved in water (150 mL) and re-precipitated by the addition of EtOH (144 mL) followed by centrifugation (7200 rpm, 5 min) to obtain a white solid. The solid was dried overnight under high vacuum to yield **C1** as a white solid (0.3444 g, 68% yield). Mp > 300 °C; IR (ATR, cm^{-1}): 3456 (w), 1720 (m), 1472 (m), 1378 (w), 1226 (m), 1101 (s), 1023 (m), 972 (w), 790 (w); ^{1}H NMR (400 MHz, D_2O) 6.71 (s, 4H), 5.67 (d, J = 15.4 Hz, 2H), 5.57 (d, J = 15.8 Hz, 4H), 5.46 (d, J = 8.9 Hz, 2H), 5.42 (d, J = 8.9 Hz, 2H), 5.41 (d, J = 16.3 Hz, 4H), 4.45–4.40 (m, 4H), 4.35–4.30 (m, 4H), 4.27 (d, J = 15.8 Hz, 2 × 4H), 4.25–4.18 (m, 4H), 4.18–4.13 (m, 4H), 4.12 (d, J = 15.4 Hz, 2H), 1.78 (s, 6H), 1.75 (s, 6H); ^{13}C NMR (100 MHz, D_2O/acetone-d_6 6:1 (v:v)) 156.7, 155.9, 150.5, 129.3, 116.1, 78.6, 77.4, 71.2, 69.5, 67.4, 52.5, 48.4, 35.0, 16.3, 15.4 ppm; ESIMS (m/z): 751.13 ([M − 2Na]$^{2-}$), calcd for $[C_{50}H_{56}N_{16}Na_2S_4O_{28}]^{2-}$, 751.1064.

Supporting Information

The X-ray crystal structure of **C1** is deposited with the Cambridge Crystallographic Data Centre (CCDC 2411723).

Supporting Information File 1

Synthesis and characterization of compounds, solubility determination, ^{1}H NMR dilution experiments, ^{1}H NMR and ITC binding studies.
[https://www.beilstein-journals.org/bjoc/content/supplementary/1860-5397-21-55-S1.pdf]

Funding

We thank the National Science Foundation (CHE-1807486) for past financial support. We thank the National Institute of General Medical Sciences of the National Institutes of Health (R35GM153362) for current financial support of this project.

Conflict of Interest

L.I. is co-founder and holds equity in Reversal Therapeutics (National Harbor, Maryland). L.I. holds equity in Clear Scientific (Cambridge, Massachusetts). The other authors declare no competing financial interests.

Author Contributions

Christian Akakpo: investigation; writing – original draft. Peter Y. Zavalij: investigation. Lyle Isaacs: conceptualization; funding acquisition; project administration; resources; supervision; visualization; writing – original draft; writing – review & editing.

ORCID® iDs

Christian Akakpo - https://orcid.org/0000-0002-3870-974X
Peter Y. Zavalij - https://orcid.org/0000-0001-5762-3469
Lyle Isaacs - https://orcid.org/0000-0002-4079-332X

Data Availability Statement

Data generated and analyzed during this study is openly available in Digital Repository at the University of Maryland (UMD DRUM) at https://doi.org/10.13016/4gal-sini.

References

1. Pedersen, C. J. *Angew. Chem., Int. Ed. Engl.* **1988,** *27,* 1021–1027. doi:10.1002/anie.198810211
2. Cram, D. J. *Angew. Chem., Int. Ed. Engl.* **1988,** *27,* 1009–1020. doi:10.1002/anie.198810093
3. Lehn, J.-M. *Angew. Chem., Int. Ed. Engl.* **1988,** *27,* 89–112. doi:10.1002/anie.198800891
4. Anslyn, E. V. *J. Org. Chem.* **2007,** *72,* 687–699. doi:10.1021/jo0617971
5. Kolesnichenko, I. V.; Anslyn, E. V. *Chem. Soc. Rev.* **2017,** *46,* 2385–2390. doi:10.1039/c7cs00078b
6. Aida, T.; Meijer, E. W.; Stupp, S. I. *Science* **2012,** *335,* 813–817. doi:10.1126/science.1205962
7. Stoddart, J. F. *Angew. Chem., Int. Ed.* **2017,** *56,* 11094–11125. doi:10.1002/anie.201703216
8. Borsley, S.; Leigh, D. A.; Roberts, B. M. W. *Angew. Chem., Int. Ed.* **2024,** *63,* e202400495. doi:10.1002/anie.202400495
9. Feringa, B. L. *Angew. Chem., Int. Ed.* **2017,** *56,* 11060–11078. doi:10.1002/anie.201702979
10. Rekharsky, M. V.; Inoue, Y. *Chem. Rev.* **1998,** *98,* 1875–1918. doi:10.1021/cr970015o
11. Gutsche, C. D. *Acc. Chem. Res.* **1983,** *16,* 161–170. doi:10.1021/ar00089a003
12. Dale, E. J.; Vermeulen, N. A.; Juríček, M.; Barnes, J. C.; Young, R. M.; Wasielewski, M. R.; Stoddart, J. F. *Acc. Chem. Res.* **2016,** *49,* 262–273. doi:10.1021/acs.accounts.5b00495
13. Jordan, J. H.; Gibb, B. C. *Chem. Soc. Rev.* **2015,** *44,* 547–585. doi:10.1039/c4cs00191e
14. Diederich, F. *Angew. Chem., Int. Ed. Engl.* **1988,** *27,* 362–386. doi:10.1002/anie.198803621
15. Rebek, J., Jr. *Acc. Chem. Res.* **2009,** *42,* 1660–1668. doi:10.1021/ar9001203
16. Ogoshi, T.; Yamagishi, T.-a.; Nakamoto, Y. *Chem. Rev.* **2016,** *116,* 7937–8002. doi:10.1021/acs.chemrev.5b00765
17. Xue, M.; Yang, Y.; Chi, X.; Zhang, Z.; Huang, F. *Acc. Chem. Res.* **2012,** *45,* 1294–1308. doi:10.1021/ar2003418
18. Wu, J.-R.; Yang, Y.-W. *Chem. Commun.* **2019,** *55,* 1533–1543. doi:10.1039/c8cc09374a
19. Harris, K.; Fujita, D.; Fujita, M. *Chem. Commun.* **2013,** *49,* 6703–6712. doi:10.1039/c3cc43191f
20. Zarra, S.; Wood, D. M.; Roberts, D. A.; Nitschke, J. R. *Chem. Soc. Rev.* **2015,** *44,* 419–432. doi:10.1039/c4cs00165f
21. Febreze.com “Ingredients”. https://www.febreze.com/en-us/ingredients-safety/our-ingredients (accessed March 27, 2025).
22. Meadows, M. K.; Anslyn, E. V. Three Tales of Supramolecular Analytical Chemistry. In *Macrocyclic and Supramolecular Chemistry: How Izatt–Christensen Award Winners Shaped the Field;* Izatt, R. M., Ed.; John Wiley & Sons: Chichester, UK, 2016; pp 92–126. doi:10.1002/9781119053859.ch5
23. Rajewski, R. A.; Stella, V. J. *J. Pharm. Sci.* **1996,** *85,* 1142–1169. doi:10.1021/js960075u
24. Stella, V. J.; Rajewski, R. A. *Pharm. Res.* **1997,** *14,* 556–567. doi:10.1023/a:1012136608249
25. Davis, A. P. *Chem. Soc. Rev.* **2020,** *49,* 2531–2545. doi:10.1039/c9cs00391f
26. Tromans, R. A.; Samanta, S. K.; Chapman, A. M.; Davis, A. P. *Chem. Sci.* **2020,** *11,* 3223–3227. doi:10.1039/c9sc05406e
27. Isaacs, L. *Acc. Chem. Res.* **2014,** *47,* 2052–2062. doi:10.1021/ar500075g
28. Sindelar, V.; Silvi, S.; Kaifer, A. E. *Chem. Commun.* **2006,** 2185–2187. doi:10.1039/b601959e
29. Ko, Y. H.; Kim, E.; Hwang, I.; Kim, K. *Chem. Commun.* **2007,** 1305–1315. doi:10.1039/b615103e
30. del Barrio, J.; Ryan, S. T. J.; Jambrina, P. G.; Rosta, E.; Scherman, O. A. *J. Am. Chem. Soc.* **2016,** *138,* 5745–5748. doi:10.1021/jacs.5b11642
31. Zhang, G.; Emwas, A.-H.; Shahul Hameed, U. F.; Arold, S. T.; Yang, P.; Chen, A.; Xiang, J.-F.; Khashab, N. M. *Chem* **2020,** *6,* 1082–1096. doi:10.1016/j.chempr.2020.03.003
32. Zhang, G.; Lin, W.; Huang, F.; Sessler, J.; Khashab, N. M. *J. Am. Chem. Soc.* **2023,** *145,* 19143–19163. doi:10.1021/jacs.3c06175
33. Ghale, G.; Nau, W. M. *Acc. Chem. Res.* **2014,** *47,* 2150–2159. doi:10.1021/ar500116d
34. Sinn, S.; Biedermann, F. *Isr. J. Chem.* **2018,** *58,* 357–412. doi:10.1002/ijch.201700118
35. Sun, C.; Zhang, H.; Li, S.; Zhang, X.; Cheng, Q.; Ding, Y.; Wang, L.-H.; Wang, R. *ACS Appl. Mater. Interfaces* **2018,** *10,* 25090–25098. doi:10.1021/acsami.8b06598
36. Zou, L.; Braegelman, A. S.; Webber, M. J. *ACS Cent. Sci.* **2019,** *5,* 1035–1043. doi:10.1021/acscentsci.9b00195
37. Walker, S.; Oun, R.; McInnes, F. J.; Wheate, N. J. *Isr. J. Chem.* **2011,** *51,* 616–624. doi:10.1002/ijch.201100033
38. Gu, A.; Wheate, N. J. *J. Inclusion Phenom. Macrocyclic Chem.* **2021,** *100,* 55–69. doi:10.1007/s10847-021-01055-9
39. Sasmal, R.; Das Saha, N.; Pahwa, M.; Rao, S.; Joshi, D.; Inamdar, M. S.; Sheeba, V.; Agasti, S. S. *Anal. Chem. (Washington, DC, U. S.)* **2018,** *90,* 11305–11314. doi:10.1021/acs.analchem.8b01851
40. Sasmal, R.; Som, A.; Kumari, P.; Nair, R. V.; Show, S.; Barge, N. S.; Pahwa, M.; Das Saha, N.; Rao, S.; Vasu, S.; Agarwal, R.; Agasti, S. S. *ACS Cent. Sci.* **2024,** *10,* 1945–1959. doi:10.1021/acscentsci.4c01080
41. Aqdot Limited Home Page, “Odour & VOC Elimination Technology”. https://aqdot.com/our-technology/ (accessed March 27, 2025).
42. Ganapati, S.; Isaacs, L. *Isr. J. Chem.* **2018,** *58,* 250–263. doi:10.1002/ijch.201700098
43. Bauer, D.; Andrae, B.; Gaß, P.; Trenz, D.; Becker, S.; Kubik, S. *Org. Chem. Front.* **2019,** *6,* 1555–1560. doi:10.1039/c9qo00156e
44. Jiang, S.; Lan, S.; Mao, D.; Yang, X.; Shi, K.; Ma, D. *Chem. Commun.* **2018,** *54,* 9486–9489. doi:10.1039/c8cc05552a
45. Wu, Y.; Yang, J.; Zhuang, S.-Y.; Yu, S.-B.; Zong, Y.; Liu, Y.-Y.; Wu, G.; Qi, Q.-Y.; Wang, H.; Tian, J.; Zhou, W.; Ma, D.; Zhang, D.-W.; Li, Z.-T. *J. Med. Chem.* **2024,** *67,* 2176–2187. doi:10.1021/acs.jmedchem.3c02110
46. Zhang, S.; Zhou, C.; Gao, C.; Yang, J.; Liao, X.; Yang, B. *J. Mol. Liq.* **2023,** *390,* 122942. doi:10.1016/j.molliq.2023.122942
47. Zhu, P.; Kong, L.; Zhang, Y.; Liu, Q.; Liao, X.; Song, Y.; Yang, B. *J. Mol. Liq.* **2023,** *372,* 121198. doi:10.1016/j.molliq.2023.121198
48. Peng, W.-C.; Lei, Z.; Lin, Q.-H.; Wu, Y.; Yang, J.-Y.; Wang, H.; Zhou, W.; Zhang, D.-W.; Li, Z.-T.; Ma, D. *ChemPlusChem* **2023,** *88,* e202300465. doi:10.1002/cplu.202300465
49. Feng, K.; Liu, Y.-Y.; Zong, Y.; Lei, Z.; Wu, Y.; Yang, J.; Lin, F.; Qi, Q.-Y.; Li, Q.; Zhuang, S.-Y.; Zhang, J.; Tian, J.; Zhou, W.; Ma, D.; Zhang, D.-W.; Li, Z.-T.; Yu, S.-B. *J. Med. Chem.* **2024,** *67,* 17905–17918. doi:10.1021/acs.jmedchem.4c01960
50. Huo, M.; Song, S.-Q.; Dai, X.-Y.; Li, F.-F.; Hu, Y.-Y.; Liu, Y. *Chem. Sci.* **2024,** *15,* 5163–5173. doi:10.1039/d4sc00160e
51. Stancl, M.; Hodan, M.; Sindelar, V. *Org. Lett.* **2009,** *11,* 4184–4187. doi:10.1021/ol9017886

52. Gilberg, L.; Zhang, B.; Zavalij, P. Y.; Sindelar, V.; Isaacs, L. *Org. Biomol. Chem.* **2015,** *13,* 4041–4050. doi:10.1039/c5ob00184f
53. Ma, D.; Hettiarachchi, G.; Nguyen, D.; Zhang, B.; Wittenberg, J. B.; Zavalij, P. Y.; Briken, V.; Isaacs, L. *Nat. Chem.* **2012,** *4,* 503–510. doi:10.1038/nchem.1326
54. Ma, D.; Zhang, B.; Hoffmann, U.; Sundrup, M. G.; Eikermann, M.; Isaacs, L. *Angew. Chem., Int. Ed.* **2012,** *51,* 11358–11362. doi:10.1002/anie.201206031
55. Hoffmann, U.; Grosse-Sundrup, M.; Eikermann-Haerter, K.; Zaremba, S.; Ayata, C.; Zhang, B.; Ma, D.; Isaacs, L.; Eikermann, M. *Anesthesiology* **2013,** *119,* 317–325. doi:10.1097/aln.0b013e3182910213
56. Haerter, F.; Simons, J. C. P.; Foerster, U.; Moreno Duarte, I.; Diaz-Gil, D.; Ganapati, S.; Eikermann-Haerter, K.; Ayata, C.; Zhang, B.; Blobner, M.; Isaacs, L.; Eikermann, M. *Anesthesiology* **2015,** *123,* 1337–1349. doi:10.1097/aln.0000000000000868
57. Diaz-Gil, D.; Haerter, F.; Falcinelli, S.; Ganapati, S.; Hettiarachchi, G. K.; Simons, J. C. P.; Zhang, B.; Grabitz, S. D.; Moreno Duarte, I.; Cotten, J. F.; Eikermann-Haerter, K.; Deng, H.; Chamberlin, N. L.; Isaacs, L.; Briken, V.; Eikermann, M. *Anesthesiology* **2016,** *125,* 333–345. doi:10.1097/aln.0000000000001199
58. Ganapati, S.; Grabitz, S. D.; Murkli, S.; Scheffenbichler, F.; Rudolph, M. I.; Zavalij, P. Y.; Eikermann, M.; Isaacs, L. *ChemBioChem* **2017,** *18,* 1583–1588. doi:10.1002/cbic.201700289
59. Thevathasan, T.; Grabitz, S. D.; Santer, P.; Rostin, P.; Akeju, O.; Boghosian, J. D.; Gill, M.; Isaacs, L.; Cotten, J. F.; Eikermann, M. *Br. J. Anaesth.* **2020,** *125,* e140–e147. doi:10.1016/j.bja.2020.02.019
60. Brockett, A. T.; Deng, C.; Shuster, M.; Perera, S.; DiMaggio, D.; Cheng, M.; Murkli, S.; Briken, V.; Roesch, M. R.; Isaacs, L. *Chem. – Eur. J.* **2021,** *27,* 17476–17486. doi:10.1002/chem.202102919
61. Mao, D.; Liang, Y.; Liu, Y.; Zhou, X.; Ma, J.; Jiang, B.; Liu, J.; Ma, D. *Angew. Chem., Int. Ed.* **2017,** *56,* 12614–12618. doi:10.1002/anie.201707164
62. Liu, W.; Lu, X.; Meng, Z.; Isaacs, L. *Org. Biomol. Chem.* **2018,** *16,* 6499–6506. doi:10.1039/c8ob01575a
63. Lu, X.; Samanta, S. K.; Zavalij, P. Y.; Isaacs, L. *Angew. Chem., Int. Ed.* **2018,** *57,* 8073–8078. doi:10.1002/anie.201803132
64. Zhang, B.; Isaacs, L. *J. Med. Chem.* **2014,** *57,* 9554–9563. doi:10.1021/jm501276u
65. Murkli, S.; Klemm, J.; King, D.; Zavalij, P. Y.; Isaacs, L. *Chem. – Eur. J.* **2020,** *26,* 15249–15258. doi:10.1002/chem.202002874
66. DiMaggio, D.; Brockett, A. T.; Shuster, M.; Murkli, S.; Zhai, C.; King, D.; O'Dowd, B.; Cheng, M.; Brady, K.; Briken, V.; Roesch, M. R.; Isaacs, L. *ChemMedChem* **2022,** *17,* e202200046. doi:10.1002/cmdc.202200046
67. Brady, K. G.; Gilberg, L.; Sigwalt, D.; Bistany-Riebman, J.; Murkli, S.; Klemm, J.; Kulhánek, P.; Šindelář, V.; Isaacs, L. *Supramol. Chem.* **2020,** *32,* 479–494. doi:10.1080/10610278.2020.1795173
68. Sigwalt, D.; Moncelet, D.; Falcinelli, S.; Mandadapu, V.; Zavalij, P. Y.; Day, A.; Briken, V.; Isaacs, L. *ChemMedChem* **2016,** *11,* 980–989. doi:10.1002/cmdc.201600090
69. Lu, X.; Zebaze Ndendjio, S. A.; Zavalij, P. Y.; Isaacs, L. *Org. Lett.* **2020,** *22,* 4833–4837. doi:10.1021/acs.orglett.0c01637
70. Zhang, B.; Zavalij, P. Y.; Isaacs, L. *Org. Biomol. Chem.* **2014,** *12,* 2413–2422. doi:10.1039/c3ob42603c
71. Xue, W.; Zavalij, P. Y.; Isaacs, L. *Org. Biomol. Chem.* **2019,** *17,* 5561–5569. doi:10.1039/c9ob00906j
72. Barrow, S. J.; Kasera, S.; Rowland, M. J.; del Barrio, J.; Scherman, O. A. *Chem. Rev.* **2015,** *115,* 12320–12406. doi:10.1021/acs.chemrev.5b00341
73. Masson, E.; Ling, X.; Joseph, R.; Kyeremeh-Mensah, L.; Lu, X. *RSC Adv.* **2012,** *2,* 1213–1247. doi:10.1039/c1ra00768h
74. Cao, L.; Šekutor, M.; Zavalij, P. Y.; Mlinarić-Majerski, K.; Glaser, R.; Isaacs, L. *Angew. Chem., Int. Ed.* **2014,** *53,* 988–993. doi:10.1002/anie.201309635
75. Mock, W. L.; Shih, N.-Y. *J. Org. Chem.* **1986,** *51,* 4440–4446. doi:10.1021/jo00373a018
76. Wiseman, T.; Williston, S.; Brandts, J. F.; Lin, L.-N. *Anal. Biochem.* **1989,** *179,* 131–137. doi:10.1016/0003-2697(89)90213-3
77. Broecker, J.; Vargas, C.; Keller, S. *Anal. Biochem.* **2011,** *418,* 307–309. doi:10.1016/j.ab.2011.07.027
78. Velazquez-Campoy, A.; Freire, E. *Nat. Protoc.* **2006,** *1,* 186–191. doi:10.1038/nprot.2006.28

License and Terms

BEILSTEIN JOURNAL OF ORGANIC CHEMISTRY

Dicarboxylate recognition based on ultracycle hosts through cooperative hydrogen bonding and anion–π interactions

Wen-Hui Mi[‡1,2], Teng-Yu Huang[‡1], Xu-Dong Wang[1], Yu-Fei Ao[1,2], Qi-Qiang Wang[*1,2] and De-Xian Wang[*1,2]

Letter

Open Access

Address:
[1]Beijing National Laboratory for Molecular Sciences, CAS Key Laboratory of Molecular Recognition and Function, Institute of Chemistry, Chinese Academy of Sciences, Beijing 100190, China and [2]University of Chinese Academy of Sciences, Beijing 100049, China

Email:
Qi-Qiang Wang[*] - qiqiangw@iccas.ac.cn; De-Xian Wang[*] - dxwang@iccas.ac.cn

* Corresponding author ‡ Equal contributors

Keywords:
anion–π interactions; anion recognition; hydrogen bonding; dicarboxylates; ultracycles

Beilstein J. Org. Chem. **2025,** *21,* 884–889.
https://doi.org/10.3762/bjoc.21.72

Received: 03 March 2025
Accepted: 24 April 2025
Published: 06 May 2025

This article is part of the thematic issue "Novel macrocycles: from synthesis to supramolecular function".

Guest Editor: C. Gaeta

Abstract

The efficient binding of dicarboxylates represents an important yet challenging issue in supramolecular chemistry. In this study, we designed functional ultracycles as hosts to accommodate large organic dicarboxylate anions. These ultracycles were synthesized via a one-pot strategy starting from macrocyclic precursors. Host–dicarboxylate binding was investigated using ^{1}H NMR titrations, revealing that **B4aH** exhibits strong binding affinities toward a series of dicarboxylates, with association constants reaching up to 6896 M^{-1}. The selectivity for heptanedioate (**C7**$^{2-}$) was attributed to cooperative hydrogen bonding, anion–π interactions, and a size-matching effect, as supported by DFT optimizations.

Introduction

Macrocycles containing more than 50 atoms in the macrocyclic skeleton are denoted as ultracycles [1]. These very large macrocycles are prevalent in nature and exhibit unique functions. For instance, the archaeal lipid GDGT-0 enables archaea to thrive in extreme environments [2]; cycloamyloses enhance the stability of drug metabolism [3,4]; cyclic peptides play critical roles in plant or bacterial defenses and as well as animal hormone signaling [5,6]; cyclic proteins exhibit diverse therapeutic functions [7]; and cyclic nucleotides are essential for molecular cloning and hold potential for disease treatment [8]. In contrast, synthetic ultracycles remain relatively unexplored due to the significant synthetic challenges [9-19]. Among these, very large macrocycles constructed from smaller macrocyclic building units are particularly underexplored. Such macrocycle-containing ultracycles are anticipated to exhibit high association efficiency and selectivity for large guests, driven by cooperative effects of their convergent macrocyclic elements.

Dicarboxylates are crucial species in biological system and chemistry [20]. Examples such as malonate, succinate, and

glutarate play key roles in cellular metabolism; they regulate the activity of numerous enzyme receptors, and serve as intermediates in the synthesis of more complex biomolecules [21]. However, excessive consumption or production, as well as insufficient clearance of dicarboxylates, can lead to various health problems [22]. Additionally, dicarboxylates like tartrate, adipate or citrate are widely used as food additives [23,24]. Furthermore, functional materials based on dicarboxylates are expected to play a significant role in future technologies [25]. Therefore, the recognition and detection of dicarboxylates are of great importance. Despite the development of a number of receptors for dicarboxylates [21,26,27], their recognition remains a challenging task due to their strong hydrophilicity (−400 kJ/mol) [28,29], dispersed negative charges at both ends, complex shapes, and flexible conformations. Moreover, the similar carbon skeletons of many dicarboxylates make selective recognition particularly difficult. To address these challenges, we envisioned that ultracycles composed of macrocycles with anion-binding capabilities could serve as suitable hosts for efficient and selective dicarboxylate recognition. In this study, we report the design of ultracycles constructed from functional tetraoxacalix[2]arene[2]triazine submacrocycles. These submacrocycles feature hydroxy groups as hydrogen-bonding (HB) donors on the lower rim, which, in combination with electron-deficient triazines, create cooperative HB and anion–π binding sites to enhance anion binding [30]. The recognition capabilities of these ultracycles toward a range of dicarboxylates were successfully demonstrated.

Results and Discussion

Synthesis and structure

The ultracycles **B4aH**, **B5aH**, and **B6aH** were synthesized following the previously reported procedure [29,31]. A one-pot reaction of submacrocycle **1a** and 2-(benzyloxy)benzene-1,3-diol (**2a**) in the presence of 8.0 equivalents of CsF yielded the ultracycle precursor compounds. Three reorganized products **B4a**, **B5a**, and **B6a** with different ring sizes were isolated. As previously observed, the structural reorganization likely involves the cleavage and re-formation of the dynamic $C_{triazine}$–OAr bonds, and the presence of an excess of base could facilitate the formation of the thermodynamic-favored reorganized products [29,31]. The benzyl groups were subsequently removed under Pd/C and H_2 conditions to afford the target ultracyclic hosts. The synthesized ultracycles were fully characterized by spectrometric and elemental analysis (Scheme 1 and Schemes S1–S3 in Supporting Information File 1).

Single crystals of **B4aH** were obtained by slow vapor diffusion of ethyl ether into an acetonitrile/chloroform 1:1 (v/v) solution of the compound at 4 °C, enabling structural analysis of the ultracycle. As illustrated in Figure 1, the backbone of **B4aH** adopts a Z-like shape with a flexible conformation. The two oxacalix[2]arene[2]triazine subcavities are positioned along the short axis in a staggered face-to-face arrangement, while the glycol chains are oriented along the long axis in the opposite orientations. In packing mode, the submacrocycle units form close contacts through intermolecular hydrogen bonding, C–H···π, and lone pair–π interactions, resulting in a 1D linear assembly.

Anion recognition

With the functional ultracycles in hand, we investigated the binding between the [2 + 2] ultracycle **B4aH**, which contains two electron-deficient cavities, and a series of dicarboxylate anions (**C2**$^{2-}$–**C8**$^{2-}$ as tetrabutylammonium salts) by ^{1}H NMR titration experiments (Figure 2). Taking **C6**$^{2-}$ as an example, when it was added dropwise to a solution of **B4aH**, the aromatic proton H^a exhibited continuous upfield shifts, while H^b initially shifted upfield and then downfield upon the addition of 1.5 equiv of **C6**$^{2-}$ (Figure 2b and Figure S8 in Supporting Information File 1). These chemical shift changes indicate the interaction between the carboxylate heads and the submacrocycles. Additionally, the protons H^d and H^e on the glycol chain showed initial downfield shifts followed by upfield shifts. These discontinuous chemical shift movements suggest the host–dicarboxylate interactions and the simultaneous conformational changes in the host upon guest inclusion. Similar chemical shift changes of **B4aH** were observed for other dicarboxylates, indicating a consistent binding mode across the series (Figure 2b and c and Figures S4–S10 in Supporting Information File 1).

The titration curves (H^a) were analyzed using the Bindfit program [32-34] to determine the binding constants of **B4aH** with guests. A 1:1 binding stoichiometry best fit the titration curves for **C5**$^{2-}$–**C8**$^{2-}$, with binding constants following the order of **C7**$^{2-}$ > **C8**$^{2-}$ ≈ **C6**$^{2-}$ > **C5**$^{2-}$, suggesting a dependence on the length of the dicarboxylates (Figure 2c and d). We proposed that the dicarboxylates interact with each subcavity of **B4aH** through their terminal anionic groups, utilizing cooperative hydrogen bonding and anion–π interactions. The optimal size matching between dicarboxylate and the host cavity, as seen with **C7**$^{2-}$, enhances the synergistic effect between the two subcavities, resulting in a higher binding strength. Dicarboxylates longer or shorter than **C7**$^{2-}$ (e.g., **C8**$^{2-}$, **C6**$^{2-}$, or **C5**$^{2-}$) exhibit weaker binding due to their less-matched host–guest sizes. For the shorter dicarboxylates (**C2**$^{2-}$–**C4**$^{2-}$), the binding behavior is more complex. For instance, the [**B4aH**·**C2**$^{2-}$] complex fits a 1:2 binding model, with two-step binding constants of K_{11} = 259 M^{-1} and K_{12} = 251 M^{-1}, implying that **B4aH** can accommodate two **C2**$^{2-}$ anions as a dimer within its cavity [29]. Malonate (**C3**$^{2-}$) and succinate (**C4**$^{2-}$) exhibited irregular titra-

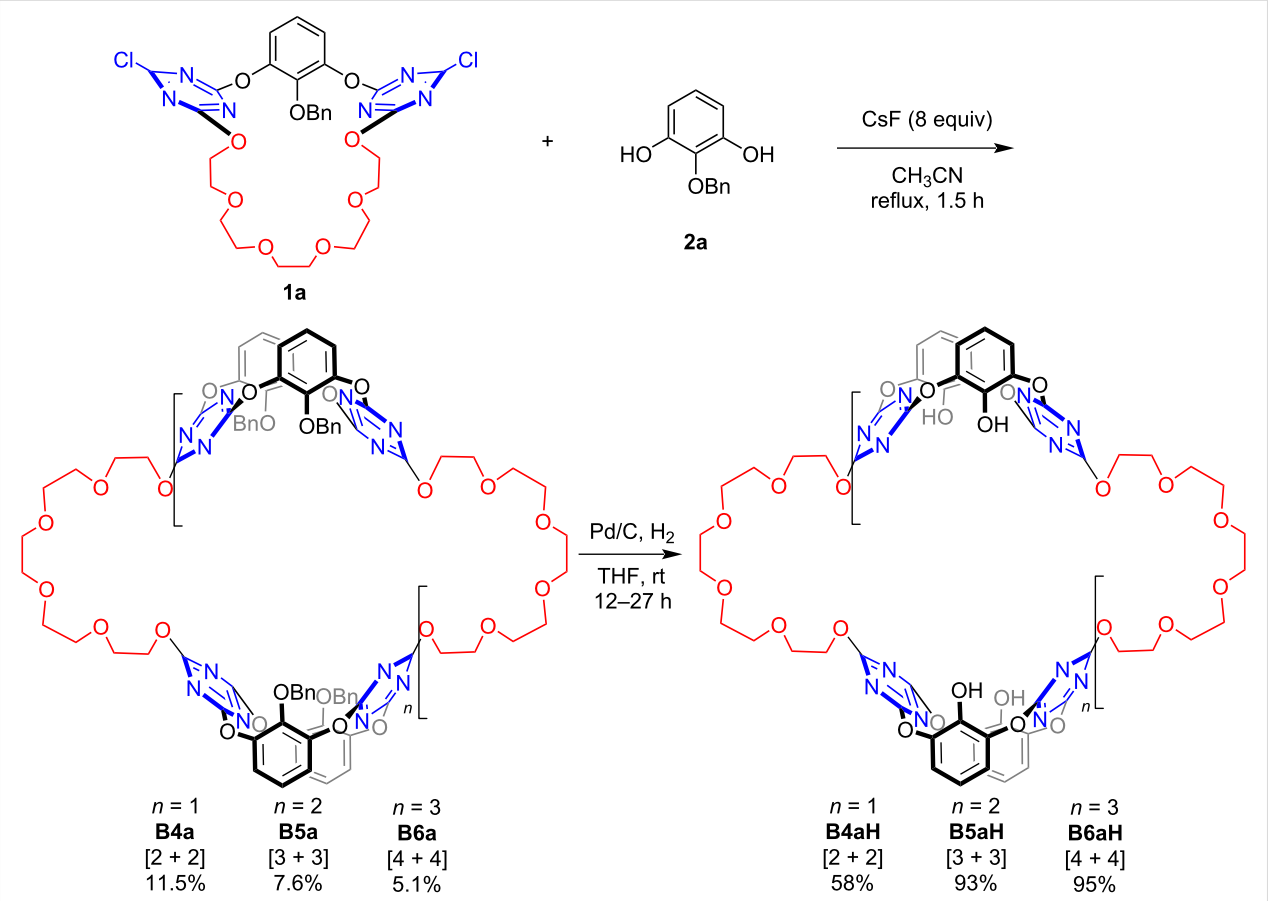

Scheme 1: Synthesis of ultracycles.

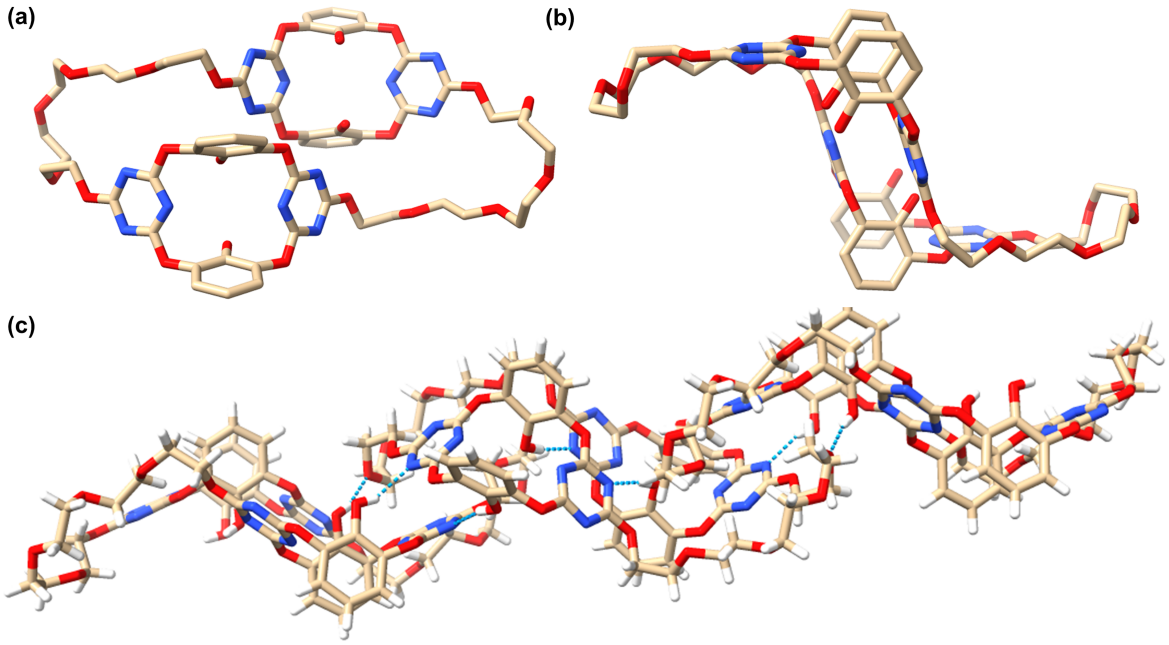

Figure 1: (a, b) Crystal structure of **B4aH** (hydrogen atoms are omitted for clarity), and (c) the stacking structure of the crystal of **B4aH** (the blue dotted lines represent hydrogen bonds).

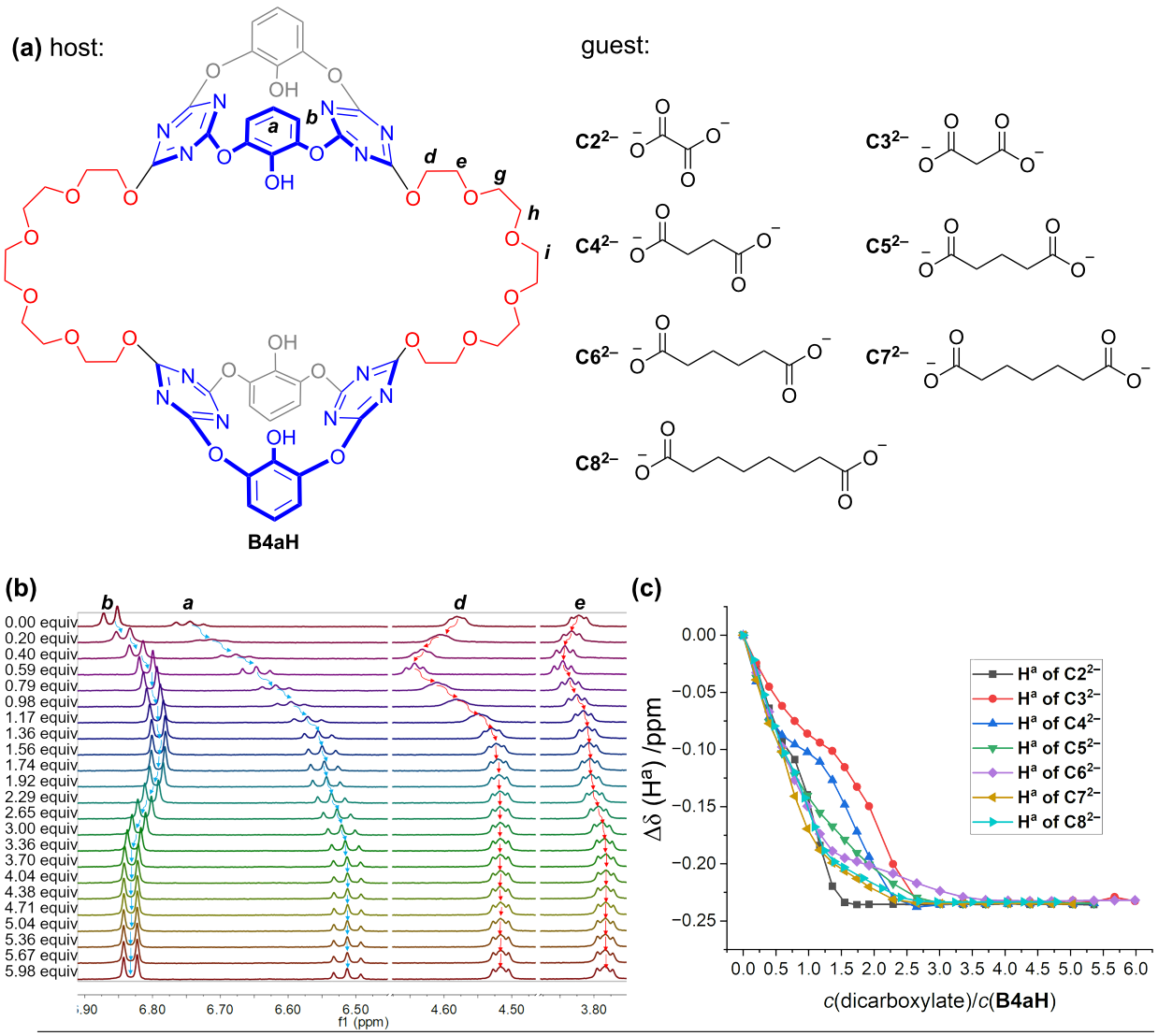

(d)

Guest	$C2^{2-}$	[a]$C3^{2-}$	[a]$C4^{2-}$	$C5^{2-}$	$C6^{2-}$	$C7^{2-}$	$C8^{2-}$
K_{11} (M^{-1})	259	–	–	2853	4455	6896	4423
K_{12} (M^{-1})	251						

[a] no reliable constants were obtained

Figure 2: (a) The structures of host and guests, (b) ^{1}H NMR spectra (298 K, 400 MHz, CD_3CN) of **B4aH** upon titration with $\mathbf{C6^{2-}}$ (*c*(**B4aH**) = 1 mM), (c) chemical shift changes of H^a versus titration equivalents *c*(dicarboxylate)/*c*(**B4aH**), and (d) association constants of host and guests.

tion curves (Figure 2c), and no reliable binding constants could be obtained using either 1:1 or 1:2 binding models. This is likely due to their intermediate size of chain lengths, which are neither long enough for 1:1 binding nor capable of squeezing a dimer for 1:2 complexation. Notably, the unsubstituted ultracycle **B4** [31] without the pendant OH groups on the lower rim, which relies on solely anion–π interactions, showed weak binding affinity for $\mathbf{C6^{2-}}$ (Figure S11 in Supporting Information File 1). This underscores the importance of cooperative hydrogen bonding and anion–π interactions for the efficient dicarboxylate binding.

To visualize the proposed synergistic hydrogen bonding and anion–π interactions between the host and guest, we carried out geometry optimizations using M06-2X at the 6-31G(d) level of theory, taking the [$\mathbf{B4aH{\cdot}C7^{2-}}$] complex as a representative example [35,36]. The optimized structure, shown in Figure 3, reveals a 1:1 complex in which the dicarboxylate $\mathbf{C7^{2-}}$ is

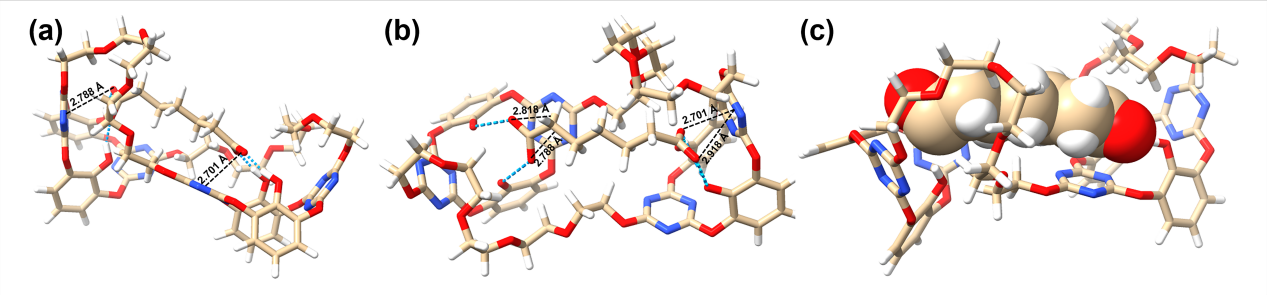

Figure 3: (a–c) DFT-optimized structure of the **B4aH-C7**$^{2-}$ complex. The blue dotted lines represent hydrogen bonds and the black dotted lines represent anion–π interactions.

included within the cavity of **B4aH**. The two subcavities interact synergistically with the included dicarboxylate; the two terminal carboxylate groups are respectively positioned within electron-deficient cavities of the submacrocycles, forming hydrogen bonds (2.49–2.59 Å) with the two hydroxy groups and engaging in anion–π interactions (2.70–2.92 Å) with the triazine rings (Figure 3). Additionally, the glycol arms of the macrocycle may further stabilize the anion binding through van der Waals interactions with the alkyl chains of the dianions. Driven by these multiple noncovalent interactions, the host undergoes conformational adjustments: the distance between the two submacrocycles increases, and the glycol chains adopt extended conformations compared to the structure shown in Figure 1. These results suggest that the experimentally observed strong binding capability and selectivity of **B4aH** for **C7**$^{2-}$ likely arise from cooperative noncovalent interactions and a size-matching effect.

Conclusion

In conclusion, we synthesized a series of hydroxy-substituted ultracycles of varying sizes on the lower-rim using a one-pot cyclization strategy. ^{1}H NMR titration experiments indicate that the introduction of lower-rim hydroxy substituents effectively enhances the dicarboxylate binding through cooperative hydrogen bonding and anion–π interactions. The selective recognition of long and flexible dicarboxylates holds exciting promise for the use of dicarboxylate sensors in medicine and industry.

Supporting Information

Supporting Information File 1

Experimental details and characterization data (including ^{1}H NMR, ^{13}C NMR, IR, and HRMS of precursor compounds and ultracycles, X-ray data for **B4aH**, theoretical calculations, and NMR titration data).
[https://www.beilstein-journals.org/bjoc/content/supplementary/1860-5397-21-72-S1.pdf]

Funding

Financial support from the National Natural Science Foundation of China (Nos. 22171271, 22371285) and Beijing National Laboratory for Molecular Sciences (BNLMS-CXXM-202002) is gratefully acknowledged.

ORCID® iDs

Yu-Fei Ao - https://orcid.org/0000-0002-9415-2181
Qi-Qiang Wang - https://orcid.org/0000-0001-5988-1293
De-Xian Wang - https://orcid.org/0000-0002-9059-5022

Data Availability Statement

All data that supports the findings of this study is available in the published article and/or the supporting information of this article.

References

1. Prautzsch, V.; Ibach, S. *J. Inclusion Phenom. Macrocyclic Chem.* **1999,** *33,* 427–458. doi:10.1023/a:1017193104870
2. Gräther, O.; Arigoni, D. *J. Chem. Soc., Chem. Commun.* **1995,** 405–406. doi:10.1039/c39950000405
3. Fujii, K.; Minagawa, H.; Terada, Y.; Takaha, T.; Kuriki, T.; Shimada, J.; Kaneko, H. *Appl. Environ. Microbiol.* **2005,** *71,* 5823–5827. doi:10.1128/aem.71.10.5823-5827.2005
4. Srisimarat, W.; Powviriyakul, A.; Kaulpiboon, J.; Krusong, K.; Zimmermann, W.; Pongsawasdi, P. *J. Inclusion Phenom. Macrocyclic Chem.* **2011,** *70,* 369–375. doi:10.1007/s10847-010-9890-5
5. Thorstholm, L.; Craik, D. J. *Drug Discovery Today: Technol.* **2012,** *9,* e13–e21. doi:10.1016/j.ddtec.2011.07.005
6. Empting, M. An Introduction to Cyclic Peptides. In *Cyclic Peptides: From Bioorganic Synthesis to Applications;* Koehnke, J.; Naismith, J.; van der Donk, W. A., Eds.; The Royal Society of Chemistry: Cambridge, UK, 2017; pp 1–14. doi:10.1039/9781788010153
7. Conlan, B. F.; Gillon, A. D.; Craik, D. J.; Anderson, M. A. *Pept. Sci.* **2010,** *94,* 573–583. doi:10.1002/bip.21422
8. Li, J.; Mohammed-Elsabagh, M.; Paczkowski, F.; Li, Y. *ChemBioChem* **2020,** *21,* 1547–1566. doi:10.1002/cbic.202000003
9. Ma, C.; Lo, A.; Abdolmaleki, A.; MacLachlan, M. J. *Org. Lett.* **2004,** *6,* 3841–3844. doi:10.1021/ol0483549
10. Kawano, S.-i.; Ishida, Y.; Tanaka, K. *J. Am. Chem. Soc.* **2015,** *137,* 2295–2302. doi:10.1021/ja510585u

11. Gregoliński, J.; Ślepokura, K.; Paćkowski, T.; Panek, J.; Stefanowicz, P.; Lisowski, J. *J. Org. Chem.* **2016,** *81,* 5285–5294. doi:10.1021/acs.joc.6b00531
12. Zhang, Z.-Y.; Li, C. *Acc. Chem. Res.* **2022,** *55,* 916–929. doi:10.1021/acs.accounts.2c00043
13. Moore, J. S.; Zhang, J. *Angew. Chem., Int. Ed. Engl.* **1992,** *31,* 922–924. doi:10.1002/anie.199209221
14. Höger, S.; Enkelmann, V. *Angew. Chem., Int. Ed. Engl.* **1995,** *34,* 2917–2919. doi:10.1002/anie.199527131
15. Itoh, Y.; Chen, S.; Hirahara, R.; Konda, T.; Aoki, T.; Ueda, T.; Shimada, I.; Cannon, J. J.; Shao, C.; Shiomi, J.; Tabata, K. V.; Noji, H.; Sato, K.; Aida, T. *Science* **2022,** *376,* 738–743. doi:10.1126/science.abd0966
16. Zhang, Y.; Wada, T.; Sasabe, H. *Chem. Commun.* **1996,** 621–622. doi:10.1039/cc9960000621
17. Vögtle, F.; Puff, H.; Friedrichs, E.; Müller, W. M. *Angew. Chem., Int. Ed. Engl.* **1982,** *21,* 431. doi:10.1002/anie.198204311
18. Lhoták, P.; Kawaguchi, M.; Ikeda, A.; Shinkai, S. *Tetrahedron* **1996,** *52,* 12399–12408. doi:10.1016/0040-4020(96)00738-7
19. Hoffmann, M.; Kärnbratt, J.; Chang, M.-H.; Herz, L. M.; Albinsson, B.; Anderson, H. L. *Angew. Chem., Int. Ed.* **2008,** *47,* 4993–4996. doi:10.1002/anie.200801188
20. Butler, S. M.; Jolliffe, K. A. *Org. Biomol. Chem.* **2020,** *18,* 8236–8254. doi:10.1039/d0ob01761b
21. Curiel, D.; Más-Montoya, M.; Sánchez, G. *Coord. Chem. Rev.* **2015,** *284,* 19–66. doi:10.1016/j.ccr.2014.09.010
22. Hoppe, B. *Nat. Rev. Nephrol.* **2012,** *8,* 467–475. doi:10.1038/nrneph.2012.113
23. Koo, O. M. Y., Ed. *Pharmaceutical Excipients: Properties, Functionality, and Applications in Research and Industry;* John Wiley & Sons: Hoboken, NJ, USA, 2016. doi:10.1002/9781118992432
24. Hou, M.-L.; Lu, C.-M.; Lin, C.-H.; Lin, L.-C.; Tsai, T.-H. *Molecules* **2016,** *21,* 367. doi:10.3390/molecules21030367
25. Dang, S.; Zhu, Q.-L.; Xu, Q. *Nat. Rev. Mater.* **2018,** *3,* 17075. doi:10.1038/natrevmats.2017.75
26. Wang, Q.-Q.; Day, V. W.; Bowman-James, K. *Chem. Sci.* **2011,** *2,* 1735–1738. doi:10.1039/c1sc00292a
27. Fitzmaurice, R. J.; Kyne, G. M.; Douheret, D.; Kilburn, J. D. *J. Chem. Soc., Perkin Trans. 1* **2002,** 841–864. doi:10.1039/b009041g
28. Marcus, Y. *J. Chem. Soc., Faraday Trans.* **1991,** *87,* 2995–2999. doi:10.1039/ft9918702995
29. Mi, W.-H.; Huang, T.-Y.; Ao, Y.-F.; Wang, X.-D.; Wang, Q.-Q.; Wang, D.-X. *Chin. Chem. Lett.* **2024,** *35,* 109077. doi:10.1016/j.cclet.2023.109077
30. Wang, X.-D.; Li, S.; Ao, Y.-F.; Wang, Q.-Q.; Huang, Z.-T.; Wang, D.-X. *Org. Biomol. Chem.* **2016,** *14,* 330–334. doi:10.1039/c5ob02291f
31. Luo, J.; Ao, Y.-F.; Wang, Q.-Q.; Wang, D.-X. *Angew. Chem., Int. Ed.* **2018,** *57,* 15827–15831. doi:10.1002/anie.201810836
32. *Bindfit,* v0.5; Supramolecular.org, http://supramolecular.org.
33. Thordarson, P. *Chem. Soc. Rev.* **2011,** *40,* 1305–1323. doi:10.1039/c0cs00062k
34. Hibbert, D. B.; Thordarson, P. *Chem. Commun.* **2016,** *52,* 12792–12805. doi:10.1039/c6cc03888c
35. Petersson, G. A.; Bennett, A.; Tensfeldt, T. G.; Al-Laham, M. A.; Shirley, W. A.; Mantzaris, J. *J. Chem. Phys.* **1988,** *89,* 2193–2218. doi:10.1063/1.455064
36. Zhao, Y.; Truhlar, D. G. *Theor. Chem. Acc.* **2008,** *120,* 215–241. doi:10.1007/s00214-007-0310-x

License and Terms

BEILSTEIN JOURNAL OF ORGANIC CHEMISTRY

Selective monoformylation of naphthalene-fused propellanes for methylene-alternating copolymers

Kenichi Kato*[1], Tatsuki Hiroi[1], Seina Okada[1], Shunsuke Ohtani[1] and Tomoki Ogoshi*[1,2]

Full Research Paper

Open Access

Address:
[1]Department of Synthetic Chemistry and Biological Chemistry, Graduate School of Engineering, Kyoto University, Katsura, Nishikyo-ku, Kyoto, 615-8510, Japan and [2]WPI Nano Life Science Institute, Kanazawa University, Kakuma-machi, Kanazawa, 920-1192, Japan

Email:
Kenichi Kato* - katok@sbchem.kyoto-u.ac.jp; Tomoki Ogoshi* - ogoshi@sbchem.kyoto-u.ac.jp

* Corresponding author

Keywords:
alternating copolymer; building block; formylation; gas adsorption; propellane

Beilstein J. Org. Chem. **2025,** *21,* 1183–1191.
https://doi.org/10.3762/bjoc.21.95

Received: 15 April 2025
Accepted: 05 June 2025
Published: 18 June 2025

This article is part of the thematic issue "Novel macrocycles: from synthesis to supramolecular function".

Guest Editor: C. Gaeta

Abstract

Development of three-dimensional (3D) building blocks is a key to change tight molecular assemblies of rigid π-conjugated planes into organic functional materials endowed with molecular-size cavities. To increase the diversity of available 3D building blocks, we herein report electrophilic formylation of naphthalene-fused [3.3.3]- and [4.3.3]propellanes as the first selective single-point functionalization by virtue of through-space electronic communications between the naphthalene units. The propellane skeletons have well-defined 3D structures and moderate flexibility at the same time. Therefore, the monoformyl products are good precursors for soft materials which show molecular-size cavities and require desymmetrized building blocks. As a proof of concept, methylene-alternating copolymers were prepared by reduction to corresponding alcohols followed by acid-mediated condensation. The linear copolymers show good solubility and carbon dioxide adsorption.

Introduction

Combination of sp^2- and sp^3-hybridized atoms in core π-skeletons [1-3] is a key to go beyond common organic functional materials composed of rigid π-conjugated planes and flexible peripheral substituents. Because larger π-conjugated planes mostly display low solubility and dense packing due to the π–π stacking and CH–π interactions, surrounding alkyl and other flexible moieties are widely adopted to improve the solubility and modulate the molecular assemblies [4-9]. By contrast, the presence of sp^3-hybridized atoms in core π-skeletons can lead to three-dimensional (3D) structures with appropriate rigidity, thereby giving macrocyclic arenes [10,11], molecule-based cages and frameworks [12-19], polymers of intrinsic microporosity [20-24], and so forth. Characteristically, they possess molecular-size cavities, which contribute to intricate molecular recognition [25], confined spaces for reactions [26], and small-molecule storage and transport [27-29]. Further progress in such

unique organic materials largely depends on the exploitation of 3D π-building blocks. However, the variety of building blocks are limited to a few families such as tetraphenylmethane and triptycene [30-39].

Widespread use of 3D π-skeletons requires not only efficient construction of the skeletons but also functionalization with precise control of substitution numbers and positions. Along this line, fully π-fused [4.4.4]- and [3.3.3]propellanes [40-43] were able to be brominated and nitrated at six positions while retaining molecular symmetry (Figure 1) [44-46]. One functional group was selectively introduced to each naphthalene ring of fully π-fused [4.3.3]- and [3.3.3]propellane, **[4.3.3]** and **[3.3.3]**, respectively [47-55]. In this work, we report the introduction of a single functional group to a whole skeleton of **[4.3.3]** and **[3.3.3]**, using formylation [55,56]. The reaction is

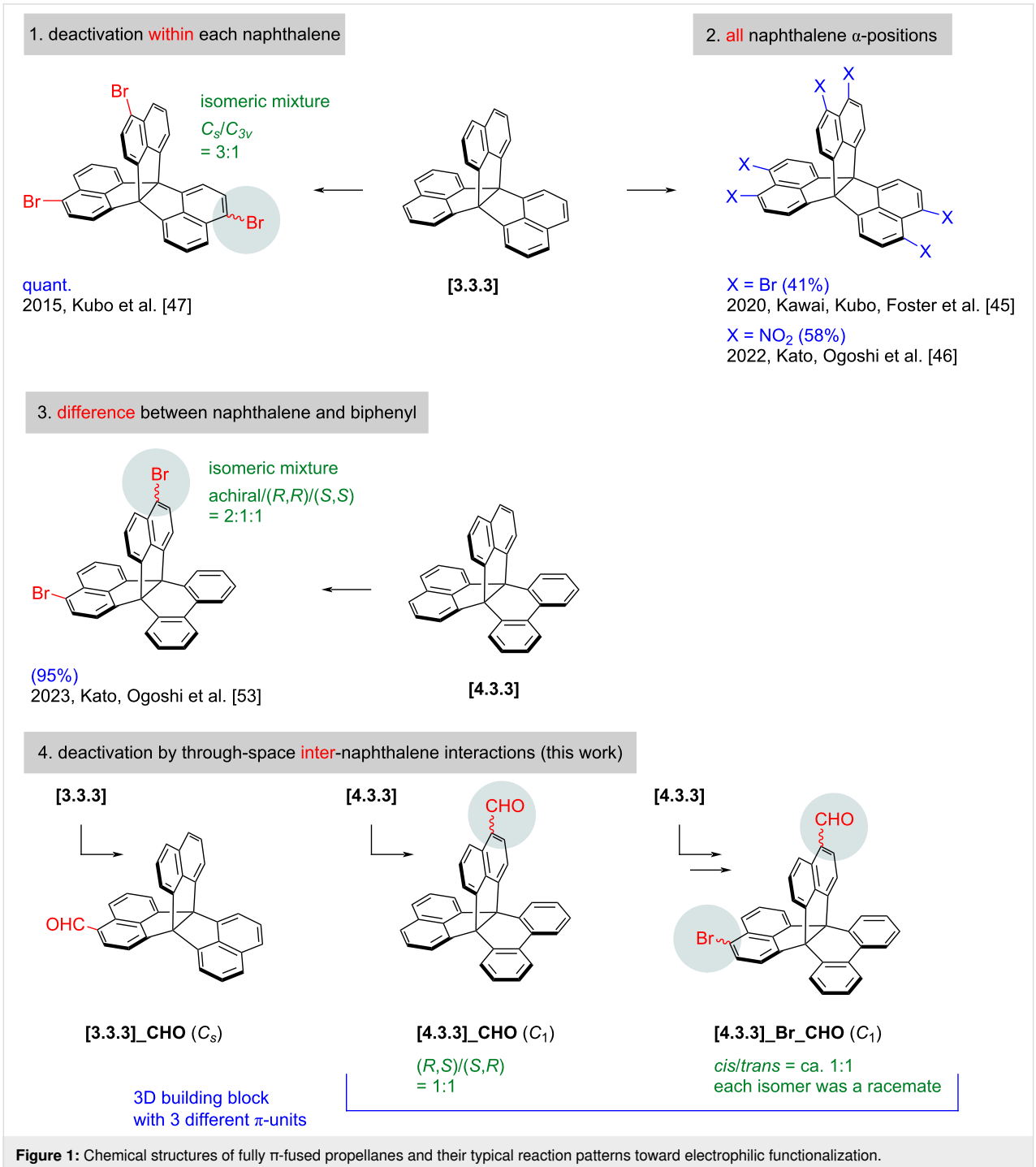

Figure 1: Chemical structures of fully π-fused propellanes and their typical reaction patterns toward electrophilic functionalization.

electrophilic, and the substrates are effectively deactivated toward further reactions upon introduction of an electron-withdrawing formyl group because of through-space electronic interactions between the naphthalene units. The monoformyl products are reduced to corresponding alcohols, which are then reacted under Friedel–Crafts conditions. Amorphous methylene-alternating copolymers are obtained without particular macrocyclic oligomers. Due to the 3D components, the linear copolymers display good solubility in $CHCl_3$ and THF and adsorption properties for CO_2 gas.

Results and Discussion

Selective monoformylation

Initially, we tried introducing formyl groups into a fully π-fused [4.3.3]propellane via organometal species, which had been effective for functional π-extended systems [57-60]. This scheme also enables control of the number of formyl groups by starting materials and reagents. Brominated [4.3.3]propellane was reacted with *n*-BuLi or iPrMgCl·LiCl to generate an organometal species, which was quenched with *N*,*N*-dimethylformamide (DMF) as an electrophile (Table S201 in Supporting Information File 1). Despite several trials, the reactions led to complicated mixtures owing to decomposition and debromination or predominant recovery of the starting material, respectively.

Then, we turned our attention to electrophilic formylation. Vilsmeier–Haack [61] and Duff [62] reactions led to recovery of starting material or a complicated mixture probably owing to the modestly electron-rich and sterically demanding naphthalene α-positions (Table S202, entries 1–3, Supporting Information File 1). By contrast, a combination of dichloromethyl methyl ether and $TiCl_4$ (Rieche reaction) [55,56,63-66] yielded the monoformyl product **[4.3.3]_CHO**, in a selective manner (Table 1, entry 1). To suppress decomposition in the overnight reaction at room temperature, the reaction time was reduced to 1.5 h, which afforded **[4.3.3]_CHO** in an isolated yield of 80% (Table 1, entry 2). The same protocol was successfully applicable to pristine π-fused [3.3.3]propellane **[3.3.3]**, giving **[3.3.3]_CHO** selectively in 67% yield (Table 1, entry 3).

In electrophilic aromatic substitutions, multifold reactions are possible, and the number of substitution is sometimes difficult to control by tuning reaction temperature and time. Indeed, bromination of **[3.3.3]** and **[4.3.3]** was reported as three/six- and two-fold reactions, respectively [45,47,53]. If the amount of bromine was limited, the resulting nearly random mixtures of brominated compounds would be practically impossible to separate by chromatography on silica gel because of their low polarity and poor solubility in *n*-hexane. On the other hand, nitration of **[3.3.3]** gave solely the six-fold nitrated product due to low solubility of the starting material [46]. The current reaction is the first practical method for the selective monofunctionalization of **[3.3.3]** and **[4.3.3]**, to the best of our knowledge. It is also noteworthy that this reaction further desymmetrized the [4.3.3]propellane skeleton of **[4.3.3]** into a 3D building block bearing three different fused π-units.

Diformylation and computed electronic structures

In the formylation of **[3.3.3]**, diformylated product **[3.3.3]_2CHO** was obtained in 5.1% yield. In expectation of successful multifold formylation, the equivalents of dichloromethyl methyl ether and $TiCl_4$ were doubled (Table 1, entry 4). The yield of **[3.3.3]_2CHO** modestly increased to 25% with a slight decrease in the yield of **[3.3.3]_CHO** (61%). Although further increase of the equivalents and prolonged reaction time may potentially provide better results for **[3.3.3]_2CHO**, we gave up such attempts because of the competing decomposition in these strongly acidic conditions. In the case of **[4.3.3]**, diformylation gave only 1.8% of **[4.3.3]_2CHO** after 1.5 h (Table 1, entry 5), which was consistent with the absence of **[4.3.3]_2CHO** in monoformylation. Due to the low reactivity, the reaction time was elongated to 18 h (Table 1, entry 6). The yield of **[4.3.3]_2CHO** was improved to 9.9%, whereas the yield of **[4.3.3]_CHO** decreased to 33% owing to competing decomposition. As a substrate, a mixture obtained by monobromination of **[4.3.3]** could be used, giving difunctional building block **[4.3.3]_Br_CHO** in 39% yield (Table 1, entry 7). The reaction was highly successful because the bromination gave nearly random 1:2:1 mixtures of **[4.3.3]**, **[4.3.3]_Br** and **[4.3.3]_2Br**.

To gain insight into the different reactivity between **[3.3.3]** and **[4.3.3]**, theoretical calculations were performed at the ωB97X-D/6-31G(d,p) level of theory (Figures S901–S903 in Supporting Information File 1). Although distribution of the highest occupied molecular orbitals (HOMOs) was similarly delocalized to multiple naphthalene units, the energy for **[3.3.3]** (−7.23 eV) was higher than that of **[4.3.3]** (−7.32 eV). Upon formylation, the HOMO energies of **[3.3.3]** and **[4.3.3]** were stabilized to −7.44 eV and −7.55 eV by 0.21 eV and 0.23 eV, respectively. These values correlated well with the observed reactivities and selectivity.

Attempted macrocyclization leading to linear polymers

Formyl groups have diverse reactivities and enable facile condensation, dynamic covalent chemistry, and so on. In this work, we tried the synthesis of cyclic oligomers composed of naphthalene-fused propellanes simply by reduction into the correspond-

Table 1: Formylation of naphthalene-fused propellanes.

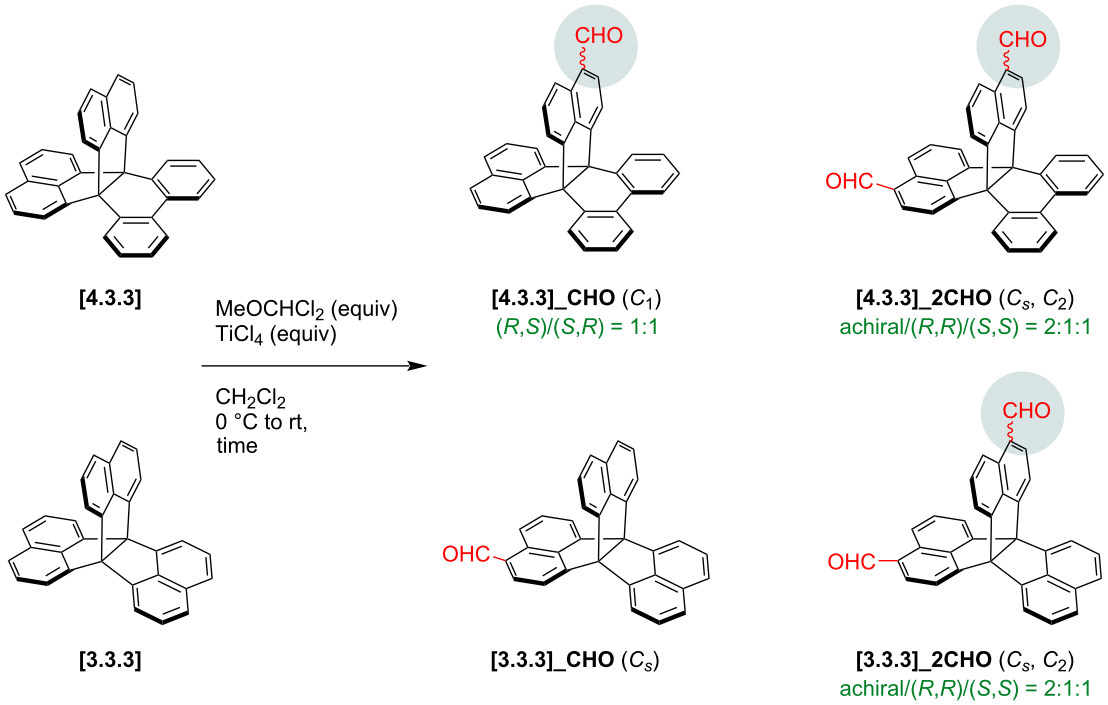

entry	substrate	equiv	time	results
1	**[4.3.3]**	1.25	29 h	**[4.3.3]_CHO** (48%)
2	**[4.3.3]**	1.2	1.5 h	**[4.3.3]_CHO** (80%), **[4.3.3]** (18%)
3	**[3.3.3]**	1.2	1.5 h	**[3.3.3]_CHO** (67%), **[3.3.3]** (12%), **[3.3.3]_2CHO** (5.1%)
4	**[3.3.3]**	2.4	1.5 h	**[3.3.3]_2CHO** (25%), **[3.3.3]_CHO** (61%)
5	**[4.3.3]**	2.4	1.5 h	**[4.3.3]_2CHO** (1.8%), **[4.3.3]_CHO** (56%)
6	**[4.3.3]**	2.4	18 h	**[4.3.3]_2CHO** (9.9%), **[4.3.3]_CHO** (33%)
7[a]	**[4.3.3]_Br**	1.2	18 h	**[4.3.3]_Br_CHO** (39% in 2 steps from **[4.3.3]**)

[a]Substrate was a 1:2:1 mixture of **[4.3.3]**, **[4.3.3]_Br**, and **[4.3.3]_2Br**, obtained by bromination of **[4.3.3]** with 1.03 equiv of Br_2 (Figure S201 in Supporting Information File 1) [53].

ing alcohols followed by acid-mediated Friedel–Crafts-type reactions (Figure 2a and Figure S201 in Supporting Information File 1) [67,68]. Reduction by $NaBH_4$ proceeded well for both monoaldehydes **[4.3.3]_CHO** and **[3.3.3]_CHO** resulting in over 90% yield. Alcohol products, **[4.3.3]_CH_2OH** and **[3.3.3]_CH_2OH**, were then tested in acidic conditions using anhydrous $FeCl_3$ as a Lewis acid. After the reactions, the alcohol proton signals at 1.54–1.58 ppm disappeared in the ^{1}H NMR spectra, and aliphatic carbon ones at 63.1–63.2 ppm were largely up-field-shifted to ca. 34 ppm in the ^{13}C NMR spectra due to conversion into methylene groups (Figure 2b and Figures S315 and S316 in Supporting Information File 1). However, all ^{1}H NMR signals were broad, and gel permeation chromatography (GPC) charts indicated broad patterns due to multiple products with varying molecular weights. These results implied that formation of well-defined cyclic oligomers was quite limited.

To increase the well-defined species, **[4.3.3]_CH_2OH** was separated into two enantiopure fractions (Supporting Information File 1, Figure S505), one of which was used for the acid-mediated reaction. Despite the stereocontrolled substrate, the resonances in the ^{1}H NMR spectrum of the product remained broad. Therefore, we concluded that these systems were difficult to give specific macrocyclic oligomers but instead provided linear polymers composed of fully π-fused propellanes.

After the reactions, each product was separated into oligomer and linear polymer by preparative GPC using $CHCl_3$ as eluent. According to analytical GPC in THF (Figures S501–504 in Supporting Information File 1), oligomer fractions were mainly composed of tetramer for **[3.3.3]_oligo** and dimer and trimer for **[4.3.3]_oligo**. Fractions of linear polymers indicated peak top molecular weights at around octamer for **[3.3.3]_linear** and

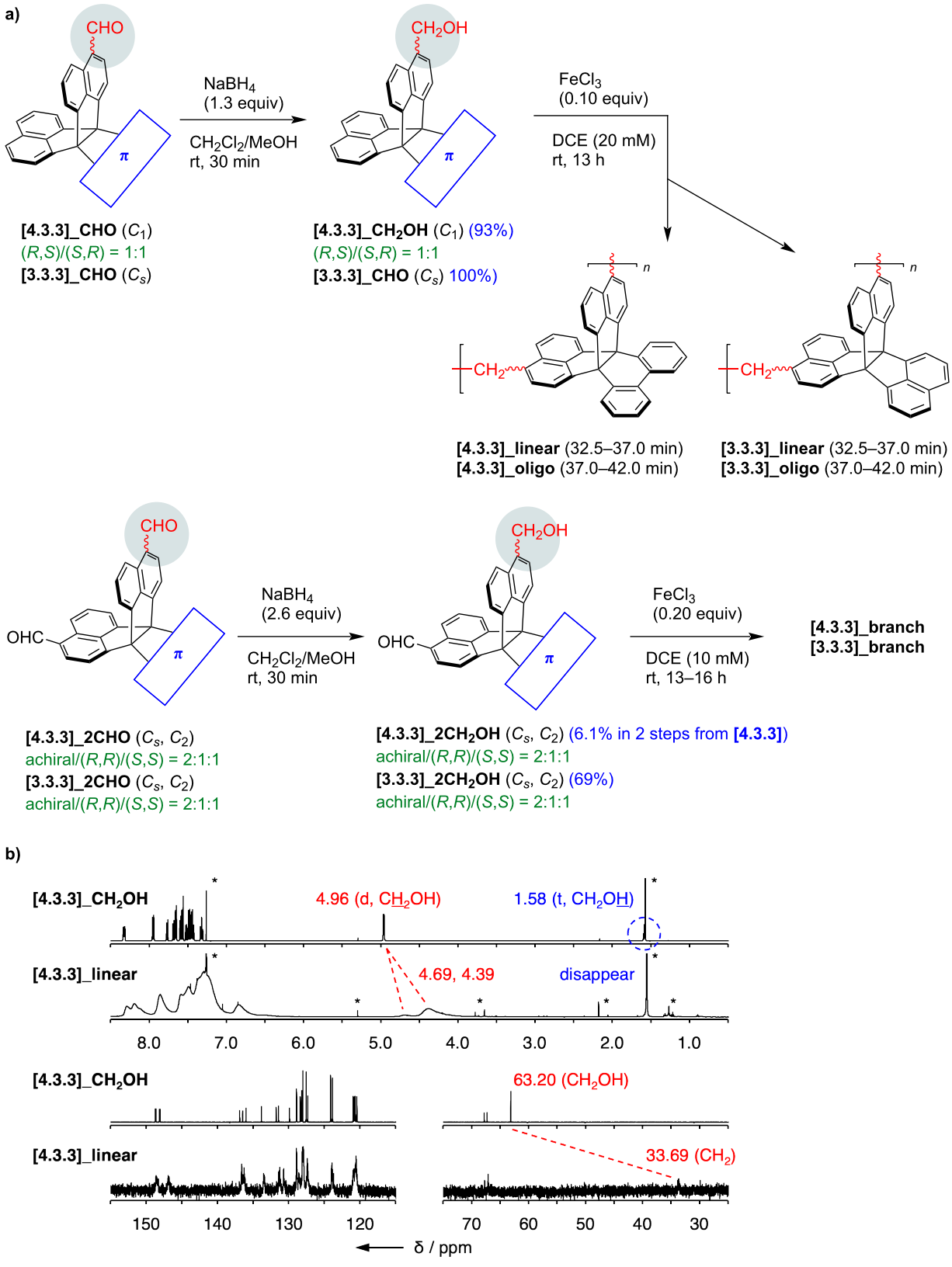

Figure 2: a) Synthesis of methylene-alternating copolymers of fully π-fused propellanes. DCE, 1,2-dichloroethane. b) ^{1}H NMR (500 MHz, top) and ^{13}C (126 MHz, bottom) NMR spectra of **[4.3.3]_CH$_2$OH** and **[4.3.3]_linear** in $CDCl_3$ at room temperature.

Table 2: Properties of methylene-alternating copolymers.[a]

	M_n	M_w	M_w/M_n	T_{90} [°C]	CY [wt %]	V (CO_2) [$cm^3\ g^{-1}$]	S_{BET} [$m^2\ g^{-1}$]
[3.3.3]_oligo	–	–	–	532	76	22	–
[3.3.3]_linear	3.29×10^3	3.79×10^3	1.15	528	68	24	–
[3.3.3]_branch	–	–	–	415	64	18	61
[4.3.3]_oligo	–	–	–	468	47	15	–
[4.3.3]_linear	2.69×10^3	3.16×10^3	1.17	491	46	15	–
[4.3.3]_branch	–	–	–	543	75	29	323

[a]M_n, number-average molar mass; M_w, mass-average molar mass; T_{90}, temperature at which weight loss reaches 10%; CY, carbonization yield; V (CO_2), CO_2 uptake (STP) at 90 kPa; S_{BET}, BET surface area.

pentamer and hexamer for **[4.3.3]_linear** (see also Table 2). In analogy with monoaldehydes, dialdehydes were reduced to dialcohols, **[3.3.3]_2CH$_2$OH** and **[4.3.3]_2CH$_2$OH**, and polymerized in acidic conditions (Figure 2a). Insoluble solids, **[3.3.3]_branch** and **[4.3.3]_branch**, were obtained due to formation of bonding networks and washed repeatedly with CH_2Cl_2, H_2O, and acetone.

Characterization of methylene-alternating copolymers

The thermal stability of the oligomers and polymers were evaluated with thermogravimetric analysis (TGA) (Figure S703 in Supporting Information File 1). Temperatures at which weight loss reached 10% (T_{90}) were 468–491 °C and carbonization yields at 900 °C (CY) were ca. 46 wt % for **[4.3.3]_oligo** and **[4.3.3]_linear**. T_{90} and CY of **[4.3.3]_branch** showed higher values of 543 °C and 75 wt % probably owing to the network structure. By contrast, soluble **[3.3.3]_oligo** and **[3.3.3]_linear** had relatively high T_{90} of 528–532 °C and CY of 68–76 wt %. The high values were ascribed to two unsubstituted naphthalene rings in precursor **[3.3.3]_CH$_2$OH**, which caused facile branching in the reaction or heating process. T_{90} and CY of **[3.3.3]_branch** (415 °C and 64 wt %) were lower than those of **[3.3.3]_linear** because of two-step decay profile (Figure S703a in Supporting Information File 1).

All the samples showed broad powder X-ray diffraction (PXRD) patterns with unclear peaks at around 2θ = 11° and 20° (Supporting Information File 1, Figure S601) and continuous curves in differential scanning calorimetry (DSC) between −70 and 300 °C (Figures S701 and S702, Supporting Information File 1). The results indicated that the polymers were amorphous while giving relatively high thermal stability toward phase transition and decomposition.

Then, gas adsorption properties [46,69-72] were evaluated after the samples were activated in vacuo at 120 °C (Figure 3 and Figures S801 and S802 in Supporting Information File 1). Their chemical structures did not necessarily contain branched or ladder-type connections, but all of them displayed CO_2 adsorption properties at 298 K probably due to the 3D components. The uptake values at standard temperature and pressure (STP) were 15–29 $cm^3 \cdot g^{-1}$ at 90 kPa. In this series, a sample with higher T_{90} and CY values tended to exhibit a higher adsorption capacity for CO_2. By contrast, the linear oligomers and polymers did not adsorb N_2 gas at 77 K. The adsorption isotherms of branched polymers did not have major IUPAC type-I contributions either, indicating the absence of micropores suitable for N_2 adsorption. The curve for **[3.3.3]_branch** looked like type-II, and that of **[4.3.3]_branch** showed multistep uptake. In the desorption step, both samples retained most of the adsorbed N_2 molecules even at 30 kPa. These observations and slow equilibrium in the adsorption processes suggested that presence of

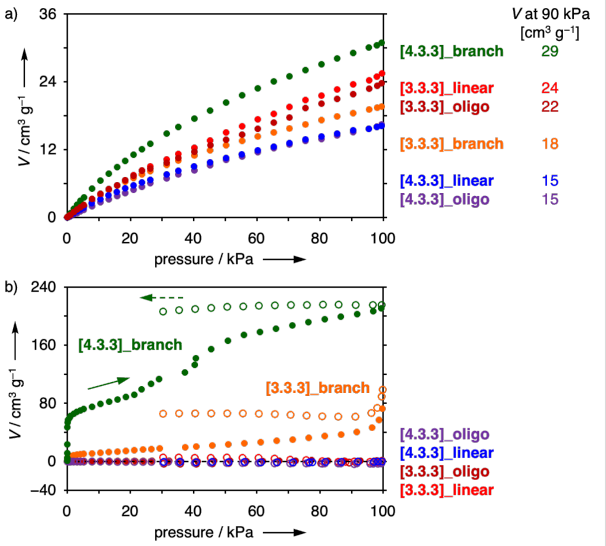

Figure 3: Gas adsorption (filled circles) and desorption (open circles) isotherms of **[3.3.3]_oligo** (dark red), **[3.3.3]_linear** (red), **[3.3.3]_branch** (orange), **[4.3.3]_oligo** (purple), **[4.3.3]_linear** (blue), and **[4.3.3]_branch** (green). a) CO_2 at 298 K and b) N_2 at 77 K.

narrow connections between molecular-size cavities disturbed smooth N_2 adsorption and desorption. Molecular design for uniform microporosity and efficient polymerization is a next challenge.

Conclusion

In this work, we developed formylation on a naphthalene ring in [3.3.3]- and [4.3.3]-type fully π-fused propellanes. High selectivity was achieved for monoformylation on a naphthalene ring. It was reported that bromination proceeded in three- or six-fold manners for a [3.3.3]propellane [45,47-52], and in two-fold one for a [4.3.3]propellane [53,54]. Nitration of the [3.3.3]propellane also yielded an exclusive six-fold product [46]. The current formylation is valuable as the first reliable method for monofunctionalization of naphthalene-fused propellanes without giving inseparable mixtures with multi-functionalized products. Due to the wide reactivities of the formyl group, the monoformyl propellanes would promote new research domains on non-branched linear polymers, macrocyclic compounds, and molecular assemblies that incorporate propellanes as key 3D components. As a proof of concept, the formylated products were reduced to the corresponding alcohols and polymerized in acidic conditions. Although the degrees of polymerization were not high, the methylene-alternating copolymers displayed gas adsorption properties. Further studies are underway towards novel functional materials containing fully π-fused propellanes as flexible 3D building blocks.

Supporting Information

Supporting information includes general information, synthetic procedures and compound data, NMR and MS spectra, HPLC charts, and results of PXRD, DSC, TGA, gas adsorption, and theoretical calculations.

Supporting Information File 1

Experimental.
[https://www.beilstein-journals.org/bjoc/content/supplementary/1860-5397-21-95-S1.pdf]

Acknowledgements

The authors acknowledge Dr. Takeshi Yamamoto and Prof. Dr. Michinori Suginome of Kyoto University for PXRD measurement.

Funding

This work was supported by JSPS KAKENHI Grant Numbers JP21K14611 (Early-Career Scientists, K.K.), JP23H04027 (Transformative Research Areas (A), K.K.), JP25K18019 (Early-Career Scientists, K.K.), and JP22H00334 and JP25H00896 (Scientific Research (A), T.O.), and MEXT World Premier International Research Center Initiative (WPI), Japan. K.K. acknowledge Tokuyama Science Foundation and Yazaki Memorial Foundation for Science and Technology.

Author Contributions

Kenichi Kato: conceptualization; funding acquisition; investigation; methodology; visualization; writing – original draft; writing – review & editing. Tatsuki Hiroi: investigation; writing – review & editing. Seina Okada: investigation; writing – review & editing. Shunsuke Ohtani: writing – review & editing. Tomoki Ogoshi: funding acquisition; project administration; supervision; writing – review & editing.

ORCID® iDs

Kenichi Kato - https://orcid.org/0000-0001-5348-5521

Data Availability Statement

The data that supports the findings of this study is available in the supporting information of this article. Further data generated and analyzed during this study is available from the corresponding author upon reasonable request.

Preprint

A non-peer-reviewed version of this article has been previously published as a preprint: https://doi.org/10.3762/bxiv.2025.23.v1

References

1. Seiki, N.; Shoji, Y.; Kajitani, T.; Ishiwari, F.; Kosaka, A.; Hikima, T.; Takata, M.; Someya, T.; Fukushima, T. *Science* **2015,** *348,* 1122–1126. doi:10.1126/science.aab1391
2. Ma, T.; Kapustin, E. A.; Yin, S. X.; Liang, L.; Zhou, Z.; Niu, J.; Li, L.-H.; Wang, Y.; Su, J.; Li, J.; Wang, X.; Wang, W. D.; Wang, W.; Sun, J.; Yaghi, O. M. *Science* **2018,** *361,* 48–52. doi:10.1126/science.aat7679
3. Koner, K.; Karak, S.; Kandambeth, S.; Karak, S.; Thomas, N.; Leanza, L.; Perego, C.; Pesce, L.; Capelli, R.; Moun, M.; Bhakar, M.; Ajithkumar, T. G.; Pavan, G. M.; Banerjee, R. *Nat. Chem.* **2022,** *14,* 507–514. doi:10.1038/s41557-022-00908-1
4. Rehahn, M.; Schlüter, A.-D.; Wegner, G.; Feast, W. J. *Polymer* **1989,** *30,* 1054–1059. doi:10.1016/0032-3861(89)90078-5
5. Rehahn, M.; Schlüter, A.-D.; Wegner, G.; Feast, W. J. *Polymer* **1989,** *30,* 1060–1062. doi:10.1016/0032-3861(89)90079-7
6. Remmers, M.; Müller, B.; Martin, K.; Räder, H.-J.; Köhler, W. *Macromolecules* **1999,** *32,* 1073–1079. doi:10.1021/ma981260s
7. Tsuda, A.; Osuka, A. *Science* **2001,** *293,* 79–82. doi:10.1126/science.1059552
8. Aratani, N.; Takagi, A.; Yanagawa, Y.; Matsumoto, T.; Kawai, T.; Yoon, Z. S.; Kim, D.; Osuka, A. *Chem. – Eur. J.* **2005,** *11,* 3389–3404. doi:10.1002/chem.200401306
9. Rieger, R.; Müllen, K. *J. Phys. Org. Chem.* **2010,** *23,* 315–325. doi:10.1002/poc.1644
10. Liu, Z.; Nalluri, S. K. M.; Stoddart, J. F. *Chem. Soc. Rev.* **2017,** *46,* 2459–2478. doi:10.1039/c7cs00185a
11. Han, X.-N.; Han, Y.; Chen, C.-F. *Chem. Soc. Rev.* **2023,** *52,* 3265–3298. doi:10.1039/d3cs00002h

12. Little, M. A.; Cooper, A. I. *Adv. Funct. Mater.* **2020,** *30,* 1909842. doi:10.1002/adfm.201909842
13. Zhang, G.; Hua, B.; Dey, A.; Ghosh, M.; Moosa, B. A.; Khashab, N. M. *Acc. Chem. Res.* **2021,** *54,* 155–168. doi:10.1021/acs.accounts.0c00582
14. El-Kaderi, H. M.; Hunt, J. R.; Mendoza-Cortes, J. L.; Côte, A. P.; Taylor, R. E.; O'Keeffe, M.; Yaghi, O. M. *Science* **2007,** *316,* 268–272. doi:10.1126/science.1139915
15. Geng, K.; He, T.; Liu, R.; Dalapati, S.; Tan, K. T.; Li, Z.; Tao, S.; Gong, Y.; Jiang, Q.; Jiang, D. *Chem. Rev.* **2020,** *120,* 8814–8933. doi:10.1021/acs.chemrev.9b00550
16. Tian, Y.; Zhu, G. *Chem. Rev.* **2020,** *120,* 8934–8986. doi:10.1021/acs.chemrev.9b00687
17. Hisaki, I.; Xin, C.; Takahashi, K.; Nakamura, T. *Angew. Chem., Int. Ed.* **2019,** *58,* 11160–11170. doi:10.1002/anie.201902147
18. Li, Z.-T.; Yu, S.-B.; Liu, Y.; Tian, J.; Zhang, D.-W. *Acc. Chem. Res.* **2022,** *55,* 2316–2325. doi:10.1021/acs.accounts.2c00335
19. Ami, T.; Oka, K.; Tsuchiya, K.; Tohnai, N. *Angew. Chem., Int. Ed.* **2022,** *61,* e202202597. doi:10.1002/anie.202202597
20. Budd, P. M.; Ghanem, B. S.; Makhseed, S.; McKeown, N. B.; Msayib, K. J.; Tattershall, C. E. *Chem. Commun.* **2004,** 230–231. doi:10.1039/b311764b
21. Budd, P. M.; Elabas, E. S.; Ghanem, B. S.; Makhseed, S.; McKeown, N. B.; Msayib, K. J.; Tattershall, C. E.; Wang, D. *Adv. Mater. (Weinheim, Ger.)* **2004,** *16,* 456–459. doi:10.1002/adma.200306053
22. Budd, P. M.; McKeown, N. B.; Fritsch, D. *J. Mater. Chem.* **2005,** *15,* 1977–1986. doi:10.1039/b417402j
23. Carta, M.; Malpass-Evans, R.; Croad, M.; Rogan, Y.; Jansen, J. C.; Bernardo, P.; Bazzarelli, F.; McKeown, N. B. *Science* **2013,** *339,* 303–307. doi:10.1126/science.1228032
24. Ghanem, B. S.; Swaidan, R.; Litwiller, E.; Pinnau, I. *Adv. Mater. (Weinheim, Ger.)* **2014,** *26,* 3688–3692. doi:10.1002/adma.201306229
25. Guo, C.; Sedgwick, A. C.; Hirao, T.; Sessler, J. L. *Coord. Chem. Rev.* **2021,** *427,* 213560. doi:10.1016/j.ccr.2020.213560
26. Grommet, A. B.; Feller, M.; Klajn, R. *Nat. Nanotechnol.* **2020,** *15,* 256–271. doi:10.1038/s41565-020-0652-2
27. Zou, L.; Sun, Y.; Che, S.; Yang, X.; Wang, X.; Bosch, M.; Wang, Q.; Li, H.; Smith, M.; Yuan, S.; Perry, Z.; Zhou, H.-C. *Adv. Mater. (Weinheim, Ger.)* **2017,** *29,* 1700229. doi:10.1002/adma.201700229
28. Huang, T.; Alyami, M.; Kashab, N. M.; Nunes, S. P. *J. Mater. Chem. A* **2021,** *9,* 18102–18128. doi:10.1039/d1ta02982g
29. Zhang, R.; Daglar, H.; Tang, C.; Li, P.; Feng, L.; Han, H.; Wu, G.; Limketkai, B. N.; Wu, Y.; Yang, S.; Chen, A. X.-Y.; Stern, C. L.; Malliakas, C. D.; Snurr, R. Q.; Stoddart, J. F. *Nat. Chem.* **2024,** *16,* 1982–1988. doi:10.1038/s41557-024-01622-w
30. Bezzu, C. G.; Carta, M.; Tonkins, A.; Jansen, J. C.; Bernardo, P.; Bazzarelli, F.; McKeown, N. B. *Adv. Mater. (Weinheim, Ger.)* **2012,** *24,* 5930–5933. doi:10.1002/adma.201202393
31. Zhu, K.; Kamochi, K.; Kodama, T.; Tobisu, M.; Amaya, T. *Chem. Sci.* **2020,** *11,* 9604–9610. doi:10.1039/d0sc02452j
32. Park, J.; Kim, J.; Yun, H.-S.; Paik, M. J.; Noh, E.; Mun, H. J.; Kim, M. G.; Shin, T. J.; Seok, S. I. *Nature* **2023,** *616,* 724–730. doi:10.1038/s41586-023-05825-y
33. Chen, Y.; Xu, J.; Gao, P. *Org. Chem. Front.* **2024,** *11,* 508–539. doi:10.1039/d3qo01735d
34. Okubo, K.; Oka, K.; Tsuchiya, K.; Tomimoto, A.; Tohnai, N. *Angew. Chem., Int. Ed.* **2024,** *63,* e202400475. doi:10.1002/anie.202400475
35. Swager, T. M. *Acc. Chem. Res.* **2008,** *41,* 1181–1189. doi:10.1021/ar800107v
36. Chong, J. H.; MacLachlan, M. J. *Chem. Soc. Rev.* **2009,** *38,* 3301–3315. doi:10.1039/b900754g
37. Zhao, L.; Li, Z.; Wirth, T. *Chem. Lett.* **2010,** *39,* 658–667. doi:10.1246/cl.2010.658
38. Chen, C.-F.; Han, Y. *Acc. Chem. Res.* **2018,** *51,* 2093–2106. doi:10.1021/acs.accounts.8b00268
39. Ueberricke, L.; Mastalerz, M. *Chem. Rec.* **2021,** *21,* 558–573. doi:10.1002/tcr.202000161
40. Wittig, G.; Schoch, W. *Justus Liebigs Ann. Chem.* **1971,** *749,* 38–48. doi:10.1002/jlac.19717490106
41. Dyker, G.; Körning, J.; Jones, P. G.; Bubenitschek, P. *Angew. Chem., Int. Ed. Engl.* **1993,** *32,* 1733–1735. doi:10.1002/anie.199317331
42. Dyker, G.; Körning, J.; Bubenitschek, P.; Jones, P. G. *Liebigs Ann./Recl.* **1997,** 203–209. doi:10.1002/jlac.199719970129
43. Hackfort, T.; Kuck, D. *Eur. J. Org. Chem.* **1999,** 2867–2878. doi:10.1002/(sici)1099-0690(199911)1999:11<2867::aid-ejoc2867>3.0.co;2-b
44. Debroy, P.; Lindeman, S. V.; Rathore, R. *Org. Lett.* **2007,** *9,* 4091–4094. doi:10.1021/ol7015466
45. Kawai, S.; Krejčí, O.; Nishiuchi, T.; Sahara, K.; Kodama, T.; Pawlak, R.; Meyer, E.; Kubo, T.; Foster, A. S. *Sci. Adv.* **2020,** *6,* eaay8913. doi:10.1126/sciadv.aay8913
46. Kato, K.; Seto, N.; Chida, K.; Yoshii, T.; Mizuno, M.; Nishihara, H.; Ohtani, S.; Ogoshi, T. *Bull. Chem. Soc. Jpn.* **2022,** *95,* 1296–1302. doi:10.1246/bcsj.20220180
47. Kubo, T.; Miyazaki, S.; Kodama, T.; Aoba, M.; Hirao, Y.; Kurata, H. *Chem. Commun.* **2015,** *51,* 3801–3803. doi:10.1039/c4cc09883h
48. Kodama, T.; Hirao, Y.; Nishiuchi, T.; Kubo, T. *ChemPlusChem* **2017,** *82,* 1006–1009. doi:10.1002/cplu.201700045
49. Kodama, T.; Miyazaki, S.; Kubo, T. *ChemPlusChem* **2019,** *84,* 599–602. doi:10.1002/cplu.201800614
50. Lv, L.; Roberts, J.; Xiao, C.; Jia, Z.; Jiang, W.; Zhang, G.; Risko, C.; Zhang, L. *Chem. Sci.* **2019,** *10,* 4951–4958. doi:10.1039/c9sc00849g
51. Lv, L.; Sun, W.; Jia, Z.; Zhang, G.; Wang, F.; Tan, Z.; Zhang, L. *Mater. Chem. Front.* **2020,** *4,* 3539–3545. doi:10.1039/c9qm00668k
52. Kato, K.; Uchida, Y.; Kaneda, T.; Tachibana, T.; Ohtani, S.; Ogoshi, T. *Chem. – Asian J.* **2024,** *19,* e202400080. doi:10.1002/asia.202400080
53. Kato, K.; Tanaka, S.; Seto, N.; Wada, K.; Gon, M.; Fa, S.; Ohtani, S.; Tanaka, K.; Ogoshi, T. *Chem. Commun.* **2023,** *59,* 7080–7083. doi:10.1039/d3cc01809a
54. Kato, K.; Tanaka, K.; Okada, S.; Kaneda, T.; Ohtani, S.; Ogoshi, T. *Chem. – Eur. J.* **2024,** *30,* e202402828. doi:10.1002/chem.202402828
55. Kodama, T.; Aoba, M.; Hirao, Y.; Rivero, S. M.; Casado, J.; Kubo, T. *Angew. Chem., Int. Ed.* **2022,** *61,* e202200688. doi:10.1002/anie.202200688
56. Kodama, T.; Hirao, Y.; Kubo, T. *Precis. Chem.* **2023,** *1,* 183–191. doi:10.1021/prechem.3c00024
57. Fujimoto, K.; Yorimitsu, H.; Osuka, A. *Eur. J. Org. Chem.* **2014,** 4327–4334. doi:10.1002/ejoc.201402391
58. Niko, Y.; Sasaki, S.; Narushima, K.; Sharma, D. K.; Vacha, M.; Konishi, G.-i. *J. Org. Chem.* **2015,** *80,* 10794–10805. doi:10.1021/acs.joc.5b01987
59. Kato, K.; Kim, W.; Kim, D.; Yorimitsu, H.; Osuka, A. *Chem. – Eur. J.* **2016,** *22,* 7041–7045. doi:10.1002/chem.201600473

60. Kato, K.; Furukawa, K.; Osuka, A. *Angew. Chem., Int. Ed.* **2018,** *57,* 9491–9494. doi:10.1002/anie.201804644
61. Vilsmeier, A.; Haack, A. *Ber. Dtsch. Chem. Ges. B* **1927,** *60,* 119–122. doi:10.1002/cber.19270600118
62. Duff, J. C.; Bills, E. J. *J. Chem. Soc.* **1932,** 1987–1988. doi:10.1039/jr9320001987
63. Rieche, A.; Gross, H.; Höft, E. *Chem. Ber.* **1960,** *93,* 88–94. doi:10.1002/cber.19600930115
64. Yamato, T.; Miyazawa, A.; Tashiro, M. *J. Chem. Soc., Perkin Trans. 1* **1993,** 3127–3137. doi:10.1039/p19930003127
65. Unikela, K. S.; Merner, B. L.; Ghasemabadi, P. G.; Warford, C. C.; Qiu, C. S.; Dawe, L. N.; Zhao, Y.; Bodwell, G. J. *Eur. J. Org. Chem.* **2019,** 4546–4560. doi:10.1002/ejoc.201900707
66. Kato, K.; Ohtani, S.; Gon, M.; Tanaka, K.; Ogoshi, T. *Chem. Sci.* **2022,** *13,* 13147–13152. doi:10.1039/d2sc04168e
67. Zhang, G.-W.; Li, P.-F.; Meng, Z.; Wang, H.-X.; Han, Y.; Chen, C.-F. *Angew. Chem., Int. Ed.* **2016,** *55,* 5304–5308. doi:10.1002/anie.201600911
68. Wang, J.-Q.; Li, J.; Zhang, G.-W.; Chen, C.-F. *J. Org. Chem.* **2018,** *83,* 11532–11540. doi:10.1021/acs.joc.8b01437
69. Taylor, R. G. D.; Bezzu, C. G.; Carta, M.; Msayib, K. J.; Walker, J.; Short, R.; Kariuki, B. M.; McKeown, N. B. *Chem. – Eur. J.* **2016,** *22,* 2466–2472. doi:10.1002/chem.201504212
70. Kato, K.; Hiroi, T.; Seto, N.; Ohtani, S.; Ogoshi, T. *Chem. Lett.* **2022,** *51,* 975–977. doi:10.1246/cl.220320
71. Chen, Y.; Zhao, Y.; Zhao, Y.; Chen, X.; Liu, X.; Li, L.; Cao, D.; Wang, S.; Zhang, L. *Angew. Chem., Int. Ed.* **2024,** *63,* e202401706. doi:10.1002/anie.202401706
72. Kato, K.; Okada, S.; Mizuno, M.; Seto, N.; Iwano, R.; Ohtani, S.; Ogoshi, T. *ChemRxiv* **2025**. doi:10.26434/chemrxiv-2025-pkb6x

License and Terms

BEILSTEIN JOURNAL OF ORGANIC CHEMISTRY

3,3'-Linked BINOL macrocycles: optimized synthesis of crown ethers featuring one or two BINOL units

Somayyeh Kheirjou[1], Jan Riebe[1], Maike Thiele[1], Christoph Wölper[2] and Jochen Niemeyer*[1]

Full Research Paper

Open Access

Address:
[1]Faculty of Chemistry (Organic Chemistry) and Center for Nanointegration Duisburg-Essen (CENIDE), University of Duisburg-Essen, 45141 Essen, Germany and [2]Faculty of Chemistry (Inorganic Chemistry), University of Duisburg-Essen, 45141 Essen, Germany

Email:
Jochen Niemeyer* - jochen.niemeyer@uni-due.de

* Corresponding author

Keywords:
BINOL; chirality; crown ethers; macrocycles; supramolecular chemistry

Beilstein J. Org. Chem. **2025,** *21,* 1719–1729.
https://doi.org/10.3762/bjoc.21.134

Received: 15 May 2025
Accepted: 31 July 2025
Published: 28 August 2025

This article is part of the thematic issue "Novel macrocycles: from synthesis to supramolecular function".

Guest Editor: C. Gaeta

Abstract

Chiral macrocycles hold significant importance in various scientific fields due to their unique structural and chemical properties. By controlling their size, shape, and substituents, chiral macrocycles offer a platform for designing and synthesizing highly efficient catalysts, chemosensors, and functional materials. We have recently made strides in developing macrocyclic organocatalysts; however, their synthesis remains challenging. In this work, we aimed to discover a straightforward method for producing a diverse range of chiral macrocycles, thereby enabling further exploration in the field of interlocked and macrocyclic organocatalysts. We successfully established optimized synthetic routes for the synthesis of chiral macrocycles containing one or two stereogenic units, featuring varying ring sizes and substituents (21 examples in total).

Introduction

Crown ethers are at the heart of supramolecular chemistry [1]. Ever since their discovery in 1960, a vast number of different crown ethers has been synthesized and their interactions with guest molecules have been studied. The pioneering works in this area by Cram, Lehn and Pedersen marked the beginning of modern supramolecular chemistry and were honoured with the Nobel Prize in Chemistry in 1987 [2-4]. Soon, it was realized that chiral crown ethers are highly promising host molecules for enantioselective molecular recognition. Different chiral backbones were used for the construction of such chiral crown ethers, especially chiral 1,2-diols such as tartaric acid [5-8], propane-1,2-diol [9-13], cyclohexane-1,2-diol [14], carbohydrates [15], 1,1'-binapthyl-2,2'-diol (BINOL) [16-23] and more [24]. Especially BINOL-based crown ethers proved to be highly useful and were applied for stereoselective molecular recognition [25-27], for catalysis [25,28-31], as stationary

phases for chromatography [32-34], but also as building blocks for incorporation into larger frameworks, such as interlocked molecules [25,35].

In most BINOL-based crown ethers, the macrocycle is attached to the BINOL unit via the oxygens in the 2,2'-positions. This structural motif has been used to construct crown ethers featuring either one or two BINOL units (see Figure 1a) [16-23].

In a related approach, a single BINOL can be equipped with two crown ethers by attaching these via the 2,3 and 2',3'-positions, respectively (see Figure 1b) [36,37]. Less frequently, the 7,7'-positions (see Figure 1c) [38-40] or the 3,3'-positions (see Figure 1d) [41-43] have been used for attaching the crown ether macrocycle, although this strategy has the advantage that the 2,2'-hydroxy groups remain intact and can be used for further binding or functionalization. Our group recently became interested in synthesizing BINOL derivatives featuring macrocyclic

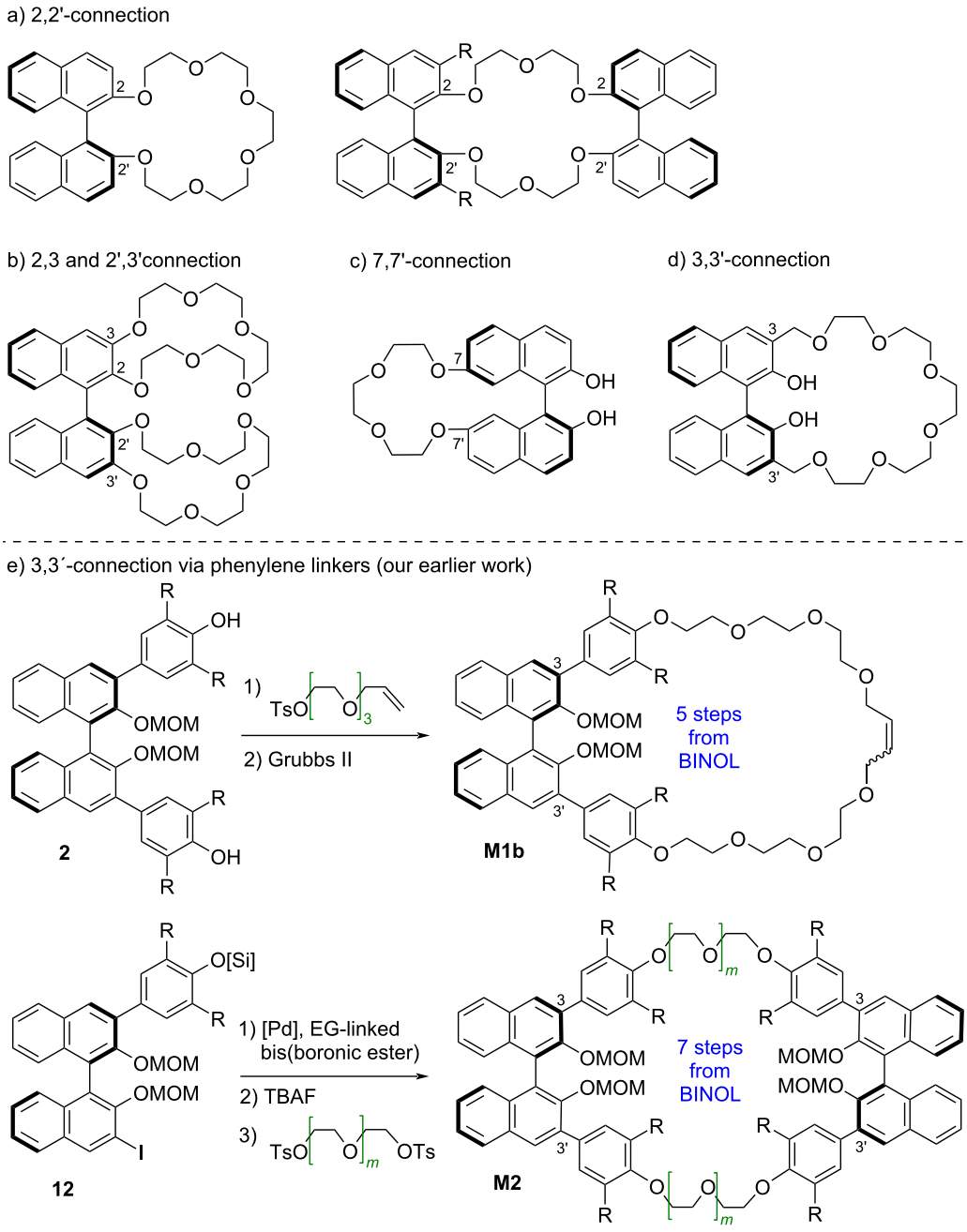

Figure 1: a–d) Selected structures of previously reported BINOL-based crown ether macrocycles; e) previous synthetic routes towards 3,3'-substituted BINOL crown ethers from our group.

crown ethers that are attached at the 3,3'-positions via additional phenylene spacers (see Figure 1e) [35,44,45]. Macrocycles **M1b** with a single BINOL unit were generated from the corresponding diol **2** by attachment of allylated linkers, followed by ring-closing metathesis [46-50]. For the synthesis of macrocycles **M2** with two BINOL units, we relied on the monoiodide **12**, which was first reacted in a two-fold Suzuki coupling to install the first linker, followed by silyl deprotection and introduction of the second linker via nucleophilic substitution [51]. Both procedures require multiple steps towards the desired macrocycles. The route towards the bis-BINOL macrocycles additionally requires the synthesis of the unsymmetric monoiodide **12**. In our previous work, the route starting from **12** had been designed to give access to macrocyclic and singly linked bis-BINOL derivatives from a single precursor, but this is unnecessary if only macrocyclic bis-BINOL derivatives are desired.

For this reason, we sought to find optimized syntheses for such BINOL-based macrocycles (see Figure 2).

After investigating different synthetic routes (vide infra), we found that Williamson-type ether syntheses were the best-yielding approach towards the desired macrocycles. This route was then applied for the synthesis of macrocycles featuring one or two BINOL units, featuring differently substituted phenylene linkers and featuring ethylene glycol linkers of different lengths.

Results and Discussion

Unless otherwise stated, all BINOL derivatives were used as the (*S*)-enantiomers and the stereochemistry will not be mentioned further.

Synthesis of macrocycles featuring one BINOL unit

We first investigated the synthesis of crown ether-type macrocycles **M1** which feature a single BINOL unit. Our previous synthetic approaches (see Figure 1e) toward BINOL macrocycles had successfully used either Williamson-type reactions or Suzuki couplings for the synthesis of intermediates. Thus, we chose to compare the use of two-fold Suzuki coupling or two-fold Williamson reaction for the synthesis of macrocycles **M1**.

For the approach via Suzuki coupling, we employed the previously reported BINOL-diiodide **1** [52], which was reacted with bisboronic acids (see Figure 3a).

Here we chose bisboronic esters **7**$_{5/6/7/8}$ which feature dimethylphenyl groups that are linked via penta/hexa/hepta/octaethylene glycol chains (throughout this publication, the suffix denotes

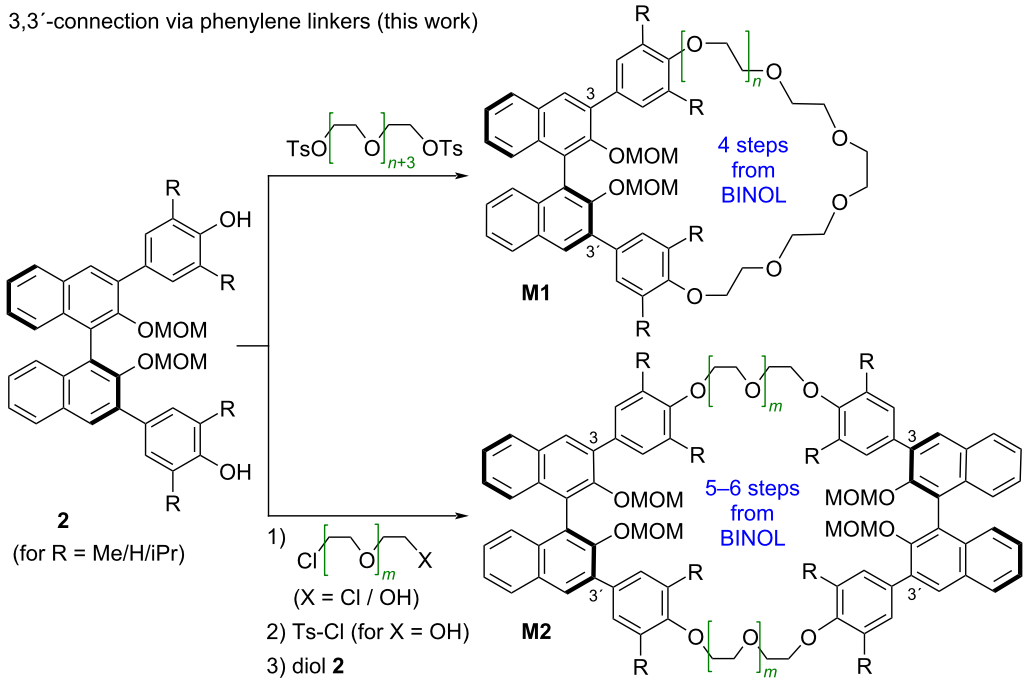

Figure 2: Optimized synthetic routes towards 3,3'-substituted BINOL crown ethers (this work).

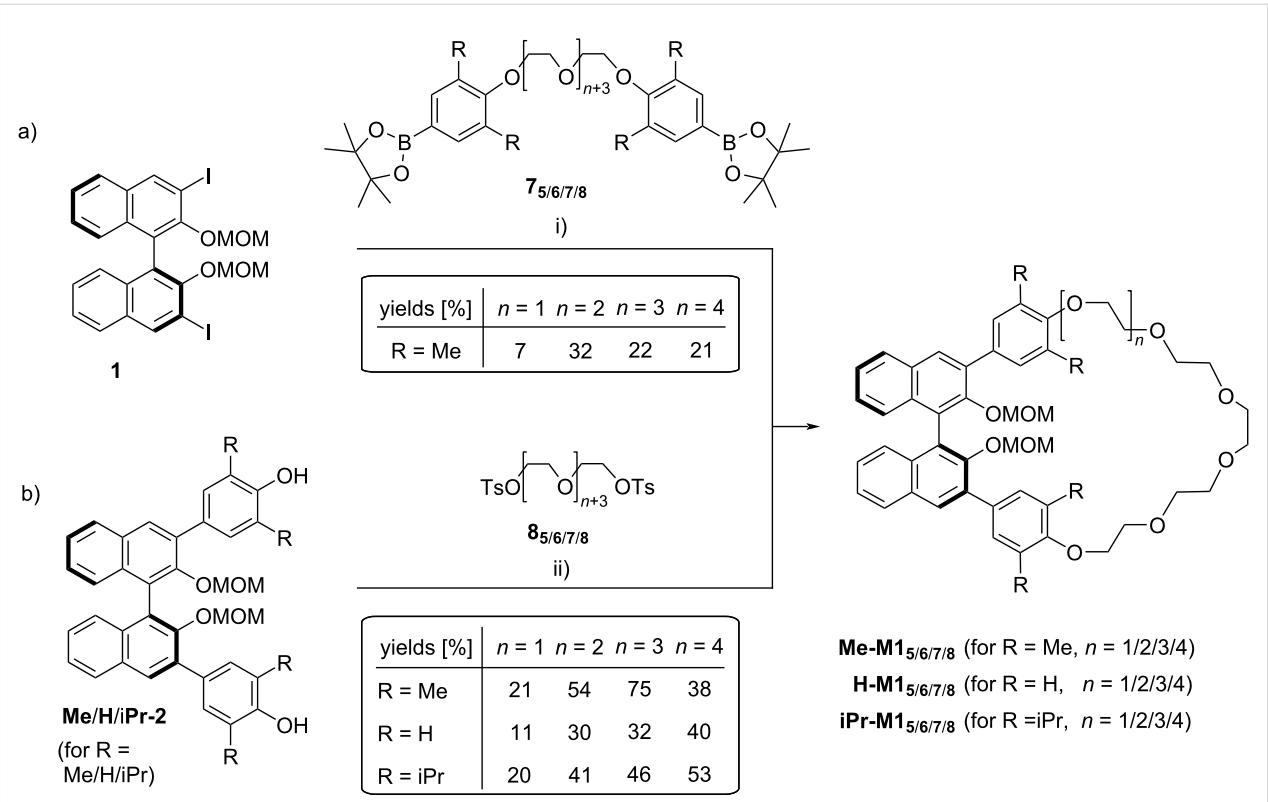

Figure 3: Synthetic routes towards macrocycles featuring one BINOL unit. a) Two-fold Suzuki coupling and b) two-fold Williamson synthesis. Reagents and conditions: i) bis(boronic ester) $\mathbf{7}_{5/6/7/8}$ (1.0. equiv), $Pd_2(dba)_3$ (0.1 equiv), P(*o*-Tol)$_3$ (0.2 equiv), *n*-$Bu_4N^+OH^-$ (3.2. equiv), toluene/H_2O 5:1, 90 °C; ii) ethylene glycol bistosylates $\mathbf{8}_{5/6/7/8}$ (1.0 equiv), Cs_2CO_3 (2.0 equiv), CH_3CN, 80 °C.

the number of ethylene glycol units in a single linker, for the structures of $\mathbf{7}_{5/6/7/8}$, see Figure 3a). The reactivity of $\mathbf{7}_{6}$ had previously been established in the reaction with the unsymmetric monoiodide **12** (see Figure 1e), which proceeded in 59% yield [51]. However, under the same coupling conditions ($Pd_2(dba)_3$, P(*o*-Tol)$_3$, *n*-$Bu_4N^+OH^-$, toluene/H_2O, 90 °C), the reaction of diiodide **1** with bisboronic acids $\mathbf{7}_{5/6/7/8}$ gave only low yields of the desired macrocycles **Me-M1** (7/32/22/21% for $\mathbf{Me\text{-}M1}_{5/6/7/8}$). Thus, the macrocyclization via two-fold Suzuki coupling was not suitable in our hands.

Therefore, we turned our attention towards the two-fold Williamson reaction (see Figure 3b). First, we employed the tetramethyl-substituted diol **Me-2**, which gives access to the same macrocyles $\mathbf{Me\text{-}M1}_{5/6/7/8}$ which we could only generate in low yields via two-fold Suzuki coupling (vide supra). To this end, **Me-2** was reacted with the bistosylated ethylene glycols $\mathbf{8}_{5/6/7/8}$ in the presence of Cs_2CO_3 as a base (CH_3CN, 80 °C). To our delight, we could isolate the macrocyles $\mathbf{Me\text{-}M1}_{5/6/7/8}$ in significantly higher yields of 21/54/75/38%. Cesium carbonate was chosen as the base, because in initial experiments, we obtained consistently higher yields and fewer side-products in comparison to other bases (such as NEt_3 or K_2CO_3), as reported in the literature for related macrocyclizations [53-55].

We then investigated the impact of different substituents on the phenylene linkers on the macrocycle formation. In comparison to the Me-derivative **Me-2**, both the unsubstituted diol **H-2** and the isopropyl derivative **iPr-2** gave generally lower yields for the smaller macrocycles (11/30/32% for $\mathbf{H\text{-}M1}_{5/6/7}$, 20/41/46% for $\mathbf{iPr\text{-}M1}_{5/6/7}$), while the yields for the largest macrocycles $\mathbf{H/iPr\text{-}M1}_{8}$ were slightly increased (40% for $\mathbf{H\text{-}M1}_{8}$, 53% for $\mathbf{iPr\text{-}M1}_{8}$). As a general trend, we observed that the pentaethylene glycol linker seems to be too short to result in efficient macrocyclization (both in Suzuki and Williamson reactions), while the longer linkers give moderate to good yields of the desired macrocycles. In the Williamson approach, we find increasing yields in the series $\mathbf{H\text{-}M1}_{5/6/7/8}$ and $\mathbf{iPr\text{-}M1}_{5/6/7/8}$, with the best yield obtained for the longest octaethylene glycol linkers in $\mathbf{H/iPr\text{-}M1}_{8}$. To our surprise, the Me-series not only gives generally better yields, but also shows the maximum yield for the shorter heptaethylene glycol macrocycle $\mathbf{Me\text{-}M1}_{7}$. The synthesis of the octaethyleneglycol derivative $\mathbf{Me\text{-}M1}_{8}$ was repeated several times but gave reproducibly lower yields than the shorter version $\mathbf{Me\text{-}M1}_{7}$.

All macrocycles were fully characterized by standard analytical methods (see Supporting Information File 1). The structure of **Me-M1$_6$** was additionally verified by single-crystal X-ray analysis (the enantiomeric compound (*R*)-**Me-M1$_6$** resulting from a separate synthesis was crystallized, see Figure 4). Due to the macrocyclic structure, the two ethylene glycol units directly attached to each dimethylphenyl linker adapt a *gauche*-conformation (∠O3–C21–C22–O4 = 66.9(3)°, ∠O4–C23–C24–O5 = −77.3(2)°), and only the central ethylene glycol can be found in a *trans*-conformation (∠O5–C25–C26–O6 = −173.0(5)°). Probably induced by the linker, the commonly preferred perpendicular orientation of the naphthyl-units in the BINOL core is slightly distorted (∠C2–C1–C1'–C2' = −79.2(3)°).

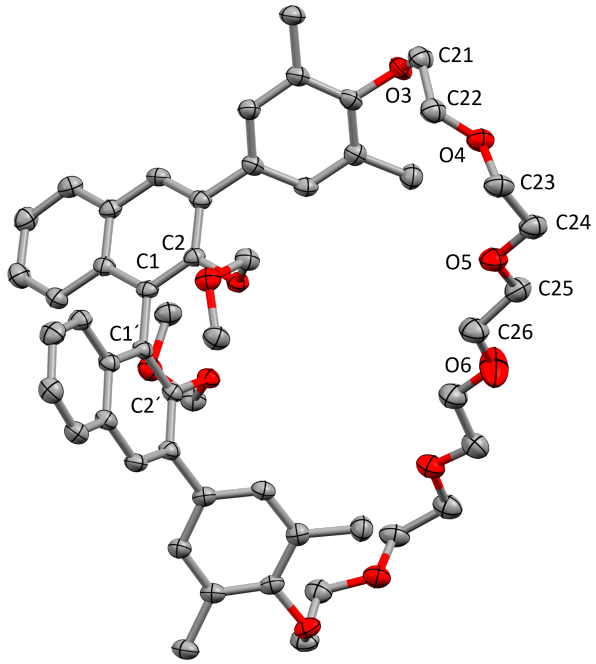

Figure 4: Molecular structure of macrocycle (*R*)-**Me-M1$_6$** in the solid state (hydrogen atoms are omitted for clarity and thermal ellipsoids are set at the 60% probability level). The ethylene glycol chain is partially disordered, only one component is shown.

In summary, we could obtain the desired macrocycles **M1** containing a single BINOL unit in satisfying yields (11–75% from diols **Me**/**H**/**iPr-2**). The previously published route based on ring-closing metathesis gave macrocycle **M1b** (see Figure 1e), which is a 38-membered macrocycle, in 38% yield. Our novel route gives access to 30/33/36/39-membered rings (**M1$_{5/6/7/8}$**), thus complementing the previous approach. Although yields are not consistently better than with the previous route, the novel route has three key advantages: Firstly, the two-step synthesis of the allyl tosyl ethylene glycol (see Figure 1e) can be avoided and the bistosylated ethylene glycol **8** (available in one step) can be used instead. Secondly, the ring-closing metathesis was substituted for an operationally simple Williamson reaction. This results in macrocycles with regular ethylene glycol linkers and removes the internal double bond, which was previously generated as an *E*/*Z*-mixture from the ring-closing metathesis. Thirdly, this route also give access to the smaller macrocylces **M1$_{5/6}$**, while similar ring sizes were difficult to obtain by ring-closing metathesis in our hands [56].

Synthesis of macrocycles featuring two BINOL units

For the synthesis of macrocycles featuring two BINOL units, our first goal was the introduction of two hexaethylene glycol chains between the two BINOL units. These derivatives had proven to be highly efficient organocatalysts in our earlier work, based on the large conformational freedom that is given by the long, flexible linkers [51].

To achieve a convergent synthesis, we first designed the hexaethylene glycol linker **9$_6$**, which features a tosylate leaving group at one end and a phenylboronic ester at the other end (see Figure 5).

This would allow a two-step synthesis of the desired macrocycles by performing a sequence of two-fold Suzuki coupling, followed by two-fold Williamson synthesis or vice versa. However, attempts to realize the first step of either sequence, i.e., reaction of the precursor **9$_6$** with either the BINOL diiodide **1** (in a two-fold Suzuki coupling) or with the BINOL-derived diol **Me-2** (in a two-fold Williamson reaction) gave no meaningful yields of the desired intermediates **Me-3$_6$** or **Me-4$_6$**, respectively.

For this reason, we resorted to an alternative synthesis of the BINOL-based bistosylates **Me**/**H**/**iPr-3$_6$**. For the long hexaethylene glycol linker, a direct reaction of the diols **Me**/**H**/**iPr-2** with a hexaethylene glycol bistosylate did not seem feasible, since this would lead to the mono-BINOL macrocycles **Me**/**H**/**iPr-M1$_6$** even in the presence of a large excess of bistosylate. Thus, we first reacted diols **Me**/**H**/**iPr-2** with chloroalcohol **10$_6$** in the presence of Cs_2CO_3 (CH_3CN, 80 °C), which gave the desired bisglycolated products **Me**/**H**/**iPr-5** (Supporting Information File 1). Subsequent reaction with tosyl chloride in the presence of triethylamine and DMAP (CH_2Cl_2, 25 °C) gave the desired BINOL bistosylates **Me**/**H**/**iPr-3$_6$** in good yields (69/61/72% over two steps, see Figure 6). However, only if temperature and reaction times in this step were carefully controlled, the reaction proceeded cleanly. Deviations from the optimized conditions (see Supporting Information File 1 for details) resulted in greatly diminished yields due to the formation of various by-products.

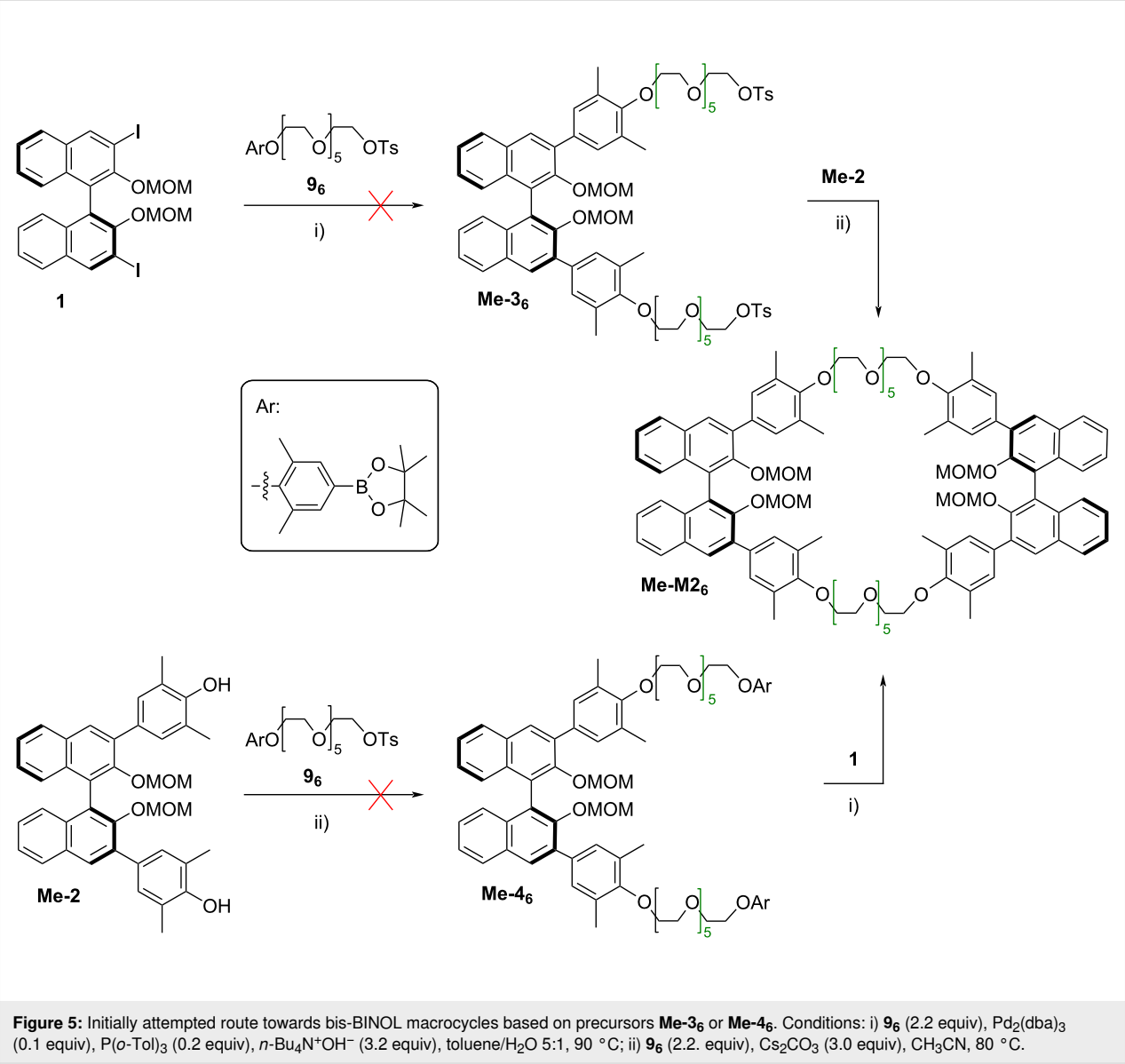

Figure 5: Initially attempted route towards bis-BINOL macrocycles based on precursors **Me-3$_6$** or **Me-4$_6$**. Conditions: i) **9$_6$** (2.2 equiv), $Pd_2(dba)_3$ (0.1 equiv), P(*o*-Tol)$_3$ (0.2 equiv), *n*-$Bu_4N^+OH^-$ (3.2 equiv), toluene/H_2O 5:1, 90 °C; ii) **9$_6$** (2.2. equiv), Cs_2CO_3 (3.0 equiv), CH_3CN, 80 °C.

Starting from the bistosylates **Me/H/iPr-3$_6$**, reaction with the diols **Me/H/iPr-2** in the presence of Cs_2CO_3 as base (CH_3CN, 80 °C) proceeded cleanly to give the desired hexaethylene glycol-linked bis-BINOL macrocycles that feature a 66-membered ring structure. Here, we successfully generated the C_2-symmetric macrocycles **Me/H/iPr-M2$_6$** (obtained in 62/67/54% yield) and the unsymmetrically substituted, C_1-symmetric derivative **HiPr-M2$_6$** (56% yield from **iPr-3$_6$** and **H-2**). Thus, the overall yields for the large macrocycles **Me/H/iPr/HiPr-M2$_6$** range from 15 to 17% (6 steps from BINOL, 35–42% over 3 steps from diols **Me/H/iPr-2**). This is an improvement in comparison to the yield obtained with the previous method, based on sequential introduction of both hexaethylene glycol linkers (see Figure 1b), which gave 11% yield for compound **Me-M2$_6$** over 7 steps from BINOL.

As a second synthetic aim, we wanted to realize the synthesis of smaller bis-BINOL macrocycles that feature two diethylene glycol linkers, thus yielding 42-membered macrocylces. In this case, it was possible to directly react diols **Me/H/iPr-2** with the corresponding dichloride **11$_2$** (Cs_2CO_3, CH_3CN, 80 °C, see Figure 7), since this is too short to result in a mono-BINOL macrocycle.

The corresponding BINOL-based dichlorides **Me/H/iPr-6$_2$** could be obtained in good yields (59/78/76%) and further reacted with the diols **Me/H/iPr-2** in the presence of Cs_2CO_3 (CH_3CN, 80 °C). This cyclization yielded the symmetrically tetrasubstitued macrocycles **Me/H/iPr-M2$_2$** in good yields of 59/78/77%. Again, we applied this protocol for the synthesis of the unsymmetric derivative **HiPr-M2$_2$**, this time in two dia-

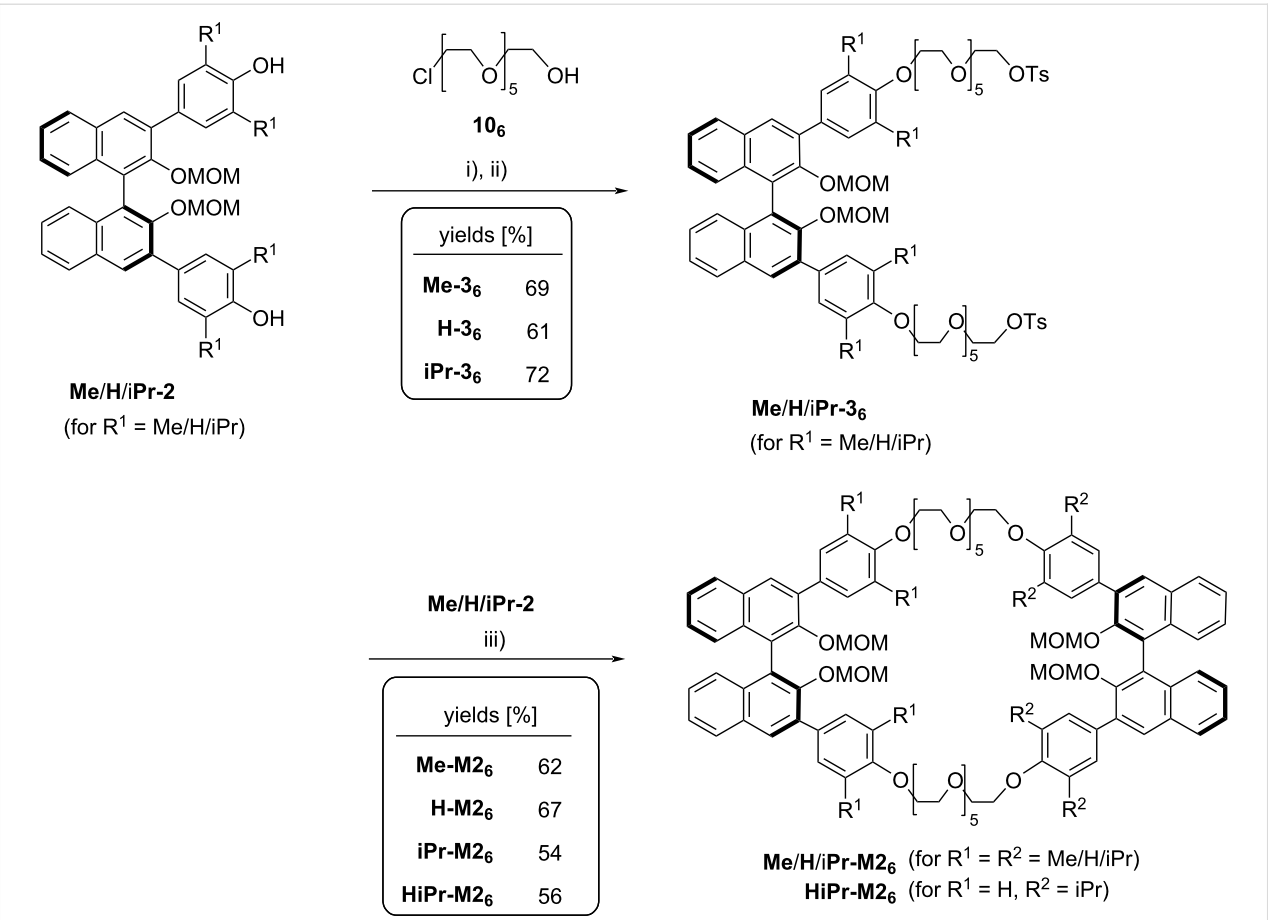

Figure 6: Synthetic route towards macrocycles featuring two BINOL units linked via hexaethylene glycol spacers. Conditions: i) chloroalcohol **10_6** (2.2 equiv), Cs_2CO_3 (2.2 equiv), CH_3CN, 80 °C; ii) tosyl chloride (2.5 equiv), triethylamine (4.0 equiv), DMAP (0.4 equiv), CH_2Cl_2, 25 °C (69/61/72% yield over two steps for **Me**/**H**/**iPr-3_6**); iii) **Me**/**H**/**iPr-2** (1.0 equiv), Cs_2CO_3 (3.2 equiv), CH_3CN, 80 °C (62/67/54/56% yield for **Me**/**H**/**iPr**/**HiPr-$M2_6$**).

stereomeric forms. In the unsymmetric case, the introduction of two BINOL units with opposite configuration does not furnish a *meso*-compound, so that we reacted either (*S*)- or (*R*)-**H-2** with the dichloride (*S*)-**iPr-6_2** to give the diastereomeric macrocycles (*S*,S)-**HiPr-$M2_2$** and (*R*,*S*)-**HiPr-$M2_2$** in 73/49% yield, respectively.

The ^{1}H NMR spectra of the C_2-symmetric derivatives (*S*,*S*)-**H**/**iPr-$M2_2$** (see Figure 8a/b) differ most significantly in the splitting of the signals corresponding to the MOM-methylene protons near 4.3 ppm (H-21), which are clearly split into two doublets for (*S*,*S*)-**H-$M2_2$**, but resemble more of a second order signal with a very small coupling constant in (*S*,*S*)-**iPr-$M2_2$**. As expected, the two BINOL units in the symmetric macrocycles only give one set of signals, e.g., one singlet for H-4 and one doublet for H-6. When comparing these to the C_1-symmetric compound (*S*,*S*)-**HiPr-$M2_2$** (see Figure 8a–c), separate signals for the 4- and 6-positions of each BINOL unit can be observed (i.e., H-4/H-27 and H-6/H-29). In contrast, the signals of the MOM-methylene protons appear closer to the shift observed for (*S*,*S*)-**H-$M2_2$**, however, also two differentiable sets for either BINOL unit can be observed. The MOM-CH_2 signals of the diisopropylphenyl-substituted BINOL unit (i.e., H-21/H-21') show a smaller splitting between the diastereomeric protons than the analogous MOM-CH_2 protons (H-36/H-36') of the phenyl-substituted BINOL unit, in line with the observations for the C_2-symmetric compounds. The two diastereomeric macrocycles (*S*,*S*)- and (*R*,*S*)-**HiPr-$M2_2$** (compare Figure 8c,d) show distinct, but small differences in the ^{1}H chemical shifts. This indicates that despite the short diethylene glycol linkers, the mutual influence of both BINOL units on each other is small in the bis-BINOL macrocycle.

Conclusion

In summary, we have developed novel approaches towards the synthesis of crown ethers that contain one or two BINOL units. The ethylene glycol units were attached to the BINOL backbone via differently substituted phenylene linkers, either featuring two methyl groups, two isopropyl groups, or no additional substituent.

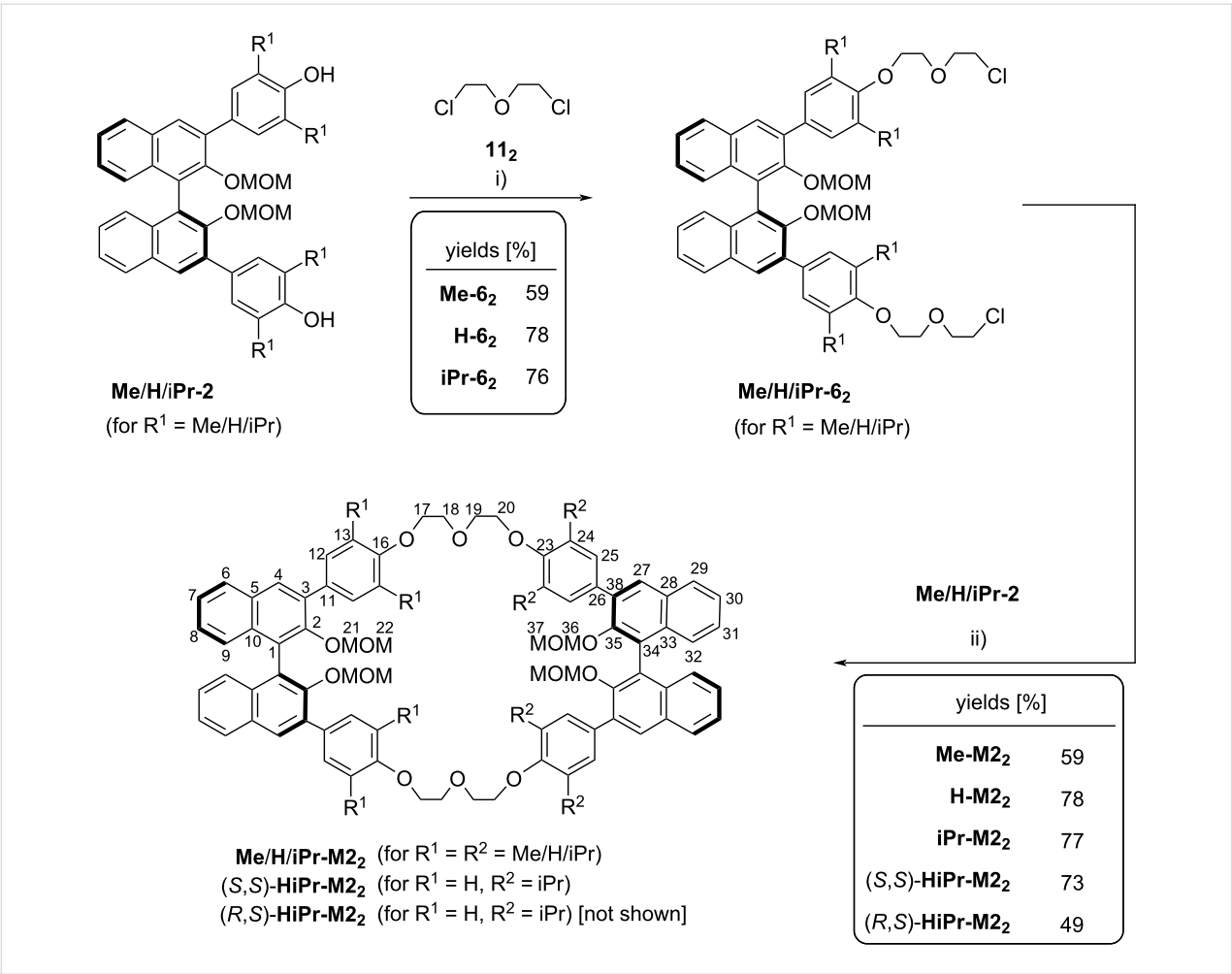

Figure 7: Synthetic route towards macrocycles featuring two BINOL units linked via diethylene glycol spacers. Conditions: i) dichloride **11₂** (2.5 equiv), Cs_2CO_3 (2.5 equiv), CH_3CN, 80 °C (59/78/76% yield for **Me/H/iPr-6₂**; ii) **Me**/(*S*)-**H**/(*R*)-**H/iPr-2** (1.0 equiv), Cs_2CO_3 (3.2 equiv), CH_3CN, 80 °C.

First, we could show that the corresponding diols **Me/H/iPr-2** can be transformed into the corresponding mono-BINOL macrocycles via two-fold Williamson reaction with ethylene glycol bistosylates. Using penta-/hexa-/hepta-/octaethylene glycol bistosylates **8₅/₆/₇/₈**, the corresponding 30/33/36/39-membered macrocycles could be synthesized from all three diols **Me/H/iPr-2**, yielding a library of 12 different mono-BINOL macrocycles. Yields for the macrocyclization step depended strongly on ring size and substitution pattern and ranged from 11–74%.

Second, we could use **Me/H/iPr-2** as starting materials for bis-BINOL macrocycles. Attachment of ethylene glycol chains with suitable leaving groups (tosylate or chloride), followed by macrocyclization with a second equivalent of diols **Me/H/iPr-2** gave access to 4 different hexaethylene glycol-based macrocycles **M2₆** (66-membered rings) and 5 different diethylene glycol-based macrocycles **M2₂** (42-membered rings). Here, the yields for the macrocyclization were consistently high and ranged from 49–78%. In this fashion, we could not only generate the symmetrically tetrasubstituted macrocycles with either hexaethylene glycol linkers (**Me/H/iPr-M2₆**) or diethylene glycol linkers (**Me/H/iPr-M2₂**), but also the unsymmetrically substituted macrocycles **HiPr-M2₆** and **HiPr-M2₂**. Furthermore, the latter compound was generated in both diastereomeric forms, namely (*S*,*S*)- and (*R*,*S*)-**HiPr-M2₂**.

We believe that these systems are highly promising candidates for further application in enantioselective chemosensing or organocatalysis, e.g., after transformation into the corresponding BINOL phosphoric acids. However, at this point, the application of BINOL-based crown ethers with 3,3'-appended ethylene glycol chains remains underdeveloped, partially due to the lack of simple and high-yielding synthetic routes. Thus, we believe that our newly developed optimized synthetic strategy

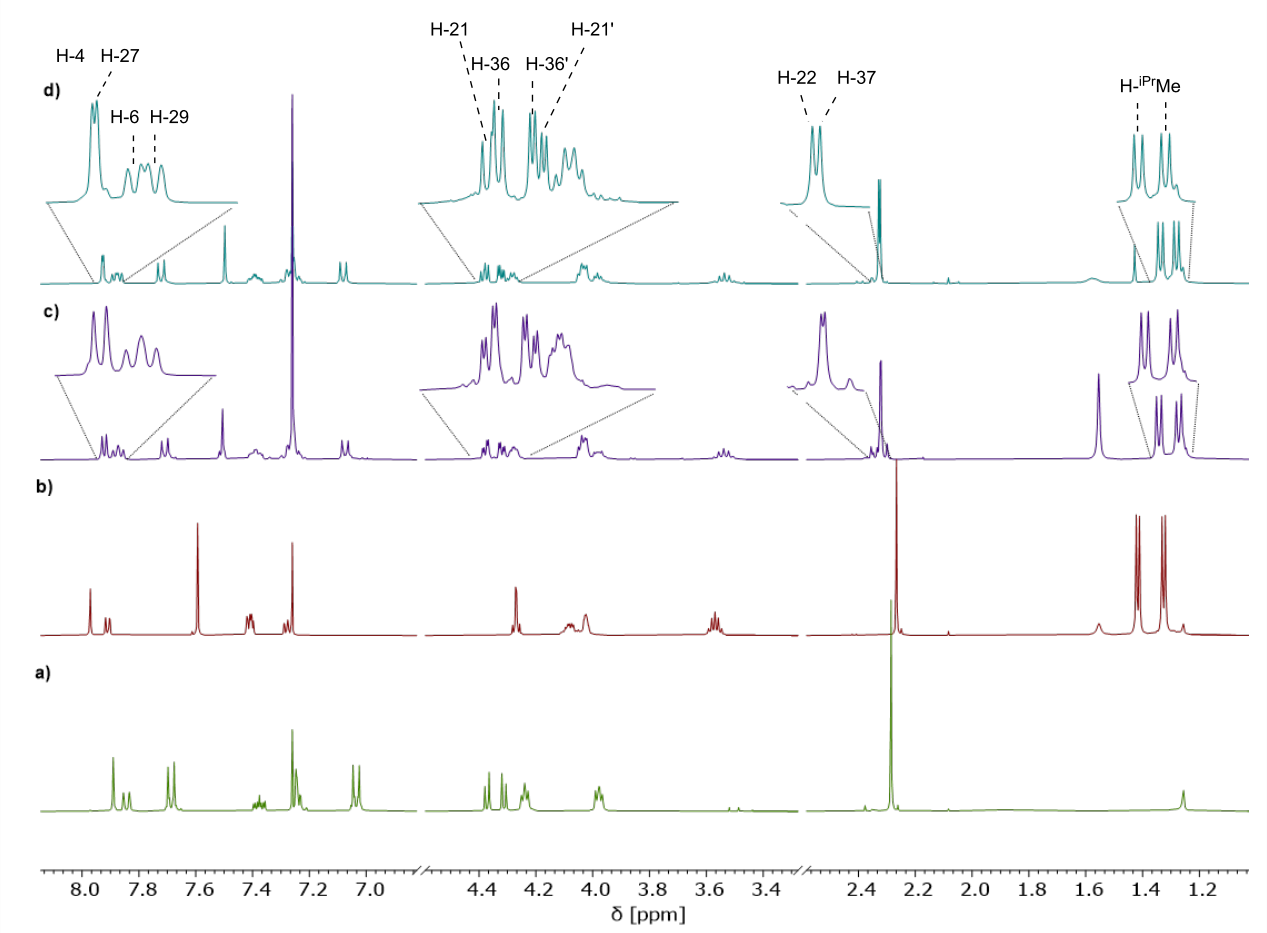

Figure 8: ^{1}H NMR spectra of a) (*S*,*S*)-**H-M2$_2$**, b) (*S*,*S*)-**iPr-M2$_2$**, c) (*S*,*S*)-**HiPr-M2$_2$**, and d) (*R*,*S*)-**HiPr-M2$_2$** (all: 400 MHz, $CDCl_3$, 298 K, for labelling see Figure 7).

will enable further applications of these BINOL-based macrocycles.

Supporting Information

Synthetic procedures and NMR spectra for all new compounds, as well as the crystal structure data for **Me-M1$_6$**. CCDC-2427523 contains the supplementary crystallographic data for this paper. This data can be obtained free of charge from The Cambridge Crystallographic Data Centre via https://www.ccdc.cam.ac.uk/data_request/cif.

Supporting Information File 1

Experimental procedures and characterization data of new compounds.
[https://www.beilstein-journals.org/bjoc/content/supplementary/1860-5397-21-134-S1.pdf]

Supporting Information File 2

Crystallographic Information File (CIF) for the solid-state structure of (*R*)-**Me-M1$_6$**.
[https://www.beilstein-journals.org/bjoc/content/supplementary/1860-5397-21-134-S2.cif]

Funding

J.N. would like to thank the Deutsche Forschungsgemeinschaft DFG (project NI1273/2-2, project NI1273/5-1 and Heisenberg Professorship NI1273/4-1) for funding. S.K. would like to thank the Alexander von Humboldt Foundation for a postdoctoral fellowship.

ORCID® iDs

Jan Riebe - https://orcid.org/0000-0002-5555-5252
Jochen Niemeyer - https://orcid.org/0000-0002-9295-4260

Data Availability Statement

All data that supports the findings of this study is available in the published article and/or the supporting information of this article.

References

1. Steed, J. W.; Atwood, J. L. *Supramolecular Chemistry;* John Wiley & Sons: Chichester, UK, 2009. doi:10.1002/9780470740880
2. Cram, D. J. *Angew. Chem., Int. Ed. Engl.* **1988,** *27,* 1009–1020. doi:10.1002/anie.198810093
3. Lehn, J.-M. *Angew. Chem., Int. Ed. Engl.* **1988,** *27,* 89–112. doi:10.1002/anie.198800891
4. Pedersen, C. J. *Angew. Chem., Int. Ed. Engl.* **1988,** *27,* 1021–1027. doi:10.1002/anie.198810211
5. Behr, J.-P.; Girodeau, J.-M.; Hayward, R. C.; Lehn, J.-M.; Sauvage, J.-P. *Helv. Chim. Acta* **1980,** *63,* 2096–2111. doi:10.1002/hlca.19800630736
6. Behr, J.-P.; Lehn, J.-M.; Vierling, P. *Helv. Chim. Acta* **1982,** *65,* 1853–1867. doi:10.1002/hlca.19820650620
7. Lehn, J.-M.; Sirlin, C. *J. Chem. Soc., Chem. Commun.* **1978,** 949–951. doi:10.1039/c39780000949
8. Lehn, J.-M. *Pure Appl. Chem.* **1979,** *51,* 979–997. doi:10.1351/pac197951050979
9. Jones, B. A.; Bradshaw, J. S.; Izatt, R. M. *J. Heterocycl. Chem.* **1982,** *19,* 551–556. doi:10.1002/jhet.5570190320
10. Izatt, R. M.; Wang, T.; Hathaway, J. K.; Zhang, X. X.; Curtis, J. C.; Bradshaw, J. S.; Zhu, C. Y.; Huszthy, P. *J. Inclusion Phenom. Mol. Recognit. Chem.* **1994,** *17,* 157–175. doi:10.1007/bf00711856
11. Davidson, R. B.; Bradshaw, J. S.; Jones, B. A.; Dalley, N. K.; Christensen, J. J.; Izatt, R. M.; Morin, F. G.; Grant, D. M. *J. Org. Chem.* **1984,** *49,* 353–357. doi:10.1021/jo00176a026
12. Jones, B. A.; Bradshaw, J. S.; Brown, P. R.; Christensen, J. J.; Izatt, R. M. *J. Org. Chem.* **1983,** *48,* 2635–2639. doi:10.1021/jo00164a001
13. Bradshaw, J. S. *J. Inclusion Phenom. Mol. Recognit. Chem.* **1997,** *29,* 221–246. doi:10.1023/a:1007955428644
14. Naemura, K. *Coord. Chem. Rev.* **1996,** *148,* 199–219. doi:10.1016/0010-8545(95)01189-7
15. Bako, P.; Keglevich, G.; Rapi, Z.; Toke, L. *Curr. Org. Chem.* **2012,** *16,* 297–304. doi:10.2174/138527212799499877
16. Cram, D. J.; Helgeson, R. C.; Peacock, S. C.; Kaplan, L. J.; Domeier, L. A.; Moreau, P.; Koga, K.; Mayer, J. M.; Chao, Y. *J. Org. Chem.* **1978,** *43,* 1930–1946. doi:10.1021/jo00404a019
17. Kyba, E. P.; Gokel, G. W.; de Jong, F.; Koga, K.; Sousa, L. R.; Siegel, M. G.; Kaplan, L.; Sogah, G. D. Y.; Cram, D. J. *J. Org. Chem.* **1977,** *42,* 4173–4184. doi:10.1021/jo00862a001
18. Kyba, E. B.; Koga, K.; Sousa, L. R.; Siegel, M. G.; Cram, D. J. *J. Am. Chem. Soc.* **1973,** *95,* 2692–2693. doi:10.1021/ja00789a051
19. Kyba, E. P.; Timko, J. M.; Kaplan, L. J.; de Jong, F.; Gokel, G. W.; Cram, D. J. *J. Am. Chem. Soc.* **1978,** *100,* 4555–4568. doi:10.1021/ja00482a040
20. Newcomb, M.; Toner, J. L.; Helgeson, R. C.; Cram, D. J. *J. Am. Chem. Soc.* **1979,** *101,* 4941–4947. doi:10.1021/ja00511a025
21. Peacock, S. C.; Domeier, L. A.; Gaeta, F. C. A.; Helgeson, R. C.; Timko, J. M.; Cram, D. J. *J. Am. Chem. Soc.* **1978,** *100,* 8190–8202. doi:10.1021/ja00494a029
22. Peacock, S. S.; Walba, D. M.; Gaeta, F. C. A.; Helgeson, R. C.; Cram, D. J. *J. Am. Chem. Soc.* **1980,** *102,* 2043–2052. doi:10.1021/ja00526a046
23. Cram, D. J.; Helgeson, R. C.; Sousa, L. R.; Timko, J. M.; Newcomb, M.; Moreau, P.; de Jong, F.; Gokel, G. W.; Hoffman, D. H.; Domeier, L. A.; Peacock, S. C.; Madan, K.; Kaplan, L. *Pure Appl. Chem.* **1975,** *43,* 327–349. doi:10.1351/pac197543030327
24. Stoddart, J. F. *Top. Stereochem.* **1987,** *17,* 207–288. doi:10.1002/9780470147269.ch3
25. Pu, L. *Chem. Rev.* **1998,** *98,* 2405–2494. doi:10.1021/cr970463w
26. Móczár, I.; Huszthy, P. *Chirality* **2019,** *31,* 97–109. doi:10.1002/chir.23031
27. Yu, S.; Pu, L. *Tetrahedron* **2015,** *71,* 745–772. doi:10.1016/j.tet.2014.11.007
28. Ooi, T.; Maruoka, K. *Angew. Chem., Int. Ed.* **2007,** *46,* 4222–4266. doi:10.1002/anie.200601737
29. Shirakawa, S.; Maruoka, K. *Angew. Chem., Int. Ed.* **2013,** *52,* 4312–4348. doi:10.1002/anie.201206835
30. Zhang, Z.; Shao, Y.; Tang, J.; Jiang, J.; Wang, L.; Li, S. *Green Synth. Catal.* **2021,** *2,* 156–164. doi:10.1016/j.gresc.2021.03.007
31. Schettini, R.; Sicignano, M.; De Riccardis, F.; Izzo, I.; Della Sala, G. *Synthesis* **2018,** *50,* 4777–4795. doi:10.1055/s-0037-1610311
32. Polewski, L.; Springer, A.; Pagel, K.; Schalley, C. A. *Acc. Chem. Res.* **2021,** *54,* 2445–2456. doi:10.1021/acs.accounts.1c00080
33. Hyun, M. H. *J. Chromatogr. A* **2016,** *1467,* 19–32. doi:10.1016/j.chroma.2016.07.049
34. Schalley, C. A. *Mass Spectrom. Rev.* **2001,** *20,* 253–309. doi:10.1002/mas.10009
35. Krajnc, M.; Niemeyer, J. *Beilstein J. Org. Chem.* **2022,** *18,* 508–523. doi:10.3762/bjoc.18.53
36. Goldberg, I. *Acta Crystallogr., Sect. B: Struct. Crystallogr. Cryst. Chem.* **1977,** *33,* 472–479. doi:10.1107/s0567740877003884
37. Tarnowski, T. L.; Cram, D. J. *J. Chem. Soc., Chem. Commun.* **1976,** 661–663. doi:10.1039/c39760000661
38. Liu, Q.-Z.; Xie, N.-S.; Luo, Z.-B.; Cui, X.; Cun, L.-F.; Gong, L.-Z.; Mi, A.-Q.; Jiang, Y.-Z. *J. Org. Chem.* **2003,** *68,* 7921–7924. doi:10.1021/jo034831+
39. Hester, M. R.; Uyeki, M. A.; Diederich, F. *Isr. J. Chem.* **1989,** *29,* 201–212. doi:10.1002/ijch.198900028
40. Diederich, F.; Hester, M. R.; Uyeki, M. A. *Angew. Chem.* **1988,** *100,* 1775–1777. doi:10.1002/ange.19881001217
41. Ito, S.; Koizumi, K.; Fukuda, K.; Kameta, N.; Ikeda, T.; Oba, T.; Hiratani, K. *Tetrahedron Lett.* **2006,** *47,* 8563–8566. doi:10.1016/j.tetlet.2006.09.161
42. Helgeson, R. C.; Tarnowski, T. L.; Cram, D. J. *J. Org. Chem.* **1979,** *44,* 2538–2550. doi:10.1021/jo01328a045
43. Koenig, K. E.; Helgeson, R. C.; Cram, D. J. *J. Am. Chem. Soc.* **1976,** *98,* 4018–4020. doi:10.1021/ja00429a058
44. Kwamen, C.; Niemeyer, J. *Chem. – Eur. J.* **2021,** *27,* 175–186. doi:10.1002/chem.202002876
45. Kauerhof, D.; Niemeyer, J. *ChemPlusChem* **2020,** *85,* 889–899. doi:10.1002/cplu.202000152
46. Kauerhof, D.; Riebe, J.; Vonnemann, C. J.; Thiele, M.; Jansen, D.; Niemeyer, J. *Chem. Commun.* **2024,** *60,* 2393–2396. doi:10.1039/d3cc05482a
47. Pairault, N.; Zhu, H.; Jansen, D.; Huber, A.; Daniliuc, C. G.; Grimme, S.; Niemeyer, J. *Angew. Chem., Int. Ed.* **2020,** *59,* 5102–5107. doi:10.1002/anie.201913781
48. Jansen, D.; Gramüller, J.; Niemeyer, F.; Schaller, T.; Letzel, M. C.; Grimme, S.; Zhu, H.; Gschwind, R. M.; Niemeyer, J. *Chem. Sci.* **2020,** *11,* 4381–4390. doi:10.1039/d0sc01026j

49. Mitra, R.; Zhu, H.; Grimme, S.; Niemeyer, J. *Angew. Chem., Int. Ed.* **2017,** *56,* 11456–11459. doi:10.1002/anie.201704647
50. Mitra, R.; Thiele, M.; Octa-Smolin, F.; Letzel, M. C.; Niemeyer, J. *Chem. Commun.* **2016,** *52,* 5977–5980. doi:10.1039/c6cc01980c
51. Thiele, M.; Rose, T.; Lökov, M.; Stadtfeld, S.; Tshepelevitsh, S.; Parman, E.; Opara, K.; Wölper, C.; Leito, I.; Grimme, S.; Niemeyer, J. *Chem. – Eur. J.* **2023,** *29,* e202202953. doi:10.1002/chem.202202953
52. Wu, T. R.; Shen, L.; Chong, J. M. *Org. Lett.* **2004,** *6,* 2701–2704. doi:10.1021/ol0490882
53. Lee, J. C.; Yuk, J. Y.; Cho, S. H. *Synth. Commun.* **1995,** *25,* 1367–1370. doi:10.1080/00397919508013838
54. Ostrowicki, A.; Koepp, E.; Vögtle, F. *Top. Curr. Chem.* **1992,** *161,* 37–67. doi:10.1007/3-540-54348-1_7
55. van Keulen, B. J.; Kellogg, R. M.; Piepers, O. *J. Chem. Soc., Chem. Commun.* **1979,** 285–286. doi:10.1039/c39790000285
56. Brodt, N.; Niemeyer, J. *unpublished results.*

License and Terms

BEILSTEIN JOURNAL OF ORGANIC CHEMISTRY

Research progress on calixarene/pillararene-based controlled drug release systems

Liu-Huan Yi, Jian Qin, Si-Ran Lu, Liu-Pan Yang*, Li-Li Wang* and Huan Yao*

Review

Open Access

Address:
School of Pharmaceutical Science, Hengyang Medical School, University of South China, Hengyang 421001, China

Email:
Liu-Pan Yang* - yanglp@usc.edu.cn; Li-Li Wang* - wangll@usc.edu.cn; Huan Yao* - yaoh@usc.edu.cn

* Corresponding author

Keywords:
aromatic macrocycle; controlled-release drug delivery systems; stimulus response; supramolecular chemistry

Beilstein J. Org. Chem. **2025,** *21,* 1757–1785.
https://doi.org/10.3762/bjoc.21.139

Received: 21 March 2025
Accepted: 15 August 2025
Published: 03 September 2025

This article is part of the thematic issue "Novel macrocycles: from synthesis to supramolecular function".

Guest Editor: C. Gaeta

Abstract

Intelligent controlled-release drug delivery systems that are responsive to various external stimuli have garnered significant interest from researchers and have broad applications in the biomedical field. Aromatic macrocycles, including calixarenes and pillararenes, are considered ideal candidates for the construction of supramolecular drug delivery systems because of their simple synthesis, ease of modification, electron-rich and hydrophobic cavities, and highly selective molecular recognition. In recent years, numerous supramolecular drug delivery systems utilizing aromatic macrocycles have been developed. This review article provides an overview of the advancements of controlled drug release systems based on host–guest selective recognition, self-assembly, and nano-valves by the use of of calixarenes and pillararenes from five perspectives: pH, light, enzyme, hypoxia, and multi-stimuli combination responses. Furthermore, the article projects the future clinical application prospects of controlled-release technologies, with the aim of offering a reference for the utilization of aromatic macrocycles in drug-controlled release applications.

Introduction

Drugs are defined by the Food and Drug Administration (FDA) as substances used for diagnosing, relieving, treating, or preventing diseases [1]. Traditional forms of drugs typically have a systemic effect, reaching both healthy and diseased areas, leading to a lack of selectivity, low bioavailability, and limited efficacy [2-4]. Nowadays, there are technologies that can better confine the action of drugs to where they are needed. Drug delivery is a technology that administers drugs to patients, which can specifically increase the concentration of drugs in certain parts of the body, thereby enhancing the therapeutic effect [5]. However, conventional drug delivery systems (such as capsules [6], tablets [7], ointments [8], etc.) have poor bioavailability, with fluctuating plasma drug levels and an inability to achieve sustained release. The emergence of con-

trolled-release drug delivery systems has provided the possibility to improve patients' adaptability to medications [8-10]. By using biomedically compatible materials to carry drugs, these systems can release drugs at a controlled, uniform rate, maintaining stable blood drug concentrations, thereby fully exerting the therapeutic effects of the drugs [11-13]. The technology for modern controlled-release drug delivery systems began with the launch of Spansule sustained-release capsules in 1952. Since then, the development of various drug delivery systems has accelerated significantly over the past few decades. These systems include dissolution-controlled, diffusion-controlled, osmotic-controlled (which encompasses osmotic pressure and swelling control), chemically controlled, nanoparticle systems, and supramolecular controlled-release systems. Among these, supramolecular controlled-release systems have advantages such as dynamic adjustability, stimulus responsiveness, specific recognition and binding, and multi-target synergistic action [14-16]. These characteristics enable precise control of drug release and targeted drug delivery, thereby improving drug stability and bioavailability, and reducing drug toxicity and side effects.

Supramolecular chemistry, with molecular recognition at its core [17], utilizes non-covalent interactions such as electrostatic interactions, hydrogen bonding [18], and hydrophobic effects to provide valuable tools for developing new biomaterials and drug delivery systems [18-22]. This article categorizes supramolecular chemistry-based drug-controlled release systems into the following three mechanisms: (1) Drugs are identified and combined with supramolecular hosts through host–guest interactions [23-28]. By adjusting the conditions surrounding the guest molecules, such as changes in pH, light, and enzyme activity, the binding affinity between the guest and host molecules can be altered, thereby achieving controlled drug release and targeted delivery. (2) Drugs are loaded into self-assembled host–guest systems [29-32]. The chemical structure or properties of the host or guest molecules are altered upon exposure to specific stimuli, such as light, pH changes, or enzymes. This modification induces the disassembly of the host–guest complex, thereby releasing the encapsulated drugs. Fundamentally, this mechanism relies on controlling the assembly and disassembly processes. For example, supramolecular self-assembly technology enhances the targeting of chemotherapeutic drugs to tumor tissues, reducing systemic adverse reactions. (3) Macrocyclic aromatic supramolecular nano-valves have a pseudo-rotaxane structure with host–guest coordination and the kinetic properties of supramolecular interactions [33,34]. Different external stimuli, including pH changes, enzymes, light irradiation, hypoxia, and multi-stimuli responses, can alter the supramolecular structure or binding affinity to activate the opening and closing of the nano-valves. In addition to the three mechanisms that will be detailed in this article, researchers have made progress in the transport of amino acids and molecular peptides across membranes using macrocycles in recent years [35-37]. These works have paved the way for the potential application of remote-controlled membrane transport technology in the field of hydrophilic functional biomolecules, and is expected to be applied to stimulus-responsive controlled drug transport across membranes in the future. Currently, various artificially synthesized macrocyclic hosts have found extensive applications in drug-controlled release systems, for example, classic macrocycles like cyclodextrins [38] and cucurbiturils [39]. In recent years, aromatic macrocycles such as calixarenes (CAs) [40] and pillararenes (PAs) [41] have attracted widespread attention from the industry and scientists due to their simple synthesis which only require a one-step synthesis, convenient modification that can be achieved by introducing functional groups, electron rich and hydrophobic cavities that can effectively recognize electron deficient or neutral guest molecules, and high selectivity in binding with the guest. Their applications are extensive in the domain of drug-controlled release.

This article mainly reviews the supramolecular drug delivery systems constructed from aromatic macrocycles (Figure 1). These systems achieve intelligent control over drug release through reasonable manipulation of stimuli, including external factors such as pH, light, enzymatic activity, hypoxia-triggered, and multi-responsive triggers. This article, based on the mechanisms of host–guest recognition, multifunctional assembly, and supramolecular nano-valves, provides several representative examples of CAs and PAs in the field of drug-controlled release. Finally, the article looks forward to future developments in this research area.

Review

1 Aromatic macrocycles for host–guest drug release systems

Aromatic macrocycles are highly valuable in fields such as chemistry, materials science, and life science due to their rigid, electron-rich and hydrophobic cavities, and ease of modification [42]. Among these, CAs and PAs are representative aromatic macrocycles. They can be made water-soluble and exhibit good biocompatibility through carboxyl or phosphate group modification, showing great potential in biomedical carrier applications. Compared with other artificial macrocycles such as crown ethers [43], cyclodextrins, and cucurbiturils, CAs and PAs have unique advantages. Their synthesis is simple (one-step completion), and they have adjustable conformations and π-electron-rich cavities [44,45], enabling efficient recognition of electron-deficient or neutral guest molecules and high-selec-

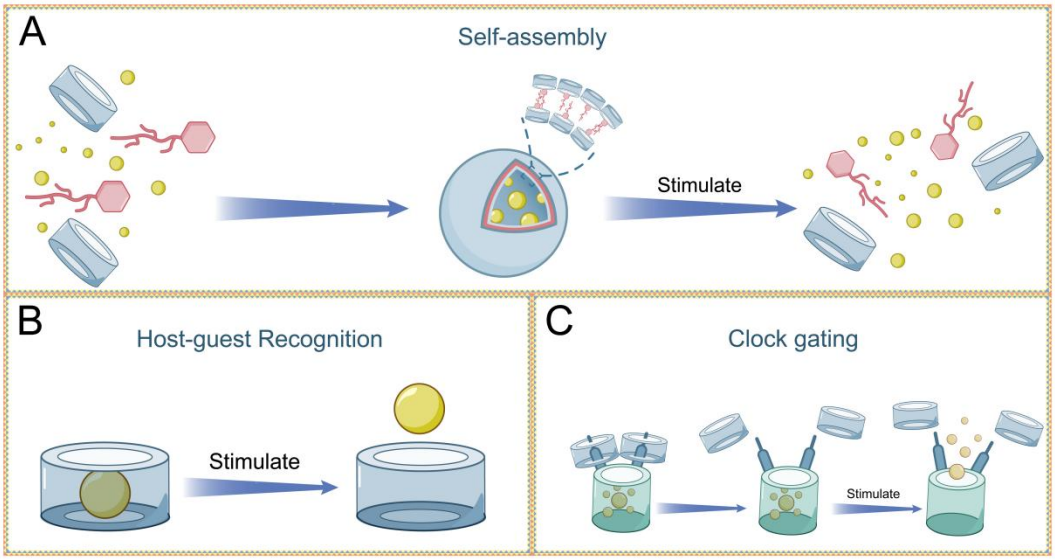

Figure 1: Schematic diagram of drug-controlled release mechanisms based on aromatic macrocycles.

tivity binding in drug-controlled release. Many calix/pillar[*n*]arene hosts are soluble in water, particularly macrocycles that are modified with carboxyl and phosphate groups. Moreover, their amphiphilic modification ability allows easy self-assembly into functional materials like vesicles, micelles and nanoparticles, overcoming the difficulties in modifying cyclodextrin and cucurbituril. These features make CAs and PAs promising candidates for stimulus responsive drug release systems [46]. Their structural diversity and functional designability offer broad prospects for targeted applications. This section will focus on the structural features and applications of CAs and PAs.

1.1 CAs: structure and properties

CAs are the third generation of supramolecular hosts [40], succeeding cyclodextrins and crown ethers. They are macrocycles composed of phenolic units condensed with formaldehyde, connected via methylene bridges. The most common CAs usually consist of 4, 6, or 8 phenolic units (Figure 2) [47-53]. The upper rim of CAs is equipped with hydrophobic alkyl groups, which, together with the benzene rings, form a hydrophobic cavity. In contrast, the lower rim consists of a series of neatly arranged hydrophilic phenolic hydroxy groups that can be selectively modified through chemical reactions [49].

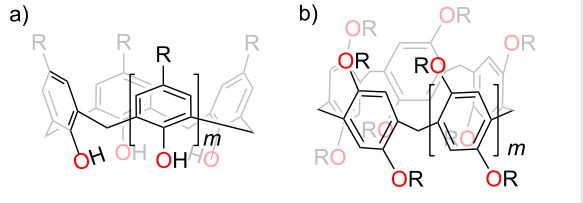

Figure 2: Chemical structure of a) calix[*n*]arene (*m* = 1,3,5), and b) pillar[*n*]arene (*m* = 1,2,3).

CAs feature large hydrophobic cavities whose size can be precisely modulated by varying the number of aromatic rings. This structural tunability enables the cavities of CAs to selectively bind drugs of different sizes through hydrophobic and π–π stacking interactions and undergo targeted modifications to enhance their affinity for various guest molecules, such as choline [54], quaternary ammonium salts [55], drug molecules [56], etc. Although they generally have poor solubility, this can be improved through derivatization. Water-soluble calixarene derivatives can be obtained through functional modifications, including the introduction of sulfonic acid, amine, and carboxylic acid groups [57-59]. These water soluble macrocycle derivatives can be used to increase the solubility of drugs. The modified CAs encapsulate drug molecules within the host through host–guest interactions. The interactions between the drug and the calixarene enhance the solubility of the drug [60]. Further functionalization of these CAs' upper and lower rims with diverse moieties (e.g., amides, imines, sulfur-containing groups, or alkyl chains) significantly expands their multifunctionality and broadens their application scope. Notably, CAs can be readily modified into amphiphilic macrocycles that can self-assemble with guests, and it exhibits superior advantages over crown ethers and cyclodextrins in terms of controllable functionalization [61]. In clinical applications, particularly for anticancer drug conjugation, CAs demonstrate remarkable cancer cell selectivity, minimized off-target effects, enhanced delivery efficiency, and reduced systemic toxicity. Additionally,

their synthetic accessibility, structural adaptability, and responsiveness to external stimuli (pH, light, enzyme, hypoxia) facilitate sustained drug release, side effect mitigation, and therapeutic efficacy, making them increasingly prominent in drug carrier research.

In recent years, the diversity of supramolecular amphiphiles has significantly expanded, bringing revolutionary breakthroughs to drug delivery systems. These structures, which possess both hydrophobic and hydrophilic characteristics, can self-assemble through non-covalent interactions to form well-defined aggregates such as micelles, vesicles, and nanoparticles [62]. Their morphologies mainly depend on molecular structure, concentration, and environmental properties. The cylindrical geometry of vesicles [63] promotes the arrangement of amphiphilic molecules with their hydrophobic tails pointing inward and hydrophilic heads pointing outward, forming a closed bilayer [64]. In contrast, micelles are usually assembled from single-tailed, conical molecules, where the smaller hydrophobic chains and larger head groups form monolayer spherical or rod-like structures [65]. Moreover, nanoparticles can be constructed through the physical or chemical cross-linking of polymers (such as PLGA and PEG), inorganic materials (such as gold and silica), or biomolecules (lipids and proteins), enabling efficient drug loading and controlled release [66-68]. Among them, amphiphilic CAs that incorporate both hydrophilic groups and hydrophobic alkyl chains through dual modifications [69]. These derivatives have emerged as a research hotspot due to their unique combination of water solubility, biocompatibility, and host–guest encapsulation capability [47,52,70]. The aggregation behavior of amphiphilic CAs is closely related to the size of the macrocycle, the length of the alkyl chain, and the nature of the polar head group [71]. Compared with traditional surfactants, amphiphilic CAs have a lower critical micelle concentration and are more likely to self-assemble into various forms of aggregates, such as spherical micelles [72], vesicles, and spherical nanoparticles [73]. Calixarene-based amphiphiles are characterized by their low cytotoxicity and ability to load drugs. The structure of calixarene-drug complexes can respond to external stimuli, causing the self-assembled complex to disassemble, which enables sustained drug release. Based on these characteristics, CAs hold potential for applications in drug delivery systems.

1.2 PAs: structure and properties

Since Ogoshi et al. first introduced pillar[*n*]arenes in 2008, these macrocycles have become essential to the synthetic macrocyclic receptor field [74]. Research on PAs and their derivatives has become a hot topic [75]. PAs can be prepared via the Friedel–Crafts condensation, which involves combining 1,4-dimethoxybenzene with paraformaldehyde in the presence of a Lewis acid. The central axis of these aromatic hydrocarbon molecules possesses *n* fold rotational symmetry [76]. PAs possess highly modifiable ring positions, and many PA derivatives with different functional groups can be obtained through the cyclization reaction of 1,4-dialkoxybenzene monomers or post-synthetic modification reactions [74]. PAs possess a unique internal cavity characterized by an electron-rich and hydrophobic environment, which significantly enhances the density of π-electrons. This structural feature makes pillar[*n*]arenes particularly effective at encapsulating guest molecules that are either electron-deficient or neutral. For example, pillar[5]arene (PA5) has a strong binding affinity for neutral guest molecules in organic solvents, [77] which is not feasible for crown ethers, CAs, and resorcinarenes. In addition, PAs can form supramolecular systems in the following ways: (1) the electron-rich cavity interacts electrostatically with cationic guests, such as methyl viologen derivatives, pyridinium salts, and quaternary ammonium salts [78]. (2) After modification with cationic groups, they can bind with anionic molecules, such as sulfonates [79]. It is worth mentioning that the cavity of PAs can encapsulate photo-responsive guests such as cationic azobenzene derivatives, providing new ideas for the innovation of drug design and therapeutic strategies. Notably, PA derivatives also exhibit specificity in recognizing important molecules in biological processes, such as acetylcholine [80], amino acids [81], doxorubicin (DOX) [82] and antibiotics [83], etc. Among the many derivatives, water-soluble pillar[5]arene (WP5) and pillar[6]arene (WP6) have become representative systems for biomedical applications due to their excellent performance in drug-controlled release [84,85].

Recent research on drug delivery has focused more on amphiphilic PAs, which are mainly constructed through two strategies: one is self-assembly after separately modifying hydrophobic and hydrophilic segments; the other is the formation of host–guest complexes between water-soluble PAs and guest molecules containing hydrophobic chains, followed by self-assembly into bilayer vesicles through host–guest interactions, hydrophobic effects, and π–π stacking interactions [86]. Their amphiphilic nature enables these systems to enter cells efficiently through endocytosis, providing a new drug delivery approach and holding great potential in precision medicine due to their programmable and stimulus-responsive features.

Additionally, PAs can be hybridized with various inorganic materials, such as metal-organic frameworks (MOFs), mesoporous silica nanoparticles (MSNs), metal nanoparticles, and carbon materials [87]. By designing through electrostatic and non-covalent interactions, PAs can be used as "molecular switches" to construct mechanized MOFs with the framework of MOFs, realizing the controlled release of drugs [88]. When integrated

with MSNs, nano valves consist of a mobile macrocyclic host that moves along a linear molecule between two or more binding sites. This movable macrocycle acts as a gate, controlling the movement of cargo into and out of the MSN pores [89]. These materials, with their ideal host–guest recognition characteristics, have provided new ideas for the design and synthesis of nano valve systems. These composite materials not only have the advantages of high specific surface area and large pore volume for drug loading, but also their unique stimulus responsive characteristics break through the limitations of traditional delivery systems: The pH, Zn^{2+}, and competitive agent-responsive characteristics can disrupt the multi-responsive supramolecular nanovalve systems based on PA5, primarily by disrupting the high-affinity host–guest interactions between PA5 and these groups (mainly through phosphonate-quaternary ammonium ion pairing) [90]. Azobenzene guest molecules can achieve dual functions (on and off) as ligands through photo-induced cis-trans isomerization. Using pillar[6]arene as the ion channel, the host–guest complexation realizes a reversible ON-OFF-ON type pseudo-monomeric ligand-gated ion transport switch [91]. The development of these pillararene-based materials has enriched the dynamic regulation methods of supramolecular structures and provided innovative approaches for prodrug design.

2 Stimulus-responsive controlled release in supramolecular systems

Many efforts have been made to prepare stimulus-responsive drug carriers, including some aimed at disease-related stimuli [92]. In the field of supramolecular materials, various stimulus strategies have been introduced to regulate the construction and destruction of aromatic macrocycles and their components. The external triggers include: pH [93], oxidation–reduction states [94], enzymatic actions [95], and light [96]. Specifically, within host–guest frameworks, the capability to meticulously regulate the assembly of complexes and synchronize them with biologically pertinent or biocompatible stimuli holds substantial potential for augmenting the precision of therapeutic interventions [97,98]. In certain scenarios, these stimuli precipitate reversible alterations in the formation of host–guest complexes, while in other cases, they may catalyze irreversible disintegration to avert reversibility. Given the benefits of the chemical stability of most aromatic macrocycles, creating stimulus-responsive complexes usually requires the guest components to undergo stimulus-triggered changes that affect their ability to bind with the host macrocycles. The controllable release of drugs is one of the most important applications of stimulus-responsive supramolecular systems and contributes to targeted therapy. Drugs are loaded into supramolecular nanosystems formed by self-assembled host–guest systems. Under specific stimuli (light, enzymes, hypoxia, pH values, etc.), changes in the host or guest molecules' chemical structure or properties lead to the host–guest system's disassembly, thereby releasing the drugs from the supramolecular systems [99]. Thus, the core principle of controlled release lies in modulating the association and dissociation of host–guest interactions. Aromat-containing macrocycles, such as CAs and PAs, are deemed exceptional hosts for fabricating host–guest nanosystems due to their versatile characteristics and capacity to self-assemble into supramolecular architectures via non-covalent interactions. These host–guest nanosystems play a vital role in controlled release, nanotechnology, materials chemistry, artificial molecular machines, and synthetic ion channels. Numerous host–guest systems have been developed based on their responsiveness to particular external triggers, including pH, enzymes, hypoxia, and light. The following section will review and discuss some of the stimulus responses.

2.1 pH-responsive controlled release

Changes in acidity are a typical stimulus for adjusting host–guest supramolecular nanosystems. It is widely recognized that the acidity levels of various organs, tissues, and cellular compartments differ. For example, the acidity of tumor and inflamed tissues is distinct from that of healthy tissues, offering a potential physiological trigger for pH-responsive drug delivery. Thus, drug release can be regulated by leveraging the variations in acidity between normal and diseased cells [100]. Developing therapeutic materials that react to shifts in pH, particularly the acidification arising from the endocytic pathway of internalized carriers or disease-induced acidification in local tissue microenvironments, is a prevalent approach for fabricating stimulus-sensitive drug carriers. Consequently, the construction of pH-responsive systems based on aromatic macrocycles has been widely promoted, with typical water-soluble carboxylated PAs and CAs frequently employed as host molecules or structural components [100]. This section will examine cases of pH-dependent degradation and drug release mechanisms.

Amphoteric CAs, known for their effective hydrophobic drug-loading capabilities, offer an excellent platform for controlled drug release. Researchers have synthesized amphoteric CAs to introduce pH-responsive properties, allowing each macrocycle to possess positively and negatively charged gates. Amphoteric CA8 were prepared by introducing positively charged groups at the lower rim of sulfonated CA8. The cavity size of the water-soluble CA8 matches with the hydrophobic drug ciprofloxacin (CPF). The efficient encapsulation of CPF (with a loading capacity of 17.8–24.5%) is achieved through the synergistic action of hydrophobic interactions and hydrogen bonding. Under physiological pH conditions (7.0–7.6), the CA8-CPF complex self-assembles into a stable multilayer structure

through electrostatic interactions. When the environmental pH deviates from the neutral range (pH < 6.0 or pH > 8.0), the charge balance is disrupted, leading to the dissociation of the complex and the release of the drug. This pH-sensitive "charge switch" mechanism enables CA8 to precisely control the release behavior of CPF, providing new insights for the development of environmentally responsive antibiotic delivery systems (Figure 3) [101]. This pH-sensitive "charge switch" mechanism enables CA8 to precisely control the release behavior of CPF, providing new insights for the development of environmentally responsive antibiotic delivery systems.

Water-soluble aromatic macrocycles are commonly utilized in drug delivery systems. Vesicles are valuable tools in biology, chemistry, and materials science. Supramolecular pH stimuli-responsiveness has applications at the cellular level and has the potential for controlling drug release in environmental protection. In 2012, Huang and colleagues [78] described the construction of supramolecular vesicles using WP6 and pyridine derivatives (G1) (Figure 4). This supramolecular system achieves controllable assembly and disassembly through pH responsiveness: under acidic conditions (pH 6.0), protonation of the WP6 carboxyl groups leads to vesicle disassembly; whereas in a neutral environment (pH 7.4), deprotonated WP6 can rebind with the guest molecules. The molecular recognition mechanism of this system is based on the synergistic effect of multiple non-covalent interactions, including electrostatic attraction, hydrophobic interactions, and π–π stacking. Researchers have further utilized this feature to achieve reversible transformation of amphiphilic guest molecules between micellar and vesicular states and have successfully applied it to the controlled release of dye molecules. Notably, the system can also effectively neutralize the toxicity of paraquat through host–guest interactions, providing a new approach for the treatment of environmental pollutants. This pH-responsive supramolecular platform shows broad application prospects in targeted drug delivery and environmental remediation.

Later, in 2014, Huang and colleagues synthesized a water-soluble pillar[7]arene (WP7) by adding 14 anionic carboxylic acid groups to both sides [102]. They explored the pH-dependent complexation of WP7 with paraquat derivative G1 in water. The host WP7 and guest G1 form a 1:1 pseudorotaxane, with an association constant of $(2.96 \pm 0.31) \times 10^5$ M^{-1}. Furthermore, they leveraged this new molecular recognition motif to create a supramolecular amphiphilic reagent using WP7 and an amphiphilic paraquat derivative G2. This pH-responsive drug delivery system has considerable potential for future medical applications. Hydrophilic supramolecular polymers that respond to stimuli, especially those formed in aqueous solutions, are poten-

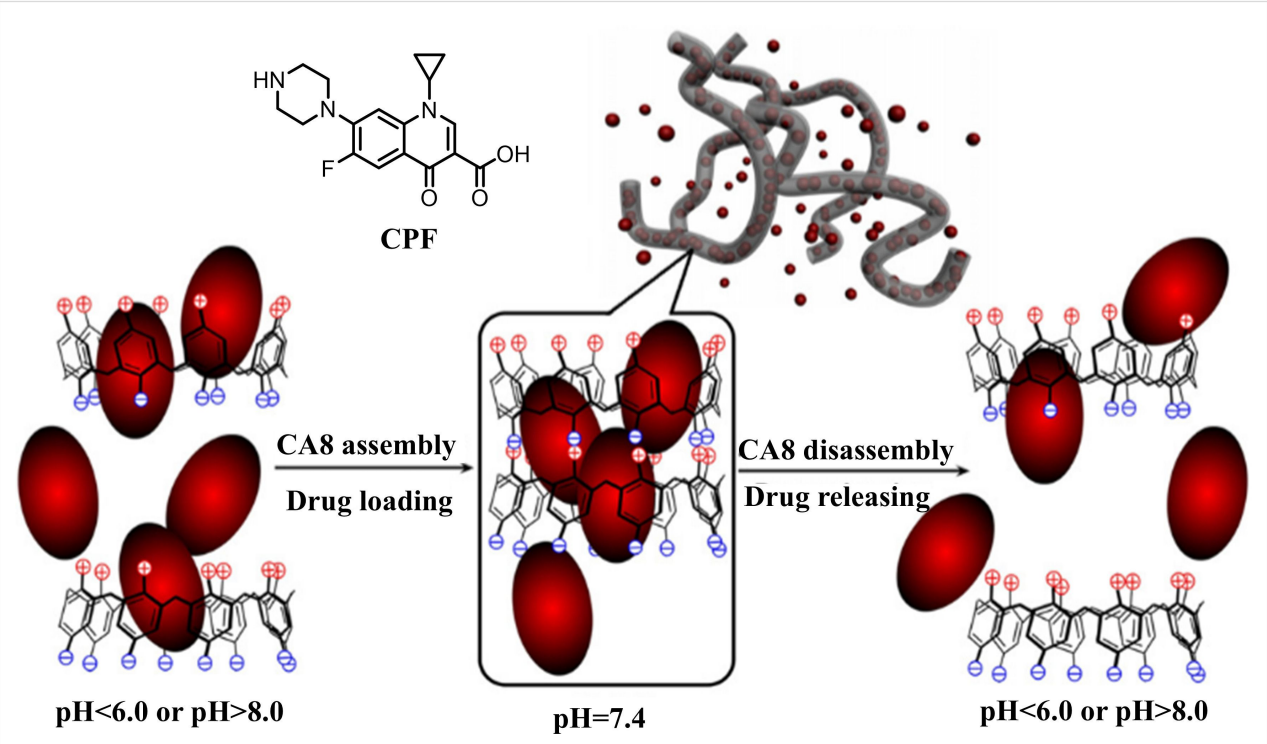

Figure 3: Changes in pH conditions cause the release of drugs from CA8 host–guest complexes [101]. Figure 3 was adapted with permission from [101], *Colloids and Surfaces B: Biointerfaces*, vol. 101, by Y. Xue; Y. Guan; A. Zheng; H. Xiao, "Amphoteric calix[8]arene-based complex for pH-triggered drug delivery", pages 55–60, Copyright (2012), with permission from Elsevier. This content is not subject to CC BY 4.0.

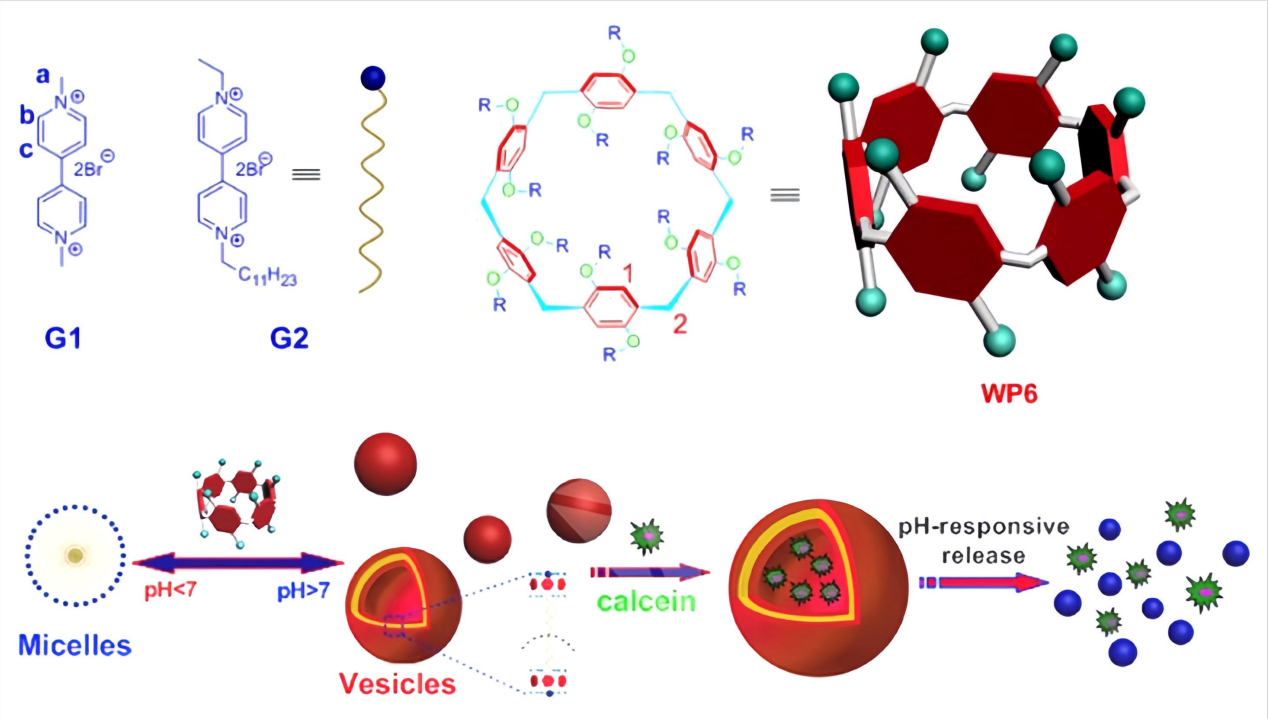

Figure 4: The illustration of the pH-mediated 1:1 complex formation between the host and guest molecules in aqueous solution, along with the pH-triggered release mechanism [78]. Figure 4 was adapted with permission from [78], Copyright 2012 American Chemical Society. This content is not subject to CC BY 4.0.

tial candidates for mimicking biocompatibility or creating important functional materials.

In 2021, Maiti et al. employed small-molecule mannose-modified CA4 to create the core structure CA4-Man3 and produce nano-micelles known as CA4-Man3-NPs (Figure 5) [103]. CA4-Man3-NPs achieve efficient targeted drug delivery through a unique self-assembly mechanism. This system leverages the unique polymeric characteristics of CA4, which reduces the critical aggregation concentration and enhance intermolecular orderliness to form structurally stable nanocarriers [52]. The key design features are: 1) The mannose groups at the upper rim confer specific recognition ability for cancer cell surface receptors; 2) The hydrophobic core formed by the alkyl chains at the lower rim and the hydrogen-bonding network constructed by the thiourea unit can efficiently encapsulate DOX. This structure integrates multiple non-covalent interactions, such as hydrophobic interactions and π–π stacking, endowing the micelles with both structural stability and pH responsiveness. When targeted to the tumor microenvironment (acidic pH), the core of the micelles dissociates to achieve specific release of DOX, significantly improving the delivery efficiency and tumor targeting of hydrophobic drugs.

The release of DOX from PAs also can be regulated by a pH-responsive mechanism. In 2015, Wang and coworkers synthesized a novel supramolecular prodrug nanoparticle exploiting the host–guest interactions between WP6 and DOX-derived prodrugs (Figure 6) [104]. As demonstrated in previous studies, WP6 has shown good biocompatibility and acid-responsive properties in aqueous media [78,105]. Meanwhile, it has been proven that WP6 has a strong binding [106,107] affinity for pyridinium salts in water driven by hydrophobic and electrostatic interactions. DOX-based prodrugs are synthesized by directly conjugating hydrophobic DOX with pyridinium-modified flexible alkyl chains (G3) or short EGn (ethylene glycol) chains (G4) via acid-cleavable hydrazone bonds. The above-mentioned WP6-G3 and WP6-G4 supramolecular complexes, based on their amphiphilic nature, have the ability to form higher-order aggregates in weakly alkaline phosphate-buffered saline (PBS). The resulting supramolecular nanoparticles exhibited stability under physiological conditions. The cumulative release of DOX reached nearly 100% within 30 minutes at a pH of 5.5, which simulates the lysosomal environment at 37 °C. Both CAs and PAs are effective supramolecular platforms for the controlled release of DOX, demonstrating significant potential for various applications.

In 2013, Wang and others reported [93] that WP6 and hydrophobic ferrocene derivatives (FC) self-assembled into supramolecular vesicles loaded with mitoxantrone (MTZ) exhibiting significant pH-responsive behavior in aqueous solutions, excep-

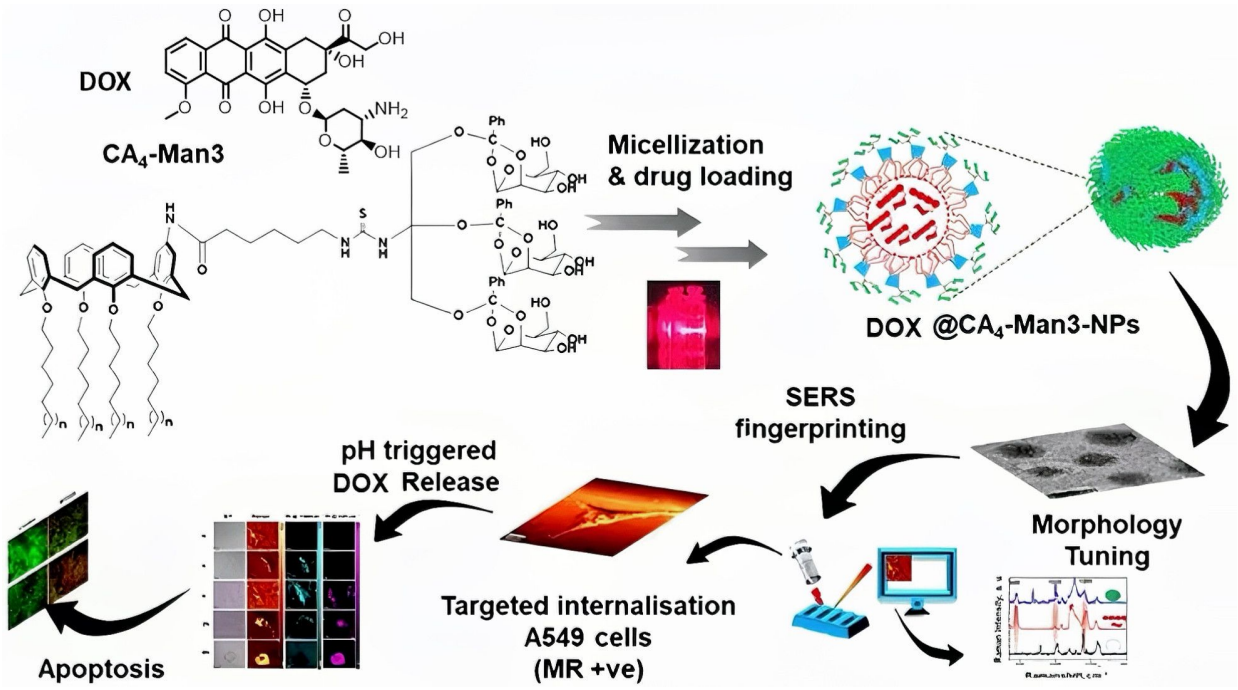

Figure 5: Illustration of the pH-responsive self-assembly of mannose-modified CA4 into micelles and the subsequent release of DOX [103]. Figure 5 was adapted with permission from [103], *Journal of Controlled Release*, vol. 339, by Sreedevi, P.; Nair, J. B.; Joseph, M. M.; Murali, V. P.; Suresh, C. H.; Varma, R. L.; Maiti, K. K, "Dynamic self-assembly of mannosylated-calix [4] arene into micelles for the delivery of hydrophobic drugs", pages 284–296, Copyright (2021), with permission from Elsevier. This content is not subject to CC BY 4.0.

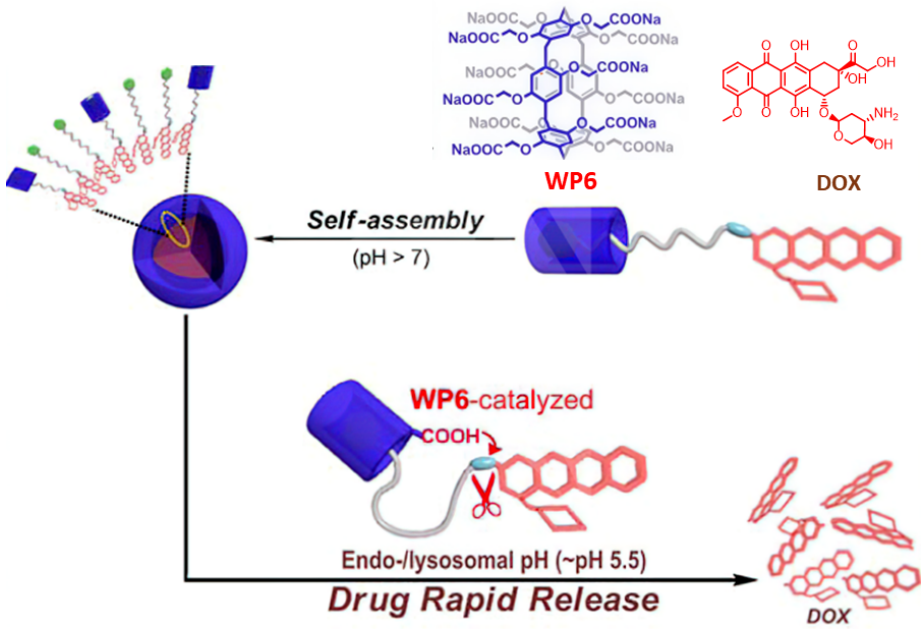

Figure 6: Illustration of the assembly of supramolecular prodrug nanoparticles from WP6 and DOX-derived prodrugs (G3 and G4) for WP6-mediated rapid release of the drug [104]. Figure 6 was adapted with permission from [104], Copyright 2015 American Chemical Society. This content is not subject to CC BY 4.0.

tionally rapid release of MTZ in a low pH environment (Figure 7). The complex exhibits significant amphiphilicity: the carboxylate residues of WP6 confer hydrophilicity, while the alkyl chains of FC contribute hydrophobicity, driving the molecules to self-assemble into supramolecular vesicles in the aqueous phase. The vesicle structure features a bilayer characteristic, with two hydrophilic carboxylate shell layers enveloping a hydrophobic alkyl chain core. The assembly driving force directly relies on the host–guest interaction between WP6 and FC. Further studies have shown that by regulating the deprotonation/protonation state of the WP6 carboxyl groups through pH control, the reversible dissociation and reassembly of the vesicle structure can be achieved, thereby constructing a pH-responsive drug carrier. The novel supramolecular vesicles assembled from WP6 and guest molecules in aqueous environments are promising for controlled release and drug delivery applications. They have established a foundation for pH-responsive controlled release systems based on WP6, encouraging increased research participation within this domain.

Photothermal construction and manipulation of optical materials are crucial in pharmaceutical or biological fields. In 2016, Zhang and colleagues [108] developed a supramolecular nanovesicle with improved photodynamic therapy (PDT) capabilities. This system was based on the host–guest interactions between polyethylene glycol-functionalized pillar[5]arene (PEG-P[5]A) and a pyridinium-capped porphyrin derivative containing a disulfide bond (TPPC6-SS-Py). The supramolecular amphiphile could self-assemble into spherical micelles, demonstrating excellent colloidal stability in aqueous solutions, as evidenced by transmission electron microscopy (TEM) and dynamic light scattering (DLS). The PEG-P[5]A/TPPC6-SS-Py micelles showed rapid release of the porphyrin photosensitizer under reducing conditions. Furthermore, in 2023, Zhang and colleagues [109] constructed a tumor microenvironment (TME)-activated supramolecular nanoplatform (Figure 8) which was consisted of a pillar[5]arene-based amphiphilic polymer (POPD), a phototherapeutic agent (Cy7-CN), an antimalarial drug with respiratory function (atovaquone, ATO), and a chemotherapeutic agent (pyridinium camptothecin, CPT-Py). This platform was designed for imaging-guided phototherapy to alleviate hypoxia. They created a new supramolecular amphiphile that enabled rapid drug release and efficient cellular internalization, potentially providing a robust platform for drug delivery and controlled release systems.

The excellent biocompatibility of both supramolecular vesicles and nano-fragments with the body indicates that aromatic macrocycles have great potential for biomedical applications. These macrocycles are distinguished by their unique structures and superior performance in host–guest interactions. Creating functional and intelligent supramolecular nano-drug carriers for controlled drug delivery is promising. In this context, water-soluble carboxylated arenes are the primary host molecules for most pH-responsive nanosystems. The nanosystem is broken down by the highly acidic environment of tumor cells, which acts as an exogenous or endogenous stimulus to enable the con-

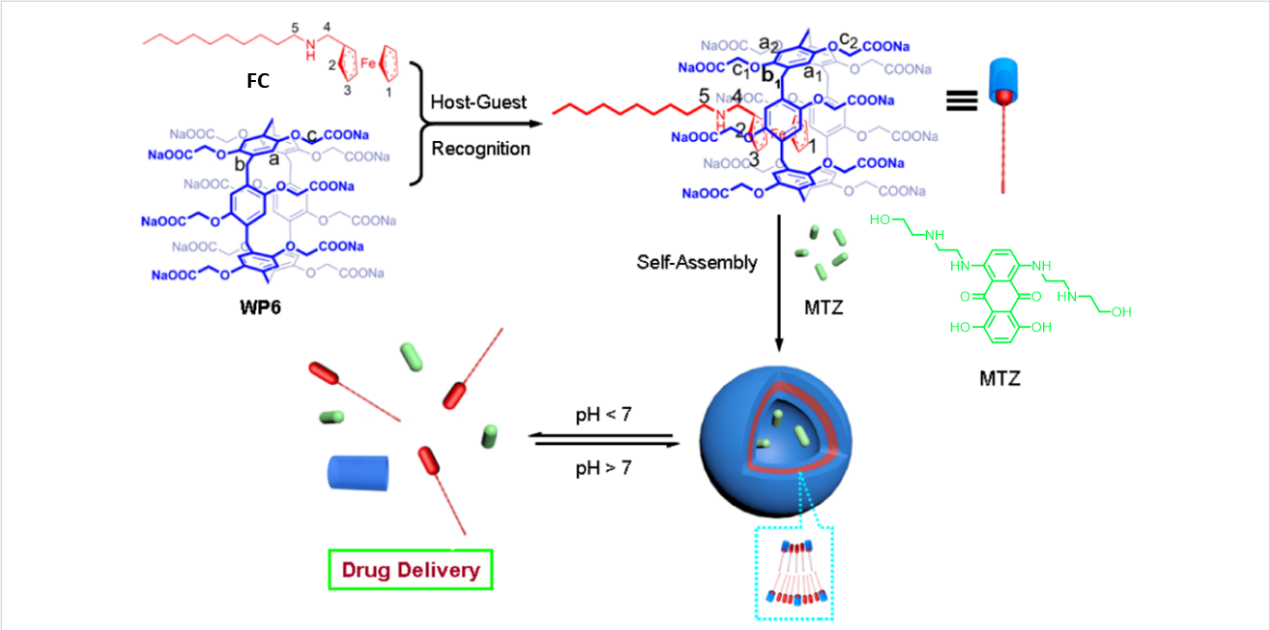

Figure 7: Illustration of the formation of supramolecular vesicles and their pH-dependent drug release [93]. Figure 7 was adapted with permission from [93], Copyright 2013 American Chemical Society. This content is not subject to CC BY 4.0.

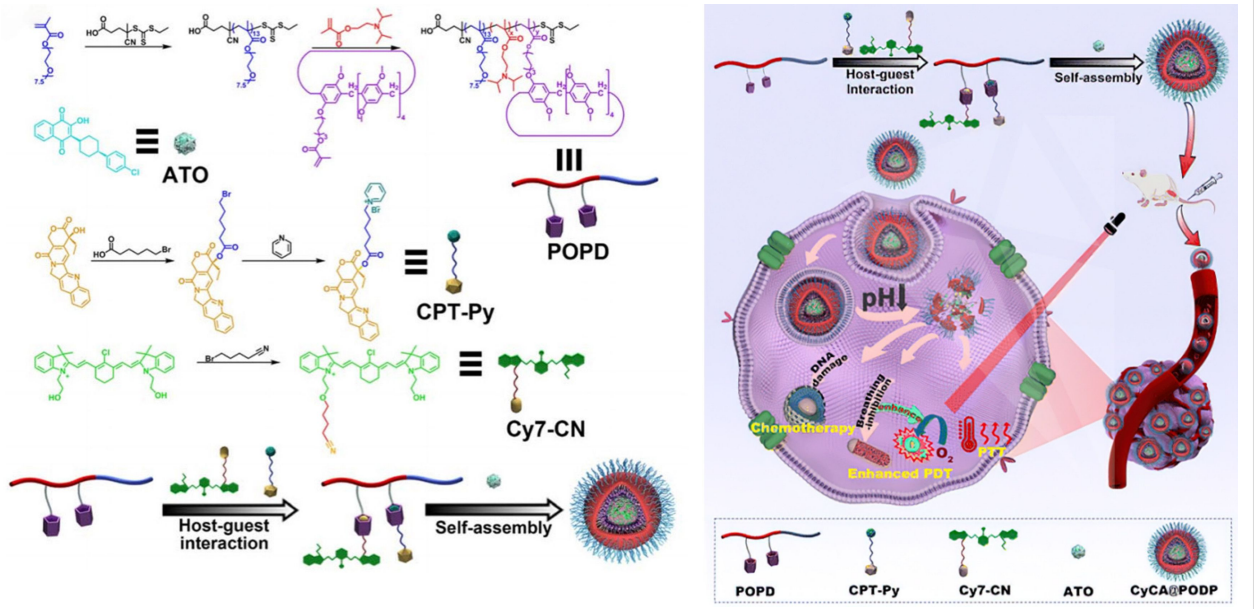

Figure 8: Schematic illustration of the application of the multifunctional nanoplatform CyCA@POPD in combined PDT, photothermal therapy (PTT), and chemotherapy [109]. Figure 8 was reproduced from [109] ("A supramolecular nanoplatform for imaging-guided phototherapies via hypoxia tumour microenvironment remodeling", © 2023 W. J. Zhou et al., published by The Royal Society of Chemistry, distributed under the terms of the Creative Commons Attribution-NonCommercial 3.0 Unported License, https://creativecommons.org/licenses/by-nc/3.0/). This content is not subject to CC BY 4.0.

trolled release of the encapsulated drugs. These nanosystems are highly compatible with the body and comprise biocompatible, water-dispersible, and low-toxicity small molecules.

2.2 Light-responsive controlled release

Light is an ideal external stimulus due to its ease of use, low cost, and safety [110,111]. Its unique advantages include being easily turned on and off, providing high spatial and temporal resolution with precise control over irradiation wavelength and intensity, and facilitating rapid responses in confined spaces [111]. Its tunable parameters, such as wavelength, duration, and intensity, along with these characteristics, have contributed to its extensive application in innovative materials and molecular devices. Ultraviolet light, in particular, is commonly employed as an external trigger for supramolecular systems. Azobenzene can regulate geometry, shape, and interfacial curvature under ultraviolet or visible light irradiation. It undergoes *cis–trans* isomerization, which can trigger alterations in bioactivity or assembly configurations. Methods for creating photo-responsive cages or capsules include fabricating cages and capsules from photoactive building blocks, and developing cages and capsules encapsulating photo-responsive guest molecules [112,113]. Incorporating supramolecular amphiphiles into photo-sensitized systems has propelled the creation of novel multifunctional photo-responsive materials. This section will discuss drug molecule capture and release systems based on two hosts.

The photo-sensitive assembly has drawn considerable interest in degradable materials, drug delivery systems, and tissue engineering. Anthracene (AnPy) derivatives are recognized for their high reactivity when exposed to light and are frequently employed as photo-degradable molecules. Liu described a photo-sensitized system composed of amphiphilic 9-alkoxy-substituted AnPy and *p*-sulfonato calix[4]arenes (SC4A) (Figure 9) [114]. SCnAs have a unique propensity to regulate the aggregation behavior of aromatic or amphiphilic molecules by reducing the critical aggregation concentration, enhancing the compactness of aggregates, and modulating the orderliness within aggregates, which is referred to as calixarene-induced aggregation (CIA) [52]. Taking the SC4A-AnPy system as an example, SC4A encapsulates the pyridine group of AnPy with its electron-rich cavity, neutralizing the electrostatic repulsion of the cationic head group and promoting the close packing of the AnPy rings through hydrophobic interactions and π-π stacking, while its deprotonated phenolic groups maintain water solubility. This assembly approach not only suppresses the fluorescence self-quenching of AnPy in the aggregated state (enhancing the yield of singlet oxygen) [115], but also boosts its photo-sensitivity – under light irradiation, the anthracene in the complex can be efficiently converted to the active drug form, anthraquinone [116]. The CIA strategy effectively improves the solubility, bioavailability, and light-response efficiency of hydrophobic photo-sensitizing drugs, offering new ideas for light-controlled drug delivery systems.

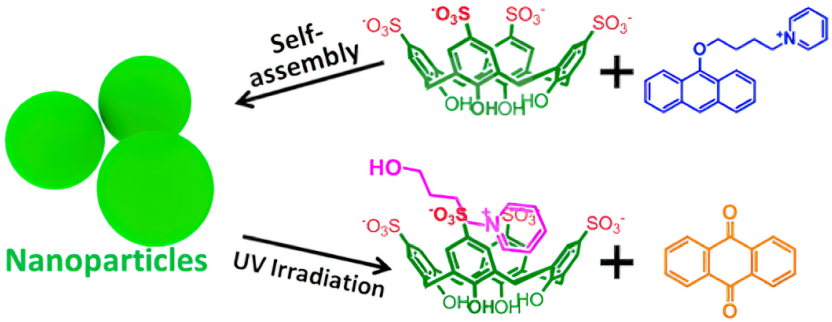

Figure 9: Illustration of the photolysis of an amphiphilic assembly via CA-induced aggregation [114]. Figure 9 was reprinted with permission from [114], Copyright 2015 American Chemical Society. This content is not subject to CC BY 4.0.

In 2018, Sun and colleagues designed and synthesized a chiral CA named chiral azo-calix[4]arene derivative (FC4AD) (Figure 10) [117]. Its interaction with enantiomers of aminoindanol in solution was investigated. It was found that FC4AD has high selective binding and release for (1*R*,2*S*)-1-amino-2-indanol, forming a 1:1 complex. *S*-phenethylamine was used as a chiral ligand, which was modified on the upper rim of calixarene through hydrogen bonding. An azobenzene group

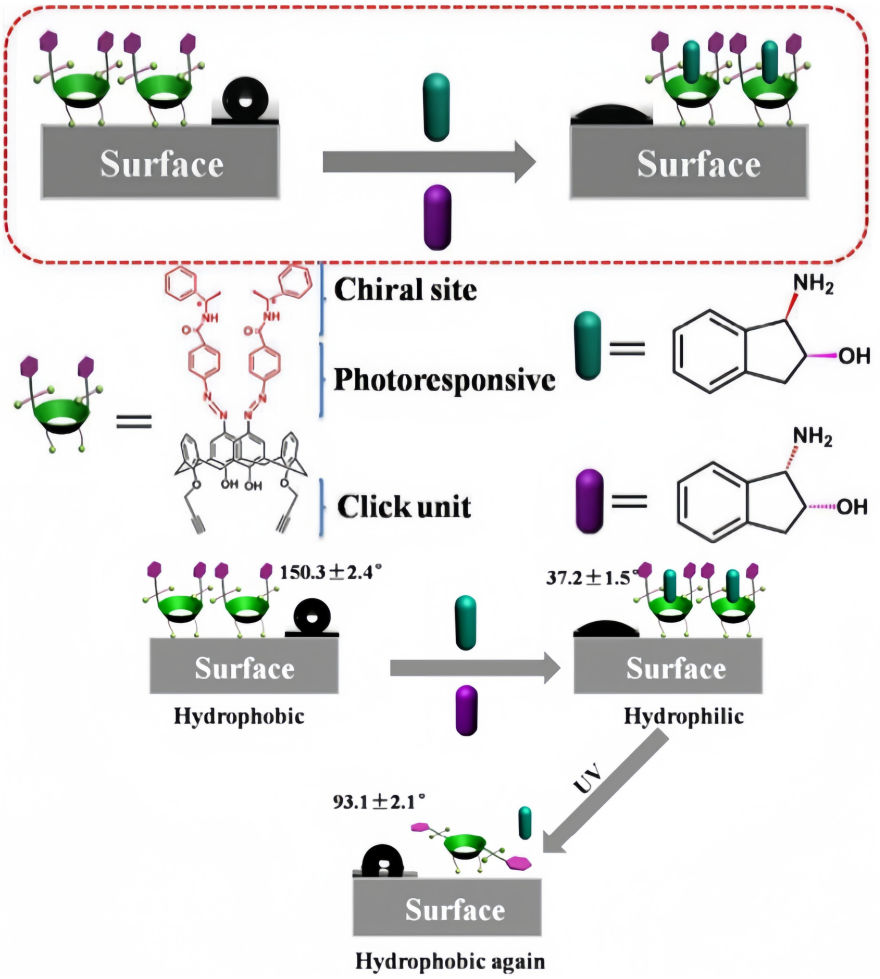

Figure 10: Schematic illustration of drug release controlled by the photo-responsive macroscopic switch based on FC4AD [117]. Figure 10 was used with permission of The Royal Society of Chemistry, from [117] ("A photo-responsive macroscopic switch constructed using a chiral azo-calix[4]arene functionalized silicon surface" by H. Pang et al., *Chem. Commun.*, vol. 54, issue 24, © 2018); permission conveyed through Copyright Clearance Center, Inc. This content is not subject to CC BY 4.0.

was introduced as the photo-regulating part at the upper edge of calixarene. The alkyne at the lower edge of FC4AD was used to form self-assembled monolayers (SAMs) on a silicon surface through Cu-catalyzed click chemistry to construct a photo-responsive macroscopic switch. This switch can achieve photo-controlled chiral reversible recognition of (1*R*,2*S*)-1-amino-2-indanol through changes in contact angle, and it holds promise for applications in chiral drug controlled release and other biotechnological fields. Further research can be conducted on the stability and performance of this switch under different environmental conditions. Its practical application in chiral drug controlled release can be expanded. Exploration of its interactions with other biomolecules can also be carried out to develop more applications in biosensing and biotechnology.

In 2024, Thongnuek and coworkers crafted a PA5-linked gelatin hydrogel incorporating the Azo-SMX drug (referred to as A-hydrogel), aiming to achieve light-regulated uptake and delivery of antibiotics (Figure 11) [118]. Azobenzene, when subjected to particular light wavelengths, displays reversible switching between its *trans* and *cis* forms, a molecular behavior well-documented in light-responsive systems. Initially, Azo-SMX, bearing an azobenzene unit, exists in a trans form and creates a stable complex with the PA5 component within the hydrogel. Upon exposure to 365 nm UV light, Azo-SMX transitions from the *trans* to the *cis* state, prompting its release from the complex. Research on antibacterial efficacy has confirmed that the modified Azo-SMX antibiotic is effective against a range of microorganisms, including both Gram-positive and Gram-negative bacteria.

2.3 Enzyme-responsive controlled release

Elevated enzyme levels often mark the microenvironment of many pathological tissues, as well as intracellular and cellular compartments. These enzymes can serve as effective triggers for drug release in stimulus-responsive systems. Owing to the specificity of enzymatic reactions, enzyme-responsive systems can act as targeted drug-delivery vehicles. Proteases such as esterases and ureases are particularly overexpressed in cancerous tissues. Thus, incorporating specific substrate groups or sequences can enhance drug release. Among the various stimuli used to control responsive assemblies, enzymatic methods offer several benefits, including biocompatibility, high efficiency, specificity, and mild reaction conditions.

Liu and colleagues reported an enzyme-responsive supramolecular ternary polymer (DiCh@a-CD-bisSC4A) (Figure 12) [95]. The supramolecular polymer with suberyl dicholine (DiCh) as the axle, with α-CD as the thread wheel and bisSC4A macrocycles as the iterative end cap units. Due to the hydrolysis of DiCh by cholinesterase, the formed supramolecular polymer assembly can be dispersed through enzymatic reactions. They

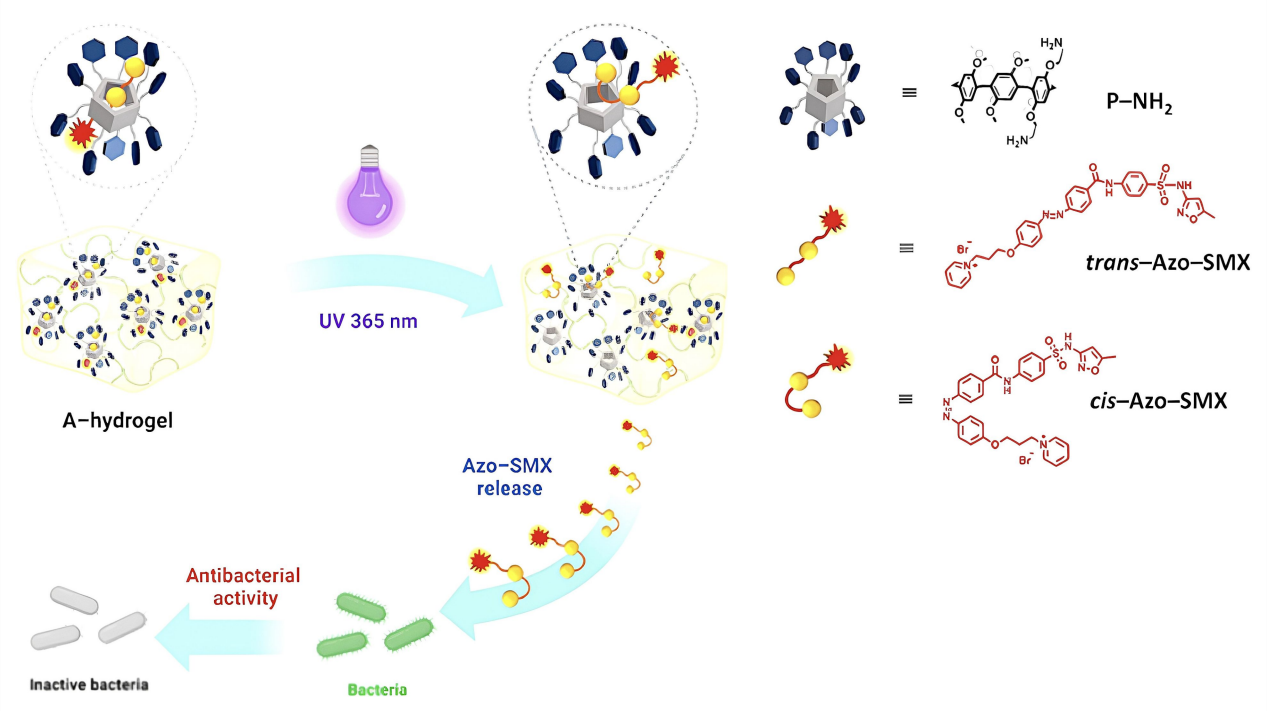

Figure 11: Schematic illustration of the formation process of Azo-SMX and its photoisomerization reaction under 365 nm UV light, transitioning from the trans to the cis form, which triggers its release from the inclusion complex [118]. Figure 11 was adapted with permission from [118], Copyright 2024 American Chemical Society. This content is not subject to CC BY 4.0.

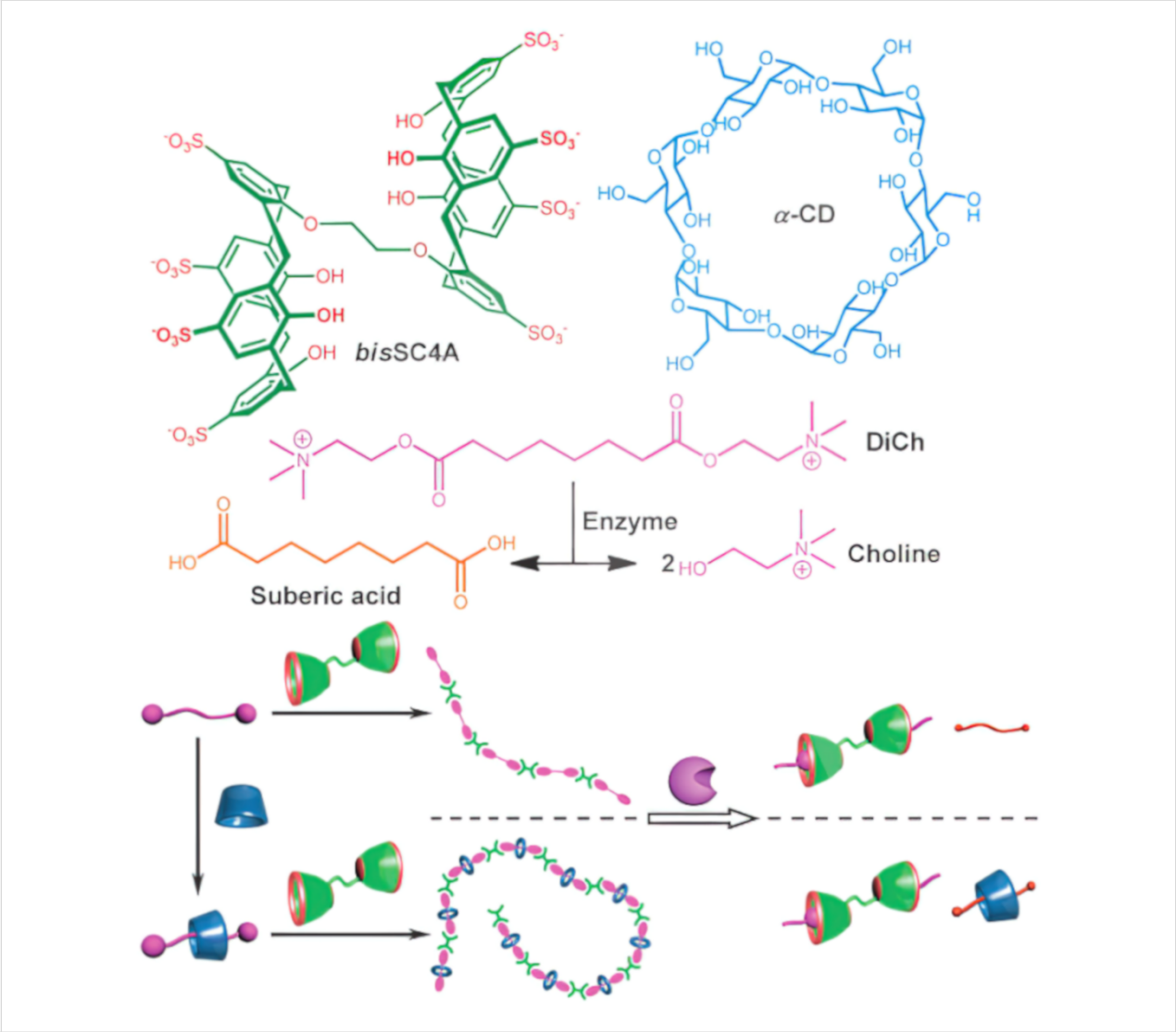

Figure 12: Schematic illustration of the enzyme-responsive behavior of supramolecular polymers [95]. Figure 12 was used with permission of The Royal Society of Chemistry, from [95] ("Enzyme-responsive supramolecular polymers by complexation of bis (*p*-sulfonatocalixarenes) with suberyl dicholine-based pseudorotaxane" by Guo, D.-S. et al., *Chem. Commun.*, vol. 49, © 2013); permission conveyed through Copyright Clearance Center, Inc. This content is not subject to CC BY 4.0.

successfully prepared a novel supramolecular ternary polymer DiCh@a-CD-bisSC4A and binary polymers DiCh@bisSC4A Compared to binary DiCh@bisSC4A, ternary DiCh@a-CD-bisSC4A has not only a larger polymer size but also a better size distribution and topological structure due to the integration of quasi rotaxanes with supramolecular polymers. Introducing α-CD onto DiCh effectively adjusts the flexibility of the spacer group, which in turn enhances supramolecular polymerization. Despite DiCh being captured by both α-CD and bisSC4A, the resultant assembly retains enzyme responsiveness, attributed to the dynamic equilibrium inherent in non-covalent interactions. Building on biocompatibility studies, they also developed an enzyme-responsive supramolecular vesicle for treating Alzheimer's disease. This vesicle is assembled via the host–guest interaction between SC4A and myristoyl choline (Figure 13) [119]. The host–guest complexation between SC4A and myristoylcholine is stabilized by the electrostatic interaction between the negatively charged sulfonate groups and the positively charged quaternary ammonium groups. The interaction between the host and guest reduces the critical aggregation concentration (CAC) to form binary vesicles, with the hydrophobic alkyl chains of myristoylcholine packing together and the inner and outer surfaces composed of the hydrophilic phenolic OH groups of SC4A exposed to the aqueous solution. Subsequently, cholinesterase (acetylcholinesterase (AChE) and butyrylcholinesterase (BChE)) specifically converts myristoylcholine into myristic acid and choline [120]. SC4A binds to the non-amphiphilic choline but not to the amphiphilic myristic

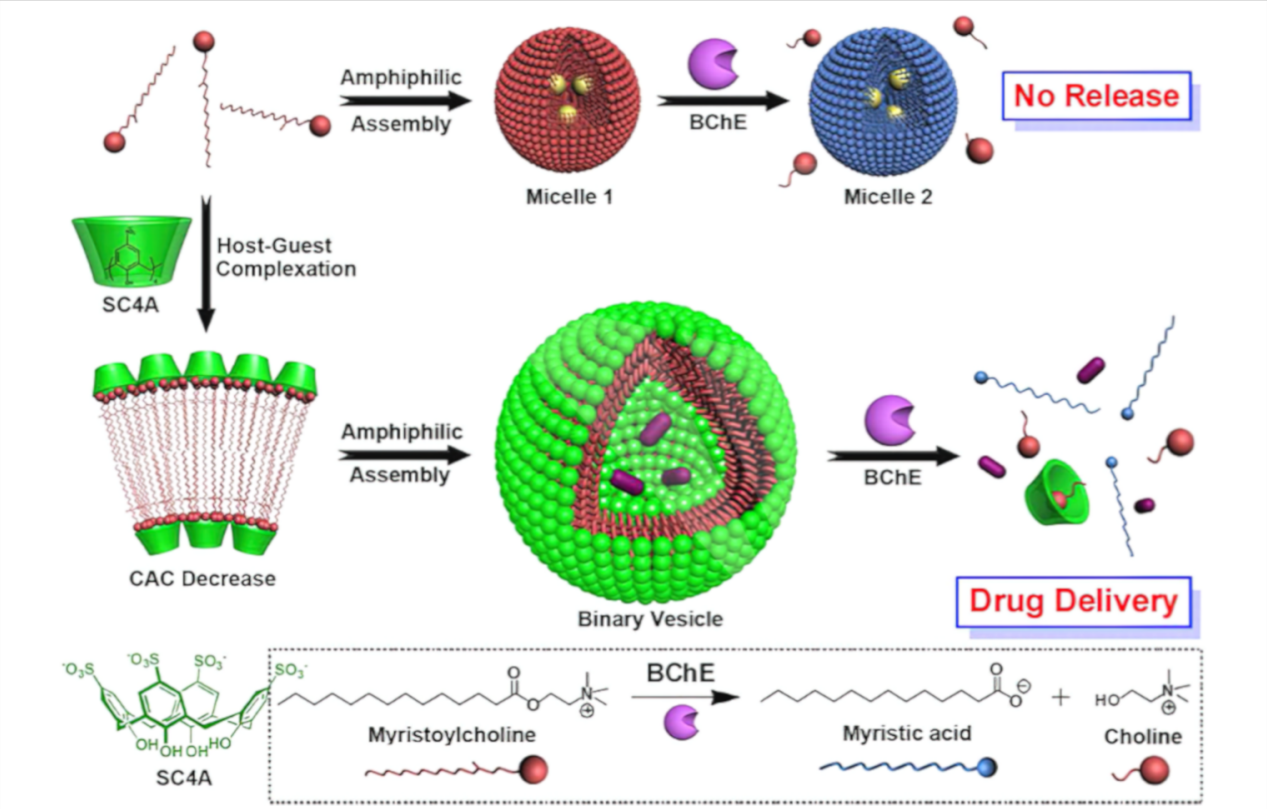

Figure 13: Schematic illustration of the amphiphilic assembly of SC4A and its enzyme-responsive applications [119]. Figure 13 was reprinted with permission from [119], Copyright 2012 American Chemical Society. This content is not subject to CC BY 4.0.

acid, leading to the disassembly of the composite vesicles. Currently, the clinical treatment of Alzheimer's disease is mainly based on cholinesterase inhibitors, such as tacrine. Therefore, this vesicle system may be suitable for the controlled release of Alzheimer's disease drugs.

Extensive research has been conducted on MSN carriers fitted with supramolecular nano valves. Yang and co-workers [121] designed an enzyme-responsive supramolecular nanovalve composed of MSNs and choline sulfonatocalixarene[2]pseudorotaxane. Two different choline derivatives with distinct structures and lengths (Figure 14) were grafted onto the pores of MSNs via ester or urea linkages, serving as enzyme-cleavable sites. Negatively charged SC4A macrocycles were introduced to envelop the choline stems on the surface of MSN-NPs through host–guest interactions, forming pseudorotaxanes as the mobile/cleavable components of the nanovalves. It was experimentally demonstrated that esterase could selectively activate the ester-linked nanovalve (MSN-C1), while urease could selectively activate the urea-linked nanovalve (MSN-C2). This innovative enzyme-activated method provides inherent biocompatibility, mild reaction conditions, high efficiency, and specificity for the degradation of supramolecular polymers.

2.4 Hypoxia-responsive controlled release

In the last few years, notable strides have been achieved in boosting the targeting accuracy and clinical utility of drug release mechanisms. Tumor cells are characterized by unique attributes, such as acidity, hypoxia, and altered metabolism, which set them apart from healthy cells. These distinct features underscore the importance of focusing on the tumor microenvironment to develop supramolecular systems that are highly specific and capable of responding to multiple stimuli. These advanced systems aim to target and penetrate tumor cells effectively, mitigate drug resistance caused by tumor cell uptake, and ultimately enhance clinical efficacy.

Guo and associates developed hypoxia-responsive molecular carriers, namely carboxylated or sulfonated azo-calix[4/5]arenes [122,123]. These CAs, utilizing their azo groups that are easily reduced in low-oxygen settings, provide the potential for tumor-targeted drug release while reducing side effects. The azo-calix[4/5]arenes have demonstrated strong binding capabilities with a range of chemotherapeutic drugs, which underscores their potential as supramolecular drug carriers. They have verified the efficacy of this hypoxia-targeted therapy through both in vitro and in vivo experiments, and the carrier has made significant progress in the field of hypoxia-targeted drug delivery.

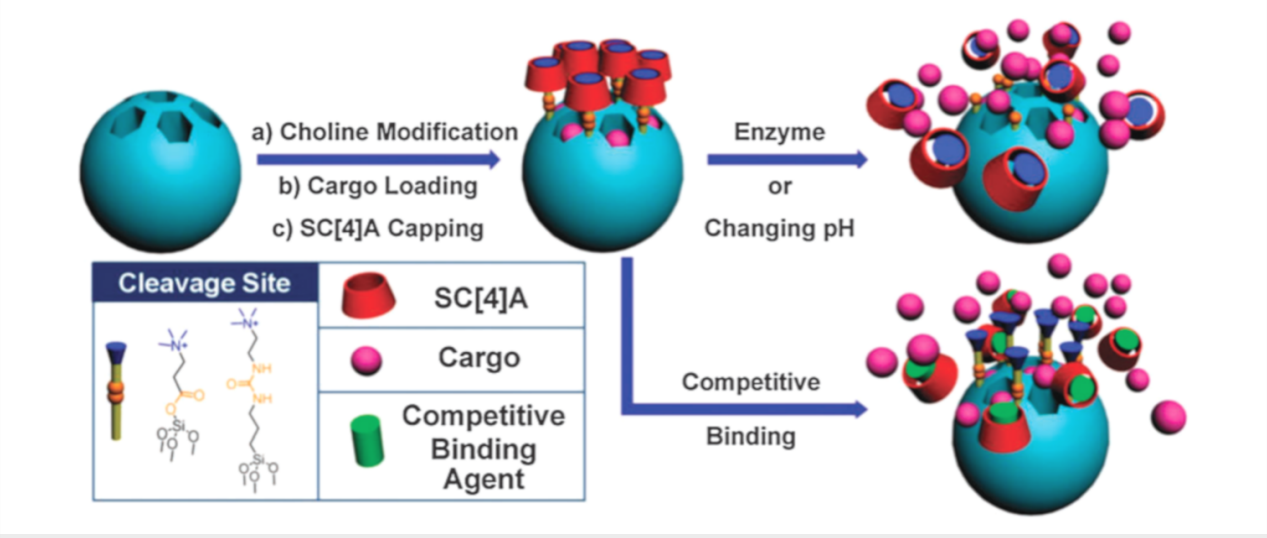

Figure 14: Stimuli-responsive nanovalves based on MSNs and choline-SC4A[2]pseudorotaxanes, MSN-C1 with ester-linked stalks and MSN-C2 with urea-linked stalks [121]. Figure 14 was used with permission of The Royal Society of Chemistry, from [121] ("Enzyme-responsive supramolecular nanovalves crafted by mesoporous silica nanoparticles and choline-sulfonatocalix [4] arene [2] pseudorotaxanes for controlled cargo release" by Sun, Y.-L. et al., *Chem. Commun.*, vol. 49, issue 79, © 2013); permission conveyed through Copyright Clearance Center, Inc. This content is not subject to CC BY 4.0.

This section highlights several recent studies on stimulus-responsive drug release within hypoxic tumor environments.

Among anti-cancer drugs, BE-43547A2 (BE) exhibits high cytotoxicity against hypoxic pancreatic cancer cells, which is in line with the current hypoxic tumor environment, making it a promising candidate for hypoxia-targeted therapies. The Guo group modified calixarene to obtain sulfonated azocalix[5]arene (SAC5A), and then combined the BE prodrug (NMP-BE) with the SAC5A to create a supramolecular complex, NMP-BE@SAC5A, that is responsive to dual hypoxia signals (Figure 15) [123]. The azo group in SAC5A endows it with hypoxia responsiveness, allowing it to enhance the accumulation of NMP-BE in tumors under hypoxic conditions in

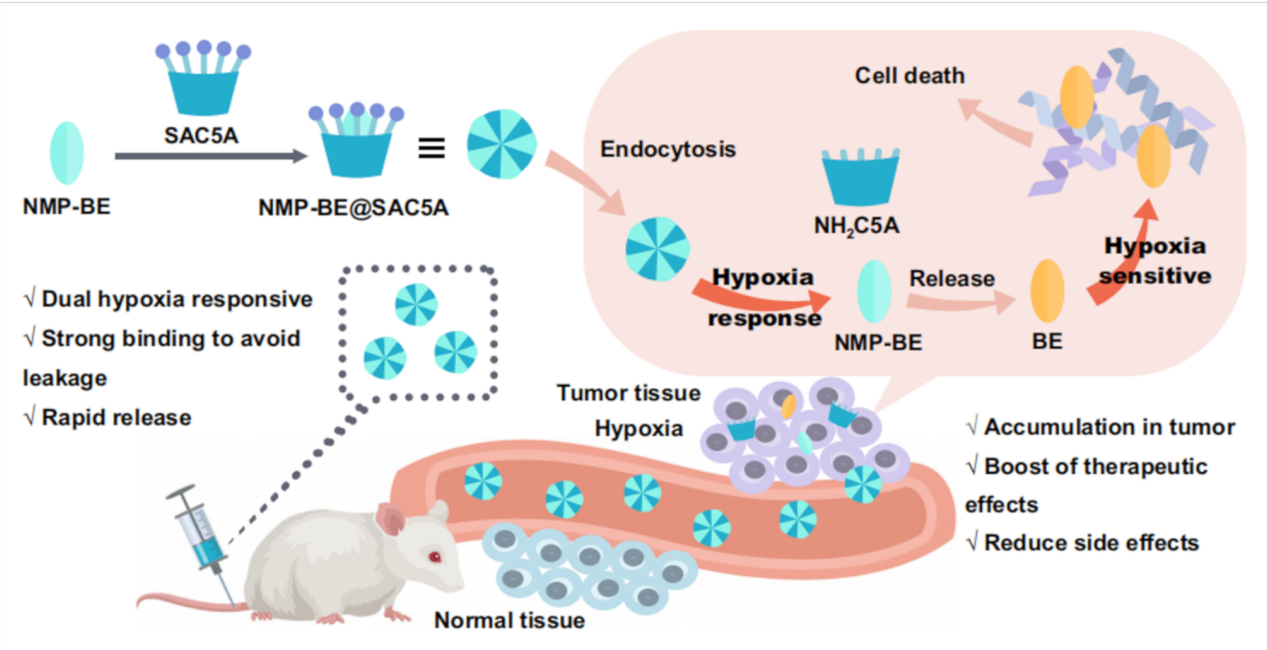

Figure 15: A schematic diagram showing the construction of a supramolecular system by host–guest interaction between SAC5A and the NMP-BE prodrug under hypoxic conditions [123]. Figure 15 was reproduced from [123] (© 2023 J.-S. Guo et al., published by Springer Nature, distributed under the terms of the Creative Commons Attribution 4.0 International License, https://creativecommons.org/licenses/by/4.0).

cancer cells. Upon intracellular release in cancer cells, NMP-BE releases the hypoxia-sensitive toxin BE, achieving the dual hypoxia-responsive therapeutic goal through host–guest interactions. Due to the specific cellular uptake and discharge process, NMP-BE@SAC5A effectively suppresses the proliferation of pancreatic cancer in a mouse model with human tumor cells at minimal concentrations, while avoiding adverse effects throughout the body. In the future, it could be attempted to combine it with more anti-tumor drugs and apply it in clinical settings.

In addition to the aforementioned SAC5A that can respond to stimuli under hypoxic conditions, they also synthesized Biotin-SAC4A by modifying SAC4A with biotin. (Figure 16) [124]. Monocarboxylated azocalixarene and aminated biotin were synthesized. Subsequently, using a coupling agent, the carboxyl group of the azocalixarene was modified through amidation to obtain biotin-modified SAC4A. The formation of amide bonds and azo linkages deepened the cavity and enhanced the interaction strength with drugs. The biotin on the upper rim endows biotin-SAC4A with the ability to actively target tumor cells based on the interaction between biotin and biotin receptors, thereby improving antitumor efficacy. DOX@biotin-SAC4A exhibited high cytotoxicity against cancer cells but low toxicity to normal cells. They further combined Biotin-SAC4A with DOX and injected it into mice. The experimental results showed that Biotin-SAC4A could firmly bind DOX and promote its release under hypoxic conditions.

In 2024, Guo and colleagues developed a SAC4A grafted self-assembled peptide hydrogel for hypoxia-responsive controlled drug release in anti-inflammatory treatment of ischemic stroke (Figure 17) [125]. Following PBS induction, the peptide hydrogel was tailored to exhibit a rheological modulus and shear-thinning behavior similar to that of brain tissue. The hydrogel's hypoxia-responsive properties were validated through three different systems: sodium dithionite (SDT), rat liver microsomes, and the oxygen-glucose deprivation (OGD) model. Under hypoxic conditions, the hydrogel achieved

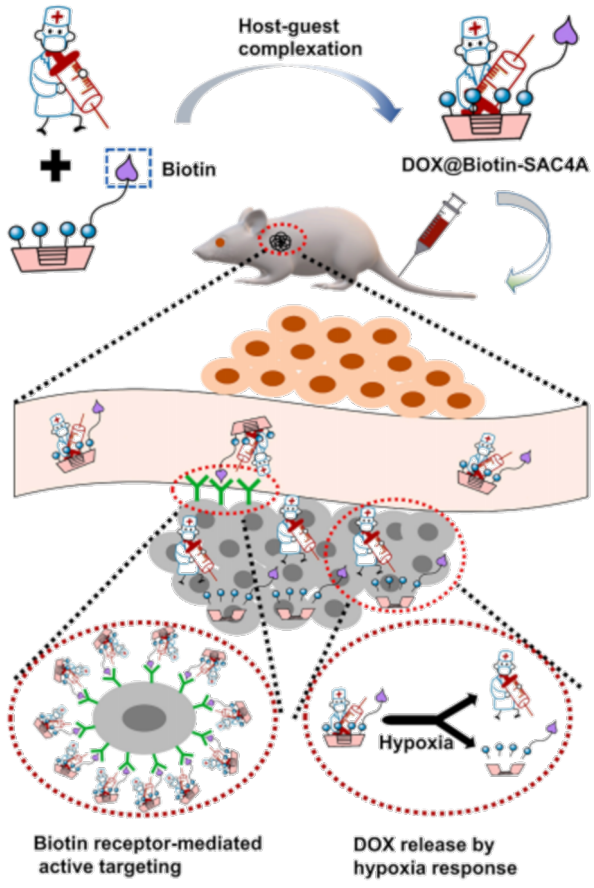

Figure 16: A schematic diagram showing the formation of the host–guest complex DOX@Biotin-SAC4A by biotin modification of SAC4 and the release of DOX under hypoxic conditions in mice [124]. Figure 16 was reprinted from [124], *Journal of Controlled Release*, vol. 368, by Chen, M.-M.; Tang, X.; Li, J.-J.; Chen, F.-Y.; Jiang, Z.-T.; Fu, R.; Li, H.-B.; Hu, X.-Y.; Geng, W.-C.; Guo, D.-S., "Active targeting tumor therapy using host–guest drug delivery system based on biotin functionalized azocalix [4] arene", pages 691–702, Copyright (2024), with permission from Elsevier. This content is not subject to CC BY 4.0.

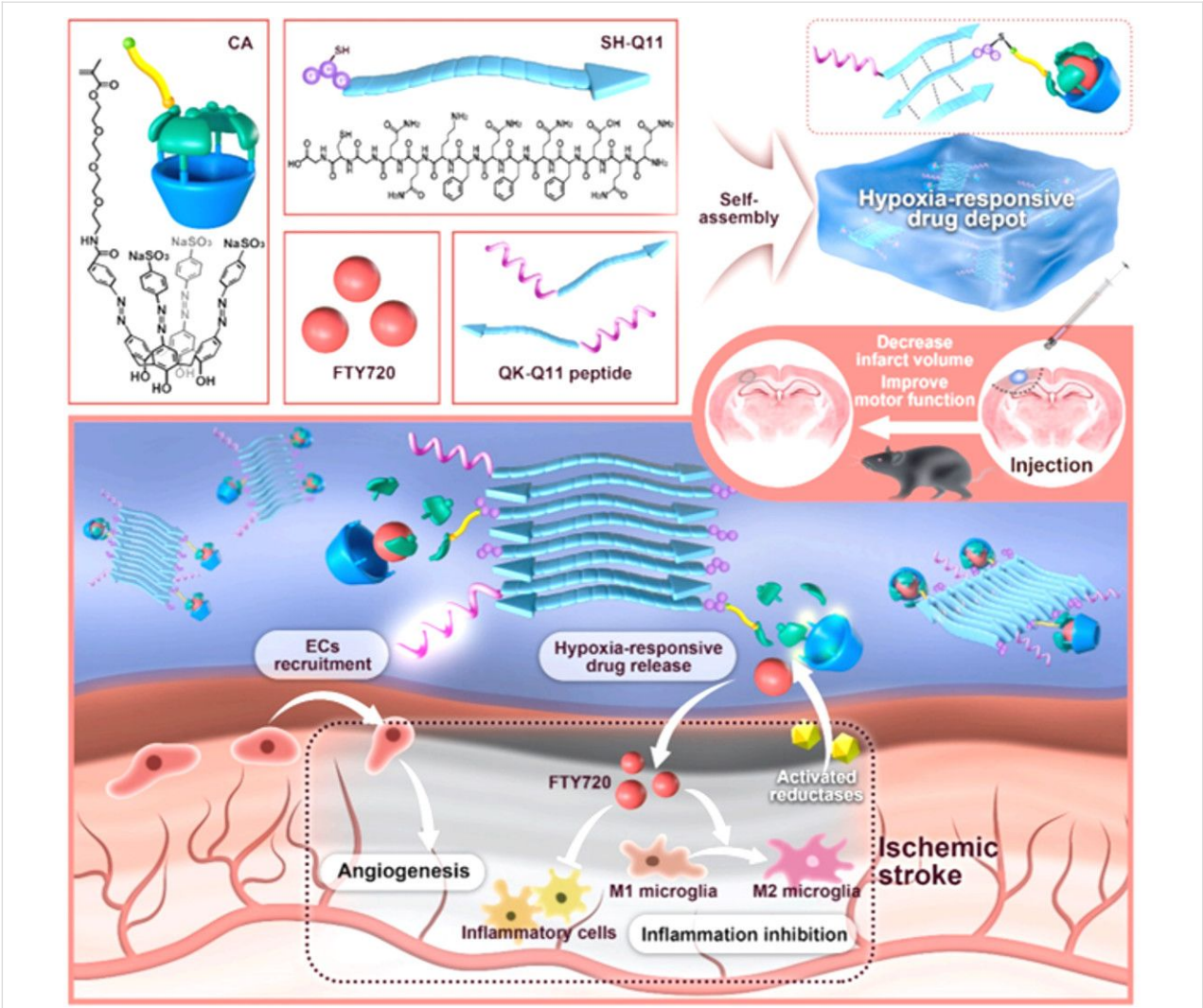

Figure 17: A schematic diagram showing the self-assembly of CA4 into a hypoxia-responsive peptide hydrogel, which achieves targeted release of CY5-DM or FTY720 in vitro [125]. Figure 17 was reprinted from [125], *Nano Today*, vol. 54, by Zheng, W.; Yao, S.-Y.; Hu, H.; Chen, X.; Qian, Z.; Liu, W.; Zhu, Y.; Mao, Z.; Guo, D.-S.; Gao, C., "Hypoxia-responsive calixarene-grafted self-assembled peptide hydrogel for inflammation suppression in ischemic stroke", article no. 102064, Copyright (2023), with permission from Elsevier. This content is not subject to CC BY 4.0.

targeted release of cyanine 5-dimethyl (CY5-DM) or fingolimod (FTY720) in vitro. Upon local administration, the hypoxia-responsive self-assembling peptide hydrogel resulted in improved motor function and reduced inflammation in vivo.

Recently, Geng and colleagues created additional binding sites by modifying the upper rim of CA4 with glucose and enhanced the overall solubility and biocompatibility of the azo-calixarene structure, designing it as a drug carrier (Figure 18) [126]. This carrier binds to the ferroptosis inhibitor liproxstatin-1 (Lip) and releases it selectively in hypoxic environments. This mechanism aims to counteract the side effects associated with intravenous thrombolysis using recombinant tissue-type plasminogen activator (rtPA) for treating ischemic stroke. The interaction between GluAC4A and Lip results in a significant improvement in Lip's solubility. The glucose modification on the upper rim of GluAC4A serves multiple functions: it expands the calixarene cavity, creates additional binding sites, and enhances the overall solubility and biocompatibility of the azo-calixarene structure. The azo moiety in GluAC4A imparts hypoxia responsiveness, enabling the targeted release of Lip specifically at ischemic sites. GluAC4A effectively promotes drug accumulation in the brain. Moreover, the Lip@GluAC4A complex significantly reduces iron deposition, blood-brain barrier leakage, and neurological deficits that are commonly observed with rtPA treatment.

2.5 Multi-responsive controlled release

The previous sections discussed the controlled drug release of single-stimulus-responsive systems, adopting a relatively simple

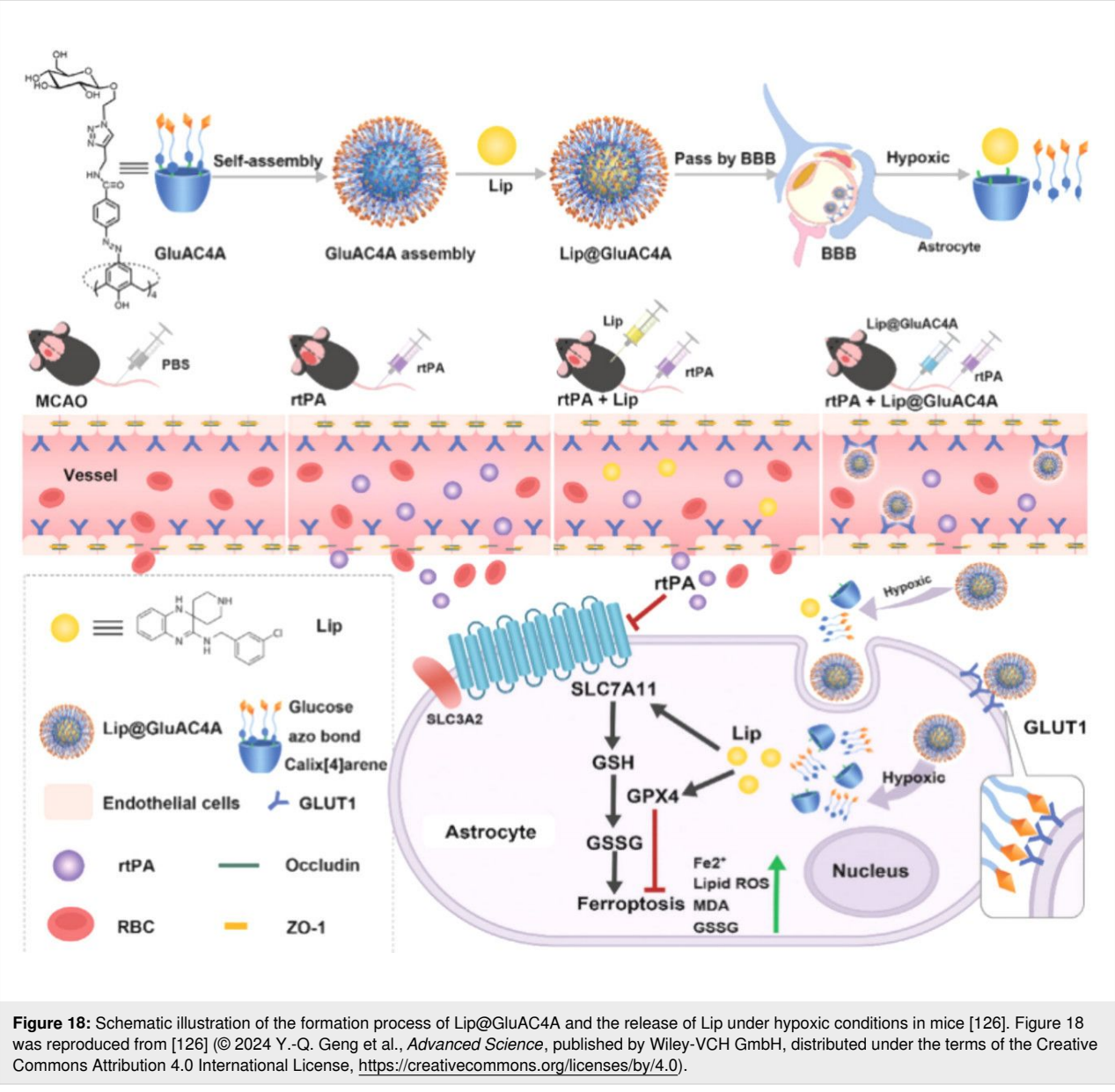

Figure 18: Schematic illustration of the formation process of Lip@GluAC4A and the release of Lip under hypoxic conditions in mice [126]. Figure 18 was reproduced from [126] (© 2024 Y.-Q. Geng et al., *Advanced Science*, published by Wiley-VCH GmbH, distributed under the terms of the Creative Commons Attribution 4.0 International License, https://creativecommons.org/licenses/by/4.0).

perspective of a single stimulus-response. Multistimuli responsiveness also holds potential applications in terms of responsiveness and efficient drug release. One of the major challenges faced by researchers in this field has long been the difficulty of incorporating two or more functional groups simultaneously when constructing multi-stimuli-responsive systems. Supramolecular materials can also be designed to be responsive to multiple stimuli. In addition to those mentioned above, multistimulus responses have a broad application prospect in controlling drug release. For example, supramolecular peptide assemblies that naturally respond to pH or ion strength can be designed to include light-responsive elements or feature-specific enzyme substrates, thus utilizing two separate stimulus-response pathways.

In 2011, Liu and colleagues [127] created a multi-stimulus-responsive supramolecular bis-vesicle through the complexation of water-soluble calixarene (C4AS) with 1-dodecyl-1'-methyl-4,4'-bipyridinium (MVC12). The term "bis-vesicle" refers to a structure with two fused or nested vesicular domains, typically featuring shared membrane interfaces or segregated internal spaces. They subsequently loaded the anticancer drug DOX into the vesicle. The formation mechanism benefits from the rigid conical structure of C4AS, which significantly reduces the critical aggregation concentration of MVC12 by 1000 times. This bis-vesicle structure possesses the following intelligent responsive characteristics: (1) temperature sensitivity originating from the enthalpy-driven nature of the host–guest interaction; (2) redox responsiveness due to the reversible electron

transfer of MVC12; (3) competitive complexation making the system sensitive to cyclodextrins. Experiments have confirmed that this carrier can efficiently encapsulate DOX and trigger drug release through multiple stimuli, demonstrating good potential for anticancer therapy in vitro. This intelligent delivery system, integrating temperature, redox, and molecular recognition responses, provides important ideas for the development of new cancer treatment strategies.

In 2021, Han et al. explored the interactions WP5 and aniline tetramer (TANI) as host and guest molecules (Figure 19) [128]. The WP5⊃TANI complex is capable of self-assembling into supramolecular vesicles. WP5 has a large hydrophobic cavity that can accommodate TANI, and the interaction between WP5 and TANI leads to the formation of an amphiphilic complex. The amphiphilicity of the WP5-TANI complex, the π–π stacking interactions between the two components, and the high hydrophobicity of TANI promote the host–guest interactions between WP5 and TANI, leading to the further formation of supramolecular vesicles by the WP5⊃TANI complex. These vesicles are non-toxic to normal cells but exhibit toxicity towards cancer cells. The WP5⊃TANI supramolecular vesicles can effectively encapsulate the anticancer drug DOX. Both the acidic microenvironment at the tumor site and photothermal effects can induce the release of DOX. DOX delivered by these vesicles, in combination with NIR light irradiation, can significantly suppress tumor growth.

Wang and colleagues [107] designed a supramolecular binary vesicle system based on WP6 and SAINT molecules (G5), which exhibits multiple stimulus-responsive characteristics to pH, Ca^{2+} and temperature (Figure 20). WP6 and G5, as amphiphilic molecules containing pyridine groups and alkyl chains, form supramolecular amphiphiles through host–guest interactions, with the assembly process driven by both hydrophobic and electrostatic interactions. The vesicles can efficiently encapsulate drug molecules such as calcein and DOX, and trigger their release under acidic conditions or Ca^{2+} stimulation. The fusion process of WP6⊃G5 vesicles can be divided into three stages: First, Ca^{2+} binds to the carboxyl groups on the outer surface of the WP6⊃G5 vesicles. Second, the binding of Ca^{2+} to WP6 further induces vesicle aggregation. Third, vesicle

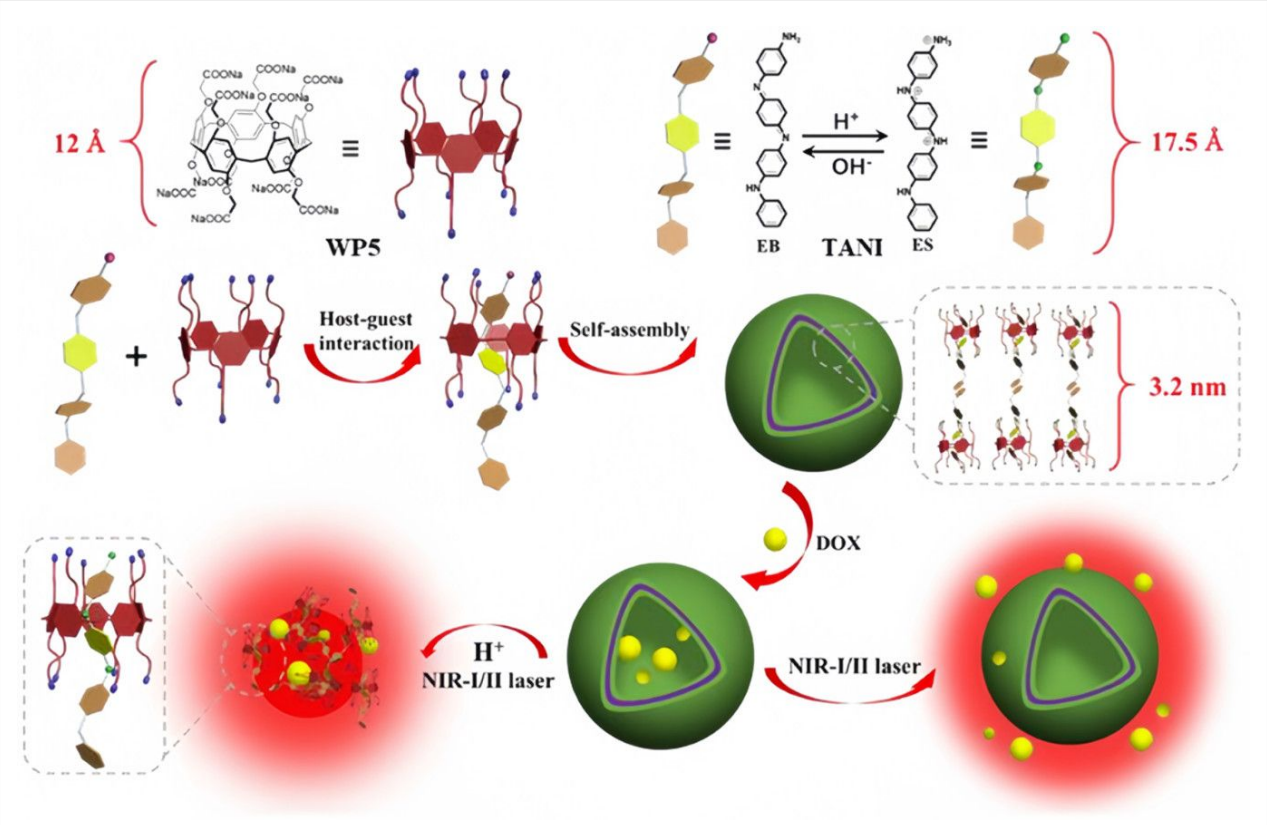

Figure 19: Schematic illustration of the construction of a supramolecular vesicle based on the host–guest complexation between WP5 and TANI, and the release of DOX under acidic conditions or NIR irradiation [128]. Figure 19 was reprinted from [128], *Chemical Engineering Journal*, vol. 403, by Chen, X.; Wang, Z.; Sun, X.; Han, Y.; Huang, Y.; Xi, J.; Bian, X.; Han, J.; Guo, R., "Photothermal supramolecular vesicles coassembled from pillar [5] arene and aniline tetramer for tumor eradication in NIR-I and NIR-II biowindows", Copyright (2020), with permission from Elsevier. This content is not subject to CC BY 4.0.

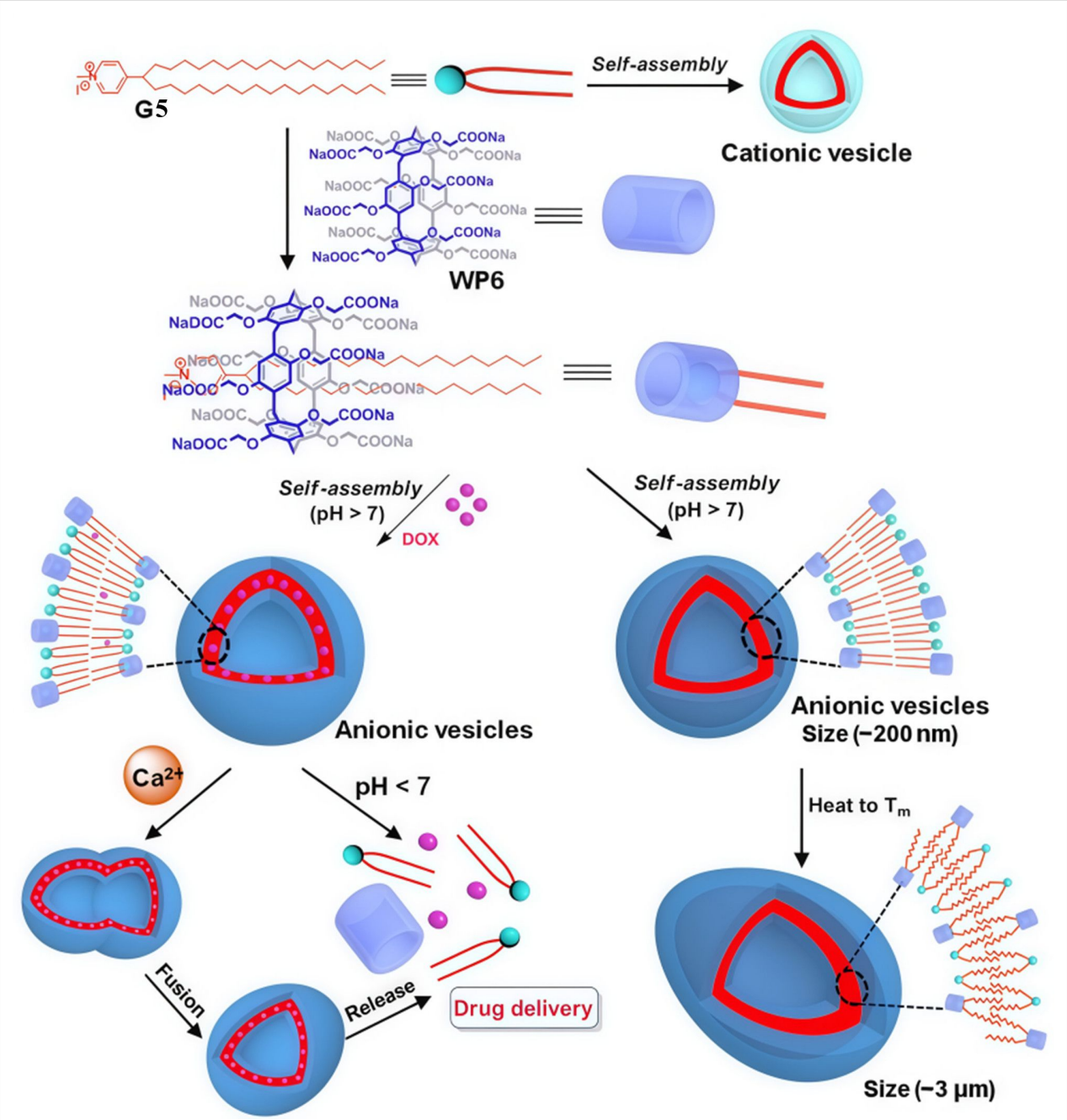

Figure 20: Schematic illustration of WP6 self-assembly at pH > 7, and the stimulus-responsive drug release behavior under varying conditions of Ca^{2+} concentration, pH, and temperature [107]. Figure 4 was adapted with permission from [107], Copyright 2014 American Chemical Society. This content is not subject to CC BY 4.0.

fusion occurs. Moreover, temperature regulation can achieve reversible changes in vesicle size; heating forms stable vesicles with an increased internal cavity and a size of approximately 3 micrometers, providing a potential carrier for bioimaging applications. This intelligent vesicle system, which combines drug-controlled release and tunable structural properties, holds significant value in the fields of targeted drug delivery and biomedical applications.

Subsequently, Wang and colleagues [129] in 2017 employed WP5 and pyridinium boronic acid derivatives (G6) to encapsulate insulin and achieve controlled release under physiological conditions (Figure 21). The host–guest binding affinity, which occurs in a 1:1 ratio, is primarily driven by synergistic electrostatic and hydrophobic interactions. The WP5⊃G6 supramolecular vesicles exhibit unique dual responsiveness to glucose and pH, originating from the specific binding of the pyridine-

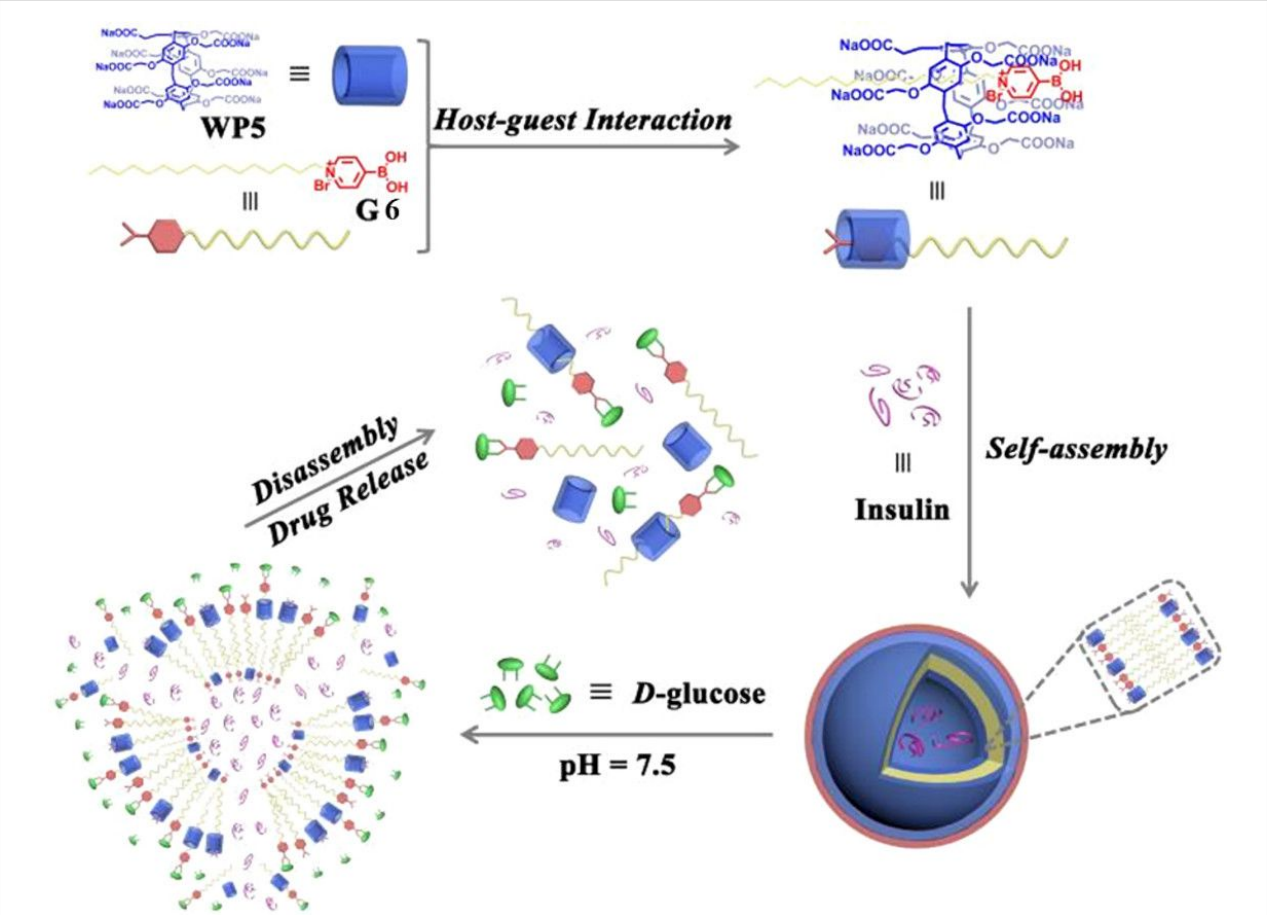

Figure 21: Schematic illustration of the formation of supramolecular vesicles based on the WP5⊃G super-amphiphile and their stimulus-responsive release [129]. Figure 21 was reproduced from [129], L. Gao et al., "Glucose-Responsive Supramolecular Vesicles Based on Water-Soluble Pillar[5]arene and Pyridylboronic Acid Derivatives for Controlled Insulin Delivery", *Chem. Eur. J.*, with permission from John Wiley and Sons. Copyright © 2017 Wiley-VCH Verlag GmbH & Co. KGaA, Weinheim. This content is not subject to CC BY 4.0.

boronic acid motif to the cis-diol of D-glucose and the pH-sensitive solubility changes. Under physiological pH conditions (7.4), the vesicle structure rapidly dissociates upon the addition of D-glucose or when the pH is lowered to 6.0, as evidenced by the disappearance of the Tyndall effect and the absence of vesicular structures in TEM images. This response mechanism is attributed to: 1) competitive binding of glucose leading to the dissociation of the host–guest complex; and 2) protonation of the WP5 carboxyl groups under acidic conditions, forming insoluble precipitates. The system can efficiently encapsulate insulin and precisely release it in response to high glucose levels or acidic environments demonstrating excellent potential for diabetes therapy. This intelligent delivery system achieves on-demand drug release and provides new insights for the development of glucose-responsive insulin formulations.

In 2022, Pei and collaborators unveiled a dual-stimuli-responsive supramolecular drug delivery system that relies on host–guest interactions, with sodium xanthate derivatives (SXD) serving as guest molecules and quaternary ammonium pillar[5]arene (QAP5) acting as host molecules (Figure 22) [130]. The hydrophobic SXD and the hydrophilic QAP5 interact through host–guest interactions driven by electrostatic forces to form the QAP5–SXD complex. The amphiphilic nature of QAP5–SXD enables its self-assembly into stable QAP5–SXD nanoparticles in aqueous solution, which are identified as vesicles by TEM. In this study, the xanthate group, which responds to both pH and hydrogen peroxide, shows great potential for the development of dual-responsive drug delivery systems. Using DOX as a model anticancer drug, they synthesized DOX@QAP5⊃SXD nanoparticles. Under conditions of low pH and high hydrogen peroxide concentration, SXD can rapidly decompose, triggering the disassembly of DOX@QAP5⊃SXD nanoparticles and the release of the encapsulated drug DOX.

Du and his team engineered MSN functionalized with dimethyl benzimidazolium (DMBI) and bipyridinium (BP) groups [131],

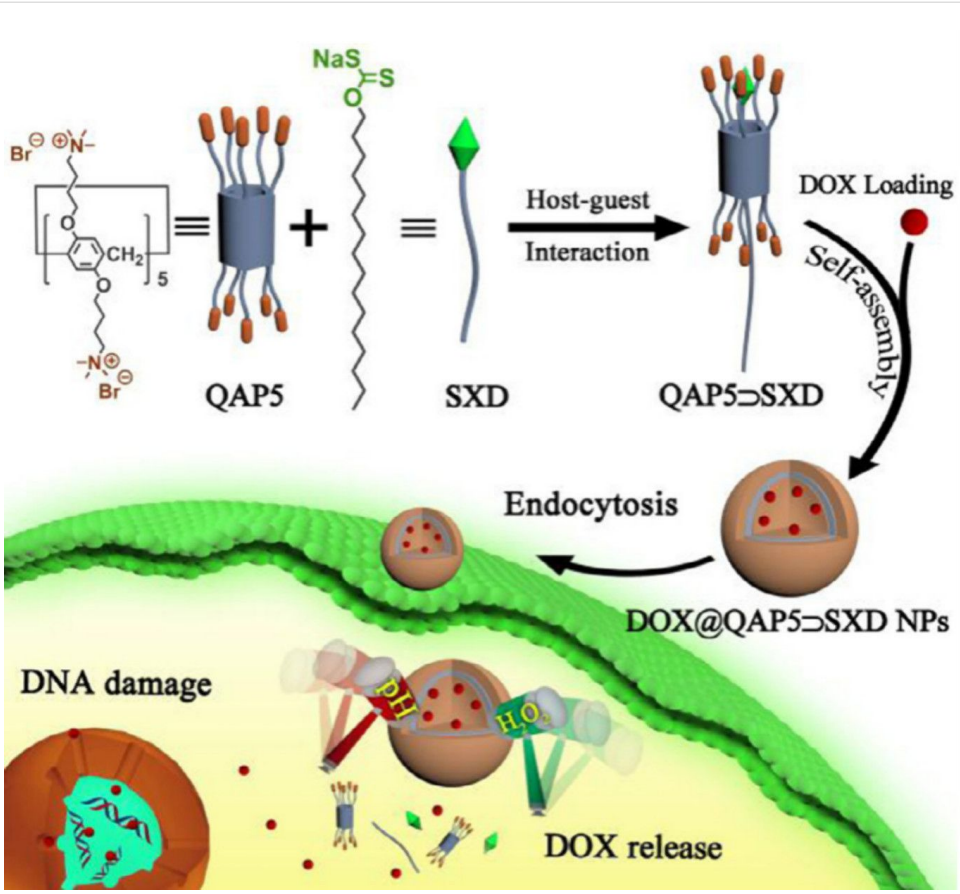

Figure 22: Schematic illustrations of the host–guest recognition of QAP5⊃SXD, the formation of the nanoparticles DOX@QAP5⊃SXD, and the stimulus-responsive release of DOX under pH and H_2O_2 conditions [130]. Figure 22 was reprinted from [130], *Chinese Chemical Letters*, vol. 33, by Shen, Z.; Ma, N.; Wang, F.; Ren, J.; Hou, C.; Chao, S.; Pei, Y.; Pei, Z., "pH-and H_2O_2-sensitive drug delivery system based on sodium xanthate: dual-responsive supramolecular vesicles from one functional group", pages 4563-4566, Copyright (2022), with permission from Elsevier on behalf of Chinese Chemical Society and Institute of Materia Medica, Chinese Academy of Medical Sciences. This content is not subject to CC BY 4.0.

as well as carboxylic acid-modified PA6 hydrocarbons (CPA6) to create multi-responsive controlled-release systems. CPA6 can rotate around DMBI or BP to form supramolecular nanovalves that encapsulate drugs within the MSN pores. The release of drugs is triggered by competitive binding at acidic pH or CPA6 de-threading, which then opens the nanovalves. In 2016, Fu and colleagues [132] designed and constructed an acid/base/Zn^{2+} stimulus-responsive controlled release system on the outer surface of a WP5-based bistable[2]pseudorotaxane (Figure 23). WP5 bonds with 1,6-hexane diamine (HDA) under neutral conditions, acting as a plug to block the retained cargo, and the two dissociate in acidic, basic, or Zn^{2+} environments, leading to controlled drug release.

Intelligent cargo delivery systems have been utilized to develop pesticide delivery nanoplatforms, thanks to their controlled release characteristics. In 2021, Yang et al. engineered a supramolecular fungicide nanoplatform using quaternary ammonium salt (Q)-modified MSN (MSN-Q NPs) as nanocarriers to encapsulate berberine hydrochloride (BH) and carboxyl pillar[5]arene (CP5A) (Figure 24) [133]. CP5A acts as a nanogate and is anchored on the surface of MSN-P through host–guest interactions between the positively charged P groups and the electron-rich cavity of CP5A, forming CP5A@MSN-P NPs loaded with BH to combat Botrytis cinerea. CP5A imparted the nanoplatform with pH or elevating temperatures-stimuli-responsive release capabilities. The encapsulated BH, a natural plant-derived fungicide, served as an eco-friendly substitute for synthetic fungicides. They employed oxalic acid (OA) secreted by B. cinerea as a trigger to release BH on demand within the pathogen microenvironment. This study capitalized on the acidic microenvironment created by B. cinerea to construct a fungicide nanoplatform that releases fungicides on demand, distinguishing it from previous nanoplatforms that relied on exogenous stimuli. Results demonstrated that the nanoplatform effectively curbed mycelial growth and spore germination, offering a novel strategy for gray mold management.

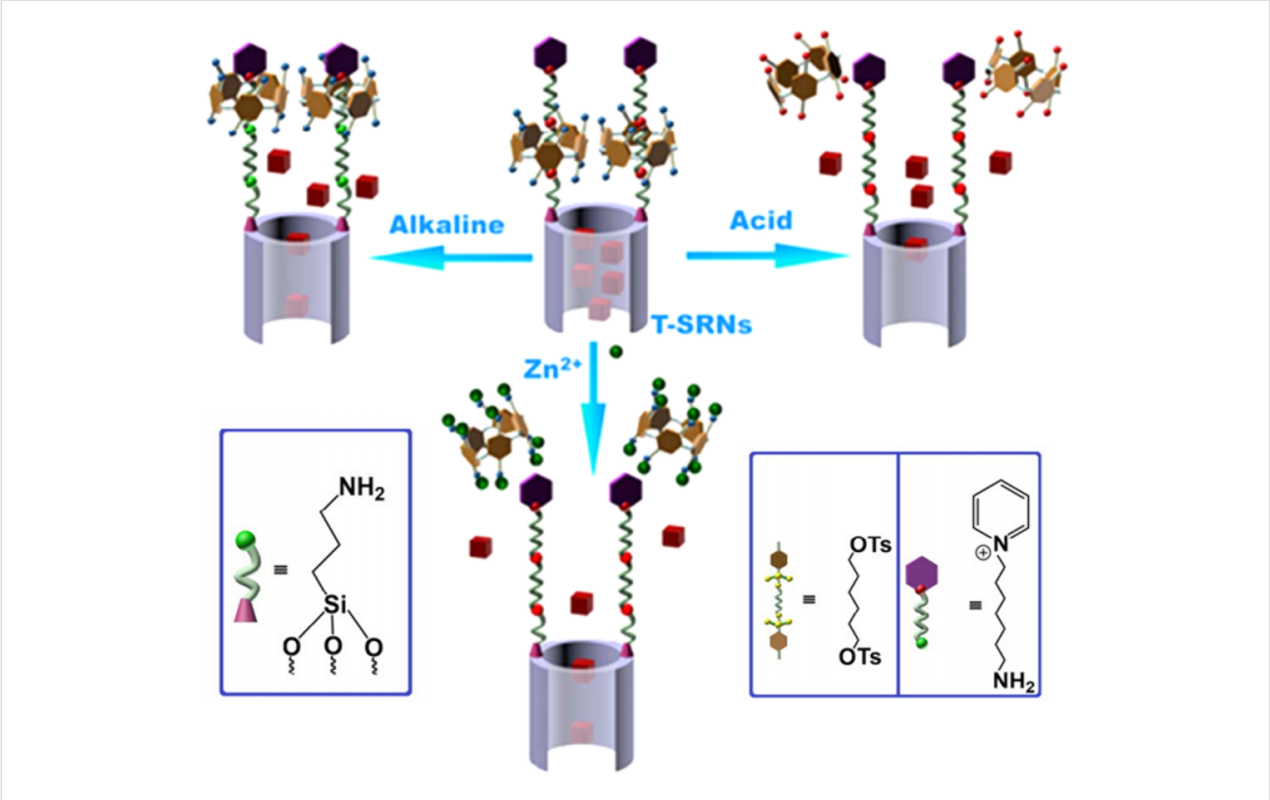

Figure 23: Schematic illustration of the activation of T-SRNs by acid, alkali, or Zn^{2+} stimuli to regulate the release of the model drug Rhodamine B (RhB) [132]. Figure 23 was used with permission of The Royal Society of Chemistry, from [132] ("Triple-stimuli-responsive nanocontainers assembled by water-soluble pillar [5] arene-based pseudorotaxanes for controlled release" by C. Ding et al., *J. Mater. Chem. B*, vol. 4, issue 16, © 2016); permission conveyed through Copyright Clearance Center, Inc. This content is not subject to CC BY 4.0.

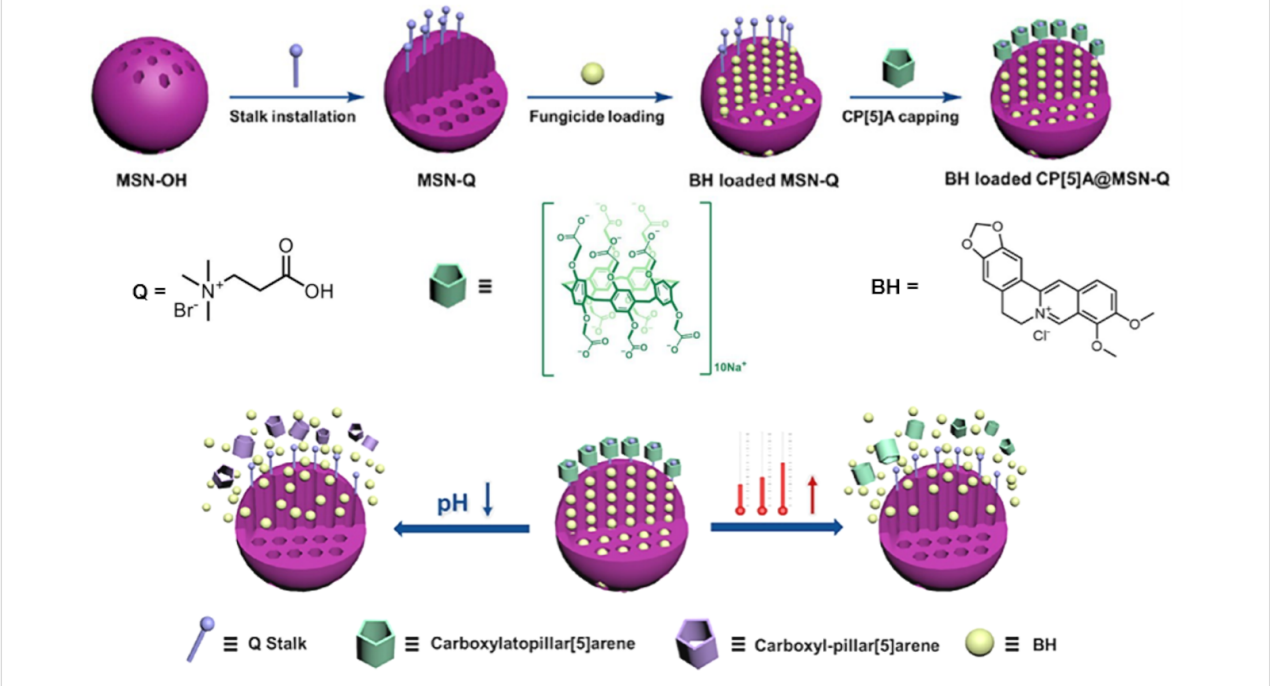

Figure 24: Illustration of the triggered release of BH from CP[5]A@MSNs-Q NPs in response to a drop in pH or a rise in temperature [133]. Figure 24 was adapted with permission from [133], Copyright 2021 American Chemical Society. This content is not subject to CC BY 4.0.

In 2022, Liu Yu and colleagues developed a pH and glutathione (GSH) dual-responsive supramolecular assembly by combining disulfide bond-containing pillar[4]arene (PA4) with tetraphenylethylene (TPE)-derived quaternary ammonium salts ($TPENC_n$, n = 6, 12) (Figure 25) [134]. The system leverages the acidic pH and reductive microenvironment of cancer cells to trigger targeted drug release. PA4, featuring acid-labile carboxylate groups and reduction-sensitive disulfide bonds, forms amphiphilic nanoparticles with $TPENC_n$ through electrostatic interactions, where the negatively charged PA4 pairs with the positively charged $TPENC_n$. The hydrophilic segments consist of PA4's carboxylate anions and $TPENC_n$'s quaternary ammonium sites, while their aromatic backbones constitute the hydrophobic core. This assembly lowers the CAC of $TPENC_n$, facilitating nanoparticle formation. Morphological studies confirmed well-structured nanoparticles optimized for cellular uptake. The dynamic non-covalent interactions enable stimulus-responsive behavior, allowing rapid drug release in acidic, high-GSH environments. Specifically, the TPENC6@PA4 nanoparticles demonstrated efficient DOX delivery, highlighting their potential as adaptive nanotherapeutics for cancer treatment.

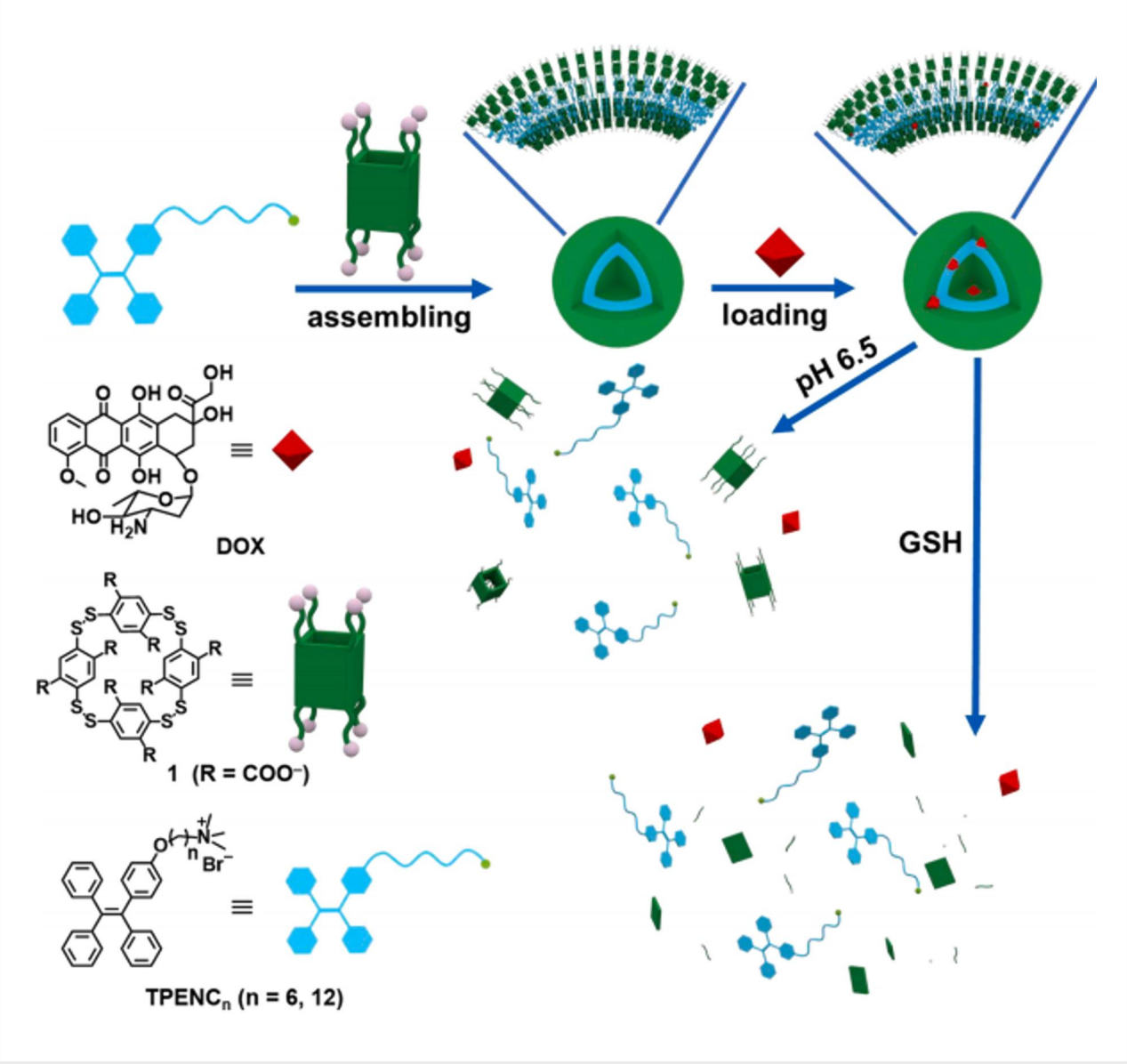

Figure 25: Illustration of the supramolecular amphiphiles $TPENC_n$@1 (n = 6 and 12) self-assembling with disulfide bond-PA4 to form vesicles, which then load DOX and respond to acidic environments and overexpressed GSH for degradation [134]. Figure 25 was reprinted from [134], *Bioorganic & Medicinal Chemistry*, vol. 57, by Tang, M.; Liu, Y. H.; Xu, X. M.; Zhang, Y. M.; Liu, Y. "Dual-responsive drug release and fluorescence imaging based on disulfide-pillar [4] arene aggregate in cancer cells", article no. 116649, Copyright (2022), with permission from Elsevier. This content is not subject to CC BY 4.0.

Conclusion

In summary, in recent years, supramolecular chemists have designed a series of easily synthesized aromatic macrocycles with electron-rich hydrophobic cavities. PAs and CAs, as intelligent hosts for drug-loading channels/holes, exhibit superior characteristics in supramolecular drug delivery systems. Most calix/pillar[*n*]arene hosts become water-soluble after modification with sulfonic acid, carboxyl, and phosphate groups. These calix/pillar[*n*]arene have good biocompatibility, ideal targeting ability, efficient operational capability, and precise response to various internal and external stimuli, and can be widely used as biomedicinal carriers. Researchers have connected functional groups that respond to specific stimuli to the aromatic macrocycle hosts. These specific functional groups endow supramolecular systems with rich responsiveness to light, pH, enzymes, and hypoxia-triggered, constructing different categories of supramolecular systems such as host–guest interactions, supramolecular self-assembly systems, and supramolecular nanovalves to achieve recognition, loading, and controlled entry and exit of drugs. It is worth mentioning that some of the constructed pH and enzyme-based controlled release systems can spontaneously generate stimulus responses in the tumor microenvironment without external human intervention to provide stimuli, thereby precisely releasing drugs, and have broad application prospects in cancer therapy.

Although there have been many reports on controlled release systems based on calix/pillar[*n*]arene in recent years, research in this field is still in its infancy, and it is challenging to conduct clinical trials for these systems. First, most stimulus-responsive nanosystems reported so far are based on SCA4 and CPA5−6. Compared to the extensive diversity of calix/pillar[*n*]arene, the currently developed types are just a tiny portion of the possible structures, greatly restricting the development of stimulus-responsive systems. Second, the known controlled release systems are usually limited to small molecules or ions, such as the anticancer drug DOX, the antibacterial MTZ, and ciprofloxacin. Due to the complexity and fragility of biomolecules, there are almost no reports on the encapsulation and release of larger biomolecules. Therefore, it is urgent to establish new stimulus-responsive controlled release systems that can contain large molecular drugs.

In view of the above, we hope that further improvement and overcoming can be achieved in future research. Different categories of aromatic macrocycles, such as tetralactam macrocycles and naphthotubes, can be tried to be modified with functional groups that respond to specific stimuli and used as hosts in release systems. Additionally, diverse stimulus-responsive systems derived from various group-modified aromatic macrocycles can be designed to align with the in vivo microenvironment, thereby facilitating the development of stimulus-responsive drug delivery systems. The photo-responsive systems based on CAs/PAs can be further optimized to improve their photo-responsive efficiency and stability. The applications of this system in more biomedical fields, such as targeted drug delivery and bioimaging, can be explored. The diversity of hypoxia-responsive systems can also be expanded by investigating CAs modified with different azobenzene structures for the treatment of tumor-related diseases. The drug release process is highly correlated with the disassembly of supramolecular nanoparticles. It can be anticipated that advanced drug loading and delivery efficiency combined with in situ monitoring of drug release will ultimately lead to effective chemotherapy and significantly inhibit tumor growth. In the future, the structure and properties of supramolecular amphiphiles can be further optimized to improve drug delivery efficiency and targeting ability. The applications of supramolecular amphiphiles in the treatment of other diseases can be explored, and the long-term safety and stability of supramolecular amphiphiles can be investigated. In the future, more biologically relevant molecules that have affinity for water-soluble CAs/PAs should be identified to achieve precise control over the size, shape, and stability of the assemblies. Other stimulus-responsive modes can be explored to expand the applications of these functional materials in other fields. Nevertheless, the clinical application of drug-controlled release systems based on aromatic macrocycles is still in its infancy. Extensive fundamental research and clinical trials are required to evaluate their safety, effectiveness, and practicality. Only through such rigorous assessment can these systems be more broadly implemented in clinical drug delivery, ultimately improving the precision and efficiency of drug administration and enhancing drug bioavailability. The development of supramolecular release systems new hope for improving drug targeting and bioavailability. Although there is still a need for innovation and progress in many aspects, we believe that with the in-depth research on stimulus-responsive host–guest chemistry, there is great potential in designing new therapies using release systems.

Acknowledgements

We are grateful to all of our co-workers for their contributions.

Funding

This research was financially supported by National Natural Science Foundation of China (No. 22174059 and 22201128). We thank USC for the technical support.

Author Contributions

Liu-Huan Yi: conceptualization; writing – original draft; writing – review & editing. Jian Qin: resources; writing – original draft. Si-Ran Lu: writing – original draft. Liu-Pan Yang:

funding acquisition; supervision; writing – review & editing. Li-Li Wang: conceptualization; funding acquisition; supervision; writing – review & editing. Huan Yao: funding acquisition; project administration; visualization; writing – review & editing.

ORCID® iDs

Li-Li Wang - https://orcid.org/0000-0001-9424-2972
Huan Yao - https://orcid.org/0000-0002-7114-1340

Data Availability Statement

Data sharing is not applicable as no new data was generated or analyzed in this study.

References

1. U.S. Food and Drug Administration. Federal Food, Drug, and Cosmetic Act, Section 201(g)(1), 21 USC §321(g)(1). 2025; https://www.accessdata.fda.gov/scripts/cdrh/cfdocs/cfcfr/CFRSearch.cfm?fr=201.128 (accessed June 28, 2025).
2. Vasan, N.; Baselga, J.; Hyman, D. M. *Nature* **2019,** *575,* 299–309. doi:10.1038/s41586-019-1730-1
3. Wu, S.; Yan, M.; Liang, M.; Yang, W.; Chen, J.; Zhou, J. *Cancer Drug Resist.* **2023,** *6,* 805–827. doi:10.20517/cdr.2023.77
4. Ward, R. A.; Fawell, S.; Floc'h, N.; Flemington, V.; McKerrecher, D.; Smith, P. D. *Chem. Rev.* **2021,** *121,* 3297–3351. doi:10.1021/acs.chemrev.0c00383
5. Tibbitt, M. W.; Dahlman, J. E.; Langer, R. *J. Am. Chem. Soc.* **2016,** *138,* 704–717. doi:10.1021/jacs.5b09974
6. Jing, Y.; Zhu, Y.; Yang, X.; Shen, J.; Li, C. *Langmuir* **2011,** *27,* 1175–1180. doi:10.1021/la1042734
7. Borgquist, P.; Körner, A.; Piculell, L.; Larsson, A.; Axelsson, A. *J. Controlled Release* **2006,** *113,* 216–225. doi:10.1016/j.jconrel.2006.05.004
8. Spang-Brunner, B. H.; Speiser, P. P. *J. Pharm. Pharmacol.* **1976,** *28,* 23–28. doi:10.1111/j.2042-7158.1976.tb04017.x
9. Mura, S.; Nicolas, J.; Couvreur, P. *Nat. Mater.* **2013,** *12,* 991–1003. doi:10.1038/nmat3776
10. Liu, M.; Du, H.; Zhang, W.; Zhai, G. *Mater. Sci. Eng., C* **2017,** *71,* 1267–1280. doi:10.1016/j.msec.2016.11.030
11. Park, K. *J. Controlled Release* **2014,** *190,* 3–8. doi:10.1016/j.jconrel.2014.03.054
12. Davoodi, P.; Lee, L. Y.; Xu, Q.; Sunil, V.; Sun, Y.; Soh, S.; Wang, C.-H. *Adv. Drug Delivery Rev.* **2018,** *132,* 104–138. doi:10.1016/j.addr.2018.07.002
13. Kamaly, N.; Yameen, B.; Wu, J.; Farokhzad, O. C. *Chem. Rev.* **2016,** *116,* 2602–2663. doi:10.1021/acs.chemrev.5b00346
14. Bernhard, S.; Tibbitt, M. W. *Adv. Drug Delivery Rev.* **2021,** *171,* 240–256. doi:10.1016/j.addr.2021.02.002
15. Yang, Y.; Li, P.; Feng, H.; Zeng, R.; Li, S.; Zhang, Q. *Molecules* **2024,** *29,* 3828. doi:10.3390/molecules29163828
16. Skorjanc, T.; Benyettou, F.; Olsen, J.-C.; Trabolsi, A. *Chem. – Eur. J.* **2017,** *23,* 8333–8347. doi:10.1002/chem.201605246
17. Liu, Y.-Y.; Yu, X.-Y.; Pan, Y.-C.; Yin, H.; Chao, S.; Li, Y.; Ma, H.; Zuo, M.; Teng, K.-X.; Hou, J.-L.; Chen, Y.; Guo, D.-S.; Wang, R.; Pei, Y.; Pei, Z.; Xu, J.-F.; Hu, X.-Y.; Li, C.; Yang, Q.-Z.; Wang, L.; Liu, Y.; Li, Z.-T. *Sci. China: Chem.* **2024,** *67,* 1397–1441. doi:10.1007/s11426-024-1971-4
18. Webber, M. J.; Langer, R. *Chem. Soc. Rev.* **2017,** *46,* 6600–6620. doi:10.1039/c7cs00391a
19. Liu, Z.; Nalluri, S. K. M.; Stoddart, J. F. *Chem. Soc. Rev.* **2017,** *46,* 2459–2478. doi:10.1039/c7cs00185a
20. Dong, R.; Zhou, Y.; Huang, X.; Zhu, X.; Lu, Y.; Shen, J. *Adv. Mater. (Weinheim, Ger.)* **2015,** *27,* 498–526. doi:10.1002/adma.201402975
21. Webber, M. J.; Appel, E. A.; Meijer, E. W.; Langer, R. *Nat. Mater.* **2016,** *15,* 13–26. doi:10.1038/nmat4474
22. Zhou, J.; Yu, G.; Huang, F. *Chem. Soc. Rev.* **2017,** *46,* 7021–7053. doi:10.1039/c6cs00898d
23. Fang, L.; Olson, M. A.; Benítez, D.; Tkatchouk, E.; Goddard III, W. A.; Stoddart, J. F. *Chem. Soc. Rev.* **2010,** *39,* 17–29. doi:10.1039/b917901a
24. Li, Y.; Li, Y.; Zhang, X.; Xu, X.; Zhang, Z.; Hu, C.; He, Y.; Gu, Z. *Theranostics* **2016,** *6,* 1293–1305. doi:10.7150/thno.15081
25. Terao, J.; Tang, A.; Michels, J. J.; Krivokapic, A.; Anderson, H. L. *Chem. Commun.* **2004,** 56–57. doi:10.1039/b311762f
26. Wang, S.; Yu, G.; Wang, Z.; Jacobson, O.; Tian, R.; Lin, L.-S.; Zhang, F.; Wang, J.; Chen, X. *Adv. Mater. (Weinheim, Ger.)* **2018,** *30,* 1803926. doi:10.1002/adma.201803926
27. Yu, G.; Ma, Y.; Han, C.; Yao, Y.; Tang, G.; Mao, Z.; Gao, C.; Huang, F. *J. Am. Chem. Soc.* **2013,** *135,* 10310–10313. doi:10.1021/ja405237q
28. Zhang, D.-W.; Zhao, X.; Li, Z.-T. *Acc. Chem. Res.* **2014,** *47,* 1961–1970. doi:10.1021/ar5000242
29. Yoon, H.-J.; Jang, W.-D. *J. Mater. Chem.* **2010,** *20,* 211–222. doi:10.1039/b910948j
30. Pitt, M. A.; Johnson, D. W. *Chem. Soc. Rev.* **2007,** *36,* 1441–1453. doi:10.1039/b610405n
31. Pluth, M. D.; Raymond, K. N. *Chem. Soc. Rev.* **2007,** *36,* 161–171. doi:10.1039/b603168b
32. Tashiro, K.; Aida, T. *Chem. Soc. Rev.* **2007,** *36,* 189–197. doi:10.1039/b614883m
33. Yang, Q.; Xu, W.; Cheng, M.; Zhang, S.; Kovaleva, E. G.; Liang, F.; Tian, D.; Liu, J.-a.; Abdelhameed, R. M.; Cheng, J.; Li, H. *Chem. Commun.* **2022,** *58,* 3255–3269. doi:10.1039/d1cc05584d
34. Lou, X. Y.; Li, Y. P.; Yang, Y. W. *Biotechnol. J.* **2018,** 14. doi:10.1002/biot.201800354
35. Peng, S.; Barba-Bon, A.; Pan, Y.-C.; Nau, W. M.; Guo, D.-S.; Hennig, A. *Angew. Chem., Int. Ed.* **2017,** *56,* 15742–15745. doi:10.1002/anie.201707979
36. Pan, Y.-C.; Barba-Bon, A.; Tian, H.-W.; Ding, F.; Hennig, A.; Nau, W. M.; Guo, D.-S. *Angew. Chem., Int. Ed.* **2021,** *60,* 1875–1882. doi:10.1002/anie.202011185
37. Martins, J. N.; Raimundo, B.; Rioboo, A.; Folgar-Cameán, Y.; Montenegro, J.; Basílio, N. *J. Am. Chem. Soc.* **2023,** *145,* 13126–13133. doi:10.1021/jacs.3c01829
38. Yu, N.; Li, G.; Gao, Y.; Liu, X.; Ma, S. *Int. J. Biol. Macromol.* **2016,** *93,* 971–977. doi:10.1016/j.ijbiomac.2016.09.068
39. Alabrahim, O. A. A.; Fahmy, S. A.; Azzazy, H. M. E.-S. *ACS Appl. Nano Mater.* **2023,** *6,* 3139–3158. doi:10.1021/acsanm.2c05391
40. Lai, G.-S.; Zhang, H.-L.; Jin, C.-M. *Electroanalysis* **2007,** *19,* 496–501. doi:10.1002/elan.200603751
41. Zhang, H.; Liu, Z.; Xin, F.; Hao, A. *Chin. J. Org. Chem.* **2012,** *32,* 219. doi:10.6023/cjoc1107141
42. Yang, L.; Zhong, L.; Yamato, K.; Zhang, X.; Feng, W.; Deng, P.; Yuan, L.; Zeng, X. C.; Gong, B. *New J. Chem.* **2009,** *33,* 729–733. doi:10.1039/b902495f

43. Liu, H.; Huang, Z.; Wen, K.; Jiang, B. *Chin. J. Org. Chem.* **2014,** *34,* 316–324. doi:10.6023/cjoc201307029
44. Jose, P.; Menon, S. *Bioinorg. Chem. Appl.* **2007,** No. 65815. doi:10.1155/2007/65815
45. Chen, L.; Cai, Y.; Feng, W.; Yuan, L. *Chem. Commun.* **2019,** *55,* 7883–7898. doi:10.1039/c9cc03292d
46. Li, P.; Chen, Y.; Liu, Y. *Chin. Chem. Lett.* **2019,** *30,* 1190–1197. doi:10.1016/j.cclet.2019.03.035
47. Basilio, N.; Francisco, V.; Garcia-Rio, L. *Int. J. Mol. Sci.* **2013,** *14,* 3140–3157. doi:10.3390/ijms14023140
48. Guo, D.-S.; Liu, Y. *Chem. Soc. Rev.* **2012,** *41,* 5907–5921. doi:10.1039/c2cs35075k
49. Ovsyannikov, A.; Solovieva, S.; Antipin, I.; Ferlay, S. *Coord. Chem. Rev.* **2017,** *352,* 151–186. doi:10.1016/j.ccr.2017.09.004
50. Chen, M.; Wang, C.; Fang, W.; Wang, J.; Zhang, W.; Jin, G.; Diao, G. *Langmuir* **2013,** *29,* 11858–11867. doi:10.1021/la4017799
51. Español, E. S.; Villamil, M. M. *Biomolecules* **2019,** *9,* 90. doi:10.3390/biom9030090
52. Guo, D.-S.; Liu, Y. *Acc. Chem. Res.* **2014,** *47,* 1925–1934. doi:10.1021/ar500009g
53. Ludwig, R. *Microchim. Acta* **2005,** *152,* 1–19. doi:10.1007/s00604-005-0422-8
54. Abd El-Rahman, M. K.; Mazzone, G.; Mahmoud, A. M.; Sicilia, E.; Shoeib, T. *Microchem. J.* **2019,** *146,* 735–741. doi:10.1016/j.microc.2019.01.046
55. Arduini, A.; Demuru, D.; Pochini, A.; Secchi, A. *Chem. Commun.* **2005,** 645–647. doi:10.1039/b411883a
56. Ostos, F. J.; Lebrón, J. A.; Moyá, M. L.; López-López, M.; Sánchez, A.; Clavero, A.; García-Calderón, C. B.; Rosado, I. V.; López-Cornejo, P. *Chem. – Asian J.* **2017,** *12,* 679–689. doi:10.1002/asia.201601713
57. Wang, J.; Ding, X.; Guo, X. *Adv. Colloid Interface Sci.* **2019,** *269,* 187–202. doi:10.1016/j.cis.2019.04.004
58. Li, R.; Liu, N.; Liu, R.; Jin, X.; Li, Z. *Curr. Drug Delivery* **2024,** *21,* 184–192. doi:10.2174/1567201820666230417084210
59. Ma, X.; Tian, H. *Acc. Chem. Res.* **2014,** *47,* 1971–1981. doi:10.1021/ar500033n
60. Ukhatskaya, E. V.; Kurkov, S. V.; Matthews, S. E.; El Fagui, A.; Amiel, C.; Dalmas, F.; Loftsson, T. *Int. J. Pharm.* **2010,** *402,* 10–19. doi:10.1016/j.ijpharm.2010.09.011
61. Xu, Z. Y.; Zhang, Y. C.; Lin, J. L.; Wang, H.; Zhang, D. W.; Li, Z. T. *Prog. Chem.* **2019,** *31,* 1540–1549. doi:10.7536/pc190817
62. Feng, W. W.; Jin, M.; Yang, K.; Pei, Y. X.; Pei, Z. C. *Chem. Commun.* **2018,** *54,* 13626–13640. doi:10.1039/c8cc08252a
63. Antimisiaris, S. G.; Mourtas, S.; Marazioti, A. *Pharmaceutics* **2018,** *10,* 218. doi:10.3390/pharmaceutics10040218
64. Xing, P.; Zhao, Y. *Small Methods* **2018,** *2,* 1700364. doi:10.1002/smtd.201700364
65. Gao, H.; Gao, L.; Lin, J.; Lu, Y.; Wang, L.; Cai, C.; Tian, X. *Macromolecules* **2020,** *53,* 3571–3579. doi:10.1021/acs.macromol.0c00146
66. Liu, J.-H.; Wu, X.; Zhang, Y.-M.; Liu, Y. *Asian J. Org. Chem.* **2018,** *7,* 2444–2447. doi:10.1002/ajoc.201800552
67. Estapé Senti, M.; de Jongh, C. A.; Dijkxhoorn, K.; Verhoef, J. J. F.; Szebeni, J.; Storm, G.; Hack, C. E.; Schiffelers, R. M.; Fens, M. H.; Boross, P. *J. Controlled Release* **2022,** *341,* 475–486. doi:10.1016/j.jconrel.2021.11.042
68. Lu, B.; Lv, X.; Le, Y. *Polymers (Basel, Switz.)* **2019,** *11,* 304. doi:10.3390/polym11020304
69. Tian, H.-W.; Xu, Z.; Li, H.-B.; Hu, X.-Y.; Guo, D.-S. *Supramol. Chem.* **2021,** *33,* 527–533. doi:10.1080/10610278.2022.2087523
70. Wang, Y.-X.; Guo, D.-S.; Duan, Y.-C.; Wang, Y.-J.; Liu, Y. *Sci. Rep.* **2015,** *5,* 9019. doi:10.1038/srep09019
71. Basílio, N.; Garcia-Rio, L.; Martín-Pastor, M. *Langmuir* **2012,** *28,* 2404–2414. doi:10.1021/la204004h
72. Suwinska, K.; Lesniewska, B.; Jebors, S.; Coleman, A. W. *Acta Crystallogr., Sect. A: Found. Crystallogr.* **2009,** *65,* s90. doi:10.1107/s0108767309098237
73. Lee, M.; Lee, S.-J.; Jiang, L.-H. *J. Am. Chem. Soc.* **2004,** *126,* 12724–12725. doi:10.1021/ja045918v
74. Ogoshi, T.; Kanai, S.; Fujinami, S.; Yamagishi, T.-a.; Nakamoto, Y. *J. Am. Chem. Soc.* **2008,** *130,* 5022–5023. doi:10.1021/ja711260m
75. Ogoshi, T.; Yamagishi, T.-a.; Nakamoto, Y. *Chem. Rev.* **2016,** *116,* 7937–8002. doi:10.1021/acs.chemrev.5b00765
76. Cao, M.; Hao, Y.; Xu, Z.; Hua Liu, S.; Yin, J. *Curr. Org. Chem.* **2016,** *20,* 1299–1313. doi:10.2174/1385272819666151022221121
77. Shu, X.; Chen, W.; Hou, D.; Meng, Q.; Zheng, R.; Li, C. *Chem. Commun.* **2014,** *50,* 4820–4823. doi:10.1039/c4cc00800f
78. Yu, G.; Zhou, X.; Zhang, Z.; Han, C.; Mao, Z.; Gao, C.; Huang, F. *J. Am. Chem. Soc.* **2012,** *134,* 19489–19497. doi:10.1021/ja3099905
79. Chen, W.; Zhang, Y.; Li, J.; Lou, X.; Yu, Y.; Jia, X.; Li, C. *Chem. Commun.* **2013,** *49,* 7956–7958. doi:10.1039/c3cc44328k
80. Yu, G.; Yang, J.; Xia, D.; Yao, Y. *RSC Adv.* **2014,** *4,* 18763–18771. doi:10.1039/c4ra01820f
81. Lin, Q.; Liu, L.; Zheng, F.; Mao, P.-P.; Liu, J.; Zhang, Y.-M.; Yao, H.; Wei, T.-B. *RSC Adv.* **2017,** *7,* 34411–34414. doi:10.1039/c7ra05750d
82. Wei, P.; Gangapurwala, G.; Pretzel, D.; Wang, L.; Schubert, S.; Brendel, J. C.; Schubert, U. S. *Nanoscale* **2020,** *12,* 13595–13605. doi:10.1039/d0nr01881c
83. Peng, H.; Xie, B.; Cen, X.; Dai, J.; Dai, Y.; Yang, X.; He, Y. *Mater. Chem. Front.* **2022,** *6,* 360–367. doi:10.1039/d1qm01459e
84. Sun, Y.-L.; Yang, Y.-W.; Chen, D.-X.; Wang, G.; Zhou, Y.; Wang, C.-Y.; Stoddart, J. F. *Small* **2013,** *9,* 3224–3229. doi:10.1002/smll.201300445
85. Song, N.; Yang, Y.-W. *Sci. China: Chem.* **2014,** *57,* 1185–1198. doi:10.1007/s11426-014-5190-z
86. Wang, C.; Li, H.; Dong, J.; Chen, Y.; Luan, X.; Li, X.; Du, X. *Chem. – Eur. J.* **2022,** *28,* e202202050. doi:10.1002/chem.202202050
87. Song, N.; Lou, X.-Y.; Ma, L.; Gao, H.; Yang, Y.-W. *Theranostics* **2019,** *9,* 3075–3093. doi:10.7150/thno.31858
88. Tan, L. L.; Li, H. W.; Qiu, Y. C.; Chen, D. X.; Wang, X.; Pan, R. Y.; Wang, Y.; Zhang, S. X. A.; Wang, B.; Yang, Y. W. *Chem. Sci.* **2015,** *6,* 1640–1644. doi:10.1039/c4sc03749a
89. Colilla, M.; González, B.; Vallet-Regí, M. *Biomater. Sci.* **2013,** *1,* 114–134. doi:10.1039/c2bm00085g
90. Huang, X.; Wu, S.; Ke, X.; Li, X.; Du, X. *ACS Appl. Mater. Interfaces* **2017,** *9,* 19638–19645. doi:10.1021/acsami.7b04015
91. Hu, X.; Yang, H. *RSC Adv.* **2021,** *11,* 7450–7453. doi:10.1039/d0ra10871e
92. Braegelman, A. S.; Webber, M. J. *Theranostics* **2019,** *9,* 3017–3040. doi:10.7150/thno.31913
93. Duan, Q. P.; Cao, Y.; Li, Y.; Hu, X. Y.; Xiao, T. X.; Lin, C.; Pan, Y.; Wang, L. Y. *J. Am. Chem. Soc.* **2013,** *135,* 10542–10549. doi:10.1021/ja405014r
94. Xia, W.; Ni, M.; Yao, C.; Wang, X.; Chen, D.; Lin, C.; Hu, X.-Y.; Wang, L. *Macromolecules* **2015,** *48,* 4403–4409. doi:10.1021/acs.macromol.5b00889
95. Guo, D.-S.; Zhang, T.-X.; Wang, Y.-X.; Liu, Y. *Chem. Commun.* **2013,** *49,* 6779–6781. doi:10.1039/c3cc41918e

96. Tao, Y.; Chan, H. F.; Shi, B.; Li, M.; Leong, K. W. *Adv. Funct. Mater.* **2020,** *30,* 2005029. doi:10.1002/adfm.202005029
97. Cafeo, G.; Carbotti, G.; Cuzzola, A.; Fabbi, M.; Ferrini, S.; Kohnke, F. H.; Papanikolaou, G.; Plutino, M. R.; Rosano, C.; White, A. J. P. *J. Am. Chem. Soc.* **2013,** *135,* 2544–2551. doi:10.1021/ja307791j
98. Zhu, H.; Li, Q.; Khalil-Cruz, L. E.; Khashab, N. M.; Yu, G.; Huang, F. *Sci. China: Chem.* **2021,** *64,* 688–700. doi:10.1007/s11426-020-9932-9
99. Xu, W.; Cheng, M.; Zhang, S.; Wu, Q.; Liu, Z.; Dhinakaran, M. K.; Liang, F.; Kovaleva, E. G.; Li, H. *Chem. Commun.* **2021,** *57,* 7480–7492. doi:10.1039/d1cc01501j
100. Li, Z. T.; Yang, J.; Huang, F. H. *Chin. J. Chem.* **2018,** *36,* 59–62. doi:10.1002/cjoc.201700601
101. Xue, Y.; Guan, Y.; Zheng, A.; Xiao, H. *Colloids Surf., B* **2013,** *101,* 55–60. doi:10.1016/j.colsurfb.2012.06.022
102. Li, Z.; Yang, J.; Yu, G.; He, J.; Abliz, Z.; Huang, F. *Org. Lett.* **2014,** *16,* 2066–2069. doi:10.1021/ol500686r
103. Sreedevi, P.; Nair, J. B.; Joseph, M. M.; Murali, V. P.; Suresh, C. H.; Varma, R. L.; Maiti, K. K. *J. Controlled Release* **2021,** *339,* 284–296. doi:10.1016/j.jconrel.2021.09.038
104. Cao, Y.; Li, Y.; Hu, X.-Y.; Zou, X.; Xiong, S.; Lin, C.; Wang, L. *Chem. Mater.* **2015,** *27,* 1110–1119. doi:10.1021/cm504445r
105. Yang, J.; Yu, G.; Xia, D.; Huang, F. *Chem. Commun.* **2014,** *50,* 3993–3995. doi:10.1039/c4cc00590b
106. Yu, G.; Xue, M.; Zhang, Z.; Li, J.; Han, C.; Huang, F. *J. Am. Chem. Soc.* **2012,** *134,* 13248–13251. doi:10.1021/ja306399f
107. Cao, Y.; Hu, X.-Y.; Li, Y.; Zou, X.; Xiong, S.; Lin, C.; Shen, Y.-Z.; Wang, L. *J. Am. Chem. Soc.* **2014,** *136,* 10762–10769. doi:10.1021/ja505344t
108. Chen, Y.; Rui, L.; Liu, L.; Zhang, W. *Polym. Chem.* **2016,** *7,* 3268–3276. doi:10.1039/c6py00505e
109. Zhou, W.; Chen, S.; Ouyang, Y.; Huang, B.; Zhang, H.; Zhang, W.; Tian, J. *Chem. Sci.* **2023,** *14,* 11481–11489. doi:10.1039/d3sc03797e
110. Zhu, H.; Shangguan, L.; Xia, D.; Mondal, J. H.; Shi, B. *Nanoscale* **2017,** *9,* 8913–8917. doi:10.1039/c7nr03160b
111. Qu, D.-H.; Wang, Q.-C.; Zhang, Q.-W.; Ma, X.; Tian, H. *Chem. Rev.* **2015,** *115,* 7543–7588. doi:10.1021/cr5006342
112. Shao, L.; Hua, B.; Yang, J.; Yu, G. *Chem. Commun.* **2016,** *52,* 6573–6576. doi:10.1039/c6cc02434c
113. Shao, L.; Hua, B.; Sun, J.; Li, Q.; Yang, J.; Yu, G. *Tetrahedron Lett.* **2017,** *58,* 1863–1867. doi:10.1016/j.tetlet.2017.03.091
114. Wang, Y.-X.; Zhang, Y.-M.; Liu, Y. *J. Am. Chem. Soc.* **2015,** *137,* 4543–4549. doi:10.1021/jacs.5b01566
115. Jiang, B.-P.; Guo, D.-S.; Liu, Y.-C.; Wang, K.-P.; Liu, Y. *ACS Nano* **2014,** *8,* 1609–1618. doi:10.1021/nn405923b
116. Liu, K.; Liu, Y.; Yao, Y.; Yuan, H.; Wang, S.; Wang, Z.; Zhang, X. *Angew. Chem., Int. Ed.* **2013,** *52,* 8285–8289. doi:10.1002/anie.201303387
117. Pang, H.; Xu, P.; Li, C.; Zhan, Y.; Zhang, Z.; Zhang, W.; Yang, G.; Sun, Y.; Li, H. *Chem. Commun.* **2018,** *54,* 2978–2981. doi:10.1039/c8cc01196f
118. Prigyai, N.; Bunchuay, T.; Ruengsuk, A.; Yoshinari, N.; Manissorn, J.; Pumirat, P.; Sapudom, J.; Kosiyachinda, P.; Thongnuek, P. *ACS Appl. Mater. Interfaces* **2024,** *16,* 8250–8265. doi:10.1021/acsami.3c14760
119. Guo, D.-S.; Wang, K.; Wang, Y.-X.; Liu, Y. *J. Am. Chem. Soc.* **2012,** *134,* 10244–10250. doi:10.1021/ja303280r
120. Li, Y.; Bai, H.; Li, C.; Shi, G. *ACS Appl. Mater. Interfaces* **2011,** *3,* 1306–1310. doi:10.1021/am200101n
121. Sun, Y.-L.; Zhou, Y.; Li, Q.-L.; Yang, Y.-W. *Chem. Commun.* **2013,** *49,* 9033–9035. doi:10.1039/c3cc45216f
122. Zhang, T.-X.; Zhang, Z.-Z.; Yue, Y.-X.; Hu, X.-Y.; Huang, F.; Shi, L.; Liu, Y.; Guo, D.-S. *Adv. Mater. (Weinheim, Ger.)* **2020,** *32,* 1908435. doi:10.1002/adma.201908435
123. Guo, J.-S.; Li, J.-J.; Wang, Z.-H.; Liu, Y.; Yue, Y.-X.; Li, H.-B.; Zhao, X.-H.; Sun, Y.-J.; Ding, Y.-H.; Ding, F.; Guo, D.-S.; Wang, L.; Chen, Y. *Nat. Commun.* **2023,** *14,* 5634. doi:10.1038/s41467-023-41388-2
124. Chen, M.-M.; Tang, X.; Li, J.-J.; Chen, F.-Y.; Jiang, Z.-T.; Fu, R.; Li, H.-B.; Hu, X.-Y.; Geng, W.-C.; Guo, D.-S. *J. Controlled Release* **2024,** *368,* 691–702. doi:10.1016/j.jconrel.2024.03.017
125. Zheng, W.; Yao, S.-Y.; Hu, H.; Chen, X.; Qian, Z.; Liu, W.; Zhu, Y.; Mao, Z.; Guo, D.-S.; Gao, C. *Nano Today* **2024,** *54,* 102064. doi:10.1016/j.nantod.2023.102064
126. Geng, Y.-Q.; Qiu, L.-N.; Cheng, Y.-Q.; Li, J.-J.; Ma, Y.-L.; Zhao, C.-C.; Cai, Y.; Zhang, X.-B.; Chen, J.; Pan, Y.-C.; Wang, K.-R.; Yao, X.-H.; Guo, D.-S.; Wu, J.-L. *Adv. Sci.* **2024,** *11,* 2309517. doi:10.1002/advs.202309517
127. Wang, K.; Guo, D.-S.; Wang, X.; Liu, Y. *ACS Nano* **2011,** *5,* 2880–2894. doi:10.1021/nn1034873
128. Chen, X.; Wang, Z.; Sun, X.; Han, Y.; Huang, Y.; Xi, J.; Bian, X.; Han, J.; Guo, R. *Chem. Eng. J.* **2021,** *403,* 126423. doi:10.1016/j.cej.2020.126423
129. Gao, L.; Wang, T.; Jia, K.; Wu, X.; Yao, C.; Shao, W.; Zhang, D.; Hu, X.-Y.; Wang, L. *Chem. – Eur. J.* **2017,** *23,* 6605–6614. doi:10.1002/chem.201700345
130. Shen, Z.; Ma, N.; Wang, F.; Ren, J.; Hou, C.; Chao, S.; Pei, Y.; Pei, Z. *Chin. Chem. Lett.* **2022,** *33,* 4563–4566. doi:10.1016/j.cclet.2022.01.069
131. Huang, X.; Du, X. *ACS Appl. Mater. Interfaces* **2014,** *6,* 20430–20436. doi:10.1021/am506004q
132. Ding, C.; Liu, Y.; Wang, T.; Fu, J. *J. Mater. Chem. B* **2016,** *4,* 2819–2827. doi:10.1039/c6tb00459h
133. Wang, C.-Y.; Lou, X.-Y.; Cai, Z.; Zhang, M.-Z.; Jia, C.; Qin, J.-C.; Yang, Y.-W. *ACS Appl. Mater. Interfaces* **2021,** *13,* 32295–32306. doi:10.1021/acsami.1c08582
134. Tang, M.; Liu, Y. H.; Xu, X. M.; Zhang, Y. M.; Liu, Y. *Bioorg. Med. Chem.* **2022,** *57,* 116649. doi:10.1016/j.bmc.2022.116649

License and Terms

BEILSTEIN JOURNAL OF ORGANIC CHEMISTRY

Synthesis and characterization of a isothiouronium-calix[4]arene derivative: self-assembly and anticancer activity

Giuseppe Granata[‡1], Loredana Ferreri[‡1], Claudia Giovanna Leotta[2,3], Giovanni Mario Pitari[2,3] and Grazia Maria Letizia Consoli[*1]

Full Research Paper

Open Access

Address:
[1]CNR-Institute of Biomolecular Chemistry, Via Paolo Gaifami 18, 95126 Catania, Italy, [2]Dream Factory Lab, Vera Salus Ricerca S.r.L., Via Sigmund Freud 62/B, 96100, Siracusa, Italy and [3]J4Med Lab, Via Paolo Gaifami 9, 95126 Catania, Italy

Email:
Grazia Maria Letizia Consoli[*] - graziamarialetizia.consoli@cnr.it

* Corresponding author ‡ Equal contributors

Keywords:
anticancer agent; calixarene; nanostructure; self-assembly

Beilstein J. Org. Chem. **2025,** *21,* 2535–2541.
https://doi.org/10.3762/bjoc.21.195

Received: 07 August 2025
Accepted: 10 October 2025
Published: 14 November 2025

This article is part of the thematic issue "Novel macrocycles: from synthesis to supramolecular function".

Guest Editor: C. Gaeta

Abstract

Calix[*n*]arenes are polyphenolic macrocycles known for their remarkable synthetic versatility, which supports their broad application in various areas, including drug discovery. Their unique conformational features, functionality, and low toxicity make calixarene derivatives valuable drug candidates against cancer. The aim of the present study was the synthesis and characterization of a calix[4]arene derivative in which known anticancer isothiouronium groups were clustered on a calix[4]arene scaffold bearing long C12 alkyl chains at the lower rim. The resulting amphiphilic calix[4]arene derivative **3** spontaneously self-assembled into nanoscale aggregates in aqueous medium, as demonstrated by dynamic light scattering analysis. The cytotoxicity of compound **3** towards cancer cells was assessed using human renal carcinoma cells (786-O cells) and compared with that in non-malignant fibroblast cells (SW1 cells). Compound **3** showed a significantly greater antiproliferative effect on cancer cells (IC_{50} 37.4 μM) than on normal fibroblasts (517 μM). The importance of the isothiouronium moieties in the observed cytoxic effect was confirmed by comparison with the calix[4]arene precursor (**1**) lacking these functional units. The selective antiproliferative profile of compound **3** highlights its potential as a lead anticancer agent. Moreover, compound **3** holds promise for further development in combination multidrug therapy due to the potential to load drug molecules in the bioactive nanoassembled structure.

Introduction

Cancer remains one of the leading causes of morbidity and mortality worldwide. Despite significant advancements in chemotherapy, more effective and less toxic, targeted treatments are still urgently needed [1]. Among the most promising avenues in cancer therapy research, multivalent compounds have emerged as a powerful class of agents for tumor diagnosis, analysis, and therapy [2]. By exposing multiple functional groups within a single molecular framework, these compounds

offer the potential for enhanced therapeutic efficacy through a multivalency effect. Multivalency is a strategy employed by nature to improve selectivity, specificity, and avidity in molecular recognition events responsible for both physiological and pathological processes. Multiple ligand–receptor interactions can significantly enhance receptor binding affinity and cellular uptake, as well as more effectively modulate signal transduction pathways, for instance when receptor clustering is necessary on the cell membrane [3]. Designing multivalent bioactive compounds thus represents a promising approach to overcoming several limitations associated with traditional monovalent therapeutics, including drug resistance, off-target effects, high dosage requirements, and insufficient specificity. This strategy may pave the way for next-generation anticancer therapies more effective and precise than current treatments. Numerous multivalent constructs have been reported in literature, both as compounds with intrinsic anticancer activity [4] and nanocarriers for anticancer drug delivery [5,6].

In the development of multivalent compounds, macrocyclic scaffolds such as cyclodextrins [7], cyclic peptides [8], cucurbiturils [9], resorcinarenes [10], pillarenes [11], prismarenes [12], and calix[*n*]arenes have proven to be particularly valuable.

Calix[*n*]arenes, a family of polyphenolic macrocyclic oligomers, are widely utilized in applications ranging from materials science to life sciences [13-17]. Their synthetic versatility, ease of functionalization, conformational rigidity or flexibility, steric bulk, and low cost make them highly attractive in the development of novel, non-conventional anticancer agents with a great potential for overcoming the toxicity of cancer chemotherapy and achieving targeted treatments [18-20].

In the era of nanotechnology, a promising strategy for developing more effective treatments against cancer [21,22], calixarene derivatives are also emerging as valid building blocks for the development of nanoscale multivalent constructs [23]. Due to the nanosize, the calixarene-based nanoconstructs could preferentially accumulate in cancer tissues by exploiting the enhanced tumor permeability and retention (EPR) effect [24] or selectively penetrate cancer cells through specific ligand–receptor interactions on the surface of target cells [25,26]. A variety of calixarene-based nanoconstructs have been reported, including nanosystems with light-triggered anticancer activity [27], potential anticancer vaccine candidates [28], and nanocarriers for anticancer drug delivery [29-33].

Numerous bioactive groups have been introduced into the calixarene skeleton to develop anticancer derivatives, including proline [34], carbonyl amide [35], glycoureido [36], ureido [37], picolylamine [38], 5-bromopentyltrimethylammonium bromide and 3-bromopropyltriphenylphosphonium bromide [39], among others.

Isothiouronium salts represent another class of interest in the search for new chemotherapeutic agents. They are known inhibitors of protein kinase C [40] and agonists of the GABA-type [41] and histamine-H3 receptors [42]. *S*-Allylic isothiouronium salts substituted with aliphatic groups have shown to combine high antitumor activity against leukemia cells and low toxicity toward non-cancerous cells [43].

Therefore, the aim of this study was to evaluate whether introducing isothiouronium moieties at the upper rim of a calix[4]arene scaffold, bearing long C12 alkyl chains at the lower rim, could yield a novel derivative (compound **3**) with anticancer activity. The synthesis and structural characterization of compound **3** were carried out, and its self-assembly behavior in aqueous medium was investigated using dynamic light scattering (DLS) and electrophoretic light scattering (ELS). The anticancer potential of compound **3** was assessed in human renal carcinoma cells (786O) and normal human fibroblasts (SW1), and the tumor cells selectivity was evaluated. To elucidate the role of the isothiouronium groups, antiproliferative effects were also estimated on calix[4]arene precursor **1** lacking these functional groups.

Results and Discussion

Synthesis and characterization of compound 3

For the synthesis of isothiouronium-calix[4]arene derivative **3** (Scheme 1), the chloromethylcalix[4]arene derivative **2** was prepared by adopting a procedure reported in the literature [44].

In brief, starting from the commercial *p*-H-calix[4]arene **1**, four C-12 alkyl chains were tethered to the calixarene hydroxy groups (lower rim) by reaction with dodecyl iodide in the presence of NaH. At the upper rim of this derivative, four formyl groups were introduced by reaction with hexamethylenetetramine in trifluoroacetic acid. The formyl groups were reduced to alcohol groups by sodium borohydride and then converted to chloromethyl groups by treatment with thionyl chloride, to give compound **2**.

The reaction of compound **2** with thiourea in THF gave compound **3** as a white solid in 96% yield. Compound **3** was characterized by ^{1}H and ^{13}C NMR in DMSO-d_6 as a solvent (Figure 1). The proton signals of the NH_2 and CH_2S groups of the isothiouronium substituents were clearly observed at 9.04 ppm and 4.23 ppm, respectively. Additionally, the carbon signal of the CH_2S group appeared at 169.3 ppm. The NMR

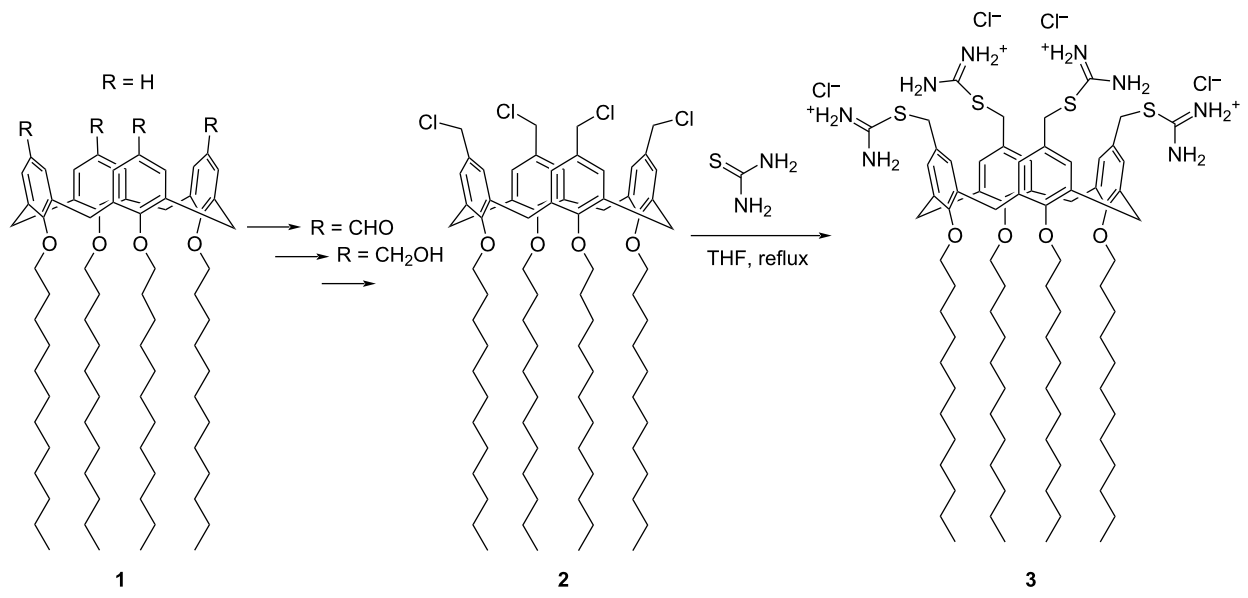

Scheme 1: Procedure for the synthesis of compound **3**.

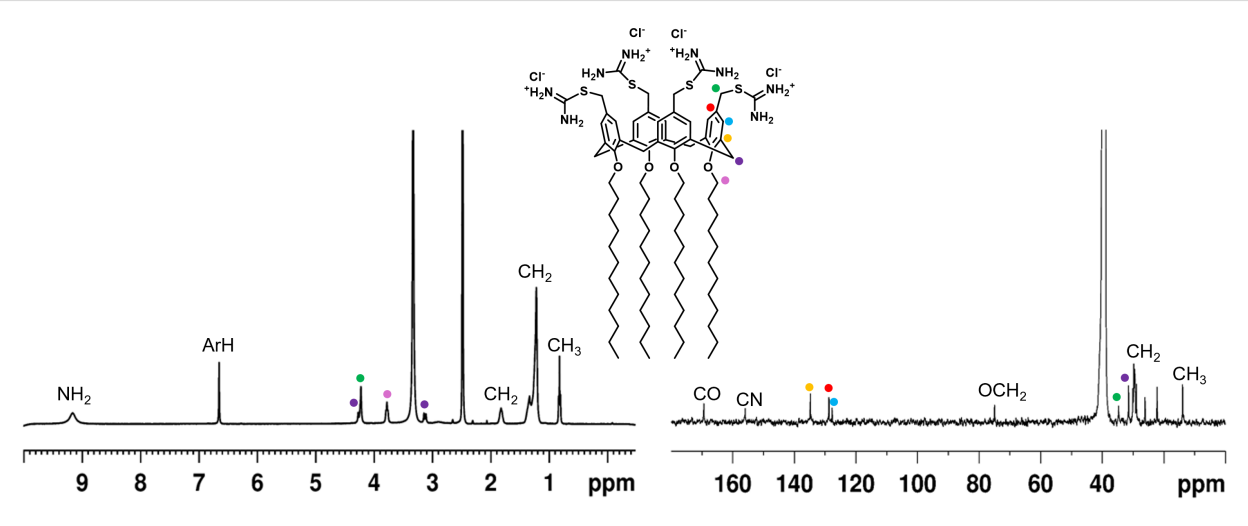

Figure 1: ^{1}H NMR (left) and ^{13}C NMR (right) spectra of compound **3** in DMSO-d_6 (400.13 MHz, 297 K).

signals, consistent with a fully symmetric structure, evidenced the exhaustive functionalization of the calix[4]arene skeleton blocked in cone conformation, as evidenced by the AX system (3.13 and 4.26 ppm) for the bridged CH_2 protons.

Spontaneous self-assembly

Due to the amphiphilic nature, compound **3** could spontaneously self-assemble in aqueous medium. This was confirmed by dynamic light scattering measurements, which showed the presence of nanoaggregates with mean hydrodynamic diameters of 125 ± 1 nm in the aqueous colloidal solution of compound **3** (Figure 2).

A polydispersity index of 0.18 ± 0.01 was indicative of a good dimensional homogeneity of the nanoaggregates in the suspension.

The zeta potential is a measure of the electrical potential between the surface of nanoaggregates and the surrounding fluid. Electrophoretic light scattering (ELS) provided for the nanoaggregates of compound **3** a zeta potential (ζ) value of +64 ± 1 mV (Figure 3), indicative of stable nanoassemblies. Indeed, it is generally accepted that values higher than ±40 mV are associated with strong stability by repulsion, preventing further aggregation phenomena.

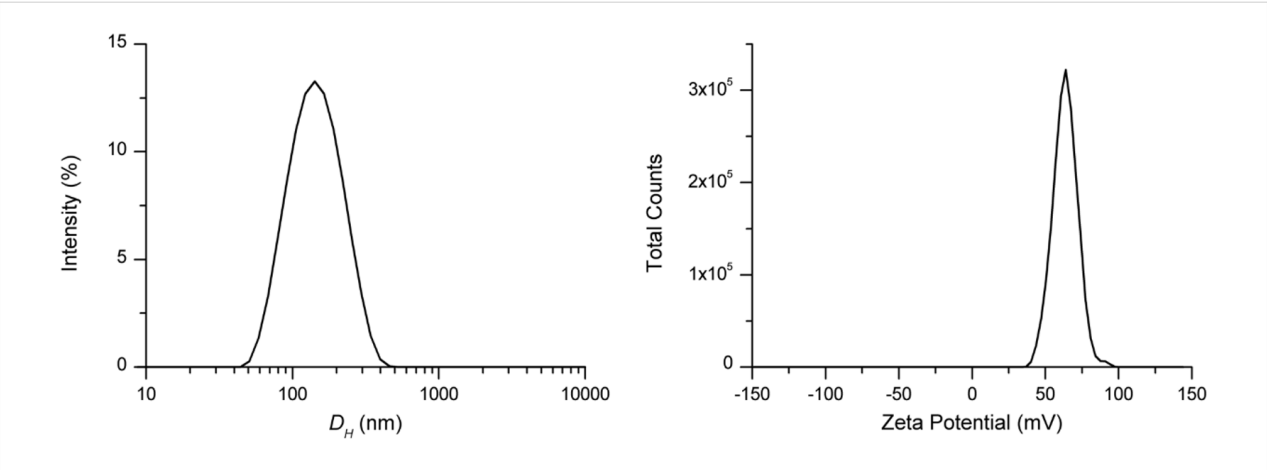

Figure 2: Intensity-weighted mean hydrodynamic diameter (left), and zeta potential distribution (right) of compound **3** (1 mg/mL water), after vortex and sonication.

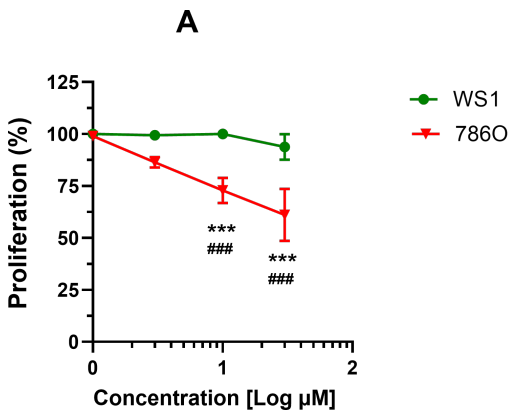

B

IC_{50} (µM)	786O	WS1
Compound **3**	37.40 ± 25.86	517.1 ± 292.74
Compound **1**	662.8 ± 342.24	1014 ± 545.48
Doxorubicin	0.34 ± 0.07	0.16 ± 0.02

Figure 3: Antiproliferative effects by compound **3** and its chemical precursor **1**. A) Results on proliferative kinetics in renal cancer 786O and skin fibroblast WS1 cells. Data represent the percentage of proliferation with respect to the correspondent vehicle DMSO controls. ***, $p < 0.001$ vs the respective vehicle control by 2-way ANOVA; ###, $p < 0.001$ vs correspondent WS1 conditions by 2-way ANOVA. B) Calculated IC_{50} for compounds **3** and **1** in renal cancer 786O and skin fibroblast WS1 cells. Doxorubicin, the positive control. Data are expressed as means ± SD.

Cytotoxicity and cancer cell selectivity

Thiouronium-containing molecules can inhibit cancer cells, inducing apoptosis or necrosis, by different mechanisms including elevation of reactive oxygen species (ROS) or interference with redox homeostasis, and inhibition of kinase or topoisomerase activities essential for cancer cell proliferation. The selective activity of thiouronium salts against cancer cells compared to non-malignant cells can be related to a specific sensitivity of cancer cells [43]. In fact, cancer cells operate under higher oxidative stress than normal cells and often overexpress kinases or topoisomerases, which make them more vulnerable than normal cells.

The anticancer effect of compound **3** was assessed on human renal carcinoma 786O cells, through evaluation of proliferative kinetics with the acridine orange staining assay [45]. The 786O cell line is a widely used in vitro model for studying clear cell renal cell carcinoma (ccRCC) [46], which accounts for over 90% of all renal malignancies and is characterized by poor responsiveness to conventional chemotherapy.

To the best of our knowledge, calixarene derivatives have not been previously tested as anticancer agents against human renal carcinoma cells.

Compound **3** suppressed the proliferation of the renal cancer cells (Figure 3) with a calculated 50% inhibitory concentration (IC_{50}) of 37.40 µM. In contrast, compound **3** was poorly effective against normal WS1 fibroblasts (Figure 3), exhibiting an IC_{50} value of 517 µM. These values yielded a selectivity index (SI) of approximately 14, indicating that tumor cells are significantly more sensitive to the cytotoxic effects of compound **3**

than healthy, non-malignant cells. In general, SI values above 12 are associated to remarkable selectivity, 6–12 to moderate selectivity and 1–5 to weak selectivity [43,47]. In contrast, the potent antineoplastic agent doxorubicin, used as the positive control for anticancer effects, did not discriminate between normal and cancer cells, as demonstrated by the calculated SI of 0.47. The high SI value by compound **3** evidenced the isothiouronium moieties retain the selective cytotoxicity towards cancer cells also when tethered to the calixarene scaffold.

Since the long alkyl chains in compound **3** could be responsible for molecular disruptive events at the cell membrane through intercalation in the lipidic bilayer, the effects of *p*-H-calix[4]arene-*O*-dodecyl derivative **1**, a precursor lacking isothiouronium moieties, on cell proliferation were also investigated. The absence of the isothiouronium groups substantially blunted the antiproliferative activity in both cancer and normal cells, as demonstrated by the higher IC_{50} values exhibited by compound **1** (Figure 3). These data clearly demonstrated that isothiouronium moieties are crucial for the anticancer activity of compound **3**.

Conclusion

The introduction of four isothiouronium functional groups at the upper rim of a calix[4]arene macrocycle, bearing four dodecyl aliphatic chains at the lower rim, yields an amphiphilic derivative that spontaneously self-assembles into nanoscale structures with a mean hydrodynamic diameter of approximately 100 nm and a positively charged surface (zeta potential + 64 mV). These values are suitable for potential applications in the field of nanomedicine. Remarkably, the isothiouronium-calix[4]arene derivative, unlike its precursor lacking isothiouronium functionalities, inhibited the proliferation of human renal carcinoma cells with notable selectivity over normal human fibroblasts. To the best of our knowledge, this is the first study evaluating the antiproliferative activity of both a thiouronium salt and a calix[4]arene derivative in renal carcinoma cells. The isothiouronium-calix[4]arene nanoassemblies may be promising candidates for further investigations as a drug delivery system. The entrapment of different drugs combined with the intrinsic anticancer activity of the nanoassemblies could provide new agents for a combination multidrug anticancer treatment.

Experimental

Materials and methods: All chemicals were purchased from Sigma-Aldrich (Milan, Italy) and used without further purification. Human renal adenocarcinoma 786-O cells were obtained from the American Type Culture Collection (ATCC; Manassas, VA, USA). Cells (passages 2-10) were maintained at 37 °C (5% CO_2) in RPMI 1640 medium, containing 10% FBS, 2 mM L-glutamine, 100 units/mL penicillin and 100 µg/mL streptomycin. All cell media and reagents were from Euroclone S.p.A. (Pero, Milan, Italy).

Procedure for the synthesis of compound 3: Compound **3** was synthesized from the chloro-methyl-calix[4]arene precursor **2** [44] adopting a procedure described for the synthesis of an analogous tetrakis(thiuroniumethyl)tetramethoxycalix[4]arene tetrachloride [48]. Compound **2** (100 mg, 0.077 mmol) and thiourea (1.5 equiv per chloromethyl unit) were dissolved in THF (4 mL) and the solution was refluxed for 15 h to give a white precipitate. After cooling, the solid precipitate was recovered by filtration and washed several times with ethyl ether, to give pure compound **3** (118 mg, 96% yield).

Characterization of compound 3: NMR spectra were acquired on a Bruker Avance 400TM spectrometer. Chemical shifts (δ, ppm) are reported referring to the residual peak of the solvent (DMSO-d_6). ^{1}H NMR (400.13 MHz, DMSO-d_6, 297 K) δ 0.83 (t, J = 6.6 Hz, 12H, 4 × dodecyl CH_3), 1.22 (br s, 72H, 36 × dodecyl CH_2), 1.34 (br s, 8H, 4 × dodecyl CH_2), 1.82 (t, 8H, 4 × dodecyl CH_2), 3.13 (d, J = 14.3 Hz, 4H, 2 × $ArCH_2Ar$), 3.78 (t, 8H, 4 × dodecyl OCH_2), 4.23 (s, 8H, 4 × $ArCH_2S$), 4.26 (d, J = 14.3 Hz, 4H, 2 × 4 $ArCH_2Ar$), 6.66 (s, 8H, 8 × ArH); ^{13}C NMR (100.6 MHz, DMSO-d_6, 297 K) δ 13.9 (q, dodecyl CH_3), 22.2, 26.2, 29.0, 29.5, 29.8, 30.1 (t, dodecyl $_{CH2}$), 31.5 (t, $ArCH_2Ar$), 34.7 (t, CH_2S), 75.0 (t, OCH_2), 127.8 (d, ArH), 128.8 (s, ArC-$_{CH2S}$), 135.0 (s, ArC-CH_2S), 156.0 (s, ArCO), 169.4 (s, C-NH_2).

Size and zeta potential measurements: DLS and ELS measurements were performed on a sample of compound **3** (1 mg) dissolved in 1 mL pure water. The colloidal solution was centrifuged at 10,000 rpm for 10 min and the supernatant was collected and analyzed by a Zetasizer NanoZS90 analyzer (Malvern Instrument, Malvern, UK) equipped with a 633 nm laser, at a scattering angle of 90° and 25 °C temperature. The size of the particles was calculated from the diffusion coefficient using the Stokes–Einstein equation:

$$D = \frac{kT}{6\eta R\pi}$$

where D is the diffusion coefficient, k is the Boltzmann constant, T is the absolute temperature, η is the solvent viscosity, and R is the solute radius.

The zeta potential (Z) was calculated by using Henry's equation

$$UE = \frac{2\varepsilon\zeta}{3\eta} f(Ka)$$

where *UE* is the electrophoretic mobility, ζ is the dielectric constant, *f*(*Ka*) is the Henry's function, and η is the viscosity.

Biological assays: Cell viability was measured by the acridine orange staining assay. Briefly, cancer cells were seeded in 96-well plates and grown at optimum culture conditions for 72 h (at a confluence of ≈60–80%). Then, cells were treated with the indicated concentrations of compounds for additional 48 h. Control cells received an equal volume of vehicle (DMSO). At the end of incubations, cells were fixed (in 4% paraformaldehyde) and stained with acridine orange solution (50 µg/mL), as previously described [45]. Acridine orange staining was then quantified as the resulting fluorescence intensity (excitation 485/20 nm, emission 528/20 nm) with a microplate reader (Synergy HT, BioTek).

Statistical analyses: Results are shown as mean ± SEM of three independent experiments, performed at least in triplicate. Statistical comparisons were performed by 2-way ANOVA. *P* values were considered significant at $p \leq 0.05$. All analyses were done with GraphPad Prism 10.4.1 (GraphPad Software, Inc., San Diego, CA).

Selectivity index determination: The selectivity index of compound **3** was calculated as the ratio of the IC_{50} in the cancer cell line to the IC_{50} in the non-malignant cell line, according to the following formula

$$SI = \frac{IC_{50}\ normal\ cells}{IC_{50}\ cancer\ cells}$$

Funding

This study was in part funded by European Union (Next-Generation EU), through the MUR-PNRR project SAMOTHRACE (ECS00000022).

Author Contributions

Giuseppe Granata: investigation; methodology. Loredana Ferreri: investigation; methodology. Claudia Giovanna Leotta: data curation; formal analysis; investigation; methodology. Giovanni Mario Pitari: conceptualization; resources; writing – review & editing. Grazia Maria Letizia Consoli: conceptualization; funding acquisition; methodology; project administration; resources; supervision; writing – original draft; writing – review & editing.

ORCID® iDs

Giuseppe Granata - https://orcid.org/0000-0001-9428-3985
Loredana Ferreri - https://orcid.org/0000-0002-3134-0409
Claudia Giovanna Leotta - https://orcid.org/0000-0002-9950-1205
Giovanni Mario Pitari - https://orcid.org/0000-0003-0698-8112
Grazia Maria Letizia Consoli - https://orcid.org/0000-0002-9608-5138

Data Availability Statement

All data that supports the findings of this study is available in the published article and/or the supporting information of this article.

References

1. Siegel, R. L.; Kratzer, T. B.; Giaquinto, A. N.; Sung, H.; Jemal, A. *Ca-Cancer J. Clin.* **2025,** *75,* 10–45. doi:10.3322/caac.21871
2. Zeng, H.; Zeng, W.; Liang, Y. *Oncol. Lett.* **2025,** *30,* 325. doi:10.3892/ol.2025.15071
3. Kiessling, L. L.; Lamanna, A. C. Multivalency in Biological Systems. In *Chemical Probes in Biology;* Schneider, M. P., Ed.; NATO Science Series, Vol. 129; Springer: Dordrecht, Netherlands, 2003; pp 345–357. doi:10.1007/978-94-007-0958-4_26
4. Carlson, C. B.; Mowery, P.; Owen, R. M.; Dykhuizen, E. C.; Kiessling, L. L. *ACS Chem. Biol.* **2007,** *2,* 119–127. doi:10.1021/cb6003788
5. Bakshi, A. K.; Haider, T.; Tiwari, R.; Soni, V. *Drug Delivery Transl. Res.* **2022,** *12,* 2335–2358. doi:10.1007/s13346-021-01103-4
6. Porębska, N.; Ciura, K.; Chorążewska, A.; Zakrzewska, M.; Otlewski, J.; Opaliński, Ł. *Biotechnol. Adv.* **2023,** *67,* 108213. doi:10.1016/j.biotechadv.2023.108213
7. Ou, C.; Li, C.; Feng, C.; Tong, X.; Vasta, G. R.; Wang, L.-X. *Bioorg. Med. Chem.* **2022,** *72,* 116974. doi:10.1016/j.bmc.2022.116974
8. Martian, P. C.; Tertis, M.; Leonte, D.; Hadade, N.; Cristea, C.; Crisan, O. *J. Pharm. Biomed. Anal.* **2025,** *252,* 116488. doi:10.1016/j.jpba.2024.116488
9. Yin, H.; Cheng, Q.; Bardelang, D.; Wang, R. *JACS Au* **2023,** *3,* 2356–2377. doi:10.1021/jacsau.3c00273
10. Della Sala, P.; Vanni, C.; Talotta, C.; Di Marino, L.; Matassini, C.; Goti, A.; Neri, P.; Šesták, S.; Cardona, F.; Gaeta, C. *Org. Chem. Front.* **2021,** *8,* 6648–6656. doi:10.1039/d1qo01048d
11. Buffet, K.; Nierengarten, I.; Galanos, N.; Gillon, E.; Holler, M.; Imberty, A.; Matthews, S. E.; Vidal, S.; Vincent, S. P.; Nierengarten, J.-F. *Chem. – Eur. J.* **2016,** *22,* 2955–2963. doi:10.1002/chem.201504921
12. Del Regno, R.; Santonoceta, G. D. G.; Della Sala, P.; De Rosa, M.; Soriente, A.; Talotta, C.; Spinella, A.; Neri, P.; Sgarlata, C.; Gaeta, C. *Org. Lett.* **2022,** *24,* 2711–2715. doi:10.1021/acs.orglett.2c00819
13. Neri, P.; Sessler, J. L.; Wang, M.-X., Eds. *Calixarenes and Beyond;* Springer International Publishing: Cham, Switzerland, 2016. doi:10.1007/978-3-319-31867-7
14. Asfari, Z.; Böhmer, V.; Harrowfield, J.; Vicens, J.; Saadioui, M., Eds. *Calixarenes 2001;* Kluwer Academic Publishers: Dordrecht, Netherlands, 2001. doi:10.1007/0-306-47522-7
15. Rodik, R.; Cherenok, S.; Kalchenko, O.; Yesypenko, O.; Lipkowski, J.; Kalchenko, V. *Curr. Org. Chem.* **2018,** *22,* 2200–2222. doi:10.2174/1385272822666181015141327
16. Mecca, T.; Consoli, G. M. L.; Geraci, C.; Cunsolo, F. *Bioorg. Med. Chem.* **2004,** *12,* 5057–5062. doi:10.1016/j.bmc.2004.07.037
17. Mecca, T.; Consoli, G. M. L.; Geraci, C.; La Spina, R.; Cunsolo, F. *Org. Biomol. Chem.* **2006,** *4,* 3763–3768. doi:10.1039/b608887b
18. Paul, S.; Jeyaprakash, R. S.; Pai, A.; Venkatachalam, H.; Jayashree, B. S. *Med. Chem.* **2023,** *19,* 939–945. doi:10.2174/1573406419666230703114605

19. Yousaf, A.; Hamid, S. A.; Bunnori, N. M.; Ishola, A. A. *Drug Des., Dev. Ther.* **2015,** *9,* 2831–2838. doi:10.2147/dddt.s83213
20. Wojaczyńska, E.; Ostrowska, M.; Lower, M.; Czyżyk, N.; Jakieła, A.; Marra, A. *Molecules* **2024,** *29,* 4240. doi:10.3390/molecules29174240
21. Sabir, S.; Thani, A. S. B.; Abbas, Q. *Front. Bioeng. Biotechnol.* **2025,** *13,* 1548588. doi:10.3389/fbioe.2025.1548588
22. Chehelgerdi, M.; Chehelgerdi, M.; Allela, O. Q. B.; Pecho, R. D. C.; Jayasankar, N.; Rao, D. P.; Thamaraikani, T.; Vasanthan, M.; Viktor, P.; Lakshmaiya, N.; Saadh, M. J.; Amajd, A.; Abo-Zaid, M. A.; Castillo-Acobo, R. Y.; Ismail, A. H.; Amin, A. H.; Akhavan-Sigari, R. *Mol. Cancer* **2023,** *22,* 169. doi:10.1186/s12943-023-01865-0
23. Baldini, L.; Casnati, A.; Sansone, F. *Eur. J. Org. Chem.* **2020,** 5056–5069. doi:10.1002/ejoc.202000255
24. Sun, R.; Xiang, J.; Zhou, Q.; Piao, Y.; Tang, J.; Shao, S.; Zhou, Z.; Bae, Y. H.; Shen, Y. *Adv. Drug Delivery Rev.* **2022,** *191,* 114614. doi:10.1016/j.addr.2022.114614
25. Consoli, G. M. L.; Granata, G.; Fragassi, G.; Grossi, M.; Sallese, M.; Geraci, C. *Org. Biomol. Chem.* **2015,** *13,* 3298–3307. doi:10.1039/c4ob02333a
26. Zhang, Y.; Xiao, J.; Cao, J.; Pan, J.; Li, C.; Zheng, Y. *J. Fluoresc.* **2025,** in press. doi:10.1007/s10895-025-04294-y
27. Consoli, G. M. L.; Forte, G.; Maugeri, L.; Consoli, V.; Sorrenti, V.; Vanella, L.; Buscarino, G.; Agnello, S.; Camarda, M.; Granata, G.; Ferreri, L.; Petralia, S. *ACS Appl. Nano Mater.* **2023,** *6,* 358–369. doi:10.1021/acsanm.2c04501
28. Geraci, C.; Consoli, G. M. L.; Granata, G.; Galante, E.; Palmigiano, A.; Pappalardo, M.; Di Puma, S. D.; Spadaro, A. *Bioconjugate Chem.* **2013,** *24,* 1710–1720. doi:10.1021/bc400242y
29. Gidwani, B.; Gupta, S. K.; Sahu, J. *Int. J. Pharm. Sci. Nanotechnol.* **2023,** *16,* 6546–6555. doi:10.37285/ijpsn.2023.16.3.8
30. Isik, A.; Oguz, M.; Kocak, A.; Yilmaz, M. *J. Inclusion Phenom. Macrocyclic Chem.* **2022,** *102,* 439–449. doi:10.1007/s10847-022-01134-5
31. Al-Ahmary, K. M.; Shafie, A.; Adnan Ashour, A.; S. Alrashdi, K.; Babalghith, A. O.; Alharthi, S. S.; Sabei, F. Y. *Crit. Rev. Anal. Chem.* **2024,** 1–26. doi:10.1080/10408347.2024.2402820
32. Li, R.; Liu, N.; Liu, R.; Jin, X.; Li, Z. *Curr. Drug Delivery* **2024,** *21,* 184–192. doi:10.2174/1567201820666230417084210
33. Basilotta, R.; Mannino, D.; Filippone, A.; Casili, G.; Prestifilippo, A.; Colarossi, L.; Raciti, G.; Esposito, E.; Campolo, M. *Molecules* **2021,** *26,* 3963. doi:10.3390/molecules26133963
34. Oguz, M.; Gul, A.; Karakurt, S.; Yilmaz, M. *Bioorg. Chem.* **2020,** *94,* 103207. doi:10.1016/j.bioorg.2019.103207
35. An, L.; Wang, C.; Zheng, Y.-G.; Liu, J.-d.; Huang, T.-h. *Eur. J. Med. Chem.* **2021,** *210,* 112984. doi:10.1016/j.ejmech.2020.112984
36. Viola, S.; Consoli, G. M. L.; Merlo, S.; Drago, F.; Sortino, M. A.; Geraci, C. *J. Neurochem.* **2008,** *107,* 1047–1055. doi:10.1111/j.1471-4159.2008.05656.x
37. Viola, S.; Merlo, S.; Consoli, G. M. L.; Drago, F.; Geraci, C.; Sortino, M. A. *Pharmacology* **2010,** *86,* 182–188. doi:10.1159/000317518
38. Oguz, M.; Gul, A.; Karakurt, S.; Yilmaz, M. *ChemistrySelect* **2020,** *5,* 12250–12254. doi:10.1002/slct.202002881
39. Oğuz, M. *Konya J. Eng. Sci.* **2022,** *10,* 189–199. doi:10.36306/konjes.1039091
40. Hendricks, R. T.; Sherman, D.; Strulovici, B.; Broka, C. A. *Bioorg. Med. Chem. Lett.* **1995,** *5,* 67–72. doi:10.1016/0960-894x(94)00460-w
41. Allan, R. D.; Dickenson, H. W.; Hiern, B. P.; Johnston, G. A. R.; Kazlauskas, R. *Br. J. Pharmacol.* **1986,** *88,* 379–387. doi:10.1111/j.1476-5381.1986.tb10214.x
42. Ganellin, C. R.; Bang-Andersen, B.; Khalaf, Y. S.; Tertiuk, W.; Arrang, J. M.; Garbarg, M.; Ligneau, X.; Rouleau, A.; Schwartz, J. C. *Bioorg. Med. Chem. Lett.* **1992,** *2,* 1231–1234. doi:10.1016/s0960-894x(00)80219-x
43. Ferreira, M.; Assunção, L. S.; Silva, A. H.; Filippin-Monteiro, F. B.; Creczynski-Pasa, T. B.; Sá, M. M. *Eur. J. Med. Chem.* **2017,** *129,* 151–158. doi:10.1016/j.ejmech.2017.02.013
44. Eggers, P. K.; Becker, T.; Melvin, M. K.; Boulos, R. A.; James, E.; Morellini, N.; Harvey, A. R.; Dunlop, S. A.; Fitzgerald, M.; Stubbs, K. A.; Raston, C. L. *RSC Adv.* **2012,** *2,* 6250–6257. doi:10.1039/c2ra20491f
45. Hathaway, W. E.; Newby, L. A.; Githens, J. H. *Cryobiology* **1965,** *2,* 143–146. doi:10.1016/s0011-2240(65)80101-8
46. Shapiro, D. D.; Virumbrales-Muñoz, M.; Beebe, D. J.; Abel, E. J. *Front. Oncol.* **2022,** *12,* 871252. doi:10.3389/fonc.2022.871252
47. Callacondo-Riva, D.; Quispe-Mauricio, A.; Lindo-Gamarra, S.; Vaisberg, A. *J. Rev. Peru. Med. Exp. Salud Publica* **2008,** *25,* 380–385.
48. Nagasaki, T.; Tajiri, Y.; Shinkai, S. *Recl. Trav. Chim. Pays-Bas* **1993,** *112,* 407–411. doi:10.1002/recl.19931120617

License and Terms

BEILSTEIN JOURNAL OF ORGANIC CHEMISTRY

Silica gel with covalently attached bambusuril macrocycle for dicyanoaurate sorption from water

Michaela Šusterová[1,2] and Vladimír Šindelář*[1,2]

Full Research Paper

Open Access

Address:
[1]Department of Chemistry, Faculty of Science, Masaryk University, Kamenice 5, 625 00 Brno, Czech Republic and [2]RECETOX, Faculty of Science, Masaryk University, Kamenice 5, 625 00 Brno, Czech Republic

Email:
Vladimír Šindelář* - sindelar@chemi.muni.cz

* Corresponding author

Keywords:
anion binding; anion extraction; anion receptor; gold mining; macrocycles

Beilstein J. Org. Chem. **2025,** *21,* 2604–2611.
https://doi.org/10.3762/bjoc.21.201

Received: 21 August 2025
Accepted: 13 November 2025
Published: 24 November 2025

This article is part of the thematic issue "Novel macrocycles: from synthesis to supramolecular function".

Guest Editor: C. Gaeta

Abstract

Anion removal from aqueous solutions remains a major challenge due to the strong hydration of anions. Here, we report the preparation of silica gel functionalized with covalently anchored bambusuril macrocycles. In aqueous solution, this material efficiently sorbs dicyanoaurate(I), the key anion in gold mining, even in the presence of competing dicyanoargentate(I) anions. We also examine the recyclability of the material and assess its stability in organic solvents, comparing its performance with that of a previously developed material containing noncovalently bound bambusuril.

Introduction

Inorganic anions play essential roles in a variety of biological and biochemical mechanisms and are also involved in many industrial and manufacturing processes. Due to their significant environmental impact, it is important to monitor their presence and control their concentrations, particularly in water. To maintain anion levels within acceptable ranges, their removal from the environment is often necessary [1,2].

Current technologies for removing anions from aqueous solutions include chemical coprecipitation [3], ion-exchange [4], or membrane filtration [5]. In the field of anion extraction, there is growing interest in solid-phase substrates functionalized with synthetic macrocyclic receptors. These materials employ a supramolecular approach based on specific host–guest interactions between the immobilized macrocycle and the guest in solution, often leading not only to improved extraction effectivity but also to enhanced selectivity [2]. Anion extractants based on functionalized polystyrene or silica gel typically incorporate calixarenes [6] and their analogues, calixpyrroles [7,8], azacalixarene derivatives [9], or expanded porphyrin-like sapphyrin [10].

Although synthetic anion receptors have attracted increasing attention in the field of supramolecular chemistry, there are still

relatively few reports of materials that employ macrocyclic receptors to recognize and selectively bind anionic species specifically in aqueous environments. For example, an amphiphilic poly(methyl methacrylate)-based polymer modified with calix[4]pyrrole was found to form micelles in water that capture anions from caesium salts and can be precipitated from solution upon heating [11]. Similarly, a hydrogel composed of poly(vinyl alcohol) cross-linked by a "Texas-sized" molecular box has been used to extract various anions from water [12].

Another family of macrocyclic compounds suitable for anion recognition and binding are bambusurils (BUs). BUs act as very potent anion receptors in both organic solvents and water. Furthermore, their portals can be variously functionalized, for instance by carboxylic moieties [13], making them available for further reactions with different substrates. We have recently presented a material (SG-BnBU) based on silica gel containing dodecabenzylbambus[6]uril (BnBU) non-covalently bound on its surface [14]. We showed that this material is able to remove dicyanoaurate(I) anion from water, the principal cyanide-based species generated during gold mining processes. However, the use of the SG-BnBU material is problematic as BnBU can leach from the material into the solution. To address this limitation, we have developed and herein report a new material, SG-NHCO-BU1, in which the BU1 macrocycle is covalently grafted onto the surface of silica gel. We demonstrate that this hybrid material can be used for the selective dicyanoaurate(I) sorption from water. Moreover, it is shown that unlike SG-BnBU, SG-NHCO-BU1 exhibits good stability in organic solvents.

Results and Discussion

Decoration of silica gel with bambusuril

For the modification of silica gel (SG), we selected previously reported bambus[6]uril BU1 (Scheme 1) containing 12 carboxyalkyl substituents [13]. This macrocycle was chosen for several reasons: BU1 can be attached to SG not only by electrostatic interactions but also covalently, the BU1 synthesis is straightforward lacking difficult and time-consuming purification, and it is obtained in relatively high yield over 60%. Once BU1 was prepared, its covalent attachment on the surface of SG was achieved in two steps. First, SG, chosen as the solid substrate, was reacted with an excess of 3-aminopropyltriethoxysilane (APTES) in toluene under reflux to obtain a-SG material with

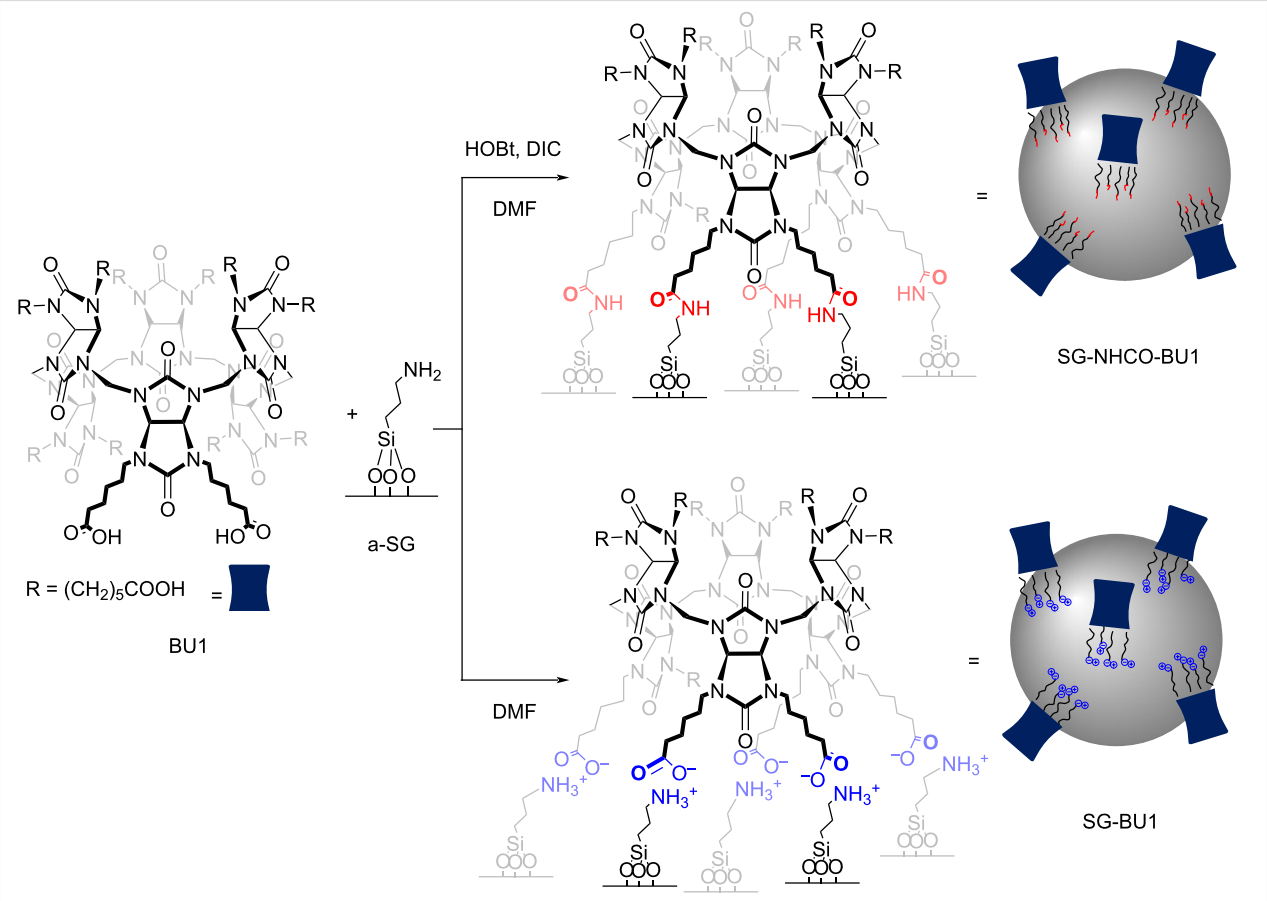

Scheme 1: Synthesis of SG-NHCO-BU1 and SG-BU1 materials based on covalently and non-covalently attached BU1 on the SG surface.

amino groups introduced on the SG surface [15,16]. In the second step, a-SG was treated with BU1, in the presence of 1-hydroxybenzotriazole (HOBt) and 1,3-diisopropylcarbodiimide (DIC) in DMF, resulting in SG-NHCO-BU1 with BU1 covalently attached through amide bonds (Scheme 1). The material was thoroughly washed with DMF, water, and methanol to remove byproducts and unreacted BU1. The grafting reaction was conducted using a 9:1 (w/w) ratio of a-SG to BU1. This ratio was selected based on our previously published results for the noncovalent SG-BnBU system [14]. Besides the covalent SG-NHCO-BU1 material, we also prepared the noncovalent SG-BU1 material, in which BU1 is attached on the SG surface through electrostatic interactions (Scheme 1). The latter reaction was also done using a 9:1 (w/w) ratio of a-SG to BU1, by treatment of a-SG with the macrocycle in DMF at ambient temperature (Scheme 1). The material was then isolated by filtration and washed with DMF and methanol.

The prepared a-SG, SG-NHCO-BU1, and SG-BU1 materials were characterized by FTIR spectroscopy (Supporting Information File 1, Figure S1). In comparison to crude silica gel, the diminished band corresponding to the –OH group (around 980 cm^{-1}) and the appearance of new bands characteristic of amino groups (around 3000 cm^{-1}) indicate the successful introduction of amino groups onto the silica gel surface, confirming the formation of a-SG. Upon modification of a-SG with BU1, additional bands characteristic of BU1 appeared. When comparing BU1 with the SG-NHCO-BU1 material, the C=O vibration band shifted from 1703 cm^{-1} to 1696 cm^{-1} indicating the formation of an amide bond. Additionally, a new absorption band at 1558 cm^{-1} was observed in the spectra of SG-NHCO-BU1 further confirming covalent attachment of BU1 through an amide bond. In the case of SG-BU1, a C=O vibrational band is observed at 1705 cm^{-1}, which corresponds to the vibration of the C=O of BU1 carboxylic acid groups. Other bands corresponding to BU1 were also visible in the spectrum, confirming the presence of the macrocycle in both materials.

The attachment of APTES and subsequently BU1 on SG was further confirmed by thermogravimetric analysis (TGA) (Figure 1A). Pure SG is highly thermally stable, undergoing only minimal decomposition at temperatures below 800 °C as

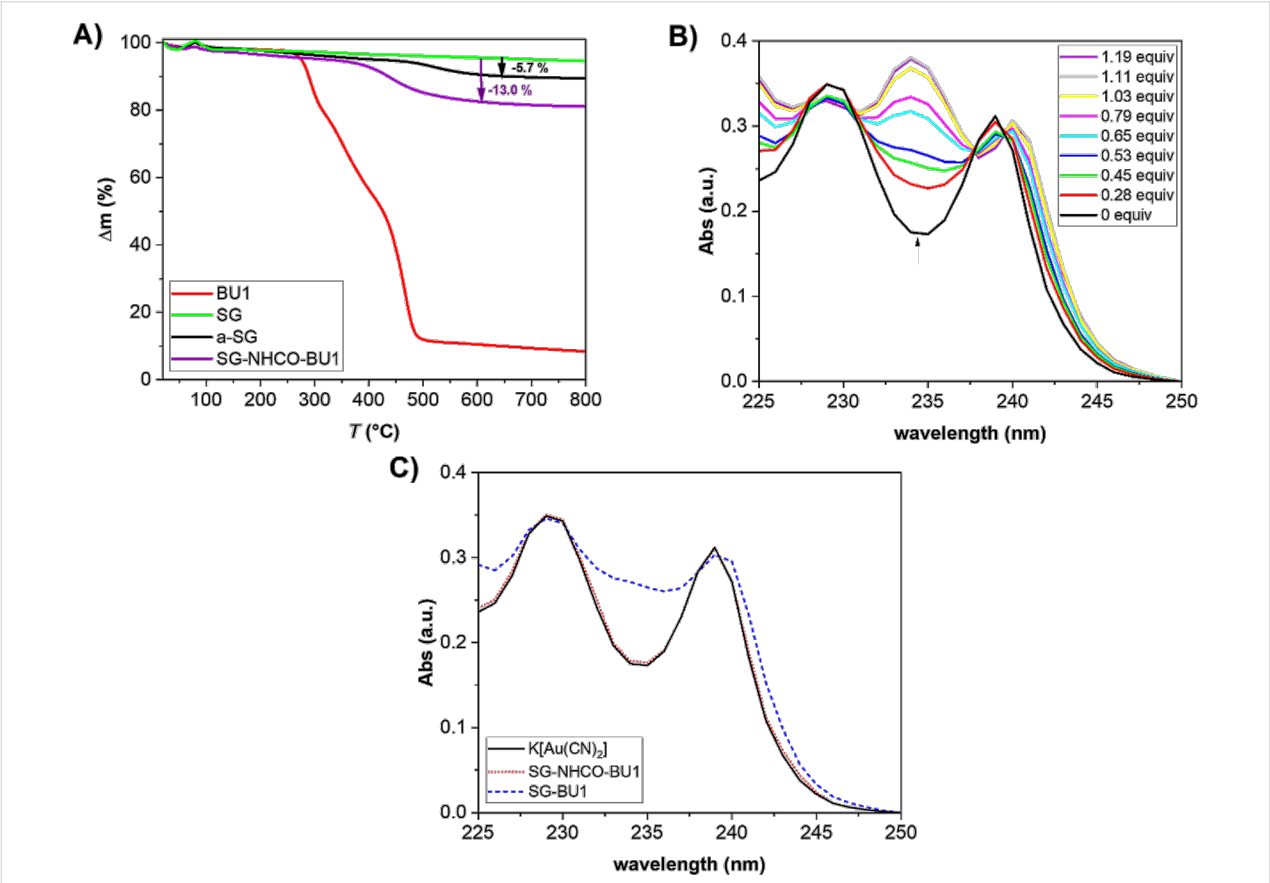

Figure 1: A) Thermogravimetric analyses of BU1, SG, a-SG, and SG-NHCO-BU1. B) UV–vis titration of $K[Au(CN)_2]$ (0.5 mM) with increasing amount of BU1. C) UV–vis spectra of $K[Au(CN)_2]$ (0.5 mM) before and after additions of supernatants obtained by treatment of SG-NHCO-BU1 and SG-BU1 with aqueous 1 M KOH.

confirmed by the analysis. In contrast, a-SG, SG-NHCO-BU1, and SG-BU1 exhibited reduced thermal stability due to the presence of organic substituents (Figure 1A and Supporting Information File 1, Figure S1C). A weight loss of 10% for BU1, SG-NHCO-BU1, and SG-BU1 was observed at 289 °C, 427 °C, and 438 °C.

Additionally, TGA allowed determination of the content of BU1 grafted on the surface in SG-NHCO-BU1 and SG-BU1. As stated above, the material was prepared by mixing of a-SG to BU1 in a 9:1 (w/w) ratio. The analysis revealed that there is approximately 7.3 wt % of BU1 in SG-NHCO-BU1, which corresponds to 74% of the used BU1 attached during its reaction with a-SG (Figure 1A). SG-BU1 contained 7.7 wt % of BU1 which is comparable with the material of covalently attached BU1 (Supporting Information File 1, Figure S1). Thus, according to the TGA, SG-NHCO-BU1 contains 73 mg of BU1 per 1 g of material, which corresponds to 0.032 mmol of BU1 per gram and SG-BU1 comprises 0.034 mol of BU1 per gram.

In order to prove that BU1 is bound through amide bonds on the substrate and it does not leach into solution, we have treated the SG-NHCO-BU1 material with 1 M KOH, followed by addition of dicyanoaurate ($[Au(CN)_2]^-$) to the supernatant. It was shown previously that the absorption spectrum of dicyanoaurate in aqueous solution changes upon formation of an inclusion complex between the anion and a bambusuril macrocycle [17]. A solution of dicyanoaurate in 1 M KOH was titrated by BU1 and the changes in the absorption spectra of the anion were in agreement with those previously reported in pure water (Figure 1B). Dicyanoaurate absorption bands with maxima at 239 and 229 nm decreased in their intensity in the presence of BU1, while a new band appeared at 234 nm. As the complex formation is almost quantitative at millimolar concentrations (association constant is 1.3×10^6 M^{-1} in water) [17], dicyanoaurate can be utilized for the determination of the BU1 content in solution in case BU1 leaches from the substrate. For comparison, SG-BU1 was treated in the same way. After the treatment of the SG-NHCO-BU1 material with 1 M KOH, the supernatant was analyzed in the presence of 1 mM dicyanoaurate by UV–vis spectroscopy (Figure 1C). The measured spectra were identical with the spectrum of pure dicyanoaurate solution revealing that SG-NHCO-BU1 did not release any BU1 and therefore, the macrocycle is indeed covalently bound in the SG-NHCO-BU1 material. This is in contrast with the SG-BU1 material, which released BU1 to the KOH solution as evidenced by marked changes of dicyanoaurate in its absorption spectra (Figure 1C).

A potential application of these materials depends on their stability in different solvents. In terms of practical implementation, BU must stay attached to the solid substrate and should not leach into solution upon usage; for example, as shown above, SG-BU1 has limitations to be used in basic environments. To investigate further the stability of the prepared materials, we compared the behavior of SG-NHCO-BU1, SG-BU1, and SG-BnBU in different solvent systems (Supporting Information File 1, Figure S3). Chloroform, dichloromethane, and methanol were investigated due to their frequent use as mobile phases in liquid chromatography; aqueous phosphate buffer (pH 7.1) was chosen to test the materials' stability in an aqueous environment. ^{1}H NMR measurements showed that neither material released BU into organic solvents in the absence of anions. This was unexpected for SG-BnBU, since BnBU is readily soluble in chloroform and dichloromethane and is only physically adsorbed on SG. However, upon addition of chloride anions, either as tetrabutylammonium (TBA) or sodium salt, BnBU formed a complex with the anion and dissolved in chloroform and dichloromethane and even in methanol. Thus, SG-BnBU remained stable only in water in the absence and presence of salt showing it is suitable for applications in an aqueous environment. SG-BU1 proved to be stable in chloroform, dichloromethane, and methanol even after addition of TBACl or NaCl, respectively. We did not detect any release of BU1 from SG-BU1 in aqueous phosphate buffer by NMR, but we observed leaching of BU1 into solution upon addition of NaCl (Supporting Information File 1, Figure S4) to this solvent system. As expected, SG-NHCO-BU1 with covalently bound BU1 remained stable in all tested solvents in the absence as well as in the presence of salts.

Anion sorption by SG-NHCO-BU1

Silica gel modified either with covalently or noncovalently immobilized BU1 was further investigated for its ability to sorb anions from water and in terms of recyclability. For this purpose, dicyanoaurate ($[Au(CN)_2]^-$) was selected as this anion can be monitored by UV–vis spectroscopy (Figure 2) and plays a central role in gold mining industry [18]. In addition, it allows comparison with the previously prepared SG-BnBU material with noncovalently bound BnBU, which was also tested using the same anion. When either SG-NHCO-BU1 or SG-BU1 was treated with a 1 mM solution of $K[Au(CN)_2]$ in water, the anion concentration in solution reached equilibrium after 15 minutes, consistent with the equilibration time previously established for the non-covalent system SG-BnBU (Supporting Information File 1, Figure S5). Therefore, all subsequent sorption experiments were performed with an equilibration time of 15 minutes.

Next, we evaluated the efficiency of the SG-NHCO-BU1 material in sorbing dicyanoaurate. First, we showed that SG-BU1 is stable under the experimental conditions (Supporting Information File 1, Figure S5C) and next, we investigated both materi-

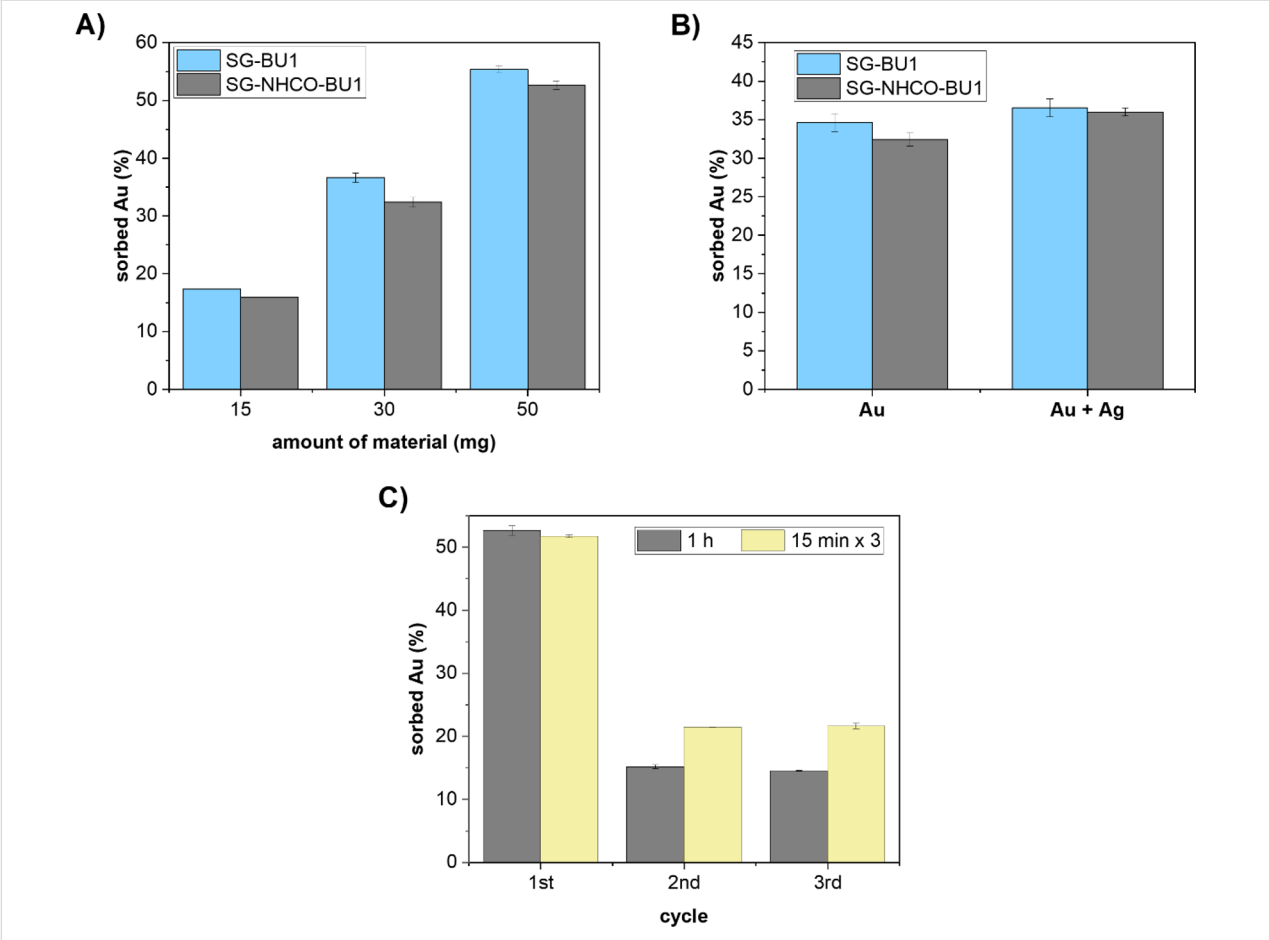

Figure 2: The efficiency of materials (blue SG-BU1, grey SG-NHCO-BU1) in sorbing dicyanoaurate from its water solution (1 mM, 3 mL). A) Depending on the amount of the used material. B) Measured in the absence (Au) and in the presence of $K[Ag(CN)_2]$ (Au + Ag); experiments were done using 30 mg of the materials. C) Dicyanoaurate sorption efficiency before (1st cycle) and after (following cycles) washing with NaBr solution (10 mM) for 1 h or 3 × 15 min; experiments were done using 50 mg of SG-NHCO-BU1.

als for dicyanoaurate sorption. Thus, we gradually increased the amount of SG-NHCO-BU1/SG-BU1 in the 1 mM water solution of $K[Au(CN)_2]$ and observed an uptake of dicyanoaurate based on the changes in the absorption spectra of $K[Au(CN)_2]$. Assuming the molar content of BU1 in the SG-NHCO-BU1/SG-BU1 materials is 0.032/0.034 mmol g^{-1} (based on TGA), we calculated that 1.3/1.4 equivalents of BU1 on the material are required to bind a single dicyanoaurate anion. A similar macrocycle-to-anion ratio was previously determined for the SG-BnBU material. In contrast, water-soluble BU and dicyanoaurate have been reported to form complexes of 1:1 stoichiometry, exhibiting near-quantitative binding at millimolar concentrations [17]. The lower binding efficiency of BUs attached to the material compared to the free macrocycle in solution can likely be attributed to the heterogeneous nature of the solid-phase system. Moreover, the anion binding ability of BU1 may be affected by its long aliphatic arms terminated with carboxylic groups, whose flexibility can enable intramolecular complexation competing for an anion binding [13].

Bambusurils are known to bind a wide range of anions with varying selectivity. Dicyanoaurate is particularly relevant to the gold mining industry, whereas dicyanoargentate is considered a contaminant in this context. To assess selectivity, we measured the sorption of dicyanoaurate from a 1 mM aqueous solution both in the absence and in the presence of an equimolar amount of dicyanoargentate. The measurements revealed that dicyanoaurate uptake was similarly high in both experiments – in the absence and in the presence of the silver salt (Figure 2B) for both materials. The minimal effect of dicyanoargentate on dicyanoaurate sorption aligns with previous findings that BU binds the former anion over 100-fold more weakly in aqueous solution [17]. The finding is also in agreement with our reported results on the noncovalent SG-BnBU system, which showed significantly higher sorption efficiency towards dicyanoaurate over dicyanoargentate [14].

We next examined the recyclability of the materials. Only SG-NHCO-BU1 was used in these experiments as SG-BU1 is

not stable under the experimental conditions as the complex of BU1@$[Au(CN)_2]^-$ was leached into the solution (Figure S6, Supporting Information File 1). After the first sorption, SG-NHCO-BU1 was washed with an excess of aqueous NaBr solution (10 mM, 3 mL, 1 h) to replace $[Au(CN)_2]^-$ in the BU1 cavity with Br^- (Figure 2C). This washing procedure was repeated three times, and the sorption efficiency after each cycle was determined. A decrease in the uptake efficiency was observed after the first washing, but the efficiency remained preserved in following cycles. Prior to the first sorption cycle, the macrocycle is anion-free, whereas in later cycles, it remains occupied by bromide ions due to NaBr treatment, which explains differences during the first and following cycles. We further optimized the regeneration procedure by replacing a single long wash (1 hour) with multiple shorter washes (3 × 15 minutes). The uptake efficiency of SG-NHCO-BU1 improved from 15% to 21% (Figure 2C). Furthermore, the ability of SG-NHCO-BU1 to capture anions was very well in accordance to how much of dicyanoaurate was released – the amount of captured dicyanoaurate corresponded to its released amount during previous washing step (Figure S6B, Supporting Information File 1).

Conclusion

In summary, we have developed organic–inorganic hybrid materials for anion extraction. Through a two-step modification of silica gel, two materials were obtained: SG-NHCO-BU1, in which the BU1 macrocycle is covalently attached to the silica surface via amide bonds, and SG-BU1, where the macrocycle is bound by electrostatic interactions. Both materials proved to be an efficient extractant of dicyanoaurate anions from water, achieving maximum sorption within 15 minutes. The covalent attachment of BU1 enables the material to be recycled using NaBr solution, while the SG-BU1 material disintegrates under similar conditions. We also showed that both SG-NHCO-BU1 and SG-BU1 are stable in organic solvents including chloroform, dichloromethane, and methanol even after addition of halide salts. This stability stands in contrast to previously published SG-BnBU, which contains noncovalently immobilized BnBU and undergoes macrocycle loss in all of three tested organic solvents after addition of halide salts. These results illustrate that the choice of material for anion sorption depends on the specific experimental conditions. While SG-BnBU and SG-NHCO-BU1 are suitable for dicyanoaurate sorption from aqueous solutions, SG-NHCO-BU1 and SG-BU1 could be used for anion extraction in organic media.

Experimental

Materials and instruments

Silica gel (Silikagel 60 (0.015–0.040 mm) for column chromatography, product number 1.15111) was dried in vacuo at 50 °C overnight before use. 3-Aminopropyltriethoxysilane (APTES), 1-hydroxybenzotriazole (HOBt), 1,3-diisopropylcarbodiimide (DIC), potassium dicyanoaurate, potassium dicyanoargentate, sodium chloride, tetrabutylammonium chloride and sodium bromide were purchased from Merck and used without further purification. Dodecakis(5-carboxypentyl)bambus[6]uril (BU1) was synthesized according to a previously published procedure [13].

Infrared spectra were recorded with an Alpha spectrophotometer (Bruker). Thermogravimetric analyses were done with a Netzsch STA 449C Jupiter and carried out in nitrogen atmosphere. The dicyanoaurate concentration in solution was determined according to UV–vis spectra recorded with a CARY 60 spectrophotometer (Agilent Technologies). NMR spectra were recorded on a Bruker Avance III 300 spectrometer (300.15 Hz, 298.15 K).

Preparation of SG-NHCO-BU1

Silica gel (8.01 g) was dispersed in toluene (24 mL) and stirred under argon atmosphere, while heated up to 115 °C. Then, APTES (6 mL) was added, and the dispersion was stirred under inert atmosphere at elevated temperature for 5 h. After cooling, the dispersion was filtered, washed thoroughly with toluene, ethanol and acetone to remove unreacted APTES and dried in vacuo (50 °C) overnight in order to get a-SG [15,16]. Further, to prepare covalent SG-NHCO-BU1, a-SG (0.9 g) was suspended in DMF (15 mL) and shaken at ambient temperature for 30 min. BU1 (0.1 g, 1 equiv) was dissolved in a minimum amount of DMF and a solution of HOBt (12 equiv) in DMF was added, followed by addition of DIC (12 equiv). Then, the activated BU1 was added to the suspension of a-SG. The reaction was performed under Ar atmosphere for 5.5 h at ambient temperature under constant shaking (180 rpm). The resulting material was filtered and thoroughly washed with DMF, water and methanol in order to remove byproducts and unreacted BU1. After air-drying, SG-NHCO-BU1 was obtained.

Preparation of SG-BU1

For the preparation of SG-BU1 with electrostatically bound BU1 on the surface of silica gel, a-SG (0.9 g) was suspended in DMF (15 mL) and BU1 (0.1 g), dissolved in a minimum amount of DMF, was added. The dispersion was mechanically shaken (180 rpm) at ambient temperature for 5.5 h. Afterwards, the dispersion was filtered, washed with DMF (5×) and methanol (5×) to remove unattached BU1. After air-drying in a hood overnight at ambient temperature, SG-BU1 was obtained.

Sorption experiments with SG-NHCO-BU1

The potential of SG-NHCO-BU1 to bind anions from solution was investigated by UV–vis spectroscopy. SG-NHCO-BU1 or

SG-BU1 was placed in a vial and anion solution (1 mM, 3 mL) was added. The system was shaken for 15 min at 250 rpm. Afterwards, SG-NHCO-BU1 or SG-BU1 was left to settle and the supernatant was analyzed. The actual concentration of the anion left in the solution was calculated from a calibration curve.

Supporting Information

Supporting Information File 1

Characterization of materials and additional experiments regarding anion uptake.
[https://www.beilstein-journals.org/bjoc/content/supplementary/1860-5397-21-201-S1.pdf]

Acknowledgements

We thank Dr. Zdeněk Moravec for the TGA measurements and Dr. Arico Del Mauro for assistance with the BU1 synthesis.

Funding

The authors thank the RECETOX Research Infrastructure (LM2023069) financed by the Ministry of Education, Youth, and Sports, and the Operational Programme Research, Development, and Education. This project was supported by the European Union's Horizon 2020 Research and Innovation Programme under grant agreement No. 857560. This publication reflects only the author's view and the European Commission is not responsible for any use that may be made of the information it contains. The authors acknowledge the support from National Infrastructure for Chemical Biology (CZ-OPENSCREEN, LM2023052).

Author Contributions

Michaela Šusterová: investigation; visualization; writing – original draft. Vladimír Šindelář: conceptualization; funding acquisition; supervision; writing – review & editing.

ORCID® iDs

Vladimír Šindelář - https://orcid.org/0000-0003-0090-5961

Data Availability Statement

All data that supports the findings of this study is available in the published article and/or the supporting information of this article.

References

1. Mohammed, F. A.; Xiao, T.; Wang, L.; Elmes, R. B. P. *Chem. Commun.* **2024,** *60,* 11812–11836. doi:10.1039/d4cc04521a
2. Zhang, Q.; Zhou, Y.; Ahmed, M.; Khashab, N. M.; Han, W.; Wang, H.; Page, Z. A.; Sessler, J. L. *J. Mater. Chem. A* **2022,** *10,* 15297–15308. doi:10.1039/d2ta03791b
3. Reyes-Serrano, A.; López-Alejo, J. E.; Hernández-Cortázar, M. A.; Elizalde, I. *Chin. J. Chem. Eng.* **2020,** *28,* 1107–1111. doi:10.1016/j.cjche.2019.12.023
4. Li, D.; Ning, X.-a.; Yuan, Y.; Hong, Y.; Zhang, J. *J. Environ. Sci.* **2020,** *91,* 62–72. doi:10.1016/j.jes.2020.01.002
5. Jiang, M.; Ye, K.; Deng, J.; Lin, J.; Ye, W.; Zhao, S.; Van der Bruggen, B. *Environ. Sci. Technol.* **2018,** *52,* 10698–10708. doi:10.1021/acs.est.8b02984
6. Memon, S.; Tabakci, M.; Roundhill, D. M.; Yilmaz, M. *React. Funct. Polym.* **2006,** *66,* 1342–1349. doi:10.1016/j.reactfunctpolym.2006.03.017
7. Sessler, J. L.; Gale, P. A.; Genge, J. W. *Chem. – Eur. J.* **1998,** *4,* 1095–1099. doi:10.1002/(sici)1521-3765(19980615)4:6<1095::aid-chem1095>3.0.co;2-1
8. Aydogan, A. *Supramol. Chem.* **2016,** *28,* 117–124. doi:10.1080/10610278.2015.1092538
9. Zhao, W.; Lou, X.; Guo, J.; Sun, P.; Jia, Y.; Zheng, L.; He, L.; Zhang, S. *J. Sep. Sci.* **2018,** *41,* 2110–2118. doi:10.1002/jssc.201701185
10. Iverson, B. L.; Thomas, R. E.; Kral, V.; Sessler, J. L. *J. Am. Chem. Soc.* **1994,** *116,* 2663–2664. doi:10.1021/ja00085a074
11. Ji, X.; Guo, C.; Chen, W.; Long, L.; Zhang, G.; Khashab, N. M.; Sessler, J. L. *Chem. – Eur. J.* **2018,** *24,* 15791–15795. doi:10.1002/chem.201804335
12. Ji, X.; Wu, R.-T.; Long, L.; Guo, C.; Khashab, N. M.; Huang, F.; Sessler, J. L. *J. Am. Chem. Soc.* **2018,** *140,* 2777–2780. doi:10.1021/jacs.7b13656
13. Havel, V.; Babiak, M.; Sindelar, V. *Chem. – Eur. J.* **2017,** *23,* 8963–8968. doi:10.1002/chem.201701316
14. Šusterová, M.; Šindelář, V. *RSC Adv.* **2025,** *15,* 12982–12986. doi:10.1039/d5ra02404h
15. Gambero, A.; Kubota, L. T.; Gushikem, Y.; Airoldi, C.; Granjeiro, J. M.; Taga, E. M.; Alcântara, E. F. C. *J. Colloid Interface Sci.* **1997,** *185,* 313–316. doi:10.1006/jcis.1996.4566
16. Lee, Y. K.; Ryu, Y. K.; Ryu, J. W.; Kim, B. E.; Park, J. H. *Chromatographia* **1997,** *46,* 507–510. doi:10.1007/bf02496369
17. Rando, C.; Vázquez, J.; Sokolov, J.; Kokan, Z.; Nečas, M.; Šindelář, V. *Angew. Chem., Int. Ed.* **2022,** *61,* e202210184. doi:10.1002/anie.202210184
18. Liu, W.; Jones, L. O.; Wu, H.; Stern, C. L.; Sponenburg, R. A.; Schatz, G. C.; Stoddart, J. F. *J. Am. Chem. Soc.* **2021,** *143,* 1984–1992. doi:10.1021/jacs.0c11769